The Dynamical Ejections of Massive Stars from Young Star Clusters

Dissertation
zur
Erlangung des Doktorgrades (Dr. rer. nat.)
der
Mathematisch-Naturwissenschaftlichen Fakultät
der
Rheinischen Friedrich-Wilhelms-Universität Bonn

von
Seungkyung Oh
aus
Busan, Republik Korea

Bonn, 2016

Dieser Forschungsbericht wurde als Dissertation von der Mathematisch-Naturwissenschaftlichen Fakultät der Universität Bonn angenommen und ist auf dem Hochschulschriftenserver der ULB Bonn `http://hss.ulb.uni-bonn.de/diss_online` elektronisch publiziert.

1. Gutachter:	Prof. Dr. Pavel Kroupa
2. Gutachter:	Prof. Dr. Karl M. Menten
Tag der Promotion:	08.11.2016
Erscheinungsjahr:	2017

Abstract

Massive stars form in star clusters or OB associations which may be expanded clusters. Such stars can be expelled with a high velocity from their birth cluster through a strong close encounter with other cluster members. In particular, massive stars can be efficiently shot out from their birth cluster via dynamical ejection processes since they are mostly found in the centre of the cluster where the stellar density is the highest. In this thesis, we perform a large set of *N*-body calculations using the direct *N*-body code NBODY6. To study the effects of initial configurations of star clusters, we vary several initial parameters, such as the initial size and mass of the clusters, initial mass segregation, and initial binary populations. We investigate several aspects of dynamical ejections of massive stars from young star clusters using the *N*-body calculations. This study constitutes the hitherto largest theoretical investigation of dynamical OB-star ejections.

Firstly, we study the effect of dynamical processes, such as dynamical ejections and stellar collisions, on the relation between the maximum stellar mass and cluster mass. We show that the initially most massive star in a cluster can be dynamically ejected from dense, massive clusters. Secondly, we study the efficiency of O-star ejections as a function of cluster mass. We discover that the ejection fraction of O-star systems peaks at a cluster mass of $10^{3.5}\,M_{\odot}$. We estimate that, for our most realistic models, about 15% of O-star systems that form in a Milky-Way-type galaxy are dynamically ejected from their birth cluster to the field. Our results show that the observed fractions of field and runaway O stars, and the binary fractions among them, can be well understood theoretically if all O stars form in embedded clusters. Thirdly, we investigate how the dynamical ejections of massive stars vary with the initial conditions of star clusters. We present several properties of ejected massive systems that are dependent on the initial conditions. The ejections of (massive) stars can change the properties of stars inside clusters. Because the ejection efficiency of stars increases with stellar mass, particularly for models that are efficient in ejecting massive stars, the mass functions become top-heavy for ejected stars and bottom-heavy for stars that remain in the cluster. Lastly, we show that a very massive ($>300\,M_{\odot}$) binary, such as R144 in the 30 Dor region in the Large Magellanic Cloud, can be dynamically ejected from a young massive star cluster like R136 through a binary–binary encounter. In addition, the R136-type cluster can populate several very massive ($\gtrsim 100\,M_{\odot}$) stars outside of the cluster through dynamical ejections. This implies that the isolated formation scenario is unnecessary for very massive stars/binaries in relative isolation.

Throughout this thesis, we show that the massive stars can be efficiently ejected from their birth cluster through energetic close encounters and that outcomes of the dynamical ejections depend on the initial conditions of star clusters and their massive star population. The latter suggests that studying massive stars outside of star clusters can help to understand how massive stars form in a star cluster, by assuming that they all form in star clusters. When a large kinematic survey of massive stars in the Galaxy becomes available, for example through the astrometric space mission *Gaia*, our models can be used to constrain the initial configurations of massive stars and their birth clusters, which are end-products of the star formation process, leading towards a better understanding of massive star formation.

Contents

CHAPTER 1

Introduction

Most, if not all, stars form in a clustered environment (Lada & Lada 2003; Kroupa 2005; Megeath et al. 2016). Even the Sun, which is now in relative isolation, was likely once a member of a star cluster that has probably dissolved a long time ago (Adams 2010; Pfalzner 2013). Therefore, soon after they were born, stars keep interacting and exchanging energy with their sibling stars by the mutual gravitational force between them.

While newly born (or forming) low-mass stars can be commonly found in less dense environments, like the Taurus-Auriga star-forming region, the majority of massive stars are found in young, dense star clusters or OB associations (Zinnecker & Yorke 2007). It is expected that massive stars likely go through more energetic experiences. On the other hand, effects of massive stars on the dynamical evolution of a cluster would be small because of their short lifetime, at most 10 Myr for O-type ($\gtrsim$15 $M_\odot$) stars, and their rareness. It is, thus, generally assumed that the dynamical evolution has hardly affected observed properties of massive stars. For globular clusters, prime objects for the N-body community, massive stars were present only shortly, and compared to their lifetime, their evolution has been dominated by low-mass stars that are the majority population and long-lived. Thus massive stars are generally ignored for most previous N-body models of globular clusters. For young star clusters, in which the majority of massive stars are found, the observed kinematic properties and binary populations of massive stars are generally assumed to be the same as the initial configuration because the clusters are considered too young to be affected by dynamical evolution. However, massive stars are mostly located in the cluster centre, from birth or by dynamical mass segregation, where the density is the highest in the cluster. This implies that a few Myr old massive stars could have gone through dynamic interactions and that studying the dynamical evolution of massive stars in the cluster is necessary for a better understanding of massive-star populations.

This thesis focuses on the dynamical evolution of massive stars that have formed in a star cluster. Not only massive stars found in the clusters but also those in relative isolation could have a dynamic history. Our particular interest goes to the origin of adventurous massive stars or those forced to leave their birth place via strong interactions with other cluster members. In this chapter we describe basic concepts of dynamical processes in a star cluster related to ejections of massive stars, issues that we investigate, and the direct N-body code we use in this thesis. The outline of the thesis follows at the end of the chapter.

1.1 Basic concepts of stellar dynamics

We briefly introduce a few basic concepts of stellar dynamics relevant to the dynamical evolution of star clusters, before we move to the topic of this thesis that is on dynamical ejections of massive stars.

Dynamical timescales Two timescales are used to evaluation of dynamical states of dense stellar systems. The *crossing time* is the time that is needed for a typical star to cross the system. For a star cluster, the crossing time $t_{\rm cr}$ is expressed as

$$t_{\rm cr} = \frac{2r_{\rm h}}{\sigma_{\rm cl}}, \tag{1.1}$$

where $r_{\rm h}$ and $\sigma_{\rm cl}$ are the half-mass radius of and the velocity dispersion in the cluster, respectively. Here, the velocity dispersion of the star cluster is the typical velocity of stars in a non-rotating cluster. The velocity dispersion at the half-mass radius is given under the assumption of virial equilibrium,

$$\sigma_{\rm cl} \approx \sqrt{\frac{GM_{\rm ecl}}{r_{\rm h}}},$$

where G and $M_{\rm ecl}$ are the gravitational constant and the mass of the cluster, respectively. The typical crossing times for globular clusters ($N \gtrsim 10^5$ stars) and open star clusters ($N \approx 100$ stars) are $\lesssim$1 Myr. For dense star clusters, such as young massive star clusters, the timescale can be lower than 0.1 Myr. The typical crossing time for galaxies is a few 100 Myr.

Stars gradually change their orbit because of small perturbations produced by gravitational forces from the other stellar members as moving through the cluster. After many crossing times, a star loses memory of its original orbit. This process is called *two-body relaxation* and its timescale is called the *relaxation time*. The half-mass relaxation time $t_{\rm rh}$ (Spitzer 1969), the relaxation time at the half-mass radius, is commonly used to estimate the relaxation time of a star cluster,

$$\begin{aligned} t_{\rm rh} &= \frac{0.17}{\ln(\lambda N)} \sqrt{\frac{r_{\rm h}^3}{GM_{\rm ecl}}} \\ &\approx \frac{0.1N}{\ln N} t_{\rm cr}, \end{aligned} \tag{1.2}$$

where $\lambda \simeq 0.1$–0.2 (Giersz & Heggie 1994; Binney & Tremaine 2008). As shown in Equation (1.2), the relaxation time typically increases with the number of particles, N, in a system.

When the relaxation time of a system is shorter than its age, the system is called *collisional*. In a collisional system, two-body relaxation has played an important role. Examples of such system are star clusters. Their typical relaxation times are a few Myr for open star clusters, the ages of which are typically a few 100 Myr and ≈100 Myr for old globular clusters, the ages of which are typically a few 10^9 to 10^{10} yr. In contrast, when the relaxation time is longer than the age of a system, the system is *collisionless*. In a collisionless system, stars move in a smooth gravitational potential of the host system and the two-body interactions are typically negligible. Examples of collisionless systems are galaxies. Their relaxation time is typically longer than a few10^{10} yr, that is longer than the age of the Universe

(Forbes & Kroupa 2011).

We note that the exact forms of these timescales can vary with the literature and can also be slightly different between the next chapters, but that the order of the timescales are similar for different formulas. Furthermore, the relaxation time is only a rough estimate and a star cluster can evolve differently depending on the assumptions used, for example, using single-mass or multi-mass components.

Energy equipartition and mass segregation Stellar interactions tend towards equipartition of kinetic energy ($mv^2/2$, where m and v are the mass and velocity of a star). Assuming there are two stars with different masses (m_1 and m_2, where $m_1 \gg m_2$) and their velocities are similar before an encounter, $v_{1,\mathrm{before}} \approx v_{2,\mathrm{befor}}$, the more massive star (m_1) has a higher kinetic energy,

$$m_1\, v_{1,\mathrm{before}}^2 \gg m_2\, v_{2,\mathrm{before}}^2.$$

After many interactions, energy exchange leads their kinetic energies to be similar,

$$m_1\, v_{1,\mathrm{after}}^2 \approx m_2\, v_{2,\mathrm{after}}^2,$$

and thus the lighter star becomes faster than the heavier star, $v_{1,\mathrm{after}} < v_{2,\mathrm{after}}$. In a system containing stars with a wide range of masses, energy equipartition leads to the massive stars losing their kinetic energy to low-mass stars and then falling deeper into the gravitational potential of the cluster (Binney & Tremaine 2008). Consequently, the lighter stars move outwards from the centre of the cluster. This is called *dynamical mass segregation* or mass stratification (Spitzer 1969, 1987).

For a star cluster, the timescale of dynamical mass segregation t_{ms} is determined by the mass ratio between the massive star and average stars in the system and by the relaxation time of the system,

$$t_{\mathrm{ms}} = \frac{\langle m \rangle}{m_{\mathrm{massive}}} t_{\mathrm{rh}},$$

where $\langle m \rangle$ and m_{massive} are the average mass of stars in the cluster and the mass of the massive star, respectively. The typical mass of stars in a cluster is $\lesssim 0.5\,\mathrm{M}_\odot$ with the canonical mass function (Kroupa 2001; Kroupa et al. 2013), and thus, the mass segregation timescale is much shorter than the relaxation time for massive stars ($m_{\mathrm{massive}} > 10\,\mathrm{M}_\odot$).

Evaporation Even though stars form together in a cluster, not all of them spend their entire life where they form. Stars in a (dense) stellar system, such as a star cluster, keep interacting and exchanging energy with other members of the system. Two-body relaxation is the result of many weak interactions between stars because most of the stellar members are situated relatively far away from each other. A fraction of stars overcome the gravitational potential of the cluster via cumulated weak gravitational interactions and leave their birth clusters, this is called evaporation (Binney & Tremaine 2008). The clusters preferentially lose low-mass stars via this process as a result of the energy equipartition such that low-mass stars are dispersed to the field more quickly.

Evaporation is also explained by using a Maxwellian velocity distribution. Relaxation tends to reach a local Maxwellian velocity distribution for stars. A fraction of stars, thus, keep being removed from the cluster since a Maxwellian distribution always has a fraction of stars with velocities exceeding the local

escape velocity.

The evaporation time, the time over which the cluster is depleted solely as a result of evaporation, can be used to estimate the lifetime of a stellar system, because the evaporation is a dominant process for the dissolution of the system. In an ideal single-mass system, in which all stars have the same mass, the evaporation time is $\approx 300\, t_{\rm rh}$ (Spitzer 1987; Binney & Tremaine 2008) or $140\, t_{\rm rh}$ using the Maxwellian velocity distribution (Binney & Tremaine 2008). For open star clusters, this timescale is <1 Gyr, while for globular clusters, it is >10 Gyr. The timescale becomes shorter for a multi-mass system (in a galactic tidal field).

Ejection While the majority of stars leave their birth cluster in the slow evaporation process, some stars can be expelled from their birth cluster in a more dramatic way. A single close encounter between two stars can lead to one of the stars having a velocity exceeding the local escape velocity: this is called the ejection process. The ejection process can happen more frequently in close encounters between binaries and/or single stars. In such encounters, the binaries transfer their binding energy to other stars as kinetic energy, thus the stars can be ejected with a high velocity. It is usually the least massive star among the interacting stars that gains the highest velocity after a few-body close encounter. The ejected star typically has a velocity of order the orbital velocity of the binary. The binary system can also be ejected from the cluster by a recoil due to momentum conservation, but the recoil is generally small and the binary soon sinks towards the cluster centre as a result of dynamical mass segregation.

A simple estimation of the ejection time (the time after which the cluster could be depopulated solely because of ejections), $t_{\rm ej}$, is about $10^4\, t_{\rm rh}$, that is much longer than the evaporation time (Binney & Tremaine 2008). Hence, evaporation is the dominant process in the evolution of star clusters relative to ejection.

Stellar binaries Binaries play a significant role in the evolution of a star cluster. Binaries can form through three-body encounters. Thus, even though a cluster does not have a binary initially, it will host binaries at some time in its evolution. Binaries behave differently depending on the ratio of their binding energy to the average kinetic energy of single stars that is of order $m\sigma_{\rm cl}^2/2$. The binding energy of a binary with semi-major axis, a, is

$$E_{\rm b} = -\frac{G m_{\rm p} m_{\rm s}}{2a},$$

where $m_{\rm p}$ and $m_{\rm s}$ are the masses of the binary components ($m_{\rm p} \geq m_{\rm s}$). A binary is called soft if the absolute value of its binding energy is much lower than the average kinetic energy of single stars in the cluster, $|E_b| \ll \langle m \rangle \sigma_{\rm cl}^2$, while hard if $|E_b| \gg \langle m \rangle \sigma_{\rm cl}^2$. For soft binaries, encounters with single stars in the cluster on average result in the binaries gaining energy (i.e. $|E_b|$ decreases), and thus the binaries become softer. This is because the internal kinetic energy of the soft binary is much less than the kinetic energy of average single stars and the internal energy increases because of the tendency towards energy equipartition (Binney & Tremaine 2008). On the other hand, the interactions of hard binaries with single stars result in the internal energy loss of the binaries, that is an increase of $|E_b|$, and thus the binaries become harder. In an extreme case, a single hard binary can hold an energy comparable to or more than the total binding energy of a star cluster. As an energy source, the hard binary is critical in star cluster evolution and in the dynamical ejection of stars. Combining both binaries is the *Heggie-Hills law*: on average, *hard binaries get harder and soft binaries get softer* (Heggie 1975; Hills 1975).

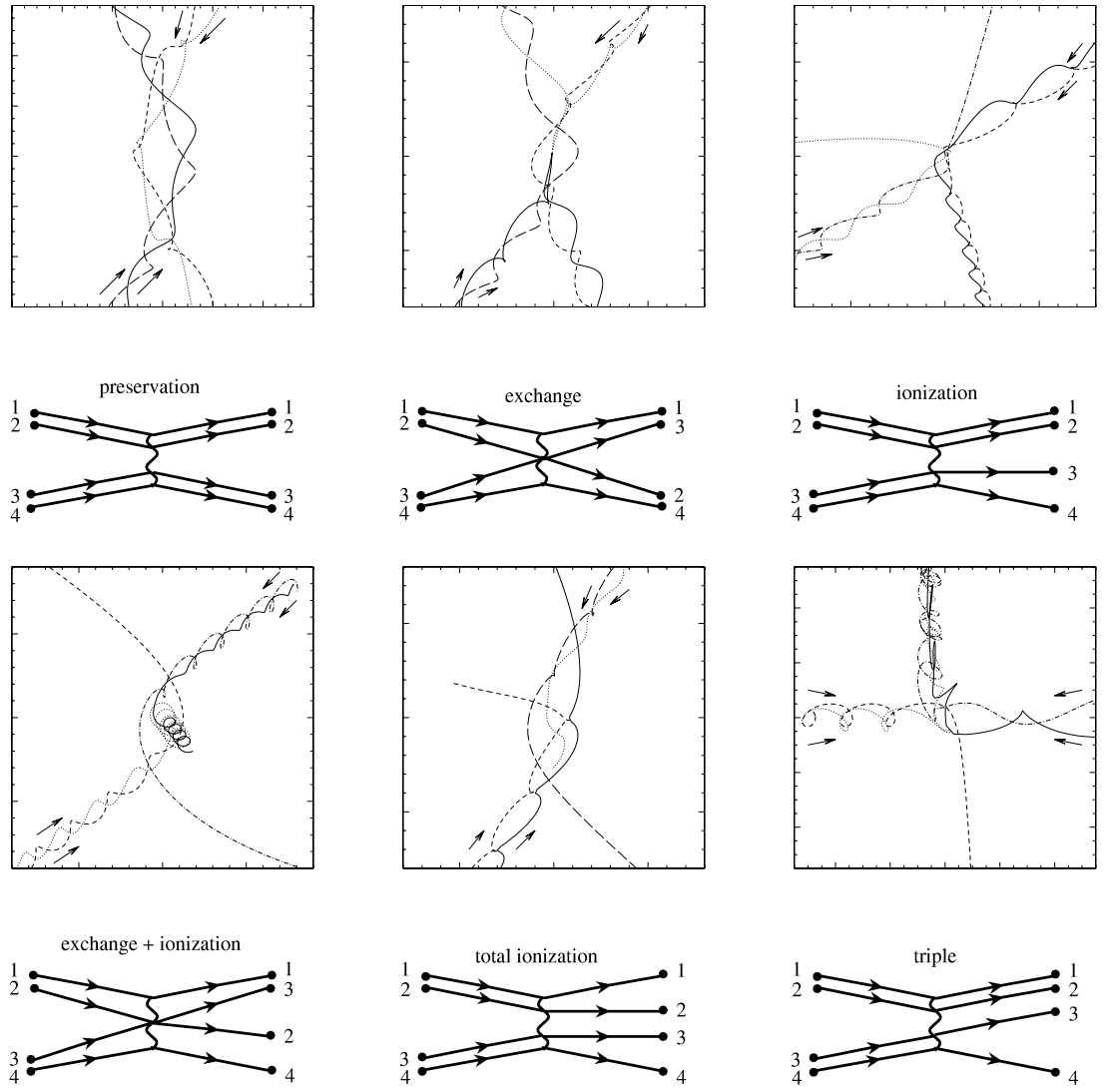

Figure 1.1. Examples of binary–binary interactions and the corresponding Feynman diagrams. Outcomes of the interactions are noted. This figure is adapted from fig. 2 of Gualandris et al. (2004) and is originally published in Volume 350, Monthly Notices of the Royal Astronomical Society.

When the internal energy of a soft binary reaches a positive value as a result of energy-gaining encounters, the binary becomes disrupted. The disruption timescale for soft binary is short, a few crossing times (Marks et al. 2011), and the disruption is soon balanced by the rate of soft binary formation due to three-body encounters (Binney & Tremaine 2008). Thus soft binaries play a less significant role in the evolution of star clusters. However, the disruptions of soft binaries are important to shape the observed period distribution of the Galactic field low-mass/solar-type star binaries (e.g. Kroupa 1995a,b; Marks & Kroupa 2012).

The outcomes of encounters involving binaries vary widely (e.g. Fig. 1.1). The encounters can result in ejections of stars with a high velocity. The binaries may exchange their components with incoming

stars/binaries, or they can be disrupted or merged (e.g. Gualandris et al. 2004). Even a triple system can be formed through this channel.

There are several important processes in the long-term evolution of star clusters, such as core collapse and tidal stripping, that are not described here. Such processes are negligible in our topic because our interest in this thesis lies in massive stars, and thus in young star clusters. For more details on the dynamical evolution of stellar systems, we refer to books on stellar dynamics, for example, "*Dynamical evolution of globular clusters*" (Spitzer 1987), "*The gravitational million-body problem*" (Heggie & Hut 2003) , and "*Galactic dynamics*" (Binney & Tremaine 2008).

1.2 Dynamical ejections of massive stars

As mentioned above, the lowest mass star is typically ejected among stars engaging in an ejection-encounter. This means that a small core composed of only massive stars are essential to produce ejections of massive stars (Poveda et al. 1967; Leonard & Duncan 1990; Clarke & Pringle 1992). Such a core can form quickly via dynamical mass segregation. In a compact massive cluster, the timescale of mass segregation (Spitzer 1987) can be shorter than 0.5 Myr for O stars (Chapter 4), which are >30 times more massive than average stars in a cluster. Considering that very young clusters have a small size of less than a pc (Testi et al. 1999; Lada & Lada 2003; Kroupa 2005; Smith et al. 2005; Tapia et al. 2014; Marks & Kroupa 2011), the dense core of massive stars forms quickly in the centre of the clusters and the dynamical ejections of massive stars from such clusters can have occurred early and efficiently (e.g. Gvaramadze & Bomans 2008; Schilbach & Röser 2008; Gvaramadze et al. 2011; Roman-Lopes 2012).

1.2.1 Runaways

Blaauw (1961) first called runaways as being OB stars that have velocities larger than $40\,\mathrm{km\,s^{-1}}$ and can be related to a known OB association. Later, the meaning of the term has extended to include all high-velocity stars whether they can be traced back to any known stellar associations or not and young massive stars that are found at a large distance from the Galactic plane. Classifying the runaway status requires velocity informations for the massive stars in question. However, they are typically at a great distance ($\gtrsim$1 kpc) from the Sun, making it difficult to measure their proper motions. Thus the velocity information of runaway stars mostly relies on radial velocities. Stone (1979) studied space velocities of O stars and shows that there are two velocity groups of stars for which velocity distributions can be approximated with Maxwellian velocity distributions. The majority of O stars belong to the low-velocity group. These stars mostly have a velocity $<25\,\mathrm{km\,s^{-1}}$ and are concentrated to known star clusters or associations (Stone 1979). In contrast to the low-velocity group, O stars in the high-velocity group show little concentration to known star clusters or associations. The stars in the high-velocity group mostly have a velocity $>25\,\mathrm{km\,s^{-1}}$ and their velocity distribution has a large velocity dispersion of $30\,\mathrm{km\,s^{-1}}$. Based on these velocity distributions, Stone (1991) estimated the true space frequency of O star runaways to be 46%. We note that the frequencies of massive runaways largely vary with different studies, from 7% to ≈50% (Gies & Bolton 1986, and references therein).

Figure 1.2. *Spitzer* image of the massive runaway star ζ Ophiuchi (the bright blue star near the centre of the image) and its bow shock. The star is as massive as $20\,M_{\odot}$ and moves supersonically through the interstellar medium with a velocity of $\approx 24\,km\,s^{-1}$. This infrared image was taken with the *Spitzer* space telescope at wavelengths of 3.6, 4.5 (blue), 8.0 (green), and 24 (red) μm. Image credit: NASA/JPL-Caltech.

There are two scenarios for the origin of runaways. Blaauw (1961) proposed that runaways were the less massive components of binary systems and would be released with a high-velocity, comparable to the original orbital velocity of the system, as a result of rapidly diminishing gravitational attraction when the more massive stars in the systems lose their significant mass and then explode as supernovae. This is called the binary-supernova scenario. The other scenario is the dynamical ejection scenario in which a massive star is ejected with a high velocity as a result of a few-body interactions in a compact core of massive stars (Poveda et al. 1967; Leonard & Duncan 1988, 1990; Clarke & Pringle 1992). Since the binary-supernova scenario requires the death of the more massive star in a binary system, the ejection can only occur later than a few (>3) Myr, which is the main sequence lifetime of massive stars, after the massive stars have formed. This suggests that the massive stars running away from young star clusters that are too young to have had a supernova (e.g. Gvaramadze & Bomans 2008; Gvaramadze et al. 2011; Roman-Lopes 2013) most likely originate from the dynamical ejection process and that the dynamical ejection may be the dominant mechanism in producing the massive stars leaving their birth cluster rather than the binary supernova scenario. This issue is also discussed in Section 3.4.

Massive stars moving supersonically through the interstellar medium (ISM) can produce a large bow shock around them in the direction of stellar motion as a result of interactions between the ISM and

their stellar wind (e.g. van Buren & McCray 1988). Thus, runaways can be identified through the existence of bow shocks, particularly those without good velocity information. Figure 1.2 shows a massive runaway, ζ Ophiuchi, and its bow shock. This 20 $M_\odot$ star is moving supersonically through the interstellar medium with a velocity of $\approx$24 km s^{-1} and produces a spectacular bow shock in the infrared wavelengths. Hoogerwerf et al. (2001) traced back the orbits of known runaways and compact objects using astrometry from *Hipparcos* and from radio observations. They claimed that ζ Ophiuchi and pulsar PSR J1932+1059 originated in a supernova explosion in a binary in the Upper Scorpius association. Since then, the star has been considered an example of the binary-supernova scenario. However, the recent study by Kirsten et al. (2015) ruled out the scenario that the star and the pulsar were in a binary system in the Upper Scorpius association, implying that the origin of the runaway star ζ Ophiuchi is uncertain. Several O stars that produce bow shocks have been found near young (<4 Myr) massive star clusters (e.g. Gvaramadze & Bomans 2008; Gvaramadze et al. 2011). This suggests that young massive star clusters actively eject their massive components via energetic few-body interactions.

1.2.2 Origin of massive stars found in apparent isolation

As mentioned before, most massive, in particular O-type, stars are found in young star clusters or OB associations. A proportion (about 20%) of the Galactic O stars are in relative isolation and are not known to be associated with stellar clusters or OB associations at the present-day (de Wit et al. 2004, and references therein). They are called field O stars. The majority of the Galactic field O stars, however, can be traced back to a young star cluster or association (e.g. Schilbach & Röser 2008) or have runaway status (Blaauw 1961; Gies & Bolton 1986; de Wit et al. 2005). de Wit et al. (2005) studied the origin of 43 field O stars and concluded that 'at present 4 ± 2% of the complete population of Galactic O-type stars cannot be traced to a formation in a cluster/OB-association', suggesting that a small fraction of massive stars may form in isolation.

The answer of whether massive stars can form in isolation is important for massive star formation theory for which there are two competing scenarios, namely competitive accretion and monolithic collapse. In *competitive accretion* (e.g. Bonnell et al. 1997, 2004), individual stars compete for the reservoir of gas that forms a cluster. Those in the centre of the cluster, where the potential is the deepest, gain more gas and become more massive. The scenario naturally expects massive stars to form in a cluster and there in the density maximum which is most likely also near the centre of a cluster. In *monolithic collapse* (e.g. Shu et al. 1987; Yorke & Sonnhalter 2002), a core of gas collapses forming a protostar and the mass of the protostar grows by accreting the remaining gas. For this scenario, the mass budget of the forming star is limited to the gas of the single core and the infalling material must not form low-mass stars. This is also a scaled-up version of low-mass star formation.

The discovery of massive stars formed in isolation can support the monolithic collapse and imply that the accretion scenario plays a role in massive star formation. Although de Wit et al. (2005) and others proposed that there is a small fraction of massive stars that may have formed in isolation (e.g. Bressert et al. 2012; Oey et al. 2013), no conclusive evidence has been given. Even some strong candidates for isolated massive star formation in de Wit et al. (2005) have been shown to be runaways (Gvaramadze et al. 2012). The two-step ejection process, according to which a binary is dynamically ejected from its cluster whereafter the primary explodes as a supernova (Pflamm-Altenburg & Kroupa 2010), deposits O stars into the field which may be very slow or even be moving towards the original cluster. Thus, even

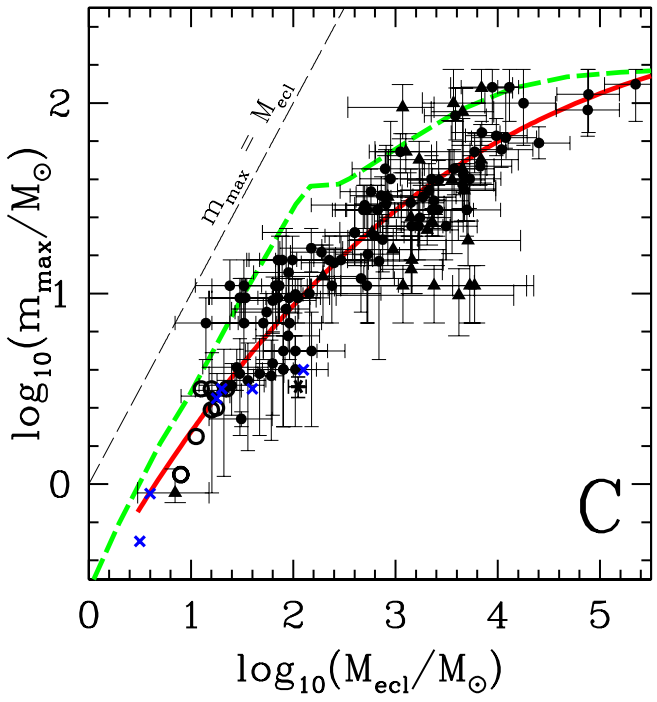

Figure 1.3. Mass of the most massive star ($m_{\rm max}$) in an embedded cluster versus the stellar mass of the embedded cluster ($M_{\rm ecl}$) from Weidner et al. (2013a). The red solid line is the third-order polynomial fit to the data (Equation 1.3, see Weidner et al. 2013a, for details). The green dashed line is the mean relation from random sampling. The thin grey dashed line marks the limit where a cluster consists of only one star ($m_{\rm max} = M_{\rm ecl}$). This figure is adapted from panel C of fig. 1 in Weidner et al. (2013a) and is originally published in Volume 434, Monthly Notices of the Royal Astronomical Society.

if all stars form in clusters, a small fraction will appear to have formed in isolation. The study on how efficiently star clusters eject their massive stars can constrain what fraction of the field O stars originate in star clusters. We refer to Chapters 3 and 4, and references therein for further discussion.

1.2.3 Dynamical ejection of the most massive star from its cluster

The most massive stars in a cluster are generally located in the centre of the cluster, from its birth or by dynamical mass segregation. As already mentioned and to be reminded frequently in the following chapters, less massive stars among those engaging in the ejection encounter obtain a high velocity. In addition, the most massive star is likely in a binary system with another massive star. Therefore, the ejection of the most massive star has been considered to be very unlikely. But it is not impossible. If a cluster is rich in massive stars, an encounter involving the most massive star and similarly massive stars can produce the ejection of the most massive star.

Relation between the maximum stellar and cluster mass

In the last decade, Weidner et al. (2013a, and references therein) have collected the masses of the most massive star in clusters and of the clusters for very young star clusters. They show that there seems to be a relation between the maximum stellar mass and the cluster mass (Fig. 1.3). The observed data is fitted

with a third-order polynomial function (equation 1 in Weidner et al. 2013a, the red line in Fig. 1.3),

$$y = \begin{cases} a_0 + a_1 x + a_2 x^2 + a_3 x^3, & 3 \leq M_{\rm ecl}/{\rm M}_\odot \leq 2.5 \times 10^5, \\ \log_{10}(150), & M_{\rm ecl}/{\rm M}_\odot > 2.5 \times 10^5, \end{cases} \tag{1.3}$$

with $x = \log_{10}(M_{\rm ecl}/{\rm M}_\odot)$, $y = \log_{10}(m_{\rm max}/{\rm M}_\odot)$, $a_0 = -0.66 \pm 0.18$, $a_1 = 1.08 \pm 0.22$, $a_2 = -0.150 \pm 0.075$, and $a_3 = 0.0084 \pm 0.0078$. The observed relation and the too-small dispersion of the data are inconsistent with the random sampling of stars from the IMF (green dashed line in Fig. 1.3) with a high significance. The existence of the relation implies that a formation of the most massive star may be regulated by the cluster mass, and thus that star formation is not a stochastic process (Kroupa 2015). A detailed introduction on the relation can also be found in Chapter 2. The existence of this relation has recently been confirmed by the work of Kirk & Myers (2011) and Ramírez Alegría et al. (2016).

Only very young (<4 Myr) star clusters are chosen in the Weidner et al. sample so that evolutionary effects are negligible. The cluster mass changes only marginally during the first few Myr of evolution, unless a cluster goes through a violent event which is very unlikely with such young age. The ejection of the most massive star will change the mass of the most massive star in the cluster. If the ejections are efficient during the very early evolution of the clusters, the observed relation can have already been altered from the true relation at the cluster birth by the dynamical process.

There has been no study focusing on the ejection of the most massive stars from very young star clusters with N-body models. We investigate how efficiently star clusters can eject their initially most massive star via dynamical ejections and how the ejections affect the relation between the maximum stellar mass and the cluster mass in Chapter 2.

1.2.4 Very massive stars/binaries in isolation

In recent years, several stars have been found to be very massive (>100 $\rm M_\odot$, e.g. Crowther et al. 2010; Bestenlehner et al. 2014; Wu et al. 2016). Their formation poses several challenges in the classical accretion star formation scenario: for example, fragmentation, radiation pressure, and ionization. In the last decade, however, it has been shown that these challenges do not prevent massive protostars growing through gas accretion (Krumholz 2015, and references therein). Some models suggest that the massive protostars can accrete without an upper mass limit (e.g. Kuiper et al. 2010, 2011), provided that the gas supply is sufficient. An alternative channel for the formation of such very massive stars is stellar collision. However, filling up the initial mass function by stellar collisions is unlikely (Moeckel & Clarke 2011; Baumgardt & Klessen 2011). Thus the collision may play a role in the formation of very massive stars but cannot be the dominant process in forming massive stars. It is still disputed how very massive stars form.

Nonetheless, one thing is clear. The formation requires lots of dense gas. Indeed, very massive stars are typically found in or close to young massive star clusters, for example, NGC 3603 ($\approx 10^4$ $\rm M_\odot$) in our Galaxy (Schnurr et al. 2008; Crowther et al. 2010) and the surroundings of R136 ($\lesssim 10^5$ $\rm M_\odot$) in the Large Magellanic Cloud (LMC, Crowther et al. 2010; Bestenlehner et al. 2014). Since they are at the high-end of the stellar initial mass function and their lifetime is short (<3 Myr), it is not surprising that only very young ($\lesssim$2 Myr) and massive ($\gtrsim 10^4$ $\rm M_\odot$) star clusters host the very massive stars. However, a

Figure 1.4. *Left*: Hubble Space Telescope image of a very massive binary R144 (≈200–300 $M_\odot$, Sana et al. 2013a) in the star forming region in the Large Magellanic Cloud . The arrow and circle respectively indicate the position of the binary system R144 and the star cluster R136. The system is at a projected distance of about 60 pc from the cluster. Image credit: NASA/ESA. *Right*: very massive star VFTS 682 (≈150 $M_\odot$, Bestenlehner et al. 2011) near R136. This star (upper left in the figure) is located at a projected distance of ≈29 pc from the centre of R136 (lower right in the figure). This image includes both visible-light and infrared images from the Wide Field Imager at the 2.2-metre MPG/ESO telescope at La Silla and the 4.1-metre infrared VISTA telescope at Paranal. Image credit: ESO/M.-R. Cioni/VISTA Magellanic Cloud survey.

few very massive stars have been found in relative isolation in the large, massive star-forming region 30 Dor in the LMC. One example is the star 30 Dor 016. The ≈ 90 $M_\odot$ star is located at a projected distance of 120 pc from the central cluster R136 of the 30 Dor region and has a peculiar radial velocity of ≈85 km s^{-1}, suggesting that it is a runaway (Evans et al. 2010). The origin of this star is likely dynamical ejection. However, discoveries of very massive single stars or binaries that show no runaway signatures, such as VFTS 682 (Bestenlehner et al. 2011) and R144 (Sana et al. 2013a) in Fig. 1.4, have raised the claim that even the most massive stars can form in isolation. This is because such massive stars are the most massive stars in a cluster if they only form in a cluster and, as mentioned previously, the dynamical ejections of the most massive stars have been considered improbable. Banerjee et al. (2012b) performed direct *N*-body calculations with an initial cluster mass of 10^5 $M_\odot$ which is close to the mass of the young massive star cluster R136. Such clusters host several very massive stars initially in the models. They show that very massive stars like VFTS 682 can be dynamically ejected through close encounters between massive binaries, and thus that isolated massive star formation is unnecessary for explaining the origin of very massive stars in the vicinity of the R136 cluster. We will discuss the origin of R144 in Chapter 5 using the same *N*-body calculations. In addition, Banerjee et al. (2012a) show that very massive stars that are more massive than the canonical stellar upper mass limit of 150 $M_\odot$ (Weidner & Kroupa 2004; Figer 2005; Oey & Clarke 2005), like those in Crowther et al. (2010), can form via stellar collisions in a

young dense star cluster or from coalescing hardened binaries after being ejected from their cluster.

1.3 Numerical experiments

Motions of individual stars in a collisional N-body system are determined by the sum of the gravitational forces from the other stellar members in the system. The acceleration, or force *per unit mass*, of the ith particle among N particles is expressed as

$$\ddot{\mathbf{r}}_i = \sum_{j=1, j\neq i}^{N} \frac{G m_j (\mathbf{r}_j - \mathbf{r}_i)}{|\mathbf{r}_j - \mathbf{r}_i|^3}, \tag{1.4}$$

where m_j and $\mathbf{r}_j$ are, respectively, the mass of the jth particle and the distance vector from the ith particle to the jth particle. Newton's equation of motion (Equation 1.4) cannot be solved analytically for systems with $N > 3$, but this can be done numerically. Since we aim to understand the dynamical evolution of star clusters, solutions of the equation for systems with $N \gg 100$ are required. Therefore, performing numerical studies is essential. In Sections 1.3.1–1.3.3, we briefly introduce the code, NBODY6, that we use in the thesis and describe how we perform numerical experiments with the code.

1.3.1 Direct N-body code: NBODY6

All work presented in this thesis are based on the calculations performed with the state-of-art direct N-body code NBODY6 (Aarseth 2003). It has been over 50 years since the first release of the NBODYx series in the 1960s. NBODY6 was introduced in1993 for realistic star cluster calculations by Sverre Aarseth (Aarseth 1999). The code is still being maintained and developed by the creator. Simple descriptions of the main features of the code are given here. The algorithms of the code are described in depth in the book *"Gravitational N-body Simulations: Tools and Algorithms"* (Aarseth 2003).

The principle of the code is simple, solving the equations of motion (Equation 1.4) for each particle in an N-particle system with the direct summation. The second-order differential equation is solved by the direct summation using the fourth-order Hermite scheme (Makino 1991) which uses a Taylor series for the force and its derivatives.

Although it looks simple, solving the equations for N stars in an N-body system (typically $N \approx 10^3$–10^5) for the age of the universe (generally comparable to the ages of globular clusters) requires complex algorithms and extensive computing power for a high accuracy and speed. Thus the code uses several algorithms to reduce computational costs while guaranteeing a good accuracy.

Individual time-step The stellar density varies within a star cluster. Motions of stars in a denser region need to be more frequently updated with a smaller time-step than those in a loose environment to achieve similar accuracies. If only a single time-step, that is optimised to the denser region (i.e. small time-step), were to be used for stars in the lower density part, force calculations with such small time-step do not give any gain but only cost more calculation time than those with a longer time-step for the stars in the lower density region in the cluster. Assigning individual time-steps to stars according to their local environment has allowed significant speed-up of the calculations while keeping a good accuracy.

Neighbour scheme To save computing expense, the code adopts the Ahmad-Cohen neighbour scheme (Ahmad & Cohen 1973; Makino & Aarseth 1992; Aarseth 1999). This neighbour scheme divides stars into two groups that are near (categorised as neighbour particles in the code) and far. The basic idea is to perform direct summation over the neighbours at suitably chosen small steps and add the predicted contributions from the distant particles. This saves the force calculation because of the less frequent direct summation on the distant particles which have slow angular speeds.

Regularization Because of the nature of a star cluster, the calculations involve a large range of time and distance scales, from a stellar binary system to the whole cluster scale, ranging from a few to $>10^6$ au. Considering the smaller sizes and the rapid change of motions for two- to few-body compact subsystems, for example binary or triple systems, such small systems require a separate treatment from that of cluster-wide integrations. Binaries and close two-body encounters are treated with Kustaanheimo-Stiefel regularization (KS, Kustaanheimo & Stiefel 1965), which uses time and coordinate transformations to avoid singularity. Strong interactions in few-body ($N \geq 3$) systems are handled with the chain regularization (Mikkola & Aarseth 1990, 1993, see also Pflamm-Altenburg & Kroupa 2006) in which the dominant two-body interactions are connected by a chain of KS-type variables.

For modelling a realistic star cluster, the code also utilises stellar evolution and a tidal field by a galaxy in which the star cluster resides. Stellar evolution is implemented in the code with the stellar evolution packages of single star evolution (SSE, Hurley et al. 2000) and of binary star evolution (BSE, Hurley et al. 2002). Several options are given for a galactic tidal field, for example, a standard tidal field (for the Solar neighbourhood), a point mass galaxy model, and a 3D-galaxy model composed of bulge, disk, and halo. In addition, one can utilise a gas cloud where a star cluster forms as a background gravitational potential and subsequently remove it in the early evolution of the cluster for modelling gas expulsion (Kroupa et al. 2001). Users can easily switch these features on and off.

Not only algorithmic development but also the advancement of hardware have remarkably improved the calculation speed of the N-body code. A series of special hardware for the calculation of the gravitational force (GRAvity PipE: GRAPE, Makino et al. 1997) was introduced in the 1990s to early 2000s, and significantly improved the speed of calculations. The separate version of the NBODYx code for this specialized hardware is NBODY4. Recent years, graphical processing units (GPUs, which cost much less than the GRAPEs) have taken over the position and the code utilises this hardware with the additional version NBODY6-GPU (Nitadori & Aarseth 2012). Also the GPU version of the code implements parallel computing. This significantly improves the speed of calculations, particularly for a large-N ($\geq 10^5$) systems. In the last year, for the first time, Wang et al. (2016) carried out the one million star simulations for 12 billion years by using their extended version of NBODY6-GPU (NBODY6++GPU, Wang et al. 2015), which is based on NBODY6++ (Spurzem 1999) that is an extensively parallelized version of NBODY6 for the usage of super computers.

The code has been applied for various topics concerning the evolution of star clusters from young to old, from low- to high-mass systems. We are interested in the products of strong encounters between massive stars in star clusters, thus the code is the most suited for our purpose since it handles such encounters with great numerical care.

We note here that the long-term evolution of globular clusters can be solved without the direct summation method. For example, there exist codes to solve this problem with the Monte Carlo method or by solving a Fokker Plank equation numerically (see Fig. 1.5). They are faster and can calculate a

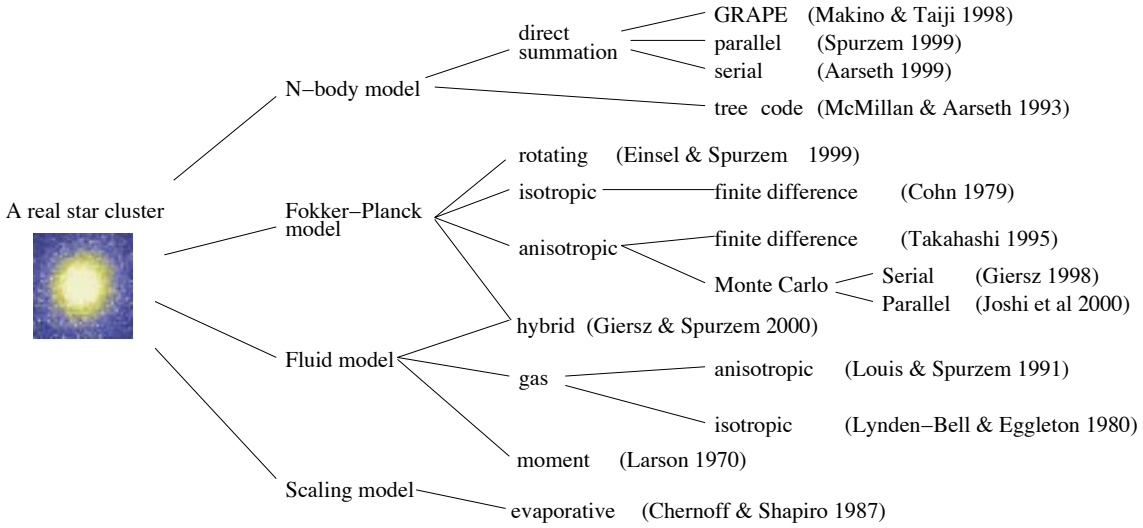

Figure 1.5. Models of the dynamics of dense stellar systems. References in the figure: Larson (1970); Cohn (1979); Lynden-Bell & Eggleton (1980); Chernoff & Shapiro (1987); Louis & Spurzem (1991); McMillan & Aarseth (1993); Takahashi (1995); Giersz (1998); Makino & Taiji (1998); Aarseth (1999); Einsel & Spurzem (1999); Spurzem (1999); Joshi et al. (2000). The picture of the star cluster (M15) was obtained using NASA's *SkyView* facility (skyview.gsfc.nasa.gov) located at NASA Goddard Space Flight Center. This figure is adapted from fig. 9.1 of the book "*The Gravitational Million-Body Problem*" by Heggie & Hut (2003) which was originally published by Cambridge University Press.

larger number of stars than the direct summation method. However, our subjects are highly collisional, and chaotic few-body interactions are essential, which non-direct summation methods cannot precisely facilitate.

1.3.2 *N*-body modelling of (young) star clusters: Initial conditions

The code requires seven initial parameters; the positions and velocities in 3 dimensional cartesian coordinates and the masses of individual particles (i.e. stars). These parameters are generated with assumed initial conditions, for example, the density profile, radius of the cluster, its equilibrium state and the mass function according to which stellar masses are distributed. Below are simple descriptions of several parameters that are required to set up initial star-cluster models studied in this thesis.

Density profile To derive positions and velocities of the stars, a density profile is assumed. The most common density profiles for star clusters are the Plummer model (Plummer 1911) and the King model (King 1966). The Plummer potential of a star cluster is given by

$$\Phi(r) = -GM_{\rm ecl}\left(1+\frac{r^2}{r_{\rm Pl}^2}\right)^{-1/2}, \tag{1.5}$$

where $r_{\rm Pl}$ is Plummer scale length, the so called Plummer radius. The potential of the Plummer model is roughly constant at small radii, $r < r_{\rm Pl}$, and proportional to r^{-2} at large radii, $r > r_{\rm Pl}$. The half-mass

radius is given by $r_{\rm h} \approx 1.3 r_{\rm Pl}$. The corresponding density profile is

$$\rho(r) = \frac{3M_{\rm ecl}}{4\pi r_{\rm Pl}^3}\left(1+\frac{r^2}{r_{\rm Pl}^2}\right)^{-5/2}. \tag{1.6}$$

The total mass of the model is finite but the radius is infinite. The density distribution of this model provides a simple and very good analytical description of globular clusters (Plummer 1911).

The distribution function of the other model, the King model, is described as

$$f(\mathcal{E}) = \begin{cases} \rho_1(2\pi\sigma^2)^{-3/2}(\mathrm{e}^{\mathcal{E}/\sigma^2}-1) & (\mathcal{E}>0) \\ 0 & (\mathcal{E}\leq 0) \end{cases}, \tag{1.7}$$

where $\mathcal{E}$ is the relative energy $\mathcal{E} = \Psi - v^2/2$ and Ψ is the relative potential. This model, also called the lowered isothermal model, has a finite mass and a finite radius. Integrating the above distribution function over all velocities, the density is

$$\rho(\Psi) = \rho_1\left[\mathrm{e}^{\Psi/\sigma^2}\mathrm{erf}\left(\frac{\sqrt{\Psi}}{\sigma}\right) - \sqrt{\frac{4\Psi}{\pi\sigma^2}}\left(1+\frac{2\Psi}{3\sigma^2}\right)\right], \tag{1.8}$$

where $\mathrm{erf}(x)$ is the error function (see Binney & Tremaine 2008, for details). King models are characterised with the dimensionless King parameter $W_0 = \Psi(0)/\sigma^2$, where $\Psi(0)$ is the central potential and σ a parameter which is approximately the velocity dispersion. And the concentration is defined as $c \equiv \log_{10}(r_{\rm t}/r_{\rm c})$, where $r_{\rm t}$ is the tidal radius at which the relative potential becomes equal to zero and $r_{\rm c}$ is the King radius or the core radius. For globular clusters the values of these parameters lie in ranges of $3 < W_0 < 9$ and $0.75 < c < 1.75$ (Kroupa 2008). The King model has been widely used for globular clusters as it improves their representation (it has an additional parameter, c or W_0).

In all calculations used in this thesis, the initial positions of stars (the centre-of-masses in the case of binaries) are generated following the Plummer model because the model is a simplest analytical description of star clusters and fits well with the density profile of observed star clusters (e.g. Röser et al. 2011).

Initial sizes of star clusters Observed star clusters typically have half-mass radii of 1 to a few pc. Considering that dynamical evolution expands the cluster, their initial size must be smaller than observed. The initial size of star clusters are thus expected to have been sub-pc. Indeed, young star clusters typically have a small size $\lesssim$1pc (Testi et al. 1999; Lada & Lada 2003; Kroupa 2005; Smith et al. 2005; Tapia et al. 2009, 2011, 2014; Marks & Kroupa 2011).

Star clusters show a very weak, if any, relation between mass and half-mass radius. Based on a relation between the initial density and cluster mass, Marks & Kroupa (2012) derive the birth cluster-mass–size (half-mass radius) relation,

$$\frac{r_{\rm h}(0)}{\rm pc} = 0.1^{+0.07}_{-0.04} \times \left(\frac{M_{\rm ecl}}{\mathrm{M}_\odot}\right)^{0.13\pm0.04},$$

where $r_{\rm h}(0)$ is the initial half-mass radius of the cluster. This agrees very well with the relation between the effective radius $R_{\rm eff}$ and cluster mass $M_{\rm cl}$ for clusters in non-interacting spiral galaxies found by

Larsen (2004), $R_{\rm cl} \propto M_{\rm cl}^{0.1\pm0.03}$.

Initial stellar mass function (IMF) The initial stellar mass function (IMF) describes the mass distribution of stars that formed in one star formation event. The IMF is typically expressed as a power-law function, $\xi(m) \propto m^{-\alpha}$. Salpeter (1955) derived $\alpha = 2.35$ for stars with a mass $0.4 < m/{\rm M}_\odot < 10$. Surprisingly, this value is found in almost every environment and this provides a basis for the hypothesis that the IMF is universal. Combining the IMF for low-mass stars, we arrive at the canonical IMF which is a two-part power law (Kroupa 2001, 2008),

$$\xi(m) = k \begin{cases} \left(\frac{m}{0.08}\right)^{-1.3}, & 0.08 \leq m/{\rm M}_\odot < 0.50, \\ \left(\frac{0.5}{0.08}\right)^{-1.3} \left(\frac{m}{0.5}\right)^{-2.3}, & 0.50 \leq m/{\rm M}_\odot \leq m_{\rm max}(M_{\rm ecl}), \end{cases} \tag{1.9}$$

where k is a normalisation constant and $m_{\rm max}$ is the upper mass limit for the stellar IMF in a cluster, which can be derived from the relation between maximum stellar and cluster mass (Section 1.2.3). Observations have shown that the IMF is universal independent of environments although its physical origin is largely unclear. However, recent studies suggest that there may be environment-dependent variations of the IMF, for example, a top-heavy IMF for high-density and low-metallicity star clusters (Marks et al. 2012) and averagely slightly bottom-heavy mass functions of young intermediate-mass clusters in the Andromeda (M31) galaxy (Weisz et al. 2015).

Our study targets young star clusters with solar metallicity in the Galaxy . They are still within the invariant IMF regime. In this thesis, thus, all calculations were started with the canonical two-part power law IMF (Equation 1.9).

Initial binary population The binary or multiple system is the dominant mode of star formation. This is due to the angular momentum problem; star-forming cloud core have too much angular momentum to form a single star (Goodman et al. 1993). Binaries by far dominate the birth stellar population because if triples or quadruples would be formed they would decay within 10^4 to 10^5 yr leaving a population with a 50% or lower binary fraction. Observed populations of 10^6 yr old star, however, indicate a binary fraction of 80% or higher (Goodwin & Kroupa 2005). To model a realistic star cluster, thus, binaries should be included from the beginning of the cluster evolution. While the positions and velocities of the centre-of-masses of the binaries are generated following a density profile as described above, relative positions and velocities of binary components are set to follow the initial distributions of orbital parameters of binaries.

Orbital parameters of late-type (low-mass or solar-type) star binaries have been intensively studied (Duquennoy & Mayor 1991; Raghavan et al. 2010) since they are numerous and a large sample of these stars are available near the Sun. Based on binaries in star-forming regions, Kroupa (1995b) derived a birth period distribution of late-type star binaries which evolves to the period distribution similar to that of field late-type binaries via dynamical processes. The birth distribution can be written

$$f(\log_{10} P) = 2.5 \frac{\log_{10} P - 1}{45 + (\log_{10} P - 1)^2}, \tag{1.10}$$

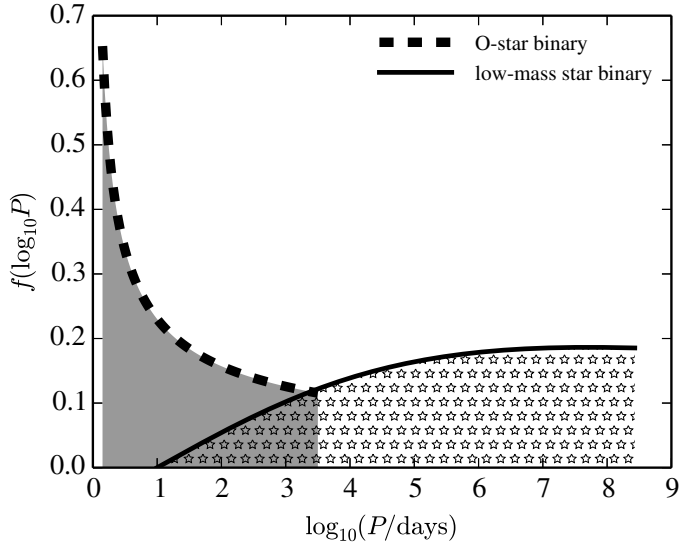

Figure 1.6. Period distributions of binaries. The thin solid line is the birth period distribution of low-mass binaries given by Equation (1.10) (Kroupa 1995b), while the thick dashed line is the intrinsic period distribution of O-star binaries deduced by Sana et al. (2012, see Equation 1.11). The area filled with star symbols is unity, that is the initial binary fraction is 1, while for the grey-filled area it is ≈0.7, which is the intrinsic O-star binary fraction for the given period range in Sana et al. (2012).

where the period P is in days. This distribution function has minimum and maximum periods of 10 and $10^{8.43}$ days, respectively. The mass-ratio distribution of these binaries is well explained with random sampling from the IMF. For the mass range of these stars, random pairing results in the distribution being close to uniform. The eccentricity (e) distribution is consistent with being the thermal distribution, $f(e) = 2e$. The binary disruption rate is almost independent of eccentricity (Heggie 1975) and thus the observed distribution can be considered as the initial one. Furthermore, stellar interactions tend to make the distribution of binaries to have $f(e) = 2e$ (Heggie 1975; Binney & Tremaine 2008).

It has been known for decades that massive stars have a high multiplicity fraction (e.g. Mason et al. 1998). However, it is only recent that distributions of their orbital parameters have been constrained (e.g. Kiminki & Kobulnicky 2012; Sana et al. 2012; Kobulnicky et al. 2014). Massive (O-star) binaries show a significantly different period distribution from that of low-mass binaries. They have a high proportion of short-period binaries compared to the low-mass binaries. Sana et al. (2012) derive the period distribution for O-star binaries in nearby young massive star clusters, that is highly biased to short-period binaries,

$$f(\log_{10} P) \approx 0.23 \times (\log_{10} P)^{-0.55}, \tag{1.11}$$

with a period range from $10^{0.15}$ to $10^{3.5}$ days. In Fig. 1.6, the period distributions for low- and high-mass binaries are compared (Equations 1.10 and 1.11). The distributions show largely different binary fractions at a given period range for the two populations. O-star binaries are observed to preferentially have an O or early-B star as a companion and their mass-ratio distribution is close to a uniform distribution, $f(q) \propto q^{-0.1}$, where q is the mass ratio and $0 < q \leq 1$. This means that the massive binary components are not randomly paired from the IMF since random pairing would result in a high proportion of low mass-ratios $q < 0.1$. Also the eccentricities of massive binaries show a rather flat distribution, with an

excess of circular binaries for short-period ($P \leq 2$ days) binaries. The large differences between orbital parameters of low- and high-mass binaries imply that separate initial binary populations should be applied to low- and high-mass binaries. In the next chapters, we will apply initial binary populations derived from low-mass binaries as well as observed massive binary populations to initial orbital parameter distributions of massive binaries to study how the initial binary populations affect the dynamical ejection of massive stars.

1.3.3 Theoretical young star cluster library

Since dynamical ejections are the outcome of strong few-body encounters, several case studies of individual runaway stars have been carried out with few-body scattering experiments (e.g. Gualandris et al. 2004; Gvaramadze et al. 2009; Gvaramadze & Gualandris 2011). Such encounters generally exhibit a chaotic behaviour (Hut & Bahcall 1983). The studies present that the outcomes of encounters largely vary with encounter parameters, such as impact parameter, relative velocities between interacting stars, orbital parameters of the binaries. They provide what kind of encounters could have happened by investigating a large parameter-space of a few-body system. However, how often do such encounters occur in a cluster? This can be answered through direct N-body calculations of star clusters. In general, N-body calculations of star clusters cannot provide the exact encounter type for each ejection case because of a finite output-time resolution and the large amount of data generated, but they give statistical quantities, such as a number and an efficiency of ejections.

The outcomes of N-body calculations largely depend on the initial conditions, like those of few-body scattering experiments do on encounter parameters. Under a certain assumption, some initial conditions can be more influential than others. In this thesis, our main subject is how the dynamical ejections of massive stars depend on initial conditions of star clusters and of massive stars. We present a vast library of theoretical young star clusters that is established with a large set of direct N-body calculations for young star clusters using the NBODY6 code. We vary the initial sizes of clusters, cluster masses, the initial binary fraction, and initial binary populations of massive binaries, such as their initial period, mass-ratio, and eccentricity distributions. We list parameters of initial conditions that are considered in our library in Table 1.1. We note that each chapter uses different, but largely overlapping, subsets of the library depending on the objective of the study. Details of the initial conditions that are considered in the chapters can be found in the model section of each chapter.

Most models were calculated with the standard NBODY6 code on workstations of the Stellar Populations and Dynamics Research (SPODYR) group at the University of Bonn. A few cluster models with the smallest size (0.1 pc) and the highest mass ($10^{4.5}$ $M_\odot$) were carried out on workstations equipped with GPUs.

Parameters	Values
cluster mass $M_{\rm ecl}$	$10–10^{4.5}\,{\rm M}_\odot$
initial size of cluster (initial half-mass radius, $r_{\rm h}(0)$)	0.1, 0.3, 0.8 pc
initial density profile	Plummer profile (Equation 1.6)
tidal field	standard (the Solar neighbourhood)
initial stellar mass function	canonical two-part power law (Equation 1.9)
lower stellar mass limit	$0.08\,{\rm M}_\odot$
upper stellar mass limit	$m_{\rm max}(M_{\rm ecl})$ (see Chapter 2)
binary fraction	0, 1
initial period distribution for low-mass binaries	Equation (1.10) (Kroupa 1995b)
initial period distribution for high-mass binaries	Equation (1.10) (Kroupa 1995b), Equation (1.11) (Sana et al. 2012)
initial mass-ratio distribution for low-mass binaries	random pairing
initial mass-ratio distribution for high-mass binaries	random pairing, ordered pairing, uniform distribution
initial eccentricity distribution for low-mass binaries	$f(e) = 2e$ (thermal distribution)
initial eccentricity distribution for high-mass binaries	thermal distribution, circular orbit only

Table 1.1. List of initial conditions that are considered in our theoretical young star cluster library. Detailed descriptions of the parameters can be found in the model sections of Chapters 2–4.

1.4 Overview

Using our theoretical young star cluster library, we study the dynamical ejections of massive stars from young star clusters according to several aspects. Each chapter is briefly introduced below.

Chapter 2 While, in general, the observed maximum stellar mass and its parent cluster mass show a relation, a spread of the data points exists. This may simply result from observational errors or stochastic effects. Despite the young ages ($\lesssim$3 Myr) of the sample, a cluster's dynamical evolution may have affected the observed relation. We study the effect of the dynamical processes, particularly ejections and mergers, on the maximum-stellar-mass–cluster-mass relation. We establish a theoretical young star cluster library with direct N-body calculations using diverse initial conditions for star clusters and their massive star population. Because the cluster mass hardly changes within a few Myr, the change of the most massive star is the subject of the study. *This chapter is published in Monthly Notices of the Royal Astronomical Society as Oh & Kroupa (2012).*

Chapter 3 We study the dependence of dynamical ejections of O-star systems on star cluster mass. We extend several N-body models in Chapter 2 to a higher cluster mass ($10^{4.5}$ $M_\odot$) and include models with the recently constrained binary population of O stars. We discover a trend that the ejection fraction of O-star systems peaks at a cluster mass of $10^{3.5}$ $M_\odot$ for all our model sequences. It is also discussed how properties of ejected O star systems, such as the mass, the velocity, and the distance distribution, vary with cluster mass. By synthesizing the cluster mass function, we estimate the fraction of O stars that are dynamically ejected from star clusters to the Galactic field and the fraction of runaway O stars among them, and compare them with the observations. *This chapter is published in the Astrophysical Journal as Oh, Kroupa & Pflamm-Altenburg (2015).*

Chapter 4 We investigate how the dynamical ejections of massive stars vary with initial conditions for the fixed cluster mass $M_{\rm ecl} = 10^{3.5}$ $M_\odot$. We study effects of the initial conditions on the ejection efficiency, for particularly massive stars. We also discuss several properties of the ejected massive systems, such as the velocity distribution, multiplicity fraction, and binary populations of ejected massive systems. Here, by considering not only O stars but also other mass ranges we study the ejection efficiency as a function of stellar mass and its impact on the present-day mass function of stars that remain in the cluster and of those ejected. *This chapter is published in Astronomy and Astrophysics as Oh & Kroupa (2016).*

Chapter 5 A recent observational study discovered that the massive star R144 (the left panel in Fig. 1.4), located in the vicinity of the young massive cluster R136 ($\lesssim 10^5$ $M_\odot$) in the Large Magellanic Cloud, is a very massive spectroscopic binary system with an estimated system mass of ≈200–300 $M_\odot$ (Sana et al. 2013a). Due to its large mass and apparent isolation, the authors claimed that the system is unlikely ejected from R136 but is a candidate for massive star formation in isolation. By revisiting direct N-body calculations of R136-like clusters by Banerjee et al. (2012b), we study whether a very massive binary, such as R144, can be dynamically ejected from a young massive cluster such as R136. We also present massive systems that are dynamically ejected from R136-type clusters. *This chapter is published in Monthly Notices of the Royal Astronomical Society as Oh, Kroupa & Banerjee (2014).*

We summarise and discuss future studies related to the topic of this thesis in Chapter 6. Additional figures and tables for Chapters 2, 3, and 4 are placed in Appendices A, B, and C, respectively.

CHAPTER 2

The influence of stellar dynamical ejections and collisions on the relation between the maximum stellar and star cluster mass

Published in Monthly Notices of the Royal Astronomical Society
Volume 424, pp 65–79, July 2012

S. Oh and P. Kroupa

ABSTRACT

We perform the largest currently available set of direct N-body calculations of young star cluster models to study the dynamical influence, especially through the ejections of the most massive star in the cluster, on the current relation between the maximum stellar mass and the star cluster mass. We vary several initial parameters such as the initial half-mass radius of the cluster, the initial binary fraction, and the degree of initial mass segregation. Two different pairing methods are used to construct massive binaries for more realistic initial conditions of massive binaries. We find that lower mass clusters ($\leq 10^{2.5}\,\mathrm{M}_\odot$) do not shoot out their heaviest star. In the case of massive clusters ($\geq 1000\,\mathrm{M}_\odot$), no most massive star escapes the cluster within 3 Myr regardless of the initial conditions if clusters have initial half-mass radii, $r_\mathrm{h}(0)$, ≥ 0.8 pc. However, a few of the initially smaller sized clusters ($r_\mathrm{h}(0) = 0.3$ pc), which have a higher density, eject their most massive star within 3 Myr. If clusters form with a compact size and their massive stars are born in a binary system with a mass ratio biased towards unity, the probability that the mass of the most massive star in the cluster changes due to the ejection of the initially most massive star can be as large as 20%. Stellar collisions increase the maximum stellar mass in a large number of clusters when clusters are relatively dense ($M_\mathrm{ecl} \geq 10^3\,\mathrm{M}_\odot$ and $r_\mathrm{h}(0) = 0.3$ pc) and binary-rich. Overall, we conclude that dynamical effects hardly influence the observational maximum stellar mass–cluster mass relation.

2.1 Introduction

Weidner, Kroupa & Bonnell (2010) compiled from the literature observational data of 100 young star clusters, whose masses lie between ≈10 and 2×10^5 $M_\odot$ and whose ages are younger than 4 Myr. They showed that observed young star clusters exhibit a well-defined correlation between the maximum stellar mass in the cluster, $m_{\rm max}$, and the mass in stars, $M_{\rm ecl}$, of the cluster. An upper age limit of 4 Myr was chosen in order to minimize any evolutionary effects on the sample. The examples of evolutionary effects discussed in their paper are as follows. First, mass-loss of massive stars due to stellar evolution may influence the cluster mass. Secondly, gas expulsion leads the cluster to lose a significant amount of its stars (i.e. cluster mass) by weakening of the gravitational potential when the residual gas is expelled from the cluster. However, these effects unlikely affect $M_{\rm ecl}$ owing to the young ages of the clusters in the Weidner et al. (2010) sample. The authors corrected $m_{\rm max}$ for stellar evolution in the case of O-type stars (note that later than O-type stars would not have evolved much at this young age), so that the $m_{\rm max}$ values provided in their paper can be considered as initial values. One process they did not take account of is the dynamical ejection of the most massive star from the cluster. The authors commented that it is highly unlikely to happen. But this has not been studied thoroughly so far. Thus, it is our aim in this study to investigate how often a young star cluster ejects its most massive member.

This observed correlation fits a semi-analytical model well (Weidner & Kroupa 2004, 2006; Weidner et al. 2010) which is deduced from there being exactly one most massive star in the cluster,

$$1 = \int_{m_{\rm max}}^{m_{\rm max*}} \xi(m)\, {\rm d}m, \tag{2.1}$$

subject to the normalization

$$M_{\rm ecl} = \int_{m_{\rm low}}^{m_{\rm max}} m\, \xi(m)\, {\rm d}m, \tag{2.2}$$

where $m_{\rm max*} \approx 150$–$300\,M_\odot$ is the fundamental upper limit of stellar masses (Weidner & Kroupa 2004, 2006; Figer 2005; Oey & Clarke 2005; Crowther et al. 2010), $m_{\rm low} = 0.08\,M_\odot$ is the hydrogen burning mass limit (brown dwarfs contribute negligibly to the cluster mass, Thies & Kroupa 2007) and $\xi(m)$ is the stellar initial mass function (IMF). A pure size-of-sample effect as expected from random sampling has been excluded as an origin of the observed correlation. Details of previous studies on the $m_{\rm max}$–$M_{\rm ecl}$ relation can be found in Weidner & Kroupa (2004, 2006), Weidner et al. (2010) and references therein. Note that Maschberger & Clarke (2008) argued that at least for the low-N clusters (i.e. low-mass clusters) observed maximum stellar masses do not much deviate from random drawing. This is basically true but leads the reader to the misinterpretation that a physical origin of the most massive star in these clusters is ruled out. But Weidner et al. (2010) show that in the mass regime considered by Maschberger & Clarke (2008) a physical $m_{\rm max}$ and a stochastic $m_{\rm max}$ cannot be distinguished from each other. The observed clusters from Weidner et al. (2010) and their semi-analytical relation are reproduced in Fig. 2.1. Interestingly, a similar relation appears in numerical simulations of star cluster formation as well. Smoothed particle hydrodynamics numerical simulations of massive star formation driven by competitive accretion (Bonnell, Vine & Bate 2004) showed that the most massive star in the forming cluster grows following the relation $m_{\rm max}(t) \propto M_{\rm ecl}(t)^{2/3}$ with time, t, which is a best fit to their simulation data. This fit agrees with the semi-analytical $m_{\rm max}$–$M_{\rm ecl}$ relation very well for clusters

with $M_{\rm ecl} \lesssim 10^3\,{\rm M}_\odot$. Furthermore, fragmentation-induced starvation scenario studied with radiation-hydrodynamical simulations of massive star formation using the adaptive-mesh code FLASH (Peters et al. 2010) also reproduced the relation found by Bonnell et al. (2004). Data from the numerical simulations of star cluster formation including the two studies mentioned above are also plotted in Fig. 2.1. The simulation data are in good agreement with the observed data.

Although most of the clusters follow the relation well, there is a spread of $m_{\rm max}$ values at a given cluster mass. Is this spread due to stochastic effects that occur during the formation of a cluster, or does it mask a true physical functional dependence of $m_{\rm max}$ on $M_{\rm ecl}$? Dynamical processes can exert an influence on the relation during the early evolution of the cluster. Stars can be dynamically ejected through energetic few body interactions. The lightest star among the interacting stars generally obtains the highest velocity and it is unlikely that the most massive star is ejected. Several theoretical studies, nevertheless, have shown that massive stars can be dynamically ejected under certain circumstances such as from a small group of massive stars lacking low-mass stars (Clarke & Pringle 1992; Gvaramadze et al. 2009; Fujii & Portegies Zwart 2011; Gvaramadze & Gualandris 2011), through binary–single (Hills & Fullerton 1980) and binary–binary interactions (Leonard & Duncan 1990). The high efficiency of dynamical ejections from dense stellar systems can indeed explain the difference between the observed and expected number of OB-type stars in the Orion Nebula Cluster (ONC; Pflamm-Altenburg & Kroupa 2006). Furthermore, dense and massive R136-type clusters are efficient in expelling massive stars (Banerjee et al. 2012b). Thus it may be possible that the heaviest star in a cluster be dynamically ejected from the cluster.

In this contribution we assume there exists an exact function, $m_{\rm max} = {\rm fn}(M_{\rm ecl})$, and we study the ejection of the heaviest star in a cluster using direct N-body integration to investigate the effect on the $m_{\rm max}$–$M_{\rm ecl}$ relation. Details of the initial conditions of the cluster models and of the calculations are described in Section 2.2 and then results are shown in Section 2.3. The discussion and the conclusions follow in Sections 2.4 and 2.5.

2.2 Models

We perform a large set of direct N-body calculations of young star clusters using NBODY6 (Aarseth 1999) with various initial conditions. Cluster masses range from 10 to $10^{3.5}\,{\rm M}_\odot$ with an interval of 0.5 on the logarithmic scale and each mass is initialized with two different half-mass radii, $r_{\rm h}(0) = 0.3$ and 0.8 pc. To study the effect of binaries, we adopt two extreme binary fractions which are 0 (all stars are single) and 1 (all stars are in binary systems). The initial binary population used in this study is described in Section 2.2.1. Single star clusters (all stars are single) are chosen for comparison purpose only since most stars in actuality form in a binary system (Goodwin & Kroupa 2005).

For each cluster mass the number of stars, $N_{\rm star}$, is assigned by dividing the cluster mass by the average stellar mass of the cluster

$$N_{\rm star} = \frac{M_{\rm ecl}}{\langle m \rangle}, \tag{2.3}$$

where the average stellar mass of the cluster, $\langle m \rangle$, is

$$\langle m \rangle = \frac{\int_{m_{\rm low}}^{m_{\rm max}} m\,\xi(m)\,{\rm d}m}{\int_{m_{\rm low}}^{m_{\rm max}} \xi(m)\,{\rm d}m}.$$

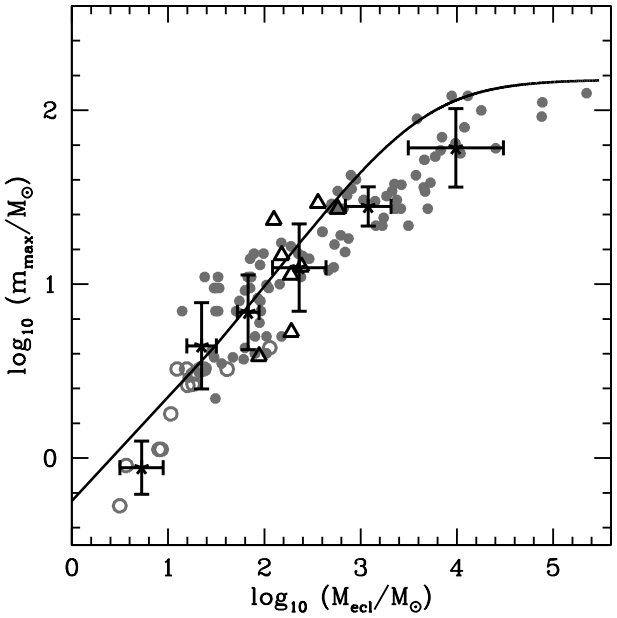

Figure 2.1. Mass of the most massive star versus cluster mass from observational data in Weidner et al. (2010). Each grey filled circle is a star cluster from their table B1. Black solid line is the semi-analytical $m_{\rm max}$–$M_{\rm ecl}$ relation from Equations (2.1) and (2.2) assuming an upper limit of the stellar mass of 150 $\mathrm{M}_\odot$ (Weidner & Kroupa 2004, 2006). The open circles are the mass of the most massive member in the group versus the total group mass in 14 young stellar groups in Taurus, Lupus3, ChaI, and IC348 (Kirk & Myers 2011). These young (low-mass) stellar groups also follow the $m_{\rm max}$–$M_{\rm ecl}$ relation well. The black points and error bars represent the average and standard deviation of $\log_{10} M_{\rm ecl}$ and $\log_{10} m_{\rm max}$ in each bin each of which contains 22 clusters for the upper five bins and four clusters for the lowest cluster mass bin. Data from several numerical simulations of star formation (Bonnell et al. 2004; Bate 2009, 2012; Smith, Longmore & Bonnell 2009; Peters et al. 2010) are included in the figure as open triangles.

We adopt the canonical two-part power-law IMF (Kroupa 2001; Kroupa et al. 2013),

$$\xi(m) \propto m^{-\alpha_i}, \tag{2.4}$$

where

$$\begin{aligned} \alpha_1 &= 1.3, \quad 0.08 \leq m/\mathrm{M}_\odot < 0.50, \\ \alpha_2 &= 2.3, \quad 0.50 \leq m/\mathrm{M}_\odot \leq m_{\rm max}. \end{aligned}$$

We use $m_{\rm max,WK} \equiv m_{\rm max}$, which is calculated using the semi-analytical relation (Equations 2.1 and 2.2) assuming the fundamental upper limit of stellar masses to be $m_{\rm max*} = 150\,\mathrm{M}_\odot$. The solid line in Fig. 2.1 represents $m_{\rm max,WK}$.

Individual masses of all stars but one (i.e. $N_{\rm star} - 1$ stars) in each cluster are randomly drawn from the IMF (Equation 2.4) with a stellar mass range from 0.08 $\mathrm{M}_\odot$ to $m_{\rm max,WK}$. To simplify the analysis, one $m_{\rm max,WK}$ star is added so that every cluster has at least one star with a mass of $m_{\rm max,WK}$.[1] This procedure removes the stochastic effects on the initial $m_{\rm max}$. This choice, however, gives a bump at the most massive

[1] This procedure would not be required if optimal sampling of stellar masses from the IMF (Kroupa et al. 2013) were used instead of random sampling. Optimal sampling was not available though at the time the present library of clusters was computed.

mass bin in the IMF of the cluster, which is especially significant in small-N (i.e. low-mass) clusters. As the dynamical ejection of massive stars occurs by close encounters between massive stars (Leonard & Duncan 1990; Clarke & Pringle 1992), our enforcement of having a $m_{\rm max,WK}$ star may enhance the ejections at a given $M_{\rm ecl}$ by overpopulating massive stars. We find that this choice would not change our conclusion (see further discussion in Section 2.4).

Positions and velocities of stars in the cluster are generated according to the Plummer model (Aarseth, Henon & Wielen 1974) which is the simplest stationary solution of the collisionless Boltzmann equation (Heggie & Hut 2003; Kroupa 2008) and is an excellent description of the nearest star cluster, the Hyades (Röser et al. 2011). To study the effect of initial mass segregation, half of our cluster models are initially mass segregated. The method for constructing initially mass segregated clusters in which positions and velocities are dependent on stellar masses is described in Section 2.2.2. For unsegregated clusters, positions and velocities are assigned to stars independently of their masses.

Dynamical timescales such as the crossing time and the median two-body relaxation time are important tools to estimate the dynamical evolution of stellar systems. The initial crossing time is

$$t_{\rm cr} = \frac{2r_{\rm h}(0)}{\sigma}, \tag{2.5}$$

where σ is initial velocity dispersion, $\sigma = \sqrt{GM_{\rm ecl}/r_{\rm grav}}$, $r_{\rm grav} \approx 2.6\, r_{\rm h}(0)$ is the gravitational radius (Binney & Tremaine 1987; Kroupa 2008). The relaxation time is

$$t_{\rm rel} = 0.1 \frac{N_{\rm star}}{\ln N_{\rm star}} t_{\rm cr}. \tag{2.6}$$

Initial conditions of all cluster models are listed in Table 2.1. Table 2.2 shows the physical properties of the 6 different-mass clusters. All clusters are evolved up to 5 Myr. And stellar evolution is taken into account using the stellar evolution library (Hurley et al. 2000) in the NBODY6 code. We carry out 100 computations for each set of initial conditions. In total 7200 models are thus calculated with a standard desktop PC. In addition, we perform 10 calculations for clusters with $M_{\rm ecl} = 10^4\,{\rm M}_\odot$ and with the same initial conditions as MS3OP in Table 2.1. We compute only the most energetic cluster model (MS3OP) in our library for $M_{\rm ecl} = 10^4\,{\rm M}_\odot$ because of the high computational cost for massive clusters. This is the largest currently existing systematically generated library of young star cluster models.

2.2.1 Primordial binaries

To set up the primordial binaries we require their initial orbital parameters such as periods, eccentricities, and mass ratios. The initial period distribution adopted in this study is equation (8) in Kroupa (1995b),

$$f_P = 2.5 \frac{\log_{10} P - 1}{45 + (\log_{10} P - 1)^2}, \tag{2.7}$$

where period, P, is in days. With this distribution function, minimum and maximum log periods, $\log_{10} P_{\rm min}$ and $\log_{10} P_{\rm max}$, are 1 and 8.43, respectively. This function shows a flat distribution at long periods and is in good agreement with the period distribution of low-density young stellar aggregates such as Taurus-Auriga (Kroupa & Petr-Gotzens 2011; Marks, Kroupa & Oh 2011). The initial eccentricity distribution follows the thermal distribution, $f(e) = 2e$ (Kroupa 2008). Pre-main-sequence eigenevolution

Model	mass segregation	$r_{\rm h}(0)$ (pc)	$f_{\rm bin,i}$
NMS3S	N	0.3	0
NMS3RP	N	0.3	1 (RP)
NMS3OP	N	0.3	1 (OP)
NMS8S	N	0.8	0
NMS8RP	N	0.8	1 (RP)
NMS8OP	N	0.8	1 (OP)
MS3S	Y	0.3	0
MS3RP	Y	0.3	1 (RP)
MS3OP	Y	0.3	1 (OP)
MS8S	Y	0.8	0
MS8RP	Y	0.8	1 (RP)
MS8OP	Y	0.8	1 (OP)

Table 2.1. The initial conditions of cluster models. Model name is in the first column. Column 2 indicates the initial mass segregation, N standing for an initially unsegregated cluster while Y signifying an initially segregated cluster. Columns 3 and 4 present the initial half-mass radius of the cluster, $r_{\rm h}(0)$, and the initial binary fraction, $f_{\rm bin,i}$, respectively. OP and RP in the $f_{\rm bin,i}$ column represent the pairing method for the massive binaries: ordered pairing and random pairing, respectively. The description of the pairing methods can be found in Section 2.2.1.

$M_{\rm ecl}$ ($M_\odot$)	$N_{\rm star}$	$m_{\rm max,i}$ ($M_\odot$)	$r_{\rm tid}$ (pc)	$t_{\rm cr}$ (Myr)		$t_{\rm rel}$ (Myr)	
				($r_{\rm h}(0)$ = 0.3 pc	0.8 pc	0.3 pc	0.8 pc)
$10^{1.0}$	28	2.1	3.5	2.56	11.13	2.14	9.35
$10^{1.5}$	76	4.5	5.1	1.44	6.26	2.52	10.98
$10^{2.0}$	214	9.7	7.4	0.81	3.52	3.22	14.03
$10^{2.5}$	618	21.2	10.9	0.45	1.98	4.37	19.03
$10^{3.0}$	1 836	43.9	16.0	0.26	1.11	6.24	27.19
$10^{3.5}$	5 584	79.2	23.5	0.14	0.63	9.30	40.50
$10^{4.0}$	17 298	114.7	34.5	0.08	–	14.32	–

Table 2.2. Characteristics of clusters with different sizes and masses. Cluster mass, $M_{\rm ecl}$, number of stars in a cluster, $N_{\rm star}$, initial mass of the most massive star in the cluster, $m_{\rm max,i}$ (from Equations 2.1 and 2.2), and the tidal radius, $r_{\rm tid}$, are presented in columns 1–4. The $r_{\rm tid}$ is obtained from $r_{\rm tid} = R_{\rm GC}(M_{\rm ecl}/(3M_{\rm gal}))^{1/3}$ by assuming $M_{\rm gal}$, the Galactic enclosed mass within the Galactocentric distance ($R_{\rm GC}$) of 8.5 kpc, to be $5 \times 10^{10}\,M_\odot$. The initial crossing, $t_{\rm cr}$, and the initial relaxation time, $t_{\rm rel}$, for two different cluster sizes, $r_{\rm h}(0)$ = 0.3 and 0.8 pc, are given in columns 5–8. Each cluster model in Table 2.1 contains all six different mass clusters ($M_{\rm ecl}$ = 10–$10^{3.5}\,M_\odot$) in this table. In total thus 72 different initial cluster configurations are used in this study, whereby 100 random realizations of each configuration are computed with Aarseth's NBODY6. The last model ($M_{\rm ecl} = 10^4\,M_\odot$) is only computed 10 times and for the MS3OP configuration.

(Kroupa 1995b) is not included in our calculations as our emphasis is on the massive stars.

Initial mass ratios of low-mass stars such as G-, K- and M-dwarf binaries can be well described with random pairing (RP; Kroupa 1995a, 2008). Observational studies of OB-type binaries, however, show that they tend to have similar mass companions (García & Mermilliod 2001; Sana, Gosset, Nazé, Rauw & Linder 2008; Sana, Gosset & Evans 2009). Sana & Evans (2011) show that the mass-ratio distribution of O star binaries seems uniform in the range $0.2 \leq m_2/m_1 \leq 1.0$, m_1 being the primary and m_2 the secondary mass. In any case the mass ratios of massive binaries are high compared to low-mass stars. RP cannot produce the observed mass-ratio distribution of massive binaries since it typically leads to massive stars being paired with low-mass stars which are the majority in the cluster. Thus, RP over the whole stellar mass-range for OB star primaries is ruled out by the observation. A different pairing method for masses of binary components is needed to create massive binaries.

In this study we introduce a simple method to generate massive binaries having mass ratios biased towards unity. First, all stellar masses are randomly drawn from the IMF and then, stars more massive than $5\,\mathrm{M}_\odot$ are sorted with decreasing mass and the others are retained in random order. We pair stellar masses in order so that a massive star has the next massive one as a companion, while stars less massive than $5\,\mathrm{M}_\odot$ have a companion which is randomly distributed. Thus binaries with primary masses more massive than $5\,\mathrm{M}_\odot$ have mass ratios biased towards unity. We call this method 'ordered pairing' (OP). Note that star clusters with masses $\lesssim 100\,\mathrm{M}_\odot$ contain no stars more massive than $5\,\mathrm{M}_\odot$ in this study; thus, OP clusters with $M_{\rm ecl} \leq 10^{1.5}\,\mathrm{M}_\odot$ are the same as RP clusters. For a deep discussion on pairing methods for binaries, see Kouwenhoven et al. (2009) and Weidner, Kroupa & Maschberger (2009) who study several pairing mechanisms.

2.2.2 Primordial mass segregation

Many young star clusters exhibit evidence for mass segregation (Gouliermis et al. 2004; Chen, de Grijs & Zhao 2007). It has been under debate whether the observed mass segregation of young star clusters is the outcome of the star formation processes or of dynamical evolution of the clusters, since a certain time is needed for it to occur dynamically. Some observed clusters seem too young for mass-segregation to have occurred. The dynamical mass segregation timescale is

$$t_{\rm ms} \approx \frac{\langle m \rangle}{m_{\rm massive}} t_{\rm rel}, \tag{2.8}$$

where $m_{\rm massive}$ is the mass of the massive star. For some clusters, $t_{\rm ms}$ could be shorter than or comparable to their age (e.g. the ONC which has $t_{\rm ms}$ of about 0.1 Myr; Kroupa 2002). Thus, it is difficult to determine whether an observed mass segregation is primordial or the result of dynamical evolution. Studying the influence of primordial mass segregation on the early dynamical evolution of clusters would give a hint for an answer to this problem. However, it is beyond the scope of this chapter as a deeper study on individual clusters is required to do that.

It is expected that initially mass-segregated clusters ought to be more efficient in ejecting massive stars thus allowing the distribution of massive stars to be used as a constraint on the issue of initial mass segregation (Clarke & Pringle 1992; Gvaramadze & Bomans 2008; Gvaramadze et al. 2011). In order to create mass-segregated clusters we use the method introduced in Baumgardt, De Marchi & Kroupa (2008). Details of setting up the segregated cluster are described in their appendix. With this method,

the heaviest star is most bound to the cluster and is located in the core of the cluster. And the cluster is initially in virial equilibrium and follows the Plummer density profile. Although one can vary the degree of mass segregation with this method, for simplicity, mass-segregated model clusters in this study are fully segregated. Thus, the segregated clusters have a core of massive stars in the centre of the cluster at the beginning of cluster evolution.

We stress that such N-body models of initially fully mass-segregated clusters with a 100% binary fraction and a mass ratio near unity for the massive binaries have never been attempted before.

2.2.3 The N-body code

NBODY6 is a fully collisional N-body code which calculates the force on a particle from other particles with direct summation. It uses the Hermite scheme for integrating the orbits of stars. The code adapts individual time steps depending on the local environment and the Ahmad-Cohen neighbour scheme (Ahmad & Cohen 1973) for calculation efficiency. For treating close encounters, Kustaanheimo-Stiefel two-body regularization and Chain regularization for higher order multiple systems are used.

Stellar evolution is implemented in the code using fitting functions with the Single Star Evolution package (Hurley et al. 2000) and the Binary Star Evolution package (Hurley, Tout & Pols 2002), which allows a collision between two components of a binary. Details of stellar evolution in NBODY6 can be found in Hurley (2008). Since we activate stellar evolution in the code, a star has a radius instead of being a point mass particle and may collide with other single stars or its companion in a binary system by close encounters and/or binary hardening. When they merge, a mass of one star is replaced by the sum of the colliding stars and the other star is replaced by a massless particle with a large distance so that it is removed from the calculation as a massless escaper (Aarseth 2003). A metallicity of $Z = 0.02$ (solar) is adopted in all our calculations.

2.3 Results

Clusters keep losing their mass due to stars escaping from them via the two-body relaxation process or through dynamical ejections besides stellar evolution, and so we only count stars found inside the tidal radius as cluster members. A cluster mass does not change much within the first few Myr (at most ≈3% on average by 3 Myr). Therefore, the change of the $m_{\rm max}$–$M_{\rm ecl}$ relation within the first few Myr is mainly caused by the change of $m_{\rm max}$. There are three ways to change the maximum stellar mass as a cluster evolves. First, stellar evolution changes the mass of the heaviest star in the cluster. Stars lose their mass with time via stellar winds. The mass-loss rate is dependent on the stellar mass. The more massive a star the larger is its mass-loss rate. In the case of the most massive cluster in our model ($M_{\rm ecl} = 10^4\,{\rm M}_\odot$), its heaviest star with an initial mass of ≈114.7 $\rm M_\odot$ loses mass to become a ≈74 $\rm M_\odot$ star at 3 Myr. On the other hand for clusters with $M_{\rm ecl} \leq 10^3\,{\rm M}_\odot$, $m_{\rm max}$ remains almost the same as the initial value since the heaviest stars in such clusters do not evolve much in a few Myr. Secondly, stars can physically collide. If two stars collide and become a more massive star than the initially heaviest star, or if the initially heaviest star collides with another star, then the new heaviest star will lie off the initial relation. Massive stars generally move into the cluster centre which has a high stellar density. Thus, a massive star may collide with another massive star in the cluster centre. Lastly, dynamical ejection of the initially heaviest star in the cluster also changes $m_{\rm max}$ by replacing it with the initially second massive star in the cluster.

Stellar evolution and dynamical ejection lead to the cluster having a smaller maximum stellar mass, while stellar collisions increase the maximum stellar mass in the cluster. In our models all three of these effects occur. However, here we concentrate only on stellar collisions and ejections as the initial masses of the heaviest stars are set to be equal for the same cluster mass. Thus, stellar evolution does not produce the $m_{\rm max}$ spread at the same cluster mass. And we are particularly interested in how often the heaviest star is ejected from the clusters.

Using direct N-body calculations, we study the dynamical effect on the $m_{\rm max}$–$M_{\rm ecl}$ relation with various initial conditions of the clusters (Tables 2.1 and 2.2). Although the clusters are evolved up to 5 Myr, we only use the results up to 3 Myr since stellar evolution begins to play a dominant role in changing the value of $m_{\rm max}$ of the $10^{3.5}$ $M_\odot$ cluster at around 3.5 Myr. The initially most massive star of the $10^{3.5}$ $M_\odot$ cluster becomes a blackhole after 4 Myr. Furthermore, most of the observed clusters used in the study of the $m_{\rm max}$–$M_{\rm ecl}$ relation (Weidner et al. 2010) are younger than 3 Myr.

For clarification, we refer to the heaviest star in the cluster at 0 Myr as $\rm S_{MAXI}$ and to the mass of the most massive star in the cluster at a given snapshot as $m_{\rm max}$.

2.3.1 Dynamical ejection of $\rm S_{MAXI}$

Stars can be ejected from a cluster via close encounters between a hard binary and a single star/binary. During the encounter, the hard binary gives its binding energy to the interacting star/stars in the form of kinetic energy and it hardens. The star that gained kinetic energy may be ejected from the cluster. Generally, the lightest one among the interacting stars attains the highest velocity after the interaction. Thus, the dynamical ejection of massive stars preferably occurs from interactions between massive stars. Leonard & Duncan (1990) showed that binary–binary interactions are the most efficient way for producing massive runaways.

We consider $\rm S_{MAXI}$ to be dynamically ejected if the star is further away from the cluster centre than the tidal radius of the cluster. The number of clusters which eject their $\rm S_{MAXI}$, $N_{\rm resc}$, is listed in Table 2.3 for all cluster models.

In the following subsections, results on the dynamical ejection of $\rm S_{MAXI}$ are discussed separately for models with different initial half-mass radii.

The $r_{\rm h}(0) = 0.8$ pc models

In Table 2.3, there are two clusters with $r_{\rm h}(0) = 0.8$ pc whose $\rm S_{MAXI}$ is located further than the tidal radius of the cluster at 3 Myr. The most massive star of one not initially mass-segregated 10 $M_\odot$ cluster was, in fact, located outside of the tidal radius of the cluster, which is ≈3.5 pc, at 0 Myr. Therefore this case is not due to dynamical ejection. Thus only one out of 3600 model clusters with $r_{\rm h}(0) = 0.8$ pc eject their $\rm S_{MAXI}$ within 3 Myr.

Fig. 2.2 shows the $m_{\rm max}$–$M_{\rm ecl}$ relation of the binary-rich clusters with $r_{\rm h}(0) = 0.8$ pc and massive binaries paired by the OP method (models NMS8OP and MS8OP) at different ages of the clusters. Even though this set of initial conditions is the most dynamic case of the cluster models with $r_{\rm h}(0) = 0.8$ pc, only one cluster, with a mass of $10^{3.5}$ $M_\odot$, ejects its $\rm S_{MAXI}$ (Table 2.3). But the initially second heaviest star of the cluster, which becomes the most massive one in the cluster after ejection of $\rm S_{MAXI}$, has a similar mass to the mass of $\rm S_{MAXI}$. Therefore, the effect of the ejection on the $m_{\rm max}$–$M_{\rm ecl}$ relation is

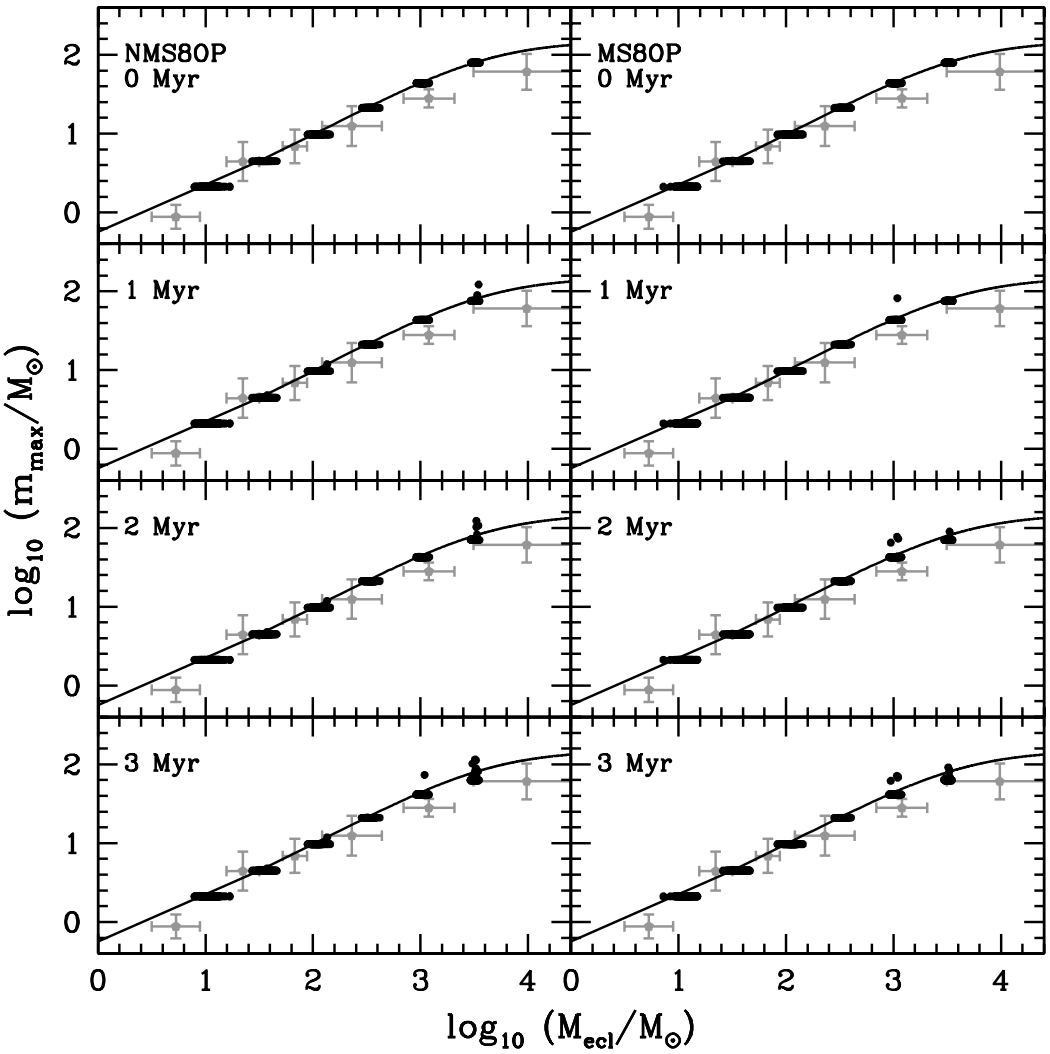

Figure 2.2. The mass of the most massive star versus the cluster mass for the unsegregated (left: NMS8OP) and the segregated (right: MS8OP) clusters with $r_{\rm h}(0)$ = 0.8 pc and massive binaries with mass ratios biased towards unity at 0, 1, 2, and 3 Myr (from top to bottom). Each black point indicates a cluster. The grey data are the average observational data as in Fig. 2.1. The solid line represents the semi-analytical model from Weidner & Kroupa (2004, 2006) assuming an upper limit of stellar mass of 150 $M_\odot$ (Equations 2.1 and 2.2). As we fix the number of stars at a certain cluster mass, the cluster mass slightly varies for each realization for the same cluster mass model. We only plot the result up to 3 Myr since the initially heaviest star of the cluster with $10^{3.5}$ $M_\odot$ loses a large amount of its initial mass within 3.5 Myr, thereafter stellar evolution affects the relation. The stars that appear above the solid curve are merger products.

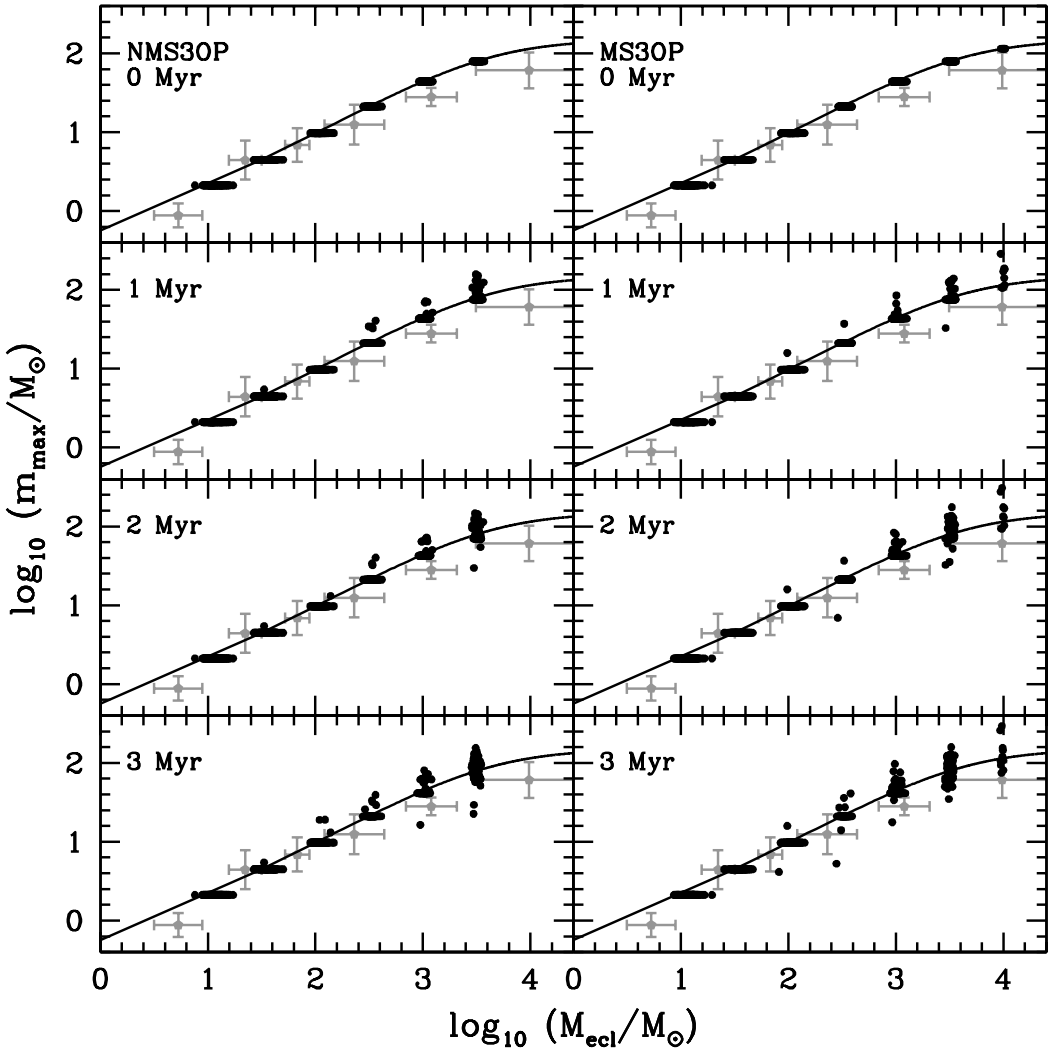

Figure 2.3. Same as Fig. 2.2, but for the OP clusters with $r_{\rm h}(0) = 0.3$ pc (left: NMS3OP; right: MS3OP).

negligible in this case.

It is unlikely that the $m_{\rm max}$–$M_{\rm ecl}$ relation is affected by dynamical ejection of $\rm S_{MAXI}$ for clusters of this size. But it is worthy to note that at 3 Myr a few OP clusters show their $\rm S_{MAXI}$ moving faster than the escape velocity, $v_{\rm esc}(r) = \sqrt{2|\Phi(r)|}$, where $\Phi(r)$ is the gravitational potential at a distance r from the cluster centre, although these clusters barely eject their $\rm S_{MAXI}$ (Table 2.3).

The $r_{\rm h}(0) = 0.3$ pc models

Fig. 2.3 shows the $m_{\rm max}$–$M_{\rm ecl}$ relation for the binary-rich cluster models with $r_{\rm h}(0) = 0.3$ pc (models NMS3OP and MS3OP). Despite the smaller size of the clusters, none of the single star clusters (NMS3S and MS3S) eject their most massive star (Table 2.3). Only two massive clusters with $M_{\rm ecl} = 10^{3.5}\,\rm M_\odot$ eject their $\rm S_{MAXI}$ when the massive binaries are randomly paired (NMS3RP and MS3RP in Table 2.3). However, binaries help the most massive star to attain a higher velocity compared to the single star clusters. The number of clusters for which the heaviest star has a speed exceeding the escape velocity is larger when the stars are initially in a binary system (Table 2.3).

Clusters with $M_{\rm ecl} \leq 10^{2.5}\,\rm M_\odot$ hardly eject their most massive star even though the clusters form in energetic initial conditions such as being binary rich and mass segregated. Among all clusters with $M_{\rm ecl} \leq 10^{2.5}\,\rm M_\odot$, only one out of 100 clusters with $M_{\rm ecl} = 10^{2}\,\rm M_\odot$ and two out of 100 clusters with $M_{\rm ecl} = 10^{2.5}\,\rm M_\odot$ eject their $\rm S_{MAXI}$ (MS3OP in Table 2.3). However, at 3 Myr there are a few clusters whose $\rm S_{MAXI}$ is inside the tidal radius but has a velocity higher than the escape velocity so that it may leave the cluster later.

For clusters with $M_{\rm ecl} \geq 10^{3}\,\rm M_\odot$, 15–40% of the most energetic models (MS3OP) have $\rm S_{MAXI}$ moving faster than the escape velocity and 2–20% of the clusters have ejected their $\rm S_{MAXI}$ at 3 Myr. When the clusters are initially mass segregated, slightly more clusters eject $\rm S_{MAXI}$.

Fig. 2.4 shows the ejection frequency of $\rm S_{MAXI}$ as a function of the cluster mass for the MS3OP models. We only plot these models since the other models barely eject their initially most massive star (see Table 2.3 for all models). The ejection probability of the $\rm S_{MAXI}$ star increases with the cluster mass as the stellar density increases. About 8 (20)% of $10^{3.5}$ (10^{4}) $\rm M_\odot$ clusters eject their $\rm S_{MAXI}$ within 3 Myr (squares in Fig. 2.4). Some massive clusters which eject their $\rm S_{MAXI}$ can be missed as we use the tidal radius as a criterion for the ejection. Some ejected $\rm S_{MAXI}$ from massive clusters may not reach the clusters' tidal radius by 3 Myr due to their large tidal radius. Thus, the real ejection frequency would be higher than the above value for the massive clusters. By using $N_{\rm vesc10}$ (Table 2.3), the number of clusters whose $\rm S_{MAXI}$ has a velocity greater than the escape velocity of the cluster and has travelled beyond 10 pc from the cluster centre, the ejection frequency increases to 40% for the cluster with $10^{4}\,\rm M_\odot$ (circles in Fig. 2.4). In order to estimate the real probability for the $\rm S_{MAXI}$ ejection, in addition, we provide in Appendix A the number of clusters whose $\rm S_{MAXI}$ is found beyond the distance criterion using the half-mass radius for all models.

From Figs 2.2 and 2.3 it is evident that collisions of massive stars may conceal the dynamical ejection of $\rm S_{MAXI}$ by the product of the collisions becoming more massive than the mass of the initially heaviest member. Thus, the dynamical behaviour of the $\rm S_{MAXI}$ needs to be considered to distinguish whether it is ejected or not. Figures 2.5 and 2.6 show the distance from the cluster centre and the velocity of the $\rm S_{MAXI}$ in NMS3OP and MS3OP clusters with 10 and $10^{3.5}\,\rm M_\odot$.

The heaviest stars are initially located at a wide range of radii up to ≈2.5 pc in the unsegregated cluster

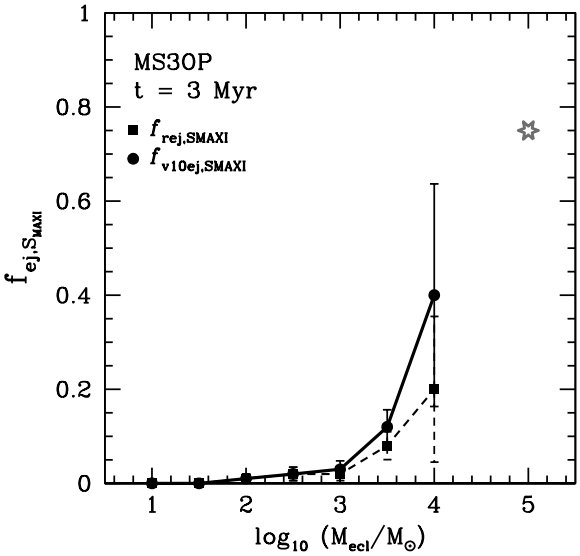

Figure 2.4. The ejection frequency of S_{MAXI} as a function of cluster mass for mass-segregated clusters with massive binaries (MS3OP) at 3 Myr. $f_{rej,S_{MAXI}}$, marked with squares, is the ratio of the number of clusters whose S_{MAXI} is located further than the tidal radius from the cluster centre, N_{resc} in Table 2.3, to the total number of the realizations, N_{run}, which is 100 in our study for each initial condition set (10 for $10^4\,M_\odot$ clusters). The error bars indicate Poisson uncertainties. All other models have $f_{rej,S_{MAXI}} \approx 0$ (Table 2.3). The circles, $f_{v10ej,S_{MAXI}}$, are the ratio of N_{vesc10} (Table 2.3) to N_{run}. $f_{v10ej,S_{MAXI}}$ is probably closer to the real ejection frequency as some massive clusters which eject their S_{MAXI} can be missed in N_{resc} due to their large tidal radii. The grey star is the ejection frequency of S_{MAXI} from clusters with $M_{ecl} = 10^5\,M_\odot$ taken from the calculations by Banerjee et al. (2012b). These authors refer to a star that is ejected when its distance from the cluster centre is larger than 10 pc. Note that the initial conditions of their calculations are different but comparable to our MS3OP models.

models (Fig. 2.5) while they are centrally concentrated in the segregated ones (Fig. 2.6). In both cases, massive stars sink towards the centre of the clusters due to dynamical friction and/or energy equipartition. This is more prominent in the unsegregated clusters since the heaviest stars already reside in the deep potential of the segregated clusters at the beginning of the calculations.

As shown in Figs 2.5 and 2.6, the heaviest stars hardly attain a high velocity if the massive stars are randomly paired into binaries. In RP, massive stars are mostly paired with low-mass stars; therefore, their mass ratios (m_2/m_1, where $m_1 \geq m_2$) are skewed to 0. Randomly paired massive binaries therefore behave like single stars. Clusters with massive binaries paired randomly do not shoot out their S_{MAXI} more frequently even though the clusters are initially mass segregated.

Clusters with massive binaries paired by OP and $M_{ecl} \geq 100\,M_\odot$ effectively produce heaviest stars with velocities exceeding the escape velocity of the cluster. For example, in the case of some initial conditions more than 20% of the clusters show that their S_{MAXI} has a velocity larger than the escape velocity at 3 Myr (Table 2.3). It is known that massive stars are ejected from the small core of massive stars in the cluster centre lacking low mass stars (Clarke & Pringle 1992). In the case of segregated clusters with OP massive binaries, the clusters already form with this kind of core; thus, the massive stars can be ejected at a very early age of the cluster (see Fig. 2.6). S_{MAXI} of one cluster with $M_{ecl} = 10^{3.5}\,M_\odot$ from the MS3OP model has travelled more than 200 pc from the cluster with a velocity of about $80\,km\,s^{-1}$ at

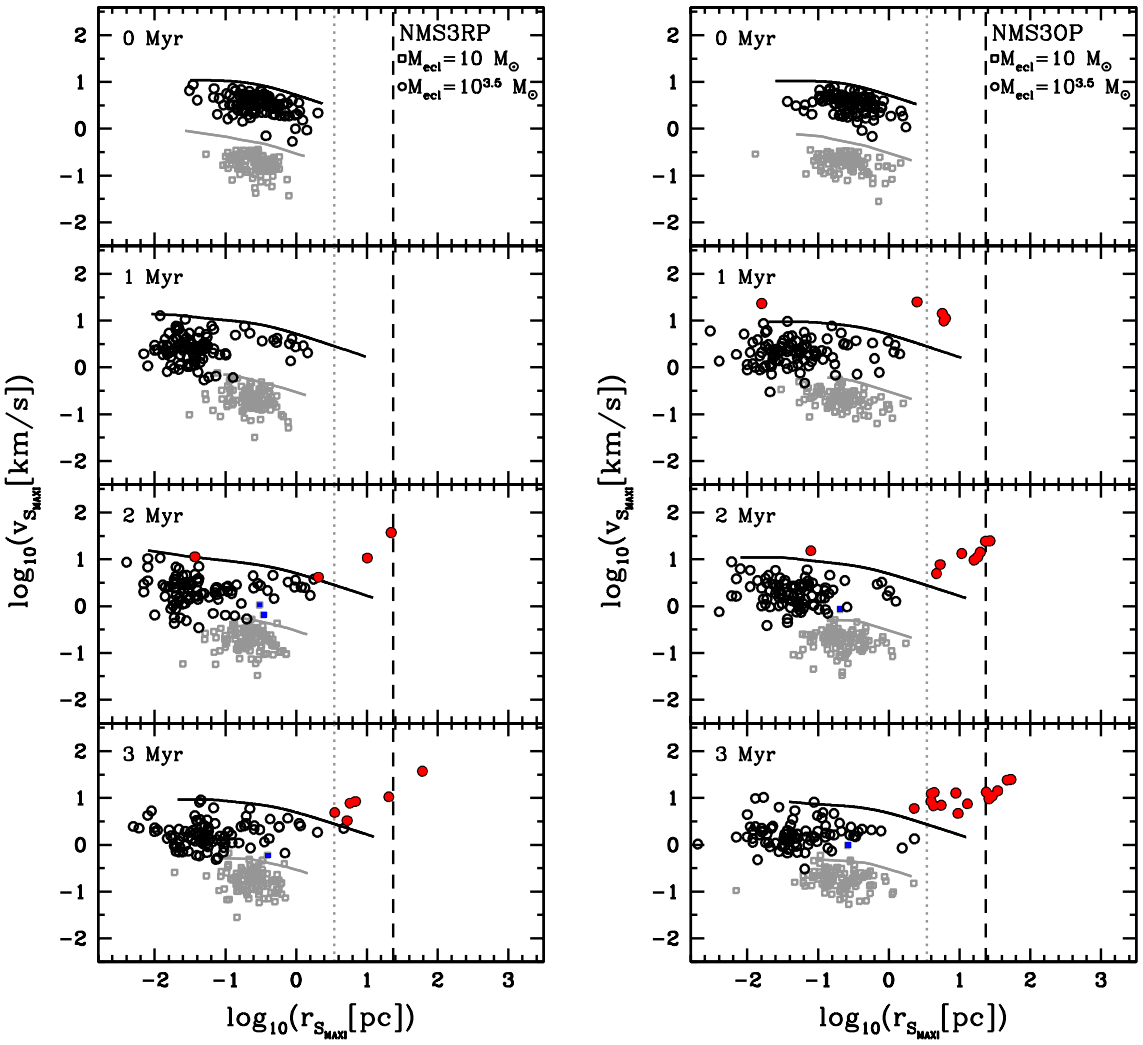

Figure 2.5. Distances from the cluster centre and velocities of S_{MAXI} stars of the initially unsegregated binary-rich clusters with $r_{\rm h}(0) = 0.3$ pc (left: NMS3RP; right: NMS3OP). Each dot denotes a cluster and in total there are 100 dots per configuration. The squares and circles are the values of S_{MAXI} in the clusters with 10 and $10^{3.5}$ $M_\odot$, respectively. The filled symbols represent S_{MAXI} stars with a speed exceeding the escape velocity. The black (grey) solid curves are the escape velocity of one cluster with $10^{3.5}$ (10) $M_\odot$ as a function of the distance from the cluster centre at each Myr. The grey dotted and the black dashed vertical lines indicate the initial tidal radius of the cluster with 10 and with $10^{3.5}$ $M_\odot$, respectively. Note how mass segregation develops by 1 Myr and how OP increases the occurrence of ejected most massive stars.

3 Myr.

Although the low-mass clusters barely eject their S_{MAXI} regardless of their initial conditions, the binary-rich or binary-poor cases show differences, for example, the number of clusters whose S_{MAXI} has a velocity greater than the escape velocity is larger for binary-rich clusters. For massive clusters, on the contrary, binary-poor and binary-rich clusters with random pairing show similar results in the case of unsegregated models. Primordial mass segregation enhances the ejection of the most massive star at earlier times and helps more clusters shoot out their S_{MAXI} within 3 Myr.

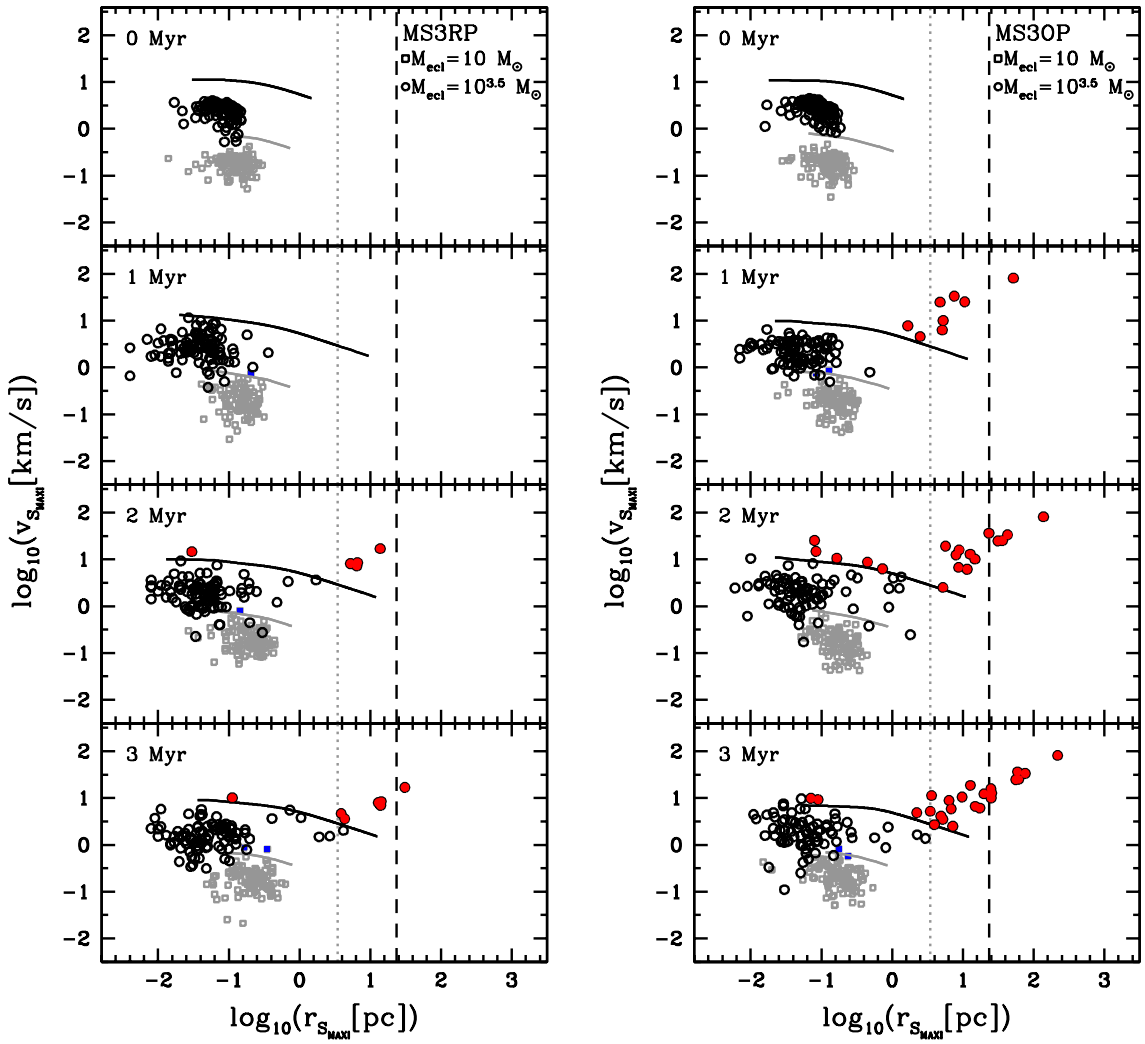

Figure 2.6. Same as Fig. 2.5 but for the initially mass-segregated, binary-rich clusters with $r_h(0) = 0.3$ pc (left: MS3RP; right: MS3OP).

$M_{\rm ecl}$ ($M_\odot$)	$N_{\rm resc}$	$N_{\rm vesc}$	$N_{\rm vesc10}$	$N_{\rm c}$	$N_{\rm resc}$	$N_{\rm vesc}$	$N_{\rm vesc10}$	$N_{\rm c}$
	Unsegregated cluster model				Mass-segregated cluster model			
	NMS3S				MS3S			
10	0	0	0	0	0	0	0	0
$10^{1.5}$	0	0	0	0	0	0	0	0
10^{2}	0	0	0	0	0	0	0	0
$10^{2.5}$	0	0	0	0	0	1	0	2
10^{3}	0	0	0	6 (1)	0	2	0	8
$10^{3.5}$	0	6	1	36 (8)	0	5	1	36 (4)
	NMS3RP				MS3RP			
10	0	1	0	0	0	2	0	0
$10^{1.5}$	0	0	0	0	0	2	0	1 (1)
10^{2}	0	1	0	1	0	0	0	2
$10^{2.5}$	0	0	0	8 (2)	0	4	0	9 (1)
10^{3}	0	2	0	17 (3)	1	4	1	23 (1)
$10^{3.5}$	1	6	2	51 (11)	1	7	4	46 (4)
	NMS3OP				MS3OP			
10	0	1	0	0	0	2	0	0
$10^{1.5}$	0	4	0	2	0	2	0	0
10^{2}	0	5	0	1	1	5	1	1
$10^{2.5}$	0	14	0	5 (1)	2	23	2	4
10^{3}	1	15	2	23 (4)	2	15	3	17 (3)
$10^{3.5}$	6	15	7	60 (23)	8	24	12	56 (14)
10^{4}					2	4	4	9 (4)
	NMS8S				MS8S			
10	1	0	0	0	0	0	0	0
$10^{1.5}$	0	0	0	0	0	0	0	0
10^{2}	0	0	0	0	0	0	0	0
$10^{2.5}$	0	0	0	0	0	0	0	0
10^{3}	0	0	0	0	0	0	0	0
$10^{3.5}$	0	0	0	1	0	0	0	0
	NMS8RP				MS8RP			
10	0	1	0	0	0	1	0	0
$10^{1.5}$	0	1	0	0	0	0	0	0
10^{2}	0	0	0	1	0	0	0	0
$10^{2.5}$	0	0	0	1	0	0	0	1
10^{3}	0	0	0	2 (1)	0	1	0	0
$10^{3.5}$	0	0	0	5	0	0	0	1 (1)

Continued on next page

$M_{\rm ecl}$ ($M_\odot$)	$N_{\rm resc}$	$N_{\rm vesc}$	$N_{\rm vesc10}$	$N_{\rm c}$	$N_{\rm resc}$	$N_{\rm vesc}$	$N_{\rm vesc10}$	$N_{\rm c}$
	Unsegregated cluster model				Mass-segregated cluster model			
	NMS8OP				MS8OP			
10	0	3	0	0	0	0	0	0
$10^{1.5}$	0	1	0	1	0	1	0	0
10^{2}	0	1	0	1 (1)	0	0	0	0
$10^{2.5}$	0	0	0	0	0	3	0	0
10^{3}	0	2	0	2	0	5	0	5 (1)
$10^{3.5}$	0	3	0	10 (4)	1	3	1	8 (6)

Table 2.3. Results at 3 Myr. $M_{\rm ecl}$ is a cluster mass in $M_\odot$ (per $M_{\rm ecl}$ value there are 100 clusters, but 10 clusters for $10^4\,M_\odot$). $N_{\rm resc}$ is the number of clusters whose $S_{\rm MAXI}$ is located beyond the tidal radius of the cluster. $N_{\rm vesc}$ is the number of clusters whose $S_{\rm MAXI}$ has a velocity larger than the escape velocity. $N_{\rm vesc10}$ is the number of clusters whose $S_{\rm MAXI}$ is located further than 10 pc from the cluster centre and has a velocity larger than the escape velocity. $N_{\rm c}$ is the number of clusters whose $m_{\rm max}$ changes due to stellar collisions. Numbers in brackets indicate the collision products that do not involve $S_{\rm MAXI}$. For example, in the case of clusters with $M_{\rm ecl} = 10^{3.5}\,M_\odot$ from the NMS3RP model, one out of 100 clusters lost their $S_{\rm MAXI}$ by dynamical ejection, $S_{\rm MAXI}$ of six clusters have a velocity greater than the escape velocity of the cluster, for two clusters out of these six clusters the star is located beyond 10 pc from the cluster centre. Stellar collisions which change the $m_{\rm max}$ have occurred in 51 clusters; for 11 clusters out of these 51 the collisions do not involve $S_{\rm MAXI}$.

2.3.2 Stellar collisions

$m_{\rm max}$ can increase by stellar collisions, either involving $S_{\rm MAXI}$ or not, which makes a star heavier than the mass of $S_{\rm MAXI}$ before the collisions occur. Although stellar collisions occur over a whole range of stellar masses, in this study, we only care about the collision that changes $m_{\rm max}$. The occurrences of the collisions are contained in Table 2.3.

For clusters with $r_{\rm h}(0) = 0.8$ pc [$2\,M_\odot\,{\rm pc}^{-3} < \rho_{0.5} < 750\,M_\odot\,{\rm pc}^{-3}$, where $\rho_{0.5} = 3M_{\rm ecl}/(8\pi r_{\rm h}(0)^3)$ is the average mass density within the half-mass radius], stellar collisions rarely occur in them due to their low density. In single star cluster models (NMS8S and MS8S), only one cluster shows that its $m_{\rm max}$ changes by a stellar collision which involves $S_{\rm MAXI}$. In the case of binary-rich models there are a few clusters whose $m_{\rm max}$ changes via stellar collisions, mostly in the most massive cluster models, but with a probability of less than 10% taking all models into account. In low-density ($r_{\rm h}(0) = 0.8$ pc) clusters a change of $m_{\rm max}$ through stellar collisions is highly improbable.

For clusters with $r_{\rm h}(0) = 0.3$ pc, the stellar collision result of low-mass clusters, $M_{\rm ecl} \leq 10^{2.5}\,M_\odot$ ($\rho_{0.5} \lesssim 1400\,M_\odot\,{\rm pc}^{-3}$), is similar to the result from clusters with $r_{\rm h}(0) = 0.8$ pc. But in the case of the massive cluster models ($M_{\rm ecl} \geq 10^3\,M_\odot$), especially the most massive one, about half of them experience a change of $m_{\rm max}$ by stellar collisions.

Most of the collisions are induced by binary encounters, in which the two components of a binary system collide due to their highly eccentric orbit generated by perturbation through other stars. Direct dynamical collisions are extremely rare. This naturally explains why $N_{\rm c}$ in Table 2.3 becomes larger when clusters are initially binary rich. And the number increases when massive binaries are paired with the OP method when compared to RP. This can be understood because both components of a massive binary in the OP method are massive stars and thus have larger sizes leading to collisions. With a different

collision channel from our result, Gaburov, Gualandris & Portegies Zwart (2008) also showed that a binary is more efficient in stellar collisions than a single star as the enhanced cross-section of a binary compared to a single star results in other stars engaging the binary, and then this can lead to a collision between one of the binary components and the incoming third star.

Both the dynamical ejection of the $S_{\rm MAXI}$ and stellar collisions that increase $m_{\rm max}$ barely take place in the same cluster within the cluster mass range we study. As shown by Baumgardt & Klessen (2011) and Moeckel & Clarke (2011), stellar collisions generally lead to the formation of a single very massive star through the merging of several massive stars rather than the formation of many massive stars. This single very massive star is hardly ejected from the cluster and its formation reduces the number of massive stars; thus, it may hamper the ejection of other massive stars. Out of 7200 cluster models (excluding the $10^4\,{\rm M}_\odot$ clusters from the MS3OP model), there are only three clusters in which both events occur. In one cluster $S_{\rm MAXI}$ is dynamically ejected, but one massive binary in the cluster merges then becoming more massive than $S_{\rm MAXI}$. In the other two clusters their $S_{\rm MAXI}$ gains mass by the collision with another star and then it is dynamically ejected.

Although this event is very rare, the most massive star in the star-forming region LH 95 in the Large Magellanic Cloud (Da Rio et al. 2012) might be an example. The peculiarities of the star, with a much younger age than the average age of other stars in the region and the mass being higher than $m_{\rm max}$ from the Weidner & Kroupa (2004) $m_{\rm max}$–$M_{\rm ecl}$ relation, could have resulted from a stellar collision between binary components with similar masses of which the primary star may have been the initially most massive star of one of the three main substructures in the region, with a mass following the $m_{\rm max}$–$M_{\rm ecl}$ relation from Weidner & Kroupa (2004). The stellar collision could have increased the stellar mass and rejuvenated the star. And the ejection of the star with a low velocity can explain the location of the star which is at a rather far ($\approx$10 pc) distance from any of the substructures but still within the region.

2.3.3 The spread of $m_{\rm max}$

Figure 2.7 presents the standard deviation of $\log m_{\rm max}$, $\sigma_{\rm lmmax}$, for the observed samples and our models. The observed larger $m_{\rm max}$ spread than what emerges from our models may be a result of stochastic effects of star formation as the dynamical processes hardly influence the change of $m_{\rm max}$ in these clusters, as shown by this study. However, numerical simulations of star cluster formation show that $m_{\rm max}$ and $M_{\rm ecl}$ evolve tightly following the relation of $m_{\rm max} \propto M_{\rm ecl}^{2/3}$ (Bonnell et al. 2004; Peters et al. 2010).

For low-mass clusters ($M_{\rm ecl} < 100\,{\rm M}_\odot$) the differences between $\sigma_{\rm lmmax}$ of the observation and our model are large despite taking into account the spread due to the different cluster masses in the bins of observational data. This could be due to the large uncertainties of the observations. Note that the homogeneous data set from Kirk & Myers (2011) is more confined to the relation than the inhomogeneous data from Weidner et al. (2010) which come from many different references.

The spread in our models for relatively massive clusters ($M_{\rm ecl} \geq 10^3\,{\rm M}_\odot$) is comparable to the observed one in the case of clusters with $r_{\rm h}(0) = 0.3$ pc and with OP for massive binaries (NMS3OP and MS3OP models).

Stellar collisions dominate the change of $m_{\rm max}$ of relatively dense clusters with $M_{\rm ecl} \geq 10^{2.5}\,{\rm M}_\odot$ and $r_{\rm h}(0) = 0.3$ pc (Table 2.3) and therefore the spread of $m_{\rm max}$ of these clusters mostly comes from the collisions. However it should be noted that the exact solution for the stellar collision process is as yet poorly understood. The treatment of stellar collisions in the code is simply adding the masses of two

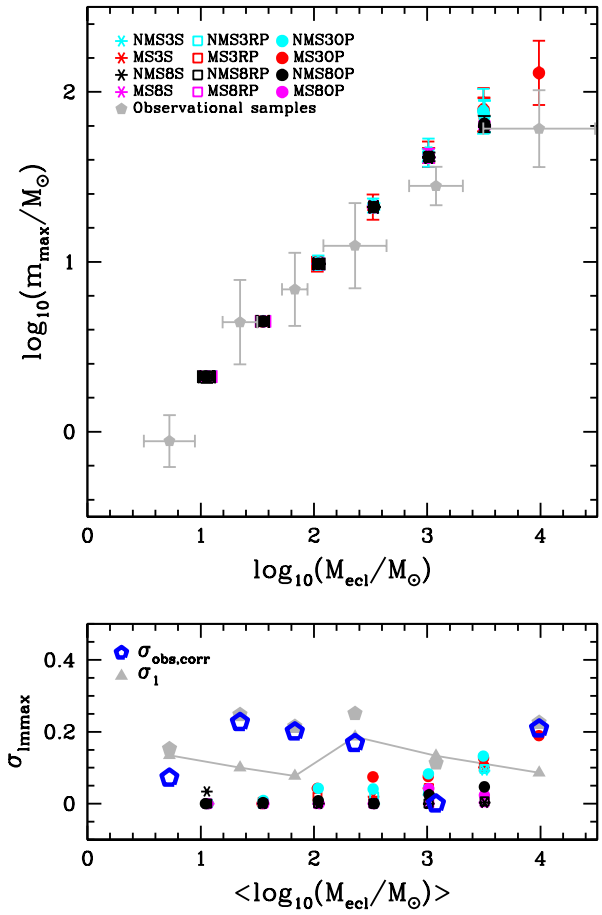

Figure 2.7. Top: average $m_{\rm max}$–$M_{\rm ecl}$ plot for all models at 3 Myr. The error bars indicate the standard deviations of $M_{\rm ecl}$ and $m_{\rm max}$. Grey symbols are the observed cluster samples as in Figs 2.2 and 2.3. The colour and symbol codes are given in the upper-left corner of the figure. Bottom: standard deviation of $\log_{10} m_{\rm max}$, $\sigma_{\rm lmmax}$, for each cluster model from the top figure. The colours and symbols are the same as in the top panel. Note that for $M_{\rm ecl} \leq 10^{2.5}\,{\rm M}_\odot$ the observed $\sigma_{\rm lmmax}$, $\sigma_{\rm obs}$, is much larger than the dispersion in the models. To quantify the deviation due to binning the cluster mass in the observed range of cluster masses in each mass bin, we obtain the $m_{\rm max}$ according to Equations (2.1) and (2.2) with $m^*_{\rm max} = 150\,{\rm M}_\odot$ for the observed cluster masses. We then calculate the standard deviation of $\log_{10} m_{\rm max}$, σ_1, by binning the clusters in the same way as for $\sigma_{\rm obs}$. This is shown as grey triangles connected with a solid line. The corrected observed $\sigma_{\rm lmmax}$, $\sigma_{\rm obs,corr} = \sqrt{\sigma^2_{\rm obs} - \sigma^2_1}$ (if $\sigma_{\rm obs} > \sigma_1$ otherwise $\sigma_{\rm obs,corr} = 0$), is plotted with blue open pentagons.

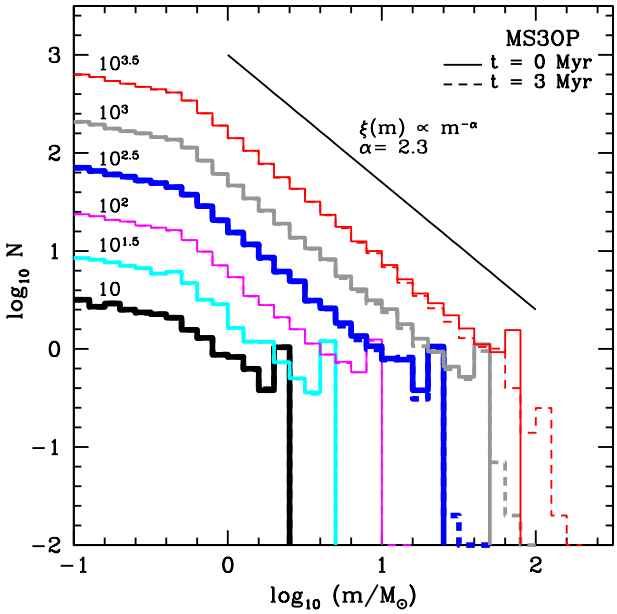

Figure 2.8. Mass functions of MS3OP clusters. Each line indicates the average mass function of clusters obtained from the 100 computations per model with a mass of 10, $10^{1.5}$, 10^2, $10^{2.5}$, 10^3 and $10^{3.5}$ $M_\odot$ from the bottom to the top. The solid and dashed histograms are mass functions at 0 (initial) and 3 Myr, respectively. A solid line on top of the histograms is the Salpeter mass function.

stars. Thus, the collision products shown in this study provide only a rough idea about merger rates and their masses. Therefore, we cannot quantify the real spread produced by the collisions but we expect that it would be smaller than our result since in reality not all the stellar mass ends up being in the merger product.

2.4 Discussion

Figure 2.8 shows the initial and the final (t = 3 Myr) mass functions of MS3OP model clusters. Massive stars are overpopulated in a cluster with a bump at the most massive stellar-mass-bin of the cluster's mass function because we enforce all clusters to have a star with a mass of $m_{\rm max,WK}$. As a necessary condition for massive star ejections is a small core of massive stars, the overpopulation of massive stars would enhance the ejection of massive stars. The other effect that might result from this choice is the overspread of $m_{\rm max}$ in low-mass (i.e. small-number) clusters if many of the clusters eject their $S_{\rm MAXI}$. When stellar masses are randomly drawn from the IMF low-mass clusters would hardly have a star with a mass close to $m_{\rm max}$ while massive clusters, that populate stars over the whole mass range, would have a few. However, the dynamical ejection of the most massive star from the low-mass cluster is highly improbable thus enforcing clusters to have a star with a $m_{\rm max,WK}$ would not have an impact on the spread.

The orbital parameters of the massive binaries are important for the ejection of massive stars. But our knowledge of their initial distribution functions is still poor. We use the same period distribution for massive binaries as that of low-mass stars. However, a high fraction of short-period massive binaries is suggested by observations (Sana & Evans 2011) implying that massive binaries may have a different

initial period distribution, compared to that of low-mass binaries. Dynamical ejections of the most massive star might become more likely than presented here. Future work taking into account the most recent constraints on the period distribution of massive star binaries will investigate this issue. The results for $M_{\rm ecl} \leq 10^3\,{\rm M}_\odot$ clusters presented here will, however, not be affected as such clusters do not contain many, if any, massive stars.

Apart from our MS3OP sequence of models, our young star cluster library does not contain clusters more massive than $10^4\,{\rm M}_\odot$ as they are computationally expensive due to the large binary population, while the observational sample contains a few clusters more massive than $10^4\,{\rm M}_\odot$. At a higher density massive clusters may show the ejection of the heaviest star with a higher probability. Indeed, 20% of the MS3OP clusters with $M_{\rm ecl} = 10^4\,{\rm M}_\odot$ eject their $\rm S_{MAXI}$ (Fig. 2.4). Furthermore, three out of four clusters with $M_{\rm ecl} = 10^5\,{\rm M}_\odot$ computed by Banerjee et al. (2012b) eject their $\rm S_{MAXI}$. Further work including such massive clusters will be carried out to study this issue.

2.5 Conclusions

We have established a large theoretical young star cluster library using Aarseth's direct N-body integration code, NBODY6 with 73 different combinations of initial conditions such as cluster size and mass, initial binary population, and primordial mass segregation. The library contains two different sizes of clusters, $r_{\rm h}(0) = 0.3$ and 0.8 pc, with two different binary fractions, zero and unity. In order to take into account that observed OB binaries likely have companions with similar masses, we generate clusters with massive binaries not only paired randomly from the IMF but also having a mass ratio close to unity. In both cases the stars follow the canonical IMF. And we model initially mass-segregated clusters as well as unsegregated clusters. Using this library we study the $m_{\rm max}$–$M_{\rm ecl}$ relation during the early evolution ($\leq$3 Myr) of the star clusters focusing on the effects on it established through dynamical ejection of the heaviest star from the cluster under the various initial conditions. Such computations of fully mass-segregated, binary-rich clusters have never been performed before.

Stellar evolution, stellar collision, and dynamical ejection can alter the $m_{\rm max}$ of the cluster. In our models, all three effects are observed to affect $m_{\rm max}$. Stellar evolution affects the relation only for the massive ($\gtrsim 10^3\,{\rm M}_\odot$) clusters since only stars more massive than $40\,{\rm M}_\odot$ significantly lose their mass within 3 Myr. Furthermore, since the mass of $\rm S_{MAXI}$ is the same for the same cluster mass, stellar evolution cannot contribute to the spread of $m_{\rm max}$ in this study. Stellar collisions influence mainly massive clusters, especially for those with the smaller radius as the clusters are denser. For clusters with $r_{\rm h}(0) = 0.3$ pc and $M_{\rm ecl} = 10^{3.5}\,{\rm M}_\odot$, for about half of the clusters their $m_{\rm max}$ has changed by stellar collisions within 3 Myr. Lastly, concerning the focus of this study, the dynamical ejection of $\rm S_{MAXI}$ only occurs in the binary-rich clusters with $r_{\rm h}(0) = 0.3$ pc and $M_{\rm ecl} > 10^2\,{\rm M}_\odot$. The number of the ejections increase when massive binaries are paired with the OP method and/or are initially concentrated in the cluster centre. As massive clusters likely have a few stars with masses close to the mass of $\rm S_{MAXI}$, $m_{\rm max}$ value would change little for massive clusters when $\rm S_{MAXI}$ is dynamically ejected. Overall we conclude that (dynamical) evolutionary effects hardly produce a spread of $m_{\rm max}$ in the relation for low-mass ($M_{\rm ecl} \lesssim 10^{2.5}\,{\rm M}_\odot$) or less dense ($r_{\rm h}(0) = 0.8$ pc) clusters. Massive ($M_{\rm ecl} \geq 10^{3.5}\,{\rm M}_\odot$), binary-rich clusters with $r_{\rm h}(0) = 0.3$ pc do show a significant spread of $m_{\rm max}$, mostly produced by stellar collisions, becoming comparable to the observed spread (Fig. 2.7).

Concerning the dynamical ejection of $S_{\rm MAXI}$, we find that in general it is very unlikely even in relatively dense clusters with massive binaries with similar mass companions. However, its probability can reach up to 20% in our cluster library depending on the initial configuration of the cluster. For example, none of the clusters without initial mass segregation but with OP binaries and with $M_{\rm ecl} = 10^{3.5}\,{\rm M}_\odot$ and $r_{\rm h}(0) = 0.8\,{\rm pc}$ (NMS8OP model) eject their $S_{\rm MAXI}$, while eight (two) out of 100 (10) mass-segregated clusters with $M_{\rm ecl} = 10^{3.5}$ $(10^4)\,{\rm M}_\odot$ and $r_{\rm h}(0) = 0.3\,{\rm pc}$ (MS3OP model) eject their $S_{\rm MAXI}$ (Table 2.3). In reality, many young star clusters are observed to fulfil the conditions which are needed to eject their massive star, such as having a compact size and massive binaries with similar component masses, so that some (up to ≈75% for $10^5\,{\rm M}_\odot$ clusters, see Fig. 2.4) of the real embedded clusters could have lost their initially most massive star by dynamical ejection within 3 Myr.

In this chapter, we are only interested in the heaviest star of the cluster. However, the dynamical ejection of other massive stars in the cluster is also interesting because it is important to understand the origin of field massive stars and OB runaways (Fujii & Portegies Zwart 2011) to help us to constrain the initial configuration of massive stars in clusters. The dynamical ejections of OB stars in our theoretical young star cluster library will be discussed in the following chapters (Oh et al. 2015; Oh & Kroupa 2016, Chapters 3 and 4), and Banerjee et al. (2012b) and Pflamm-Altenburg & Kroupa (2006) have, respectively, already demonstrated that R136-type star-burst and ONC-type clusters are very efficient in ejecting OB stars.

CHAPTER 3

Dependency of dynamical ejections of O stars on the masses of very young star clusters

Published in the Astrophysical Journal
Volume 805, article id 92, pp 1–18, June 2015
S. Oh, P. Kroupa, and J. Pflamm-Altenburg

ABSTRACT

Massive stars can be efficiently ejected from their birth clusters through encounters with other massive stars. We study how the dynamical ejection fraction of O-star systems varies with the masses of very young star clusters, $M_{\rm ecl}$, by means of direct N-body calculations. We include diverse initial conditions by varying the half-mass radius, initial mass segregation, initial binary fraction, and orbital parameters of the massive binaries. The results show robustly that the ejection fraction of O-star systems exhibits a maximum at a cluster mass of $10^{3.5}\,{\rm M}_\odot$ for all models, even though the number of ejected systems increases with cluster mass. We show that lower mass clusters ($M_{\rm ecl} \approx 400\,{\rm M}_\odot$) are the dominant sources for populating the Galactic field with O stars by dynamical ejections, considering the mass function of embedded clusters. About 15% (up to ≈38%, depending on the cluster models) of O stars of which a significant fraction are binaries, and which would have formed in a ≈10 Myr epoch of star formation in a distribution of embedded clusters, will be dynamically ejected to the field. Individual clusters may eject 100% of their original O-star content. A large fraction of such O stars have velocities up to only $10\,{\rm km\,s^{-1}}$. Synthesising a young star cluster mass function it follows, given the stellar-dynamical results presented here, that the observed fractions of field and runaway O stars, and the binary fractions among them can be well understood theoretically if all O stars form in embedded clusters.

3.1 Introduction

The majority of O stars are found in young star clusters or OB associations. It has been suggested that a small fraction of massive stars may form in isolation as a result of stochastic sampling of the stellar and cluster mass function (see de Wit et al. 2005; Parker & Goodwin 2007; Oey & Lamb 2012). However, in the case of the Galactic field O stars within 2–3 kpc from the Sun, essentially all of them can be traced back to young star clusters or associations (Schilbach & Röser 2008), suggesting the field O stars also formed in clusters (Gvaramadze et al. 2012). Some observational studies on O stars in the Large and Small Magellanic Clouds have claimed there to be evidence for isolated massive star formation (Bressert et al. 2012; Oey et al. 2013), such as e.g. apparent isolation, absence of a bow shock, and circular shape of an H II region. These claims can not, however, be conclusive since they can be explained with slowly moving runaways or former members of clusters which have already dissolved (Weidner et al. 2007). For example, only 30–40% of the Galactic OB runaways are found to have a bow shock (van Buren et al. 1995; Huthoff & Kaper 2002), and, furthermore, bow shock formation depends on the physical condition of the ambient medium through which a runaway travels (e.g. temperature and density of the ambient medium, Huthoff & Kaper 2002). Mackey et al. (2013) showed that runaways can have a circular H 2 region in the projected Hα emission. Furthermore, in the case of the 30 Dor region Bressert et al. considered, there are many young star clusters in the region. If the 30 Dor region is modelled by a population of clusters, how many O stars would be ejected or removed from their clusters in 10 Myr? This has not been investigated. Any conclusion on the issue of isolated O-star formation are, for the time being, thus premature. Finally, measuring stellar proper motions in the Large or Small Magellanic Clouds is unfeasible such that claims for O stars formed in isolation become next to impossible to confirm or reject. With *Gaia*, however, it may become possible to put constraints on this if proper motions of massive stars can be measured to a precision of a few km s^{-1} in the Magellanic Clouds. Given the above results on the well studied ensemble of O stars within 2–3 kpc around the Sun it appears physically more plausible that all O stars form in embedded clusters.

There are two mechanisms to expel O stars from a star cluster. One is the binary supernova scenario (Blaauw 1961; Portegies Zwart 2000; Eldridge et al. 2011) in which a star in a binary obtains a high velocity after the supernova explosion of the initially more massive companion star. The other is dynamical ejection through strong close encounters with other massive stars in the cluster core (Poveda et al. 1967; Leonard & Duncan 1990; Fujii & Portegies Zwart 2011; Banerjee et al. 2012b; Perets & Šubr 2012). Of the candidate isolated O stars catalogued by Schilbach & Röser (2008), 8–9% could not be traced back to any still existing star clusters or associations, but are consistent with originating in a cluster which could not be found due to several effects such as incompleteness of their cluster sample (Schilbach & Röser 2008), dissolution of the cluster (Gvaramadze et al. 2012), and having experienced the two-step-ejection process proposed by Pflamm-Altenburg & Kroupa (2010). The majority of the stars which can be traced back to clusters appear to have been ejected when their parental clusters were very young (Schilbach & Röser 2008). This may suggest that dynamical ejections through few-body interactions in the heavy-star-rich cluster core mainly populate the field O-star population (Clarke & Pringle 1992).

There have been many studies on dynamically ejected massive stars from young star clusters using numerical integrations. In most cases the studies performed few-body scattering experiments focused on runaways, which are ejected with a velocity higher than $\approx$30–40 km s^{-1} (Gualandris et al. 2004;

Pflamm-Altenburg & Kroupa 2006; Gvaramadze et al. 2009; Gvaramadze & Gualandris 2011). Full N-body calculations for a particular cluster mass have also been presented (Banerjee et al. 2012b; Perets & Šubr 2012). Fujii & Portegies Zwart (2011) performed N-body calculations for very dense star clusters composed of single stars with three different cluster masses ($\geq$6000 $M_\odot$) and showed that the clusters with the lowest mass in their models, 6000 $M_\odot$, produce runaways most efficiently. They argued that the one bullying binary formed during core collapse of the cluster is responsible for the production of runaways and that the number of runaways is almost independent of cluster mass. The runaway fraction (number of runaway stars over total number of stars still present) therefore decreases with cluster mass as the more massive clusters have more stars. Note that the lower mass limit for stars in their models is 1 $M_\odot$. Thus, if a cluster is populated with a full range of stellar masses from the hydrogen burning limit upwards, in order to have the same number of massive stars, the cluster would be twice as massive as they claimed. The relation between O-star ejection fraction and cluster mass has not been studied in detail to date.

Here we study for the first time how the dynamical ejection fraction of O stars changes with the masses of very young star clusters using direct N-body calculations with a broad range of cluster masses, from low-mass clusters containing one or two O stars to massive clusters containing a few hundred O stars, and including primordial binaries. Such an investigation based on a very large library of young cluster models has not been possible to date because the knowledge on the properties of initial stellar population, their birth configurations, and, last but not least, the computational algorithms enabling such a CPU-intensive and massive numerical challenge have not been in place. Thus, for example, how to initialize initially a mass segregated cluster in dynamical equilibrium is only known since the work of Šubr et al. (2008) and Baumgardt et al. (2008) and the statistical distribution functions of massive star binaries are becoming observationally constrained only now (e.g. Kiminki & Kobulnicky 2012; Sana et al. 2012, 2013b; Kobulnicky et al. 2014; Aldoretta et al. 2015). The N-body calculations, made possible by the relentless code and algorithmic advances by Sverre Aarseth and Seppo Mikkola, used in this study are briefly described in Section 3.2. The results are presented in Sections 3.3–3.5, and the discussion and summary follow in Sections 3.6 and 3.7, respectively.

3.2 N-body models

The data used in this study are based on the theoretical young star cluster library of model sequences over cluster mass computed by Oh & Kroupa (2012, Chapter 2) with direct N-body calculations using the NBODY6[2] code (Aarseth 2003) and various initial conditions. Among the model sequences in the library, we adopt four sequences here and, further, extend them to higher cluster masses. Additionally we perform calculations for three more sets of initial conditions for this study. Table 3.1 lists properties of the model sequences studied in this chapter. The initial setup of the models is described below.

The four model sequences that we adopt from the library for this study are composed of binary-rich clusters with initial mass segregation (MS3OP) and without initial mass segregation (NMS3OP), single-star clusters (MS3S) with an initial half-mass radius, $r_{\rm h}(0)$, of 0.3 pc, and initially mass-segregated, binary-rich clusters with $r_{\rm h}(0)$ of 0.8 pc (MS8OP).

The cluster masses, $M_{\rm ecl}$, in the library range from 10 to $10^{3.5}$ $M_\odot$ (to 10^4 $M_\odot$ for the MS3OP model

[2] The code can be freely downloaded from `http://www.ast.cam.ac.uk/~sverre/web/pages/nbody.htm`.

Name	$r_{\rm h}(0)$ (pc)	IMS	IBF	IPD	Pairing method
MS3OP	0.3	Yes	1	Kroupa95	OP
NMS3OP	0.3	No	1	Kroupa95	OP
MS3OP_SP	0.3	Yes	1	Sana et al.12	OP
MS3UQ_SP	0.3	Yes	1	Sana et al.12	Uniform q dist.
MS3S	0.3	Yes	0	–	–
MS8OP	0.8	Yes	1	Kroupa95	OP
MS1OP	0.1	Yes	1	Kroupa95	OP

Table 3.1. List of N-body model sequences studied here. Names of model sequences and initial half-mass radii ($r_{\rm h}(0)$) are listed in columns 1 and 2, respectively. Columns 3–6 present initial mass segregation (IMS), initial binary fraction (IBF), and initial period distribution (IPD), and pairing method used for massive binaries (primary mass $\geq 5\,{\rm M}_\odot$).

sequence). For extending the range of cluster masses, we additionally carried out calculations for clusters with $M_{\rm ecl} \approx 10^4$ and $10^{4.5}\,{\rm M}_\odot$ ($M_{\rm ecl} \approx 10^{4.5}\,{\rm M}_\odot$ for the MS3OP model sequence). Individual stellar masses are randomly drawn from the canonical initial mass function (IMF), which is a two-part power-law (Kroupa 2001; Kroupa et al. 2013),

$$\xi(m) = k \begin{cases} \left(\dfrac{m}{0.08}\right)^{-1.3}, & 0.08 \leq m/{\rm M}_\odot < 0.50, \\ \left(\dfrac{0.5}{0.08}\right)^{-1.3} \left(\dfrac{m}{0.5}\right)^{-2.3}, & 0.50 \leq m/{\rm M}_\odot \leq m_{\rm max}. \end{cases} \tag{3.1}$$

More details of our stellar mass sampling can be found in Oh & Kroupa (2012, Chapter 2). The mass of the most massive star in the cluster, $m_{\rm max}$, is chosen from the maximum-stellar-mass–cluster-mass relation (Weidner & Kroupa 2004; Weidner et al. 2010, 2013a, 2014). Thus only clusters with $M_{\rm ecl} \geq 10^{2.5}\,{\rm M}_\odot$ initially have O-type stars in our models. Pflamm-Altenburg et al. (2007) provide a fitting formula for $m_{\rm max}(M_{\rm ecl})$. This procedure was adopted rather than optimal sampling introduced in Kroupa et al. (2013) because the theoretical young cluster library of Oh & Kroupa (2012, Chapter 2) did not have this sampling method available.

Binary-rich models have an initial binary fraction of 100%, i.e. all stars are in a binary system at $t = 0\,{\rm Myr}$. This is motivated by the angular momentum problem of star formation since the angular momentum of a collapsing cloud core can be distributed efficiently into two stars, and also by the strong empirical evidence that star formation universally prefers the binary mode (Goodwin & Kroupa 2005; Duchêne et al. 2007; Goodwin et al. 2007; Marks & Kroupa 2012; Sana et al. 2014; Leigh et al. 2015). The Kroupa (1995b) period distribution function with minimum and maximum periods of 10 and $10^{8.43}$ days, respectively, is adopted for all binaries in the library. The Kroupa period distribution,

$$f_P(\log_{10} P) = 2.5 \frac{\log_{10} P - 1}{45 + (\log_{10} P - 1)^2}, \tag{3.2}$$

where the period (P) is in days, has been derived iteratively using binary-star data from the Galactic field

population and from star-forming regions. With this distribution, about 2.75% of all O-star binaries have a period shorter than 100 days (Fig. 3.1). Although it was derived from binaries with primary star mass $\leq 1\,M_\odot$, the same distribution is used for more massive binaries in the library since no well constrained period distribution of massive binary population was available when the N-body calculations were begun.

However, recently, Sana et al. (2012) derived an intrinsic period distribution of O stars of the form $f_P(\log_{10} P) \propto (\log_{10} P)^{-0.55}$, over the period range of $0.15 < \log_{10}(P/\text{days}) < 3.5$, from spectroscopic observations of O-star populations in nearby young open star clusters. The Sana et al. (2012) period distribution leads to ≈49% of O stars being binaries with a period shorter than 100 days (Fig. 3.1). Here we additionally perform a set of N-body integrations with massive binaries ($m \geq 5\,M_\odot$) having the Sana et al. (2012) period distribution, MS3OP_SP, but with the maximum period extended to the value $\log_{10}(P/\text{days}) \approx 6.7$ at which the cumulative binary fraction becomes unity. We thus adopt the following period distribution function for the massive binaries,

$$f_P(\log_{10} P) = 0.23 \times (\log_{10} P)^{-0.55}, \tag{3.3}$$

for which $\int_{0.15}^{6.7} f_P(\log_{10} P)\, \mathrm{d}\log_{10} P = 1$. The other initial conditions are the same as those of MS3OP. See also Kiminki & Kobulnicky (2012), Kobulnicky et al. (2014) and Aldoretta et al. (2015) for slightly different period distributions of O-star binaries derived from observations.

Stars with a mass $m < 5\,M_\odot$ are randomly paired after choosing the two masses randomly from the IMF. Again, this mass-ratio distribution is derived from the Galactic field population and from star-forming regions (Kroupa 1995a,b). Stars with $m \geq 5\,M_\odot$ are paired to imprint observations that the massive binaries favour massive companions (Pinsonneault & Stanek 2006; Kobulnicky & Fryer 2007; Kiminki & Kobulnicky 2012; Sana et al. 2012). To achieve this we first order all stars more massive than $5\,M_\odot$ in to an array of decreasing mass. The most massive star is then paired with the next massive star, the third most massive star is paired with the fourth most massive star, and so on. We refer to this procedure as ordered pairing (OP). While with this method it is easy to have a massive primary being paired with a massive companion while preserving the IMF, it gives a significant bias toward high mass ratios ($q \approx 1$ where $q = m_2/m_1$ and $m_1 \geq m_2$) which is not supported by recent observations (Kiminki & Kobulnicky 2012; Sana et al. 2012; Kobulnicky et al. 2014). The recent observations show the mass-ratio distribution of O-star binaries to be rather uniform,

$$f(q) \propto q^\eta$$

with $-0.1 \lesssim \eta \lesssim 0.1$ and $0.1 \leq q \leq 1.0$. We add a model sequence (MS3UQ_SP) with a uniform mass-ratio distribution, $\eta = 0$, for massive binaries ($m_1 \geq 5\,M_\odot$), being otherwise the same as the MS3OP_SP model sequence. First, a mass-ratio value for a primary is derived from a uniform probability function and then the secondary is chosen from the rest of the members which gives the closest q value for the derived one. This is important to preserve the IMF: it is important to first generate a full list of stars whose combined mass corresponds to the mass of the cluster and only then to create the binaries using this list only. The thermal distribution is used for the initial eccentricity distribution, i.e. $f_e(e) = 2e$, where e is the eccentricity of a binary (see Kroupa 2008).

Each model sequence has one initial half-mass radius regardless of the cluster mass since by observation there is no significant relation between the size and mass of a cluster (Bastian et al. 2005; Scheepmaker

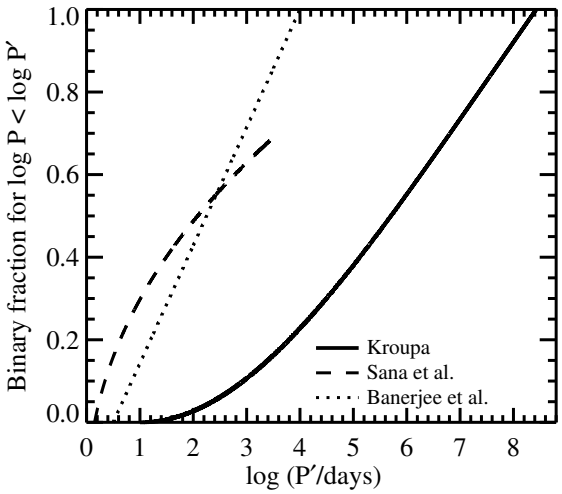

Figure 3.1. Cumulative binary fraction for $\log_{10} P < \log_{10} P'$ among all O stars. Solid and dashed lines are calculated from the Kroupa (1995b, Equation 3.2) and Sana et al. (2012, Equation 3.3) period distributions, respectively. The dotted line is a uniform period distribution with a period range of $0.5 < \log_{10}(P/\mathrm{days}) < 4$ used in Banerjee et al. (2012b) for O-star binaries. For example, 49% of all O-star systems are binaries with period shorter than 100 days according to the Sana et al. distribution.

et al. 2007) or at most only a very weak one (Larsen 2004; Marks & Kroupa 2012). The cluster-mass–initial half-mass radius relation from Marks & Kroupa (2012),

$$(r_{\rm h}(0)\,/\mathrm{pc}) = 0.1 \times (M_{\rm ecl}/\mathrm{M}_\odot)^{0.13},$$

gives initial half-mass radii of ≈0.21–0.38 pc for $M_{\rm ecl} = 10^{2.5}$–$10^{4.5}\,\mathrm{M}_\odot$. Our main, initial half-mass radius (0.3 pc) lies close to the median value and is well consistent with the typical initial half-mass radius (0.1–0.3 pc) inferred for the Milky Way clusters (Marks & Kroupa 2011). Thus, our results may be able to represent reality. Here we include two more model sequences with different half-mass radii of 0.1 and 0.8 pc, MS1OP and MS8OP, respectively. This allows us to estimate how the ejection fraction changes with cluster mass when the cluster radius varies with cluster mass. While the MS8OP model sequence is adopted from the library of Oh & Kroupa (2012, Chapter 2), the MS1OP model sequence is computed for this work. From the choices of half-mass radii, the initial central densities of our models range from ≈300 to $3.3\times10^4\,\mathrm{M}_\odot\,\mathrm{pc}^{-3}$ for $r_{\rm h}(0) = 0.8$ pc clusters, from 6.2×10^3 to $6.2\times10^5\,\mathrm{M}_\odot\,\mathrm{pc}^{-3}$ for $r_{\rm h}(0) = 0.3$ pc clusters, and from $\approx1.7\times10^5\,\mathrm{M}_\odot\,\mathrm{pc}^{-3}$ to $\approx1.7\times10^7\,\mathrm{M}_\odot\,\mathrm{pc}^{-3}$ for $r_{\rm h}(0) = 0.1$ pc clusters.

For all models, initial positions and velocities of single stars or of centres-of-masses of binaries in the clusters are generated following the Plummer density profile under the assumption that the clusters are in virial equilibrium. Initially mass-segregated clusters are produced being fully mass-segregated with the method developed in Baumgardt, De Marchi & Kroupa (2008) in which more massive systems are more bound to the cluster.

The *N*-body code regularises the motions of stars in compact configurations and incorporates a near-neighbour force evaluation scheme to guarantee the high accuracy of the solutions of the equations of motions. Stellar evolution is taken into account by using the stellar evolution library (Hurley et al. 2000, 2002) implemented in the code. All clusters are evolved up to 3 Myr, i.e. to a time before the first

supernova occurs, in order to study dynamical ejections only. Moreover the dynamical ejections of O stars are most efficient at an early age of the cluster (Oh & Kroupa 2016, see also Section 3.5), thus computations to an older cluster age would not change our conclusion on the dynamical ejections.

A standard solar-neighbourhood tidal field is adopted. The clusters are highly tidally underfilling such that the tidal field of the hosting galaxy plays no significant role for the results presented here. Our cluster models are initially gas-free, i.e. without a background gas-potential, and thus the gas-expulsion phase is not included here. While 100 realizations with different random seed numbers are performed for the clusters with $M_{\rm ecl} \leq 10^{3.5}\,{\rm M}_\odot$, 10 and 4 realizations are carried out for $M_{\rm ecl} = 10^4$ and $10^{4.5}\,{\rm M}_\odot$ clusters, respectively, as computational costs increase with the number of stars, i.e. cluster mass, and stochastic effects are reduced with a larger number of stars.

3.3 Ejection fraction of O stars as a function of $M_{\rm ecl}$

Throughout this study, an O star refers to a star with a mass of $\geq$17.5 $\rm M_\odot$ at 3 Myr and an O-star system is either a single O star or a binary system having at least one O-star component. *We regard a system as being ejected when its distance from the cluster centre is greater than* $3 \times r_{\rm h}$ *of the cluster at 3 Myr, and its velocity is larger than the escape velocity at that radius.* Such a short distance criterion for ejections is an appropriate physical condition to quantify the real ejected O-star fraction, in order to account for the O stars which have been dynamically ejected but have not travelled far from the cluster centre by 3 Myr. O stars can be ejected with a velocity of a few $\rm km\,s^{-1}$ from the lower-mass clusters, e.g. the central escape velocity of a cluster with $M_{\rm ecl} = 1000\,{\rm M}_\odot$ and an half-mass radius $r_{\rm h} = 0.3$ pc is $\approx$6 $\rm km\,s^{-1}$.

From the computational data the ejection fraction of O-star systems, ${}^{\rm com}f_{\rm ej,O}$, is defined as the number ratio of the ejected O-star systems, ${}^{\rm com}N_{\rm ej,O}$, to all O-star systems that are still present in a calculation, ${}^{\rm com}N_{\rm O}$, i.e.

$$ {}^{\rm com}f_{\rm ej,O} = \frac{{}^{\rm com}N_{\rm ej,O}}{{}^{\rm com}N_{\rm O}}. $$

Only clusters with $M_{\rm ecl} \geq 10^{2.5}\,{\rm M}_\odot$ are shown in the tables because clusters with $M_{\rm ecl} \leq 100\,{\rm M}_\odot$ do not have an O star in our models. Since values of ${}^{\rm com}f_{\rm ej,O}$ from individual clusters are diverse, especially for low-mass clusters, we mainly deal with the averaged value of ${}^{\rm com}f_{\rm ej,O}$, $\langle {}^{\rm com}f_{\rm ej,O}\rangle$, for the same cluster mass in a certain set of initial conditions.

The average ejection fractions of O-star systems for all models are shown in Fig. 3.2. Table B.1 lists averaged properties of the models, such as half-mass radius, number of O-star systems, number of ejected O-star systems, O-star ejection fraction, and O-star binary fraction in the clusters and among the ejected O-star systems, at 3 Myr. All models show a trend that $\langle {}^{\rm com}f_{\rm ej,O}\rangle$ increases with cluster mass up to $10^{3.5}\,{\rm M}_\odot$ and then decreases for a higher cluster mass. The average values of the ejection fraction with the same cluster mass vary from model to model. The peak fractions are $\approx$25% for the binary-rich cluster models with $r_{\rm h}(0) = 0.3$ pc with a weak dependency on initial mass segregation or on the initial period distribution of massive binaries, although the $\langle {}^{\rm com}f_{\rm ej,O}\rangle$ values of the other cluster masses change with the initial conditions. *Note that individual clusters in the mass range* $10^{2.5}$–$10^{3.5}\,{\rm M}_\odot$ *may eject all their O-star systems!*

The ejection fractions from the initially not mass-segregated models (NMS3OP) exhibit similar results to the MS3OP models. The difference between the two models is only seen at the lowest cluster mass,

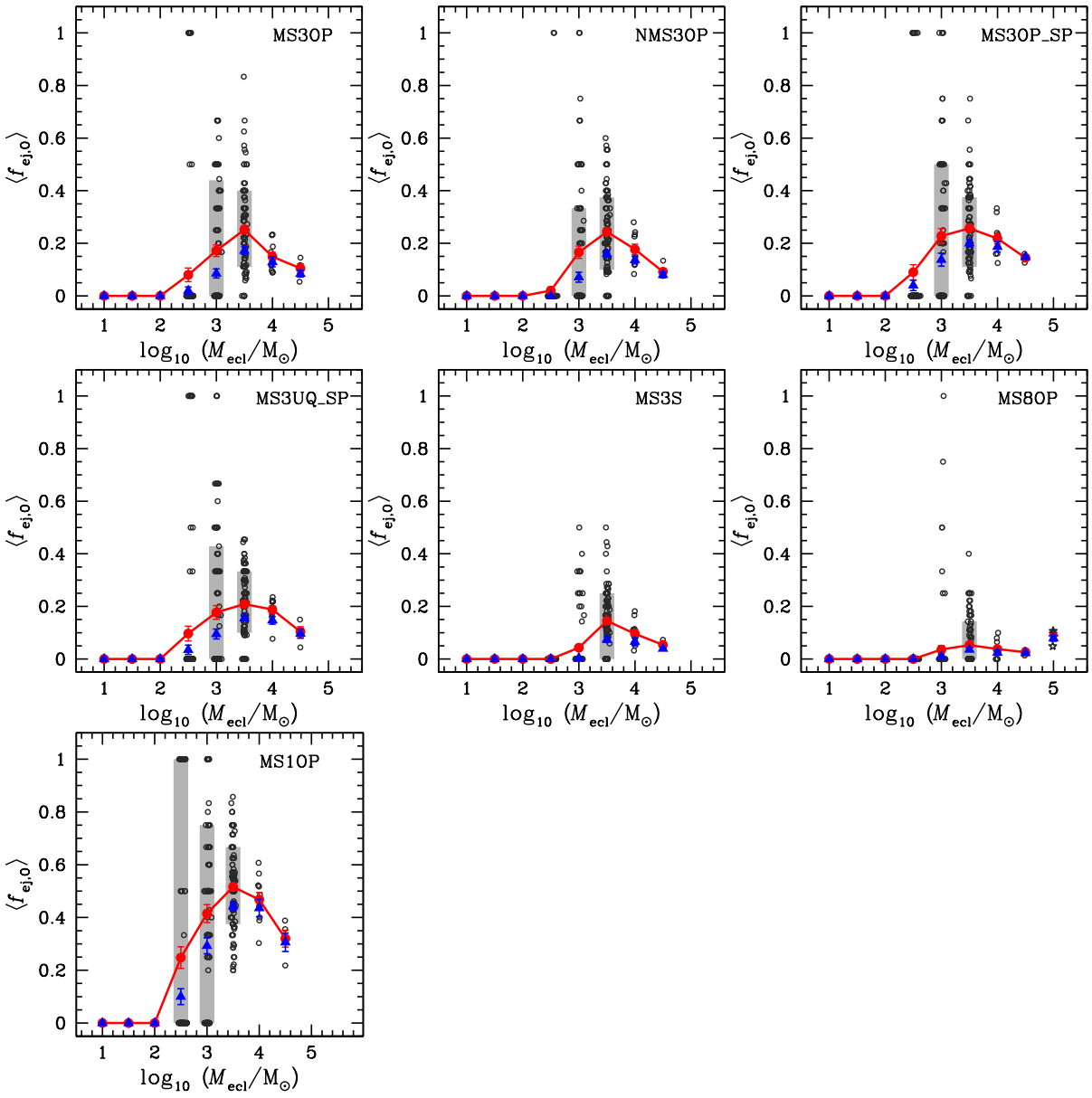

Figure 3.2. Ejection fraction of O-star systems as a function of cluster mass at 3 Myr. Red big circles are the average O-star ejection fraction for each cluster mass and open circles are the values of individual clusters. The (red) solid lines are drawn by connecting the red points to guide the dependency of the ejection fraction on the cluster mass. Grey vertical bars indicate where the central 68% of the data points lie (i.e. the points between 17 (lower) and 84 (upper) percentiles) for 10^3 and $10^{3.5}$ $M_\odot$ cluster models (for the MS1OP sequence $10^{2.5}$ $M_\odot$ clusters are included). Because more than 85% of clusters with $M_{ecl} = 10^{2.5}$ $M_\odot$ in each sequence except for clusters in the MS1OP sequence do not eject any O star, the grey bar is not plotted for this cluster mass with the exception for the MS1OP sequence. For more than 50% of the 10^3 $M_\odot$ clusters of all sequences, except for the MS1OP sequence for which only 30% of the cases, the O-star ejection fraction is 0. Due to their small number of realizations and small spread of the ejection fraction, the grey bar is not necessary for clusters with $M_{ecl} \geq 10^4$ $M_\odot$. Blue triangles are the average O-star ejection fraction using 10 pc for the ejection criterion without applying a velocity criterion. The data for the 10^5 $M_\odot$ cluster model taken from the calculations by Banerjee et al. (2012b) are marked with open stars in the MS8OP model sequence panel.

$10^{2.5}\,M_\odot$. This can be understood because dynamical mass segregation is inefficient for the lowest mass clusters due to their low density. *Initial mass segregation therefore does not have a significant impact on massive-star ejections.*

In the models using the Sana et al. (2012) period distribution (MS3OP_SP and MS3UQ_SP), the same trend of the O-star ejection fraction is present as above, but the $\langle {}^{\rm com}f_{\rm ej,O}\rangle$ values show a much broader peak than those in the model using the Kroupa (1995b) period distribution (MS3OP). The $\langle {}^{\rm com}N_{\rm ej,O}\rangle$ values of the three models are similar (see Table B.1). However, for massive clusters ($M_{\rm ecl} > 10^{3.5}\,M_\odot$), MS3OP_SP clusters not only have a smaller number of O-star systems near 3 Myr due to a higher fraction of binaries and mergers, but they also eject more O-star systems. The latter suggests that short period massive binaries are dynamically active and boost the ejection of O stars, especially for massive clusters.

The numbers of O-star systems are slightly higher in the MS3UQ_SP sequence than in the MS3OP_SP sequence (see Table B.1) because O-star binaries in the MS3OP_SP models mostly have an O star companion while companions of O-star binaries in the MS3UQ_SP models are chosen from a broader range of stellar masses. For example, when the binary fraction is unity and both sequences have the same number of individual O stars, for the MS3OP_SP sequence the number of O-star systems would be almost half of the number of individual O stars while it would larger than half in the case of the MS3UQ_SP sequence. However, the difference in the mass-ratio distributions of the two model sequences does not seem to affect the trend of the O-star ejection fraction as a function of cluster mass, having a peak at $M_{\rm ecl} = 10^{3.5}\,M_\odot$. The difference between the results of the MS3OP_SP and MS3UQ_SP models is only marginal. *Therefore, massive star ejections are not sensitive to the form of the mass-ratio distribution as long as they are paired with other massive stars, i.e.* $q > 0.1$.

For single-star clusters (MS3S), we find the same cluster mass at which the peak of the O-star ejection fraction occurs although the ejection fractions are about half those of the binary-rich model sequences. The peak appears at the same cluster mass in the sequences with different initial cluster sizes. In the case of MS8OP ($r_{\rm h}(0) = 0.8\,$pc), the ejection fraction is much smaller than in other model sequences with $r_{\rm h}(0) = 0.3\,$pc. But $\langle {}^{\rm com}f_{\rm ej,O}\rangle$ reaches ≈50% in the MS1OP model sequence ($r_{\rm h}(0) = 0.1\,$pc) at the cluster mass of the peak. *The dependency of the ejection fraction on cluster mass is thus independent of the initial cluster size, but more compact cluster do have higher ejection fractions of massive stars.*

The peak near $10^{3.5}\,M_\odot$ of the ejection fraction can be understood as a consequence of the growth of the number of O stars with cluster mass surpassing the number of ejected O stars as the cluster mass increases and the potential smoothens. Figure 3.3 shows the average number of ejected O stars at each cluster mass.

This implies that clusters a few Myr old with a mass at which the O-star ejection fraction peaks would present O-star populations most deviating from the number of O stars given by the canonical IMF. For example the estimated stellar mass in the inner 2 pc of the Orion Nebula Cluster (ONC) is ≈1800 $M_\odot$ (Hillenbrand & Hartmann 1998) and probably ≈2700 $M_\odot$ taking account of a probable binary fraction of 50% (Kroupa 2000). With these cluster masses, about 6–10 stars are expected to have a mass larger than 18 $M_\odot$ from the canonical IMF. However, only three O-type (or $m \geq 17.5\,M_\odot$) stars are found within ≈2 pc of the Trapezium stars (Hillenbrand 1997). This discrepancy may be due to the stochastic sampling of the IMF. But the probability for this is less than 5% when stellar masses are randomly drawn from the IMF with a stellar upper mass limit of 150 $M_\odot$ (but about 10% with $m_{\rm max} = 50\,M_\odot$) such that it is more likely that the ONC has ejected a significant fraction of its O-star content. Furthermore, the initial

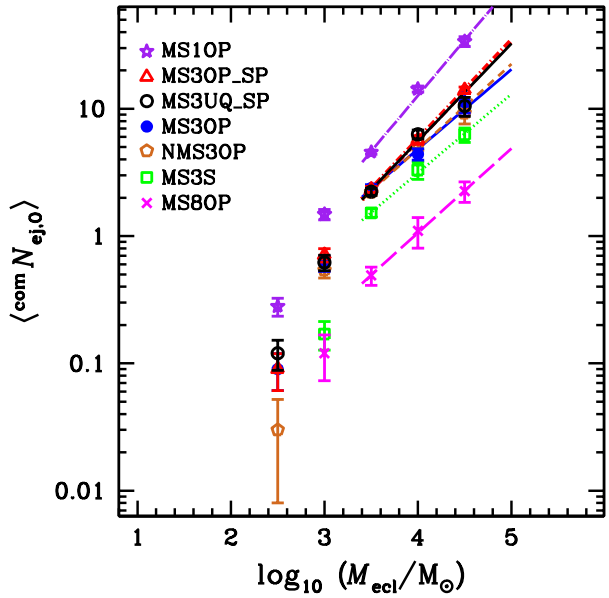

Figure 3.3. The average number of ejected O-star systems, $\langle {}^{\rm com}N_{\rm ej,O}\rangle$, as a function of cluster mass. Lines are linear fits to $\langle {}^{\rm com}N_{\rm ej,O}\rangle$ with cluster mass between $10^{3.5}$ and $10^{4.5}$ $M_\odot$ (Equation 3.11).

mass of the cluster may have been higher than observed at the present day as the cluster could have lost a significant fraction of its members during the residual gas-expulsion phase (Kroupa et al. 2001). Thus the ONC formed with a mass close to the peak mass we found in this study and could have lost a significant fraction of its massive stars through the dynamical ejection process. This may explain why the ONC's massive star population deviates from the canonical IMF (Pflamm-Altenburg & Kroupa 2006). Examples of such events would be two O-type single runaway stars, AE Aur and μ Col, and a massive binary system ι Ori which may have been ejected from the ONC through a binary–binary interaction (Gies & Bolton 1986; Hoogerwerf et al. 2001; Gualandris et al. 2004). Future proper motion surveys, such as with the *Gaia* mission, may provide further constraints on this question, because the putative ejected O stars from the ONC would have to become evident.

Very massive clusters may have small ejection fractions of O stars but the upper end of their stellar mass range could lack stars because the ejection fraction of stars more massive than 100 $M_\odot$ can be from ≈10 to ≈100% (Banerjee et al. 2012b). Furthermore, they can eject not only very massive single stars but also very massive binaries (Oh et al. 2014). This bias through the most massive stars being ejected from star-burst clusters and the observed IMF of star-burst clusters being close to the canonical value (e.g. the R136 cluster in the Large Magellanic Cloud, Massey & Hunter 1998) may imply the IMF to be top-heavy in star-burst clusters (Banerjee & Kroupa 2012). There is some evidence for a possibly systematically varying IMF above a few $M_\odot$: a number of independent arguments have shown the IMF to become increasingly top-heavy with increasing star-formation rate density on a pc scale (Marks et al. 2012), with a dependency on the metallicity. This metallicity dependence is such that metal-rich environments tend to produce a steeper (i.e. top-light) IMF slope. Evidence for this may have emerged in M31 data (Weisz et al. 2015). The models calculated here are, however, in the invariant regime.

A theoretically expected relation between the ejection fraction and the cluster mass can be found. First,

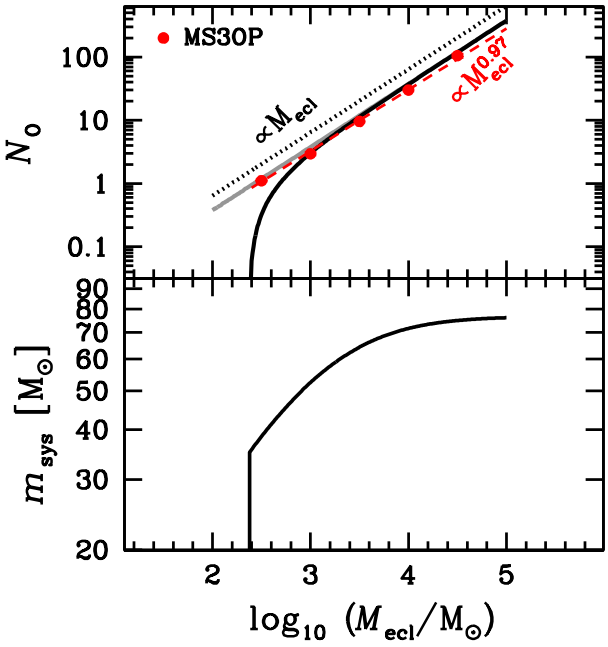

Figure 3.4. Top: number of O stars in a cluster calculated using the IMF, $N_{\rm O,IMF}$ (Equation 3.4, solid line). The dotted line indicates $N_{\rm O} \propto M_{\rm ecl}$. Red filled circles present the average number of O-star systems from N-body calculations, $\langle {}^{\rm com}N_{\rm O}\rangle$, in the MS3OP model sequence. A red dashed line indicates $\langle {}^{\rm com}N_{\rm O}\rangle \propto M_{\rm ecl}^{0.97}$ obtained by a linear fit of $\log_{10}\langle {}^{\rm com}N_{\rm O}\rangle$–$\log_{10} M_{\rm ecl}$ to the MS3OP model sequence. The other model sequences have almost the same slopes as the MS3OP model sequence (Equation 3.5). The grey solid line is the number of O stars derived from the IMF with the universal upper mass limit of 150 M$_\odot$. Bottom: assumed system mass of an O-star binary, $m_{\rm sys}$. The values are twice the average O-star mass in a cluster calculated from the IMF (Equation 3.1). Here we assumed that an O-star binary is an equal mass binary. Although the mass-ratio distribution of O-star binaries is close to a uniform distribution for $q > 0.1$ in observations (Sana et al. 2012), our assumption is sufficient to show the dependence of the average system mass of O-star binaries on cluster mass.

the number of O stars in a cluster, $N_{\rm O,IMF}$, which is a function of $m_{\rm max}(M_{\rm ecl})$ and $M_{\rm ecl}$, is

$$\begin{aligned} N_{\rm O,IMF} &= \int_{17.5\,{\rm M}_\odot}^{m_{\rm max}(M_{\rm ecl})} \xi(m)\,{\rm d}m, \\ &\approx \frac{3.390\times10^{-4} - 0.014 m_{\rm max}^{-1.3}}{0.100 - 0.062 m_{\rm max}^{-0.3}} M_{\rm ecl}, \end{aligned} \tag{3.4}$$

by using the IMF (Equation 3.1). The normalisation constant, k, in Equation (3.1) is calculated from $M_{\rm ecl} = \int_{0.08\,{\rm M}_\odot}^{m_{\rm max}} m\xi(m)\,{\rm d}m$. The top panel of Fig. 3.4 presents $N_{\rm O,IMF}$ as a function of $M_{\rm ecl}$ from Equation (3.4). Since we adopt the $m_{\rm max}$–$M_{\rm ecl}$ relation, Equation (3.4) is not a simple linear function of cluster mass especially for low-mass clusters in which $m_{\rm max}$ is highly dependent on the cluster mass. $N_{\rm O,IMF}$, however, becomes almost linearly proportional to $M_{\rm ecl}$ for massive clusters where $m_{\rm max}$ is saturated (see the upper panel of Fig. 3.4). Note that the solid line in the upper panel of Fig. 3.4 and the numbers in Table B.1 are slightly different because Equation (3.4) gives the number of all *individual* O stars from the IMF, whereas $\langle {}^{\rm com}N_{\rm O}\rangle$ listed in Table B.1 is the number of O star *systems* at 3 Myr. The difference between the number of O stars from the IMF, $N_{\rm O,IMF}$, and from our N-body calculations,

$\langle {}^{\rm com}N_{\rm O}\rangle$, at the cluster mass of $10^{2.5}\,{\rm M}_\odot$ in Fig. 3.4 arises due to our choice of forcing a cluster to have at least one $m_{\rm max}$ star initially. This would not have been required if optimal sampling (Kroupa et al. 2013) had been available when the theoretical young star cluster library was computed pre-2013.

Our stellar masses are randomly drawn from the IMF with the upper mass limit given by the $m_{\rm max}$–$M_{\rm ecl}$ relation. Therefore, our sampling would produce a slightly lower maximum stellar mass in a cluster but a similar number of O stars compared to what random sampling without the $m_{\rm max}$–$M_{\rm ecl}$ relation would give. The grey line in the upper panel of Fig. 3.4 is the expected number of O stars from the IMF with a universal upper stellar mass limit of $150\,{\rm M}_\odot$ for all cluster masses. The figure indicates that a higher number of O stars is expected in the IMF with a universal and constant $m_{\rm max} = 150\,{\rm M}_\odot$ than with the $m_{\rm max}$–$M_{\rm ecl}$ relation at lower cluster mass ($M_{\rm ecl} \lesssim$ a few $1000\,{\rm M}_\odot$, the black solid line in the same figure). But the values of $\langle {}^{\rm com}N_{\rm O}\rangle$ in our N-body models are close to the grey line because of adding one $m_{\rm max}(M_{\rm ecl})$ star in a cluster of mass $M_{\rm ecl}$ by default. So whether adopting the relation or not would have little effect on the number of O stars in our models. The proper comparison for outcomes of the two assumptions ($m_{\rm max} = 150\,{\rm M}_\odot$ or the $m_{\rm max}$–$M_{\rm ecl}$ relation) can be done by performing a large set of Monte Carlo calculations. However, it is beyond the objectives of this study. In any case, the $m_{\rm max}$–$M_{\rm ecl}$ relation is observationally well supported for young star clusters and star-forming regions in the Milky Way given the most recent data (Kirk & Myers 2011; Weidner et al. 2013a).

Fitting the number of O-star systems present, regardless of whether the systems are in the star cluster or ejected, in N-body calculations at 3 Myr to a simple power law gives,

$$\langle {}^{\rm com}N_{\rm O}\rangle \propto \begin{cases} M_{\rm ecl}^{0.97\pm0.01}, & \text{MS3OP,} \\ M_{\rm ecl}^{0.96\pm0.01}, & \text{NMS3OP,} \\ M_{\rm ecl}^{0.96\pm0.01}, & \text{MS3OP\_SP,} \\ M_{\rm ecl}^{0.96\pm0.01}, & \text{MS3UQ\_SP,} \\ M_{\rm ecl}^{1.01\pm0.01}, & \text{MS3S,} \\ M_{\rm ecl}^{0.95\pm0.01}, & \text{MS8OP,} \\ M_{\rm ecl}^{1.00\pm0.01}, & \text{MS1OP.} \end{cases} \tag{3.5}$$

The numbers of O-star systems in all model sequences are more or less linearly proportional to the cluster mass as expected from the IMF despite various binary fractions.

Next, the relation between the number of ejected O stars and cluster mass is needed. According to Verbunt (2003), the binary–single star scattering encounter rate, Γ, is

$$\Gamma \propto \frac{\rho_0^2 r_{\rm c}^3}{\sigma_{\rm cl}} a, \tag{3.6}$$

where ρ_0 is the central mass density, $\sigma_{\rm cl}$ the velocity dispersion of the cluster, $r_{\rm c}$ the core radius, and a the semi-major axis of the binary. The semi-major axis can be replaced with the system mass, $m_{\rm sys}$, and the orbital velocity, $v_{\rm orb}$, of the binary by using equation (8.142) in Kroupa (2008) as,

$$a \propto m_{\rm sys} v_{\rm orb}^{-2}. \tag{3.7}$$

Considering that binaries with a circular velocity similar to the velocity dispersion of the cluster are dynamically the most active (i.e. $v_{\rm orb} = \sigma_{\rm cl}$) and $\sigma_{\rm cl} \propto \sqrt{\rho_0} r_{\rm c}$, Equation (3.6) becomes

$$\Gamma \propto \rho_0^{0.5} m_{\rm sys} \propto M_{\rm ecl}^{0.5} m_{\rm sys}, \tag{3.8}$$

since all our cluster models in a given sequence have the same initial half-mass radius so the initial central density is only proportional to the cluster mass. A binary ejecting an O star after a strong interaction with a single star is likely a binary consisting of O stars since the least massive star is generally ejected after a close encounter between a binary and a single star. Therefore, $m_{\rm sys}$ can be approximated to twice the average mass of O stars in a cluster. We assume,

$$\begin{aligned} m_{\rm sys} &= 2 \times \langle m_{\geq 17.5 {\rm M}_\odot} \rangle = 2 \frac{\int_{17.5}^{m_{\rm max}} m \xi(m)\, {\rm d}m}{\int_{17.5}^{m_{\rm max}} \xi(m)\, {\rm d}m} \\ &\approx 8.66 \frac{m_{\rm max}^{-0.3} - 0.42}{m_{\rm max}^{-1.3} - 0.02}, \end{aligned} \tag{3.9}$$

using the IMF (Equation 3.1). Thus $m_{\rm sys}$ is a function of $m_{\rm max}$ so that $m_{\rm sys} = m_{\rm sys}(m_{\rm max})$. Due to the $m_{\rm max}$–$M_{\rm ecl}$ relation, $m_{\rm sys}$ is thus a function of the cluster mass (the lower panel of Fig. 3.4).

The number of ejections is proportional to the encounter rate,

$${}^{\rm th}N_{\rm ej,O} \propto \Gamma \propto m_{\rm sys}(m_{\rm max}) M_{\rm ecl}^{0.5}. \tag{3.10}$$

The $m_{\rm max}$–$M_{\rm ecl}$ relation has only a minor effect on the number of ejected O stars for the massive clusters, i.e. the dependence of $m_{\rm sys}$ on $M_{\rm ecl}$ becomes negligible in Equation (3.10). ${}^{\rm th}N_{\rm ej,O}$ is thus expected to be proportional to $M_{\rm ecl}^{0.5}$ for the massive clusters. We fit $\langle {}^{\rm com}N_{\rm ej,O} \rangle$ as a power law of cluster mass for clusters with $10^{3.5} \leq M_{\rm ecl}/{\rm M}_\odot \leq 10^{4.5}$ (Fig. 3.3). These fits provide for each model sequence,

$$\langle {}^{\rm com}N_{\rm ej,O} \rangle \propto \begin{cases} M_{\rm ecl}^{0.63\pm0.066}, & \text{MS3OP}, \\ M_{\rm ecl}^{0.67\pm0.066}, & \text{NMS3OP}, \\ M_{\rm ecl}^{0.78\pm0.034}, & \text{MS3OP\_SP}, \\ M_{\rm ecl}^{0.76\pm0.061}, & \text{MS3UQ\_SP}, \\ M_{\rm ecl}^{0.62\pm0.061}, & \text{MS3S}, \\ M_{\rm ecl}^{0.66\pm0.100}, & \text{MS8OP}, \\ M_{\rm ecl}^{0.87\pm0.100}, & \text{MS1OP}. \end{cases} \tag{3.11}$$

All model sequences but MS3OP_SP, MS3UQ_SP, and MS1OP exhibit slopes similar to each other within an error, in a range of 0.62–0.67. The power-law exponents we obtain from our N-body models are slightly steeper than 0.5 in Equation (3.10) but with only a marginal difference. It can be argued that this is due to a broad range of binary parameters for which binaries could have engaged in the ejection of O stars in our models and the complexity of the few-body scattering process. The model sequences MS3OP_SP and MS3UQ_SP show steeper slopes, i.e. the more massive clusters in these

model sequences eject O stars more efficiently compared to other models. As the model sequence MS1OP begins with an extreme density the results of the model significantly deviate from the simplified theoretical expectation with simple approximations.

Finally, the theoretically expected ejection fraction of O stars is

$$^{\rm th}f_{\rm ej,O} = \frac{^{\rm th}N_{\rm ej,O}}{N_{\rm O,IMF}} \propto F(m_{\rm max})\, M_{\rm ecl}^{-0.5}, \tag{3.12}$$

where $F(m_{\rm max})$ comes from the part of Equations (3.4) and (3.10) in which $m_{\rm max}$ plays a role. For massive clusters ($M_{\rm ecl} \geq 10^{3.5}\,{\rm M}_\odot$), $F(m_{\rm max})$ in Equation (3.12) becomes very weakly dependent on the cluster mass as in Equation (3.10), and thus this term can be ignored. Therefore, $^{\rm th}f_{\rm ej,O}$ is expected to be proportional to $M_{\rm ecl}^{-0.5}$ in this cluster mass regime. Figure 3.5 shows the linear fits to the O-star ejection fractions as a function of cluster mass for the massive clusters ($10^{3.5} \leq M_{\rm ecl}/{\rm M}_\odot \leq 10^{4.5}$) in a log–log scale. Within a cluster mass range $10^{3.5}$–$10^{4.5}\,{\rm M}_\odot$, the numerical data suggest the relation between O-star ejection fraction and cluster mass as follows,

$$\langle ^{\rm com}f_{\rm ej,O}\rangle \propto \begin{cases} M_{\rm ecl}^{-0.40\pm0.064}, & \text{MS3OP,} \\ M_{\rm ecl}^{-0.40\pm0.055}, & \text{NMS3OP,} \\ M_{\rm ecl}^{-0.25\pm0.029}, & \text{MS3OP\_SP,} \\ M_{\rm ecl}^{-0.20\pm0.060}, & \text{MS3UQ\_SP,} \\ M_{\rm ecl}^{-0.43\pm0.055}, & \text{MS3S,} \\ M_{\rm ecl}^{-0.31\pm0.094}, & \text{MS8OP,} \\ M_{\rm ecl}^{-0.16\pm0.036}, & \text{MS1OP.} \end{cases} \tag{3.13}$$

The results of most models are reasonably consistent with the relation between the ejection fraction and cluster mass expected from the binary–single star scattering encounter rate (Equation 3.12) when applied to massive clusters in which the maximum stellar mass is less sensitive to cluster mass.

For lower mass clusters, the number of O stars in a cluster and the ejection rate do not simply follow from the above equations due to the dependency of $m_{\rm max}$ on the cluster mass and the highly collisional nature of the cluster cores which contain but a few O stars.

The ejection fractions from individual clusters are plotted with open circles in Fig. 3.2. For lower mass clusters the O-star ejection fraction varies largely from one cluster to another, e.g. the values spread from 0 to 1 for clusters with $M_{\rm ecl} \leq 10^{3.5}\,{\rm M}_\odot$. The spread gets smaller with increasing cluster mass as the stochastic effect diminishes with a larger number of O stars in more massive clusters. For massive clusters ($M_{\rm ecl} \geq 10^4\,{\rm M}_\odot$) the individual ejection fractions mostly lie close to the average value.

Only for a comparison, we additionally show results using 10 pc as the ejection criterion in Fig. 3.2 (without a constraint on the velocity of the stars) since a larger distance criterion is more appropriate from an observational point of view. The ejection fractions using 10 pc as a distance criterion show a similar shape and the peak at the same cluster mass, only the values are smaller (max. up to ≈17 % for clusters with $r_{\rm h}(0) = 0.3$ pc) than the results using our main ejection criteria. The difference becomes smaller or almost disappears for the massive clusters. Massive clusters may eject O stars most efficiently at earlier time of the evolution due to their short dynamical (i.e. crossing) timescale, and soon their ejection

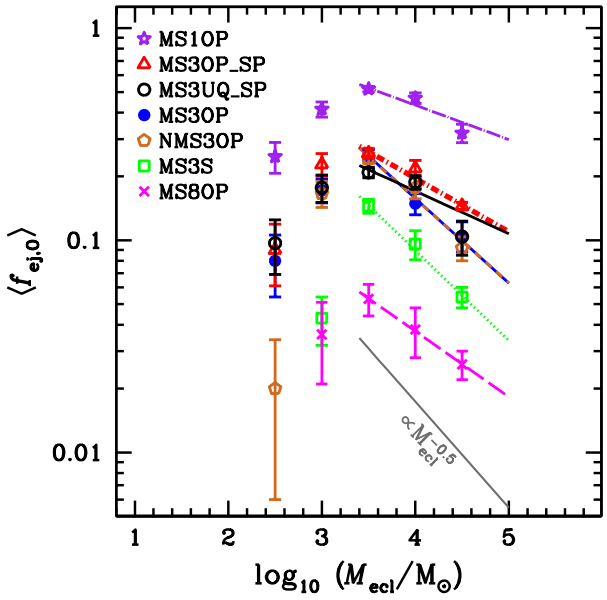

Figure 3.5. The average ejection fraction of O-star systems. Lines are linear fits of the average ejection fraction from the clusters with $M_{\rm ecl} = 10^{3.5}$–$10^{4.5}$ $M_\odot$ (Equation 3.13). The grey solid line shows the relation ${}^{\rm th}f_{\rm ej,O} \propto M_{\rm ecl}^{-0.5}$.

efficiency would drop as the O-star population is reduced in the core of the cluster. Also, in the massive clusters the velocity of the ejected systems is generally high (see Section 3.5.1) so they quickly move further than 10 pc away from the cluster centre. Low-mass clusters have longer dynamical times-scales and they eject O stars moving relatively slowly so that they need more time to reach a distance of 10 pc.

3.4 Field O stars from dynamical ejection processes

Our N-body results show that $\log_{10}\langle {}^{\rm com}N_{\rm ej,O}\rangle$ steeply increases with $\log_{10} M_{\rm ecl}$ at a lower cluster-mass range ($M_{\rm ecl} < 10^{3.5}$ $M_\odot$) while it can be approximated to a linear function of $\log_{10} M_{\rm ecl}$ at a higher cluster-mass range. In the previous section, we use data only from the clusters with $10^{3.5}$ $M_\odot \leq M_{\rm ecl} \leq 10^{4.5}$ $M_\odot$ to fit a linear relation between $\log_{10}\langle {}^{\rm com}N_{\rm ej,O}\rangle$ and $\log_{10} M_{\rm ecl}$ (Fig. 3.3). In order to fit the number of ejected O stars for the entire cluster mass range in which $\langle {}^{\rm com}N_{\rm ej,O}\rangle$ is > 0, we use the following functional form,

$$\log_{10} y = a + b \log_{10} x - \frac{1}{(\log_{10} x - \log_{10} x_0)^n}, \tag{3.14}$$

where $x > x_0$, $y = \langle {}^{\rm com}N_{\rm ej,O}\rangle$, and $x = M_{\rm ecl}/M_\odot$. In this function, $\log_{10} y$ converges to $-\infty$ for $x \to x_0$ and approximates a linear function, $a + b \log_{10} x$, for $x \gg x_0$. This function can thus be fitted to our results. The value x_0 indicates the cluster mass where the y value, i.e. $\langle {}^{\rm com}N_{\rm ej,O}\rangle$, $\approx$0. For all models but MS3S and MS8OP, we choose $x_0 = 240$ $M_\odot$ which is the maximum cluster mass at which clusters do not host single O stars initially, as given by the $m_{\rm max}$–$M_{\rm ecl}$ relation. For the other two models we choose $x_0 = 10^{2.5}$ $M_\odot$, at which mass a cluster contains O stars but $\langle {}^{\rm com}N_{\rm ej,O}\rangle$ is 0 in the N-body calculations. By performing nonlinear least squares fitting of Equation (3.14) to our results, we obtain the parameters listed in Table 3.2 and plot the results in Fig. 3.6.

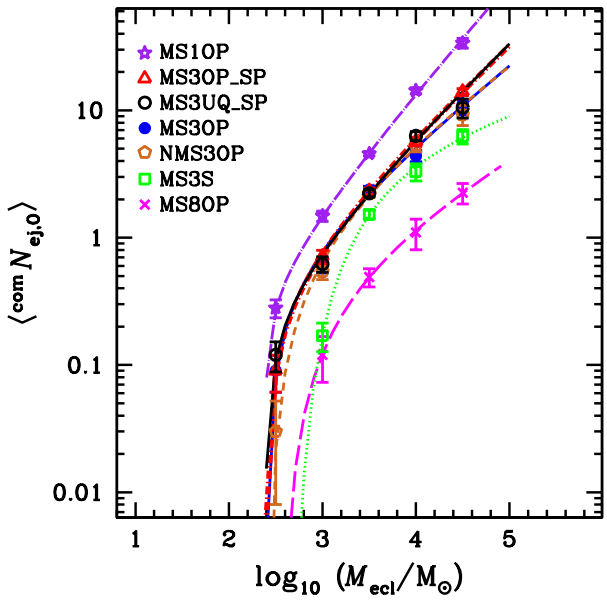

Figure 3.6. Fitting function for $\langle {}^{com}N_{ej,O} \rangle$ (Equation 3.14 and Table 3.2). The symbols and line styles are the same as in Fig. 3.3.

Model	a	b	n
MS3OP	-0.56 ± 0.25	0.53 ± 0.07	0.29 ± 0.04
NMS3OP	-0.43 ± 0.25	0.49 ± 0.07	0.42 ± 0.05
MS3OP_SP	-0.91 ± 0.16	0.64 ± 0.04	0.26 ± 0.04
MS3UQ_SP	-1.04 ± 0.25	0.67 ± 0.07	0.22 ± 0.04
MS3S	0.67 ± 0.32	0.14 ± 0.08	0.90 ± 0.10
MS8OP	-0.60 ± 0.01	0.37 ± 0.003	0.51 ± 0.03
MS1OP	-1.17 ± 0.16	0.80 ± 0.05	0.16 ± 0.03

Table 3.2. Parameters by fitting Equation (3.14) for all models.

The mass distribution of young star clusters can be described with a simple power law,

$$\xi_{\rm ecl}(M_{\rm ecl}) = k_{\rm ecl}\, M_{\rm ecl}^{-\beta}, \tag{3.15}$$

where the normalisation constant $k_{\rm ecl}$ is calculated from the total mass of all clusters which form within a certain time. Assuming a global Milky Way star formation rate (SFR) of $3\,{\rm M}_\odot\,{\rm yr}^{-1}$, a minimum cluster mass $M_{\rm ecl,min} = 10\,{\rm M}_\odot$, and $\beta = 2$ for the Milky Way, the maximum cluster mass, $M_{\rm ecl,max}$, that can form in the Galaxy becomes $\approx 1.9 \times 10^5\,{\rm M}_\odot$ (Weidner et al. 2004; Marks & Kroupa 2011, and references therein). The total mass formed in stars over time δt, $M_{\rm SCS}$, is

$$M_{\rm SCS} = {\rm SFR} \times \delta t = \int_{M_{\rm ecl,min}}^{M_{\rm ecl,max}} M_{\rm ecl}\, \xi_{\rm ecl}(M_{\rm ecl})\, {\rm d}M_{\rm ecl} \tag{3.16}$$

where δt is the cluster-population formation timescale, about 10 Myr (Weidner et al. 2004). We adopt here the $M_{\rm ecl,max}$–SFR relation derived by Weidner et al. (2004), i.e. the mass of the most massive forming cluster is dependent on the physical properties of the star-formation environment provided by a self-regulated galaxy. It has been found that the luminosity of the brightest cluster increases with the galaxy-wide SFR (Larsen 2002, and references therein) or with the total number of clusters (Whitmore 2003). The relation is treated to be the result of the size of the sample in several studies (Whitmore 2003; see also section 2.4 of Portegies Zwart et al. 2010, and references therein). Recently, Pflamm-Altenburg et al. (2013) ruled out that the relation results from the pure size-of-sample effect by studying a radial dependancy of maximum star cluster masses in M33. Randriamanakoto et al. (2013) confirm this by studying the $M_{\rm ecl,max}$ versus SFR relation in their independent observational survey. The authors noted that their result can be explained with purely random sampling but only if the luminosity function of super star clusters at the bright end is very steep (a slope >2.5), steeper than usually observed (≈2).

By combining the fitting function for the number of ejected O stars (Equation 3.14) with the cluster mass function (Equation 3.15), the number of O stars being ejected to the field contributed by clusters in the mass range $M_{\rm ecl}$ to $M_{\rm ecl} + {\rm d}M_{\rm ecl}$ is

$${\rm d}^{\rm total}N_{\rm ej,O}(M_{\rm ecl}) = \langle {}^{\rm com}N_{\rm ej,O}\rangle(M_{\rm ecl}) \times \xi_{\rm ecl}(M_{\rm ecl})\, {\rm d}M_{\rm ecl}, \tag{3.17}$$

and is shown in the upper panel of Fig. 3.7. As the number of clusters decreases more steeply ($\xi_{\rm ecl}(M_{\rm ecl}) \propto M_{\rm ecl}^{-2}$) than the number of ejected O-star systems from a cluster increases with cluster mass ($\langle {}^{\rm com}N_{\rm ej,O}\rangle(M_{\rm ecl}) \propto M_{\rm ecl}^{\gamma}$ with $0.6 < \gamma < 0.9$, Section 3.3), the number of O stars contributed to the field by dynamical ejections is a function decreasing with increasing cluster mass. The most prominent contributors to the population of ejected O stars are $\approx 400\,{\rm M}_\odot$ clusters.

In the lower panel of Fig. 3.7, cumulative numbers of ejected O-type systems as a function of cluster mass are shown. The fraction (right Y-axis) is calculated by dividing the cumulative number by the total number of O stars formed during the cluster-population forming timescale of 10 Myr, which can be deduced from Equations (3.4) and (3.15),

$${}^{\rm total}N_{\rm O} = \int_{M_{\rm ecl,min}}^{M_{\rm ecl,max}} N_{\rm O,IMF}(M_{\rm ecl})\, \xi_{\rm ecl}(M_{\rm ecl})\, {\rm d}M_{\rm ecl}. \tag{3.18}$$

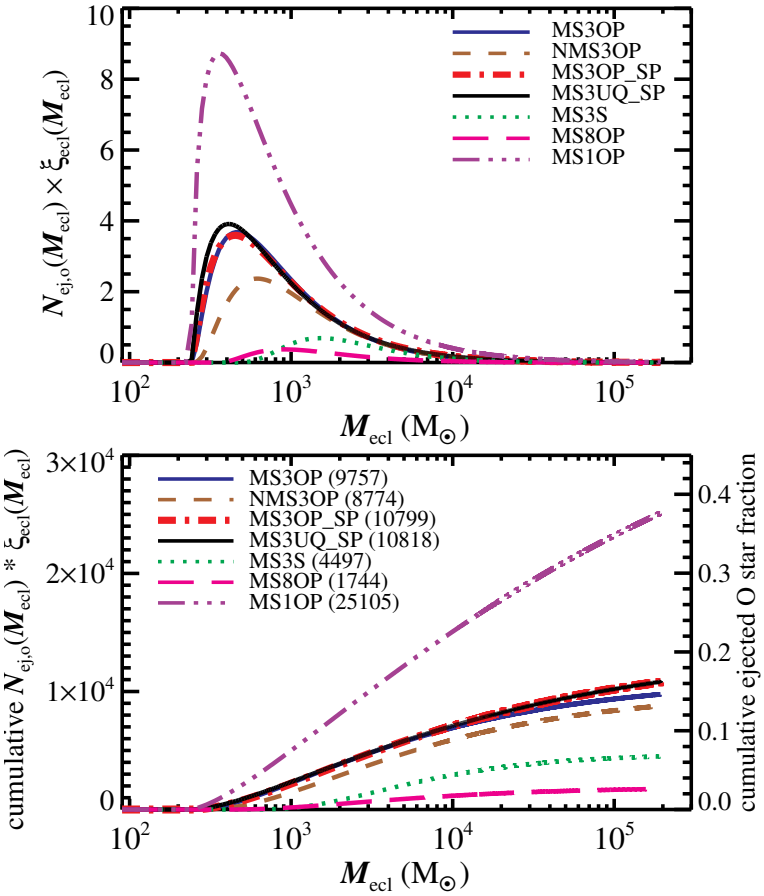

Figure 3.7. Top: total number of the ejected O-star systems per cluster mass in the Galaxy (Equation 3.17). For example, according to the most realistic model sequence (MS3UQ_SP), in total about four ejected O-star systems per 10 Myr are contributed from all clusters weighing about 400 $M_\odot$. The small numbers of ejected O-star systems contributed from massive clusters come about because the number (or probability) of such massive clusters to form is small according to the very young or embedded cluster mass function (Equation 3.15). Bottom: cumulative number of the ejected O-star systems as a function of cluster mass. Right Y-axis shows the ejected O-star fraction of the total O stars formed within 10 Myr deduced by using Milky Way type parameters. Numbers next to the model sequence names are the expected total number of ejected O-star systems which are the sum of Equation (3.17) over all clusters for each model sequence. For example, the MS1OP model sequence would imply that all clusters formed within 10 Myr eject in total almost 2.5×10^4 O-star systems assuming the SFR $= 3\,M_\odot\,yr^{-1}$ such that $M_{ecl,max} = 1.9 \times 10^5\,M_\odot$. As another example, according to the most realistic sequence of models (MS3UQ_SP), every 10 Myr, 10818 O-star systems are ejected from all clusters formed in this time interval. Clusters with a mass of almost 400 $M_\odot$ have the largest contribution to this population (upper panel) and clusters with masses up to 10^3 $M_\odot$ contribute almost 33% to this population (lower panel, right axis); 50% of all ejected O stars originate from $M_{ecl} \leq 3 \times 10^3\,M_\odot$ clusters.

The parameters which we adopt here for the Milky Way provide ${}^{\rm total}N_{\rm O} \approx 66\,749$ being formed every 10 Myr. Note ${}^{\rm total}N_{\rm O}$ is the total number of *individual* O stars which have formed within the formation timescale, while $\mathrm{d}^{\rm total}N_{\rm ej,O}(M_{\rm ecl})$ is the number of ejected O star *systems*. It is difficult to derive the total number of O-star systems from the models because a binary fraction evolves due to dynamical disruptions/captures and mergers between stars, the final binary fraction varies with cluster mass and initial conditions, and some O stars have an O-star secondary while some do not. The fraction shown in the lower panel of Fig. 3.7 can, thus, be interpreted as being a minimum value since the total number of O-star systems would be smaller than ${}^{\rm total}N_{\rm O}$ which counts all individual O stars from the IMF and cluster mass function. Our models thus yield as a lower boundary that binary-rich clusters with $r_{\rm h}(0) = 0.3$ pc can eject ≈13–16% of the total O-star systems and even ≈38% can be dynamically ejected if clusters form more compact, e.g. with $r_{\rm h}(0) = 0.1$ pc (Fig. 3.7). About 50% of ejected O-star systems come from clusters with $M_{\rm ecl} \lesssim 3000$–$5000\,{\rm M}_\odot$.

The fraction of O stars found in clusters and/or OB-associations is 70–76% (de Wit et al. 2005; Eldridge et al. 2011, depending on how to count a binary) yielding the fraction of the field O stars as being 24–30%. Our model is thus reasonably consistent with these data. Additional three processes that are not part of the present model but which increase the apparent number of field O stars are: (i) some of the observed field stars may originate from clusters which contained only a few or one O stars and which dissolved at an early age by rapid gas removal (Gvaramadze et al. 2012). That is such O stars "lost" their birth cluster through disruptive gas removal (see also Kroupa & Boily 2002; Weidner et al. 2007). (ii) Small-N clusters for which the two-body relaxation time is comparable to the crossing time also dissolve within a few initial crossing times (Moeckel et al. 2012), which is aided by stellar evolution within a few tens of Myr. (iii) Some O stars may be ejected when they are companions to primaries that explode as supernovae at an age older than 3 Myr (Eldridge et al. 2011).

In observations about 6% of O stars are found being runaways which have a velocity higher $30\,{\rm km\,s^{-1}}$ (Eldridge et al. 2011). The runaway fraction among the dynamically ejected O stars generally increases with cluster mass (upper panel of Fig. 3.8), e.g. 0% ($M_{\rm ecl} = 10^{2.5}\,{\rm M}_\odot$) to 43% ($M_{\rm ecl} = 10^{4.5}\,{\rm M}_\odot$) in the case of the MS3UQ_SP model and 81% for the $10^5\,{\rm M}_\odot$ model in Banerjee et al. (2012b). We deduce the number of the runaways first by fitting a function for the runaway fraction as a function of cluster mass with the same functional form of the number of ejected O stars (Equation 3.14, but y being the runaway fraction) and then by multiplying the fitting function by the number of ejected O stars (Equation 3.17, upper panel of Fig. 3.7). By dividing the total number of runaways by the total number of ejected stars (lower panel of Fig. 3.7), we obtain the runaway fraction among the ejected O stars. Our most realistic model sequence, MS3UQ_SP, predicts about 30% of the ejected O stars, i.e. about 5% of all O-star systems to be runaways. Eldridge et al. (2011) studied runaways assuming the binary supernova scenario, in which the companion star obtains a high velocity when one of the binary components undergoes a supernova explosion. They predicted about 0.5%[3] of O stars being runaways when only this process is accounted for. The value combining ours and Eldridge et al. (2011) is thus well consistent with the observed one.

The upper panel of Fig. 3.7 demonstrates that the presence or absence of initial mass segregation leads

[3] Eldridge et al. (2011) provides two values, 0.5% (mentioned in the text) and 2.2%, for the fraction of O-star runaways produced by a supernova explosion of the primary star in a binary system. The former is obtained using O stars with velocity larger than $30\,{\rm km\,s^{-1}}$, which is also our runaway criterion. The latter is derived with a lower velocity limit of $5\,{\rm km\,s^{-1}}$ for runaways. The latter value is applicable to process (iii) in the text.

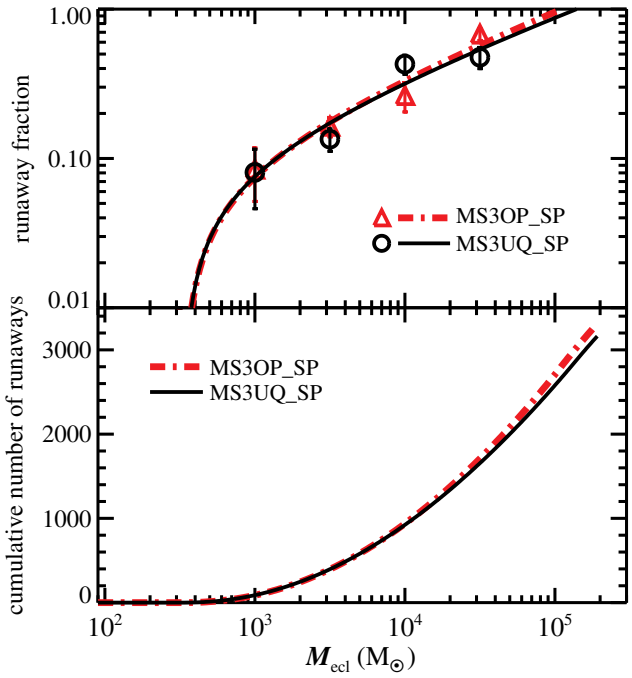

Figure 3.8. Top: runaway fraction among the ejected O stars from two model sequences, MS3OP_SP and MS3UQ_SP. The data are fitted with the same functional form of Equation (3.14) (curved lines). The error bars indicate Poisson errors. Bottom: expected cumulative number of runaways as a function of cluster mass. The numbers are derived by multiplying the fitted lines in the upper panel by the number of ejected O-star systems with cluster mass, Equation (3.17). More than 70% of O-star runaways are expected to originate in the clusters more massive than 10^4 $M_\odot$.

to differences in the numbers of ejected O stars only for lower mass clusters ($M_{\rm ecl} \lesssim 10^3$ $M_\odot$) with the constant initial half-mass radius we assume in this study. If larger $r_{\rm h}(0)$ are assumed the cluster mass at which the difference vanishes would move up to a larger cluster mass since the mass-segregation timescale gets longer.

3.5 Properties of ejected O-star systems

In this section, we study how properties such as velocities, distances from the cluster centre, and system masses of the ejected O-star systems vary with cluster mass. We remind the reader that our analysis is restricted to systems younger than 3 Myr.

3.5.1 Kinematics of the ejected O-star systems

Cumulative distributions of velocity, distance from the cluster centre, and system mass of all ejected O-star systems for each cluster mass and for each model sequence are shown in Fig. 3.9. Overall, the systems ejected from more massive clusters have velocity distributions skewed towards higher velocity. This can be understood in two ways. Firstly, the velocity dispersion of stars in a cluster increases with cluster mass under the assumption of a constant cluster size (in general, velocity dispersion is a function of both size and mass of a cluster), i.e. on average stars in more massive clusters have higher velocities.

Secondly, a star needs a velocity greater than the escape velocity, which also increases with cluster mass, in order to leave its parental cluster. For the MS8OP model sequence (with $r_{\rm h}(0) = 0.8$ pc), the trend is not as pronounced as in other models since the ejection fractions are small and so are the total number of ejected O-star systems, e.g. only in total 11 O-star systems are ejected out of four runs in the $10^{4.5}$ $M_\odot$ cluster models. Also in the case of the $10^{2.5}$ $M_\odot$ clusters in the NMS3OP sequence ($r_{\rm h}(0) = 0.3$ pc) only three O-star systems are ejected out of 100 runs.

The highest velocity of an ejected system generally increases with cluster mass, although this is not always the case, e.g, in the MS3OP model sequence, the system moving the fastest (a single star of mass 46 $M_\odot$ with a velocity of $\approx$200 km s^{-1}) is ejected from a $10^{3.5}$ $M_\odot$ cluster. The velocity distribution is dependent on the cluster model, especially on the initial half-mass radius of the cluster. The MS1OP models have velocity distributions biased towards higher velocities compared to the larger-sized cluster models (Fig. 3.9). The highest velocity of an ejected system (a single star of mass 34 $M_\odot$ from an $M_{\rm ecl} = 10^{4.5}$ $M_\odot$ cluster) is $\approx$300 km s^{-1} in the MS1OP model sequence.

As the distance distribution of the ejected systems is directly related to the velocity distribution, their shapes are similar. The slight difference between them results from the time of ejections occurring at systematically different times in different models. Owing to the systematic shift to larger ejection velocities, the ejected systems travel on average further away from the clusters in the more massive clusters. The distances of the ejected systems from $M_{\rm ecl} \geq 10^4$ $M_\odot$ clusters range from a few pc to a few 100 pc. The most extreme system (a single star with a mass of 34 $M_\odot$) ejected from an MS1OP model traveled up to $\approx$750 pc away from its birth cluster by 3 Myr.

Cumulative mass distributions of the ejected O stars are plotted in the right column of Fig. 3.9. In the case of a binary system, masses of both components are counted separately. As binary fractions of the ejected systems are low for most of the models, the cumulative distributions of system masses would be similar to those of individual stellar masses. A few models suggest that the more massive clusters may have a higher fraction of more-massive ejected stars. However, the trend is not strongly evident. For example, in the case of the MS1OP models, the mass distributions of the ejected O stars look similar to each other for different cluster masses. But only clusters with $M_{\rm ecl} \geq 10^{3.5}$ $M_\odot$ eject O stars heavier than 100 $M_\odot$ as the lower mass clusters do not have such a massive star initially, e.g. for $M_{\rm ecl} = 1000$ $M_\odot$, $m_{\rm max} \approx 44$ $M_\odot$. About 10% of the ejected O stars from clusters with $M_{\rm ecl} \gtrsim 10^{3.5}$ $M_\odot$ in the MS3OP_SP and MS3UQ_SP sequences are more massive than 100 $M_\odot$, while this is the case for $\lesssim$5% from the other models. This may result from a higher number of mergers in the MS3OP_SP and MS3UQ_SP models due to the high fraction of close, eccentric binaries in comparison to the other models.

Thin grey lines in the right column of Fig. 3.9 indicate cumulative mass distributions of O stars from the canonical IMF with the lower and the upper mass limits of, respectively, 17.5 $M_\odot$ and the mass of the most massive star among the ejected O star for each cluster-mass set. It follows that most models show that ejected stars have a shallower slope of the mass function than the canonical value (index of 2.3, see Equation 3.1) as also shown in Fujii & Portegies Zwart (2011) resembling the mass function in the cluster core.

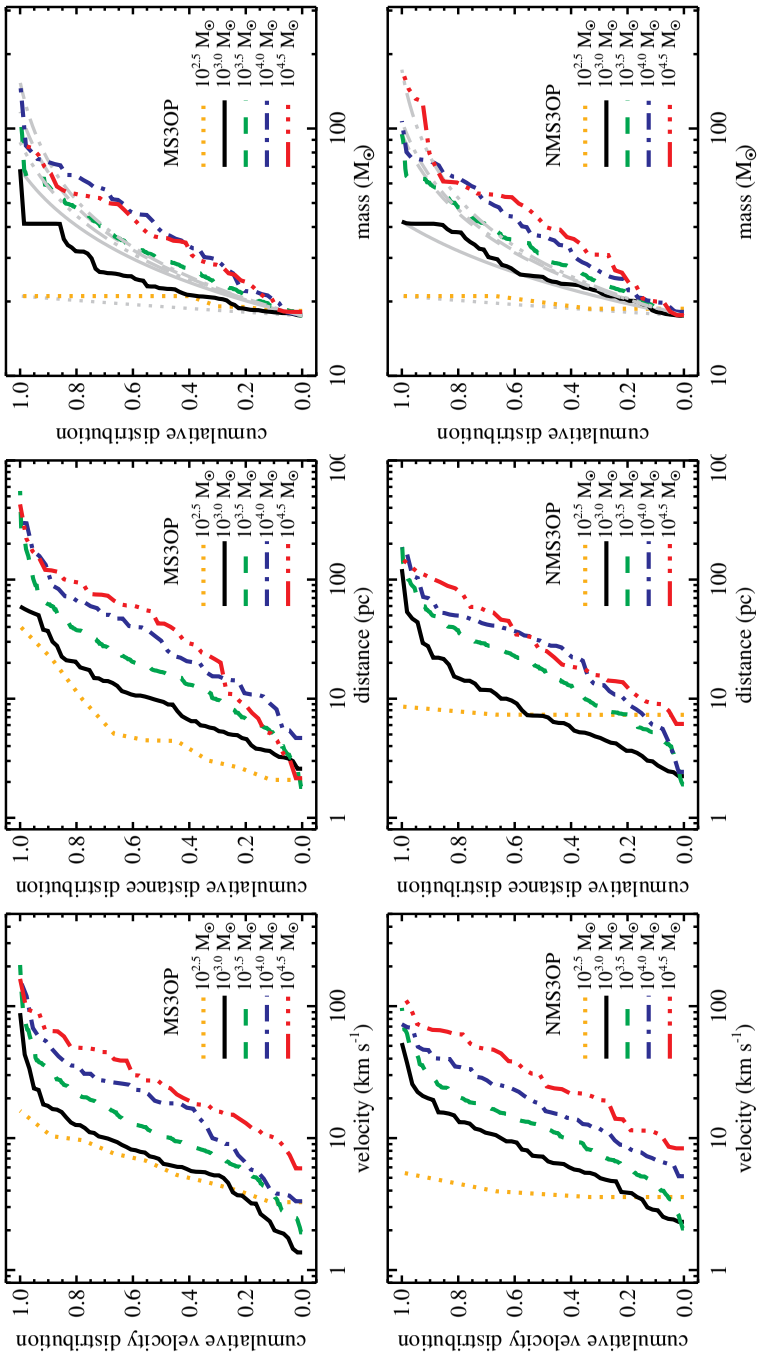

Figure 3.9. Normalised cumulative distributions of velocity (left) and of distance from the cluster centre (centre) of ejected O-star systems, and of mass of the individual ejected O stars (right) from our calculations. See the text for the grey lines in the right most column.

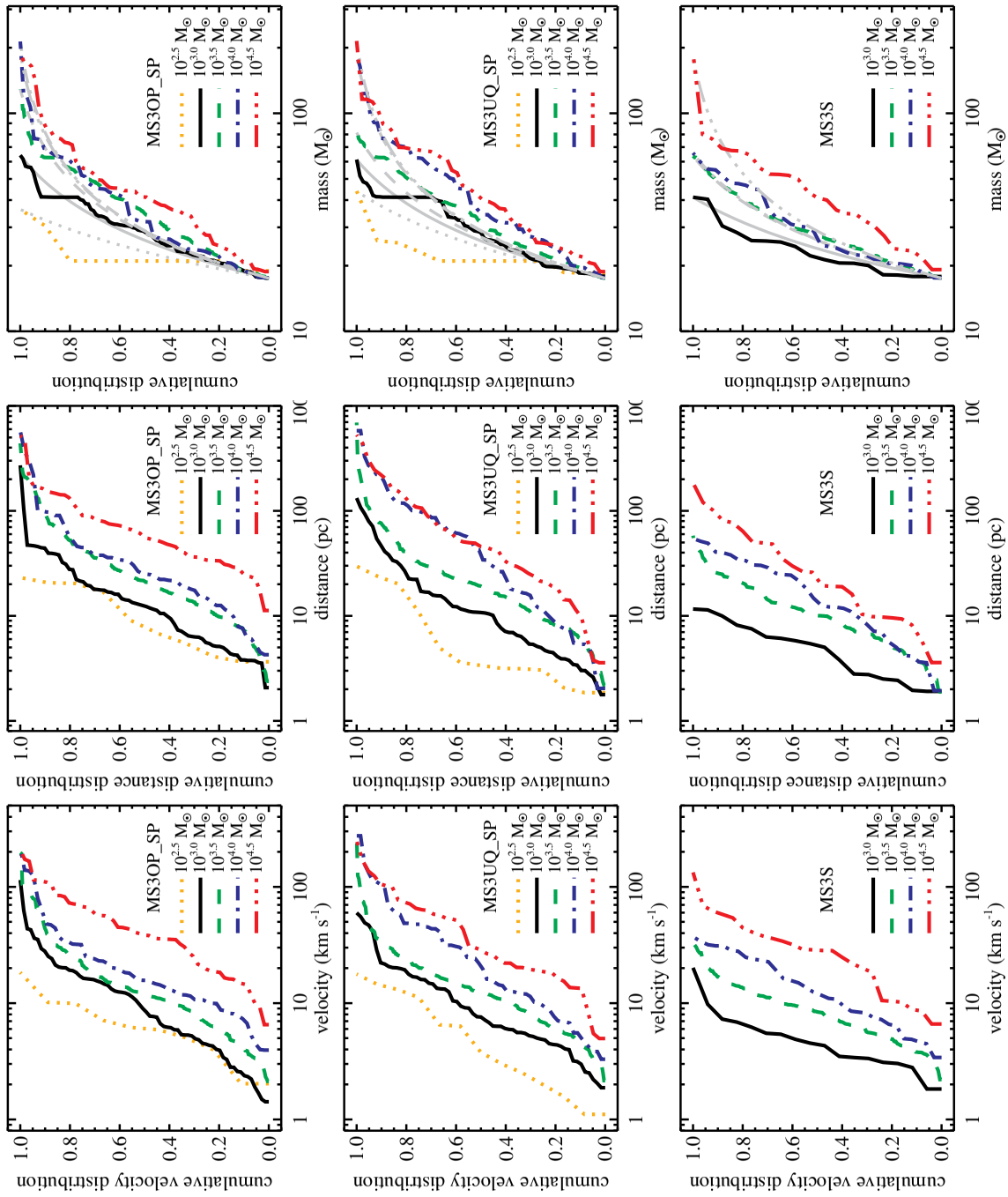

Figure 3.9. (Continued.)

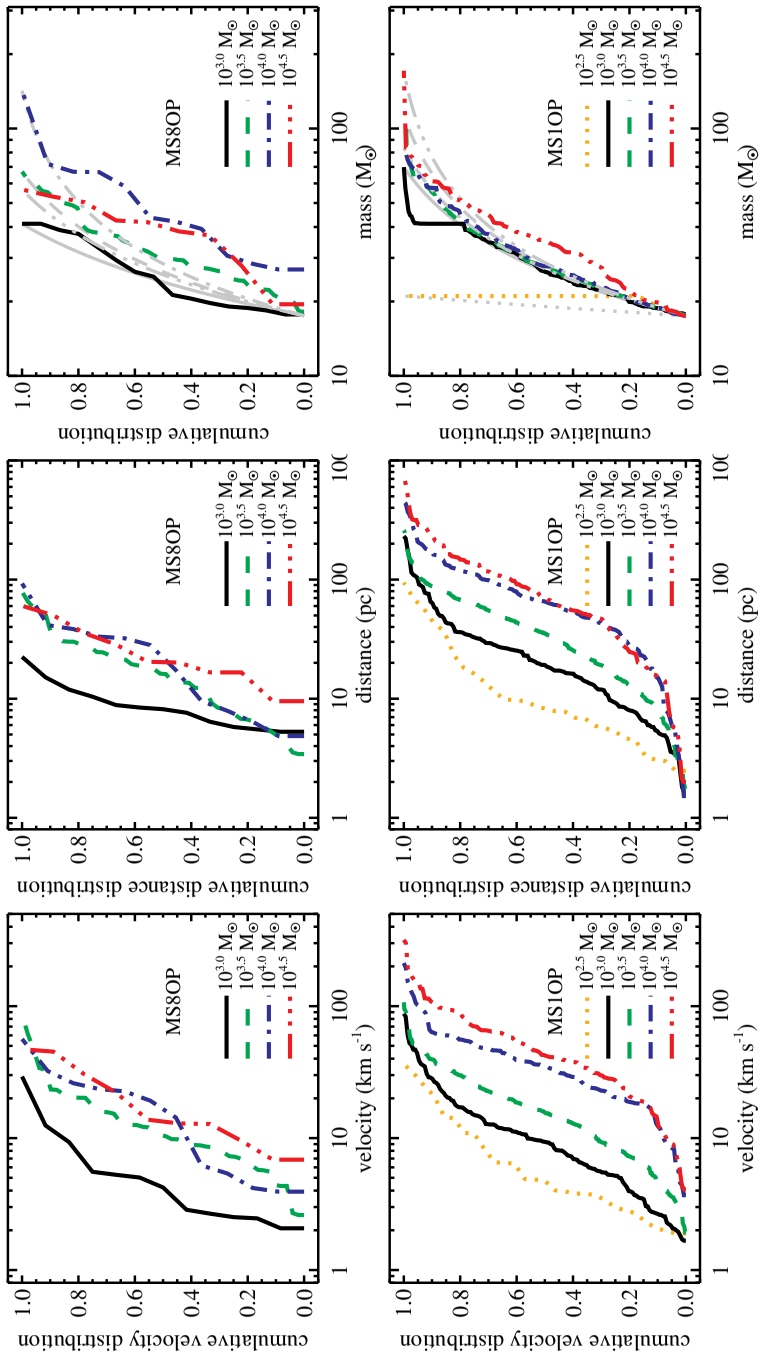

Figure 3.9. (Continued.)

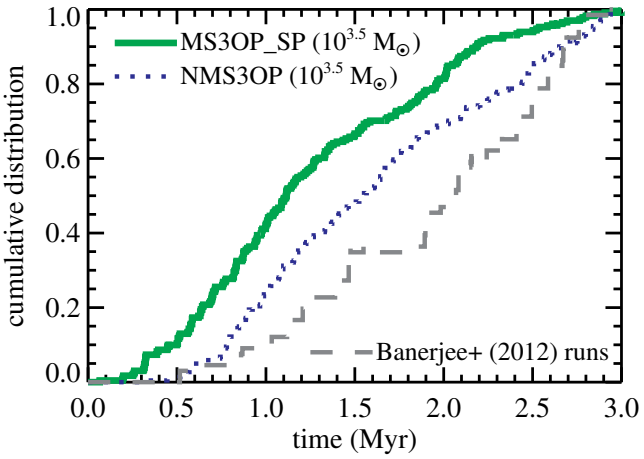

Figure 3.10. Cumulative O-star ejection as a function of time for $10^{3.5}$ M$_\odot$ clusters in models MS3OP_SP and NMS3OP, and the Banerjee et al. (2012b) model. For example, almost 45% of all ejected O-star systems are ejected by 1 Myr in the MS3OP_SP ($10^{3.5}$ M$_\odot$) model.

The normalised cumulative number of the ejected O-star systems as a function of time for a few models is shown in Fig. 3.10. In the case of the MS3OP_SP model ($M_{\rm ecl}$ = $10^{3.5}$ M$_\odot$), almost 70% of the ejected stars travel beyond three times the half-mass radius before 1.5 Myr. Initially not mass-segregated cluster models (e.g. the $10^{3.5}$ M$_\odot$ clusters of the NMS3OP model sequence in Fig. 3.10) show a delay of the ejections as the model requires time for massive stars to migrate to the cluster centre to interact with other massive stars. But about half of the ejected stars already reach a distance of three times the half-mass radius from the cluster centre before 1.5 Myr of evolution. Also the ejection rate is higher during the earlier times of evolution. Note that the time at which a star is classified as being ejected is different to when the ejection has actually happened. The time presented in the figure comprises the traveling time the stars need to reach to the ejection criterion and thus the ejections actually happened at an earlier time than shown in the figure. This can naturally explain the steeper increase of the number of ejected stars at a later time for the Banerjee et al. (2012b) model in which the initial half-mass radius of the clusters is larger ($r_{\rm h}(0)$ = 0.8 pc) than in the above two models ($r_{\rm h}(0)$ = 0.3 pc). Thus an ejected star requires more time to reach the ejection criterion in their model (see Section 3 for the criteria). A rough estimate of the time when the ejections occur peaks at around 1 Myr, though it can vary with different initial conditions (Oh & Kroupa 2016).

3.5.2 The binary fraction among the ejected O-star systems

Not only single O stars but binaries containing O-star component/s are ejected from star clusters via dynamical interactions. The binary fraction of ejected O stars can be substantial, up to ≈78% (Table B.1). Even initially single-star clusters eject O-star binaries dynamically (Table B.1). In Fig. 3.11 is plotted the average binary fraction among ejected O-star systems from the binary-rich cluster models as a function of cluster mass. A smaller fraction of binaries is ejected from the more massive clusters because the kick required to remove a system from the cluster is larger and more binaries are disrupted through interactions with other stars in the more massive clusters.

The binary fraction among ejected O stars can be significantly altered by assuming a different initial

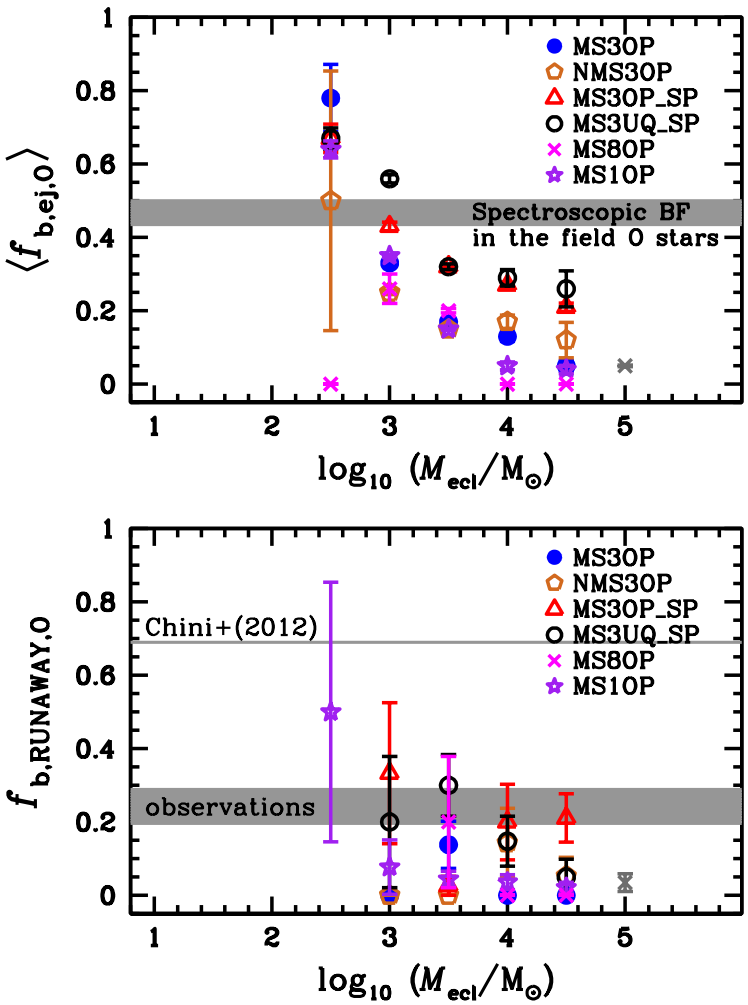

Figure 3.11. Top: averaged binary fraction among the ejected O-star systems, $\langle f_{b,ej,O} \rangle$, from initially binary-rich cluster models. A (grey) cross at $M_{ecl} = 10^5$ $M_\odot$ is the Banerjee et al. (2012b) model which adopted a uniform initial period distribution for O-star binaries. The error bars indicate standard deviations of $\langle f_{b,ej,O} \rangle$. The observed spectroscopic binary fractions in the Galactic field O stars are shown as a grey area (Gies 1987; Mason et al. 1998, 2009; Chini et al. 2012). Bottom: binary fraction among the runaway O stars from initially binary-rich cluster models. The cluster models that do not eject any runaway O star, e.g. $10^{2.5}$ $M_\odot$ cluster models from all sequences but the MS1OP sequence, are not included in the figure. The error bars indicate Poisson errors. The grey area indicates a range of the observed spectroscopic binary fractions of runaway O stars in Gies (1987) and Mason et al. (1998, 2009). The grey horizontal line is the observed value in Chini et al. (2012).

period distribution. An initially higher fraction of close binaries leads to a higher binary fraction of ejected O stars. Thus the more realistic MS3OP_SP and MS3UQ_SP models produce higher binary fractions of ejected O-star systems compared to the other models (Fig. 3.11). The observed spectroscopic binary fraction among the Galactic field O stars is 43–50% (Gies 1987; Mason et al. 1998, 2009; Chini et al. 2012). This may be reproduced readily through dynamical ejections of O stars with more realistic (than the Kroupa 1995b) period distribution function for O-star binaries, such as constrained recently by Sana et al. (2012) (Equation 3.3). This comes about because, as can be seen for the most realistic sequence (MS3UQ_SP), the dominant contributors to the population of ejected O-star systems are $\leq 10^4$ $M_\odot$ clusters (lower panel of Fig. 3.7), and these ejected O-star systems have a binary fraction $\gtrsim$30% (upper panel of Fig. 3.11). It should be noted that the given observed binary fractions are lower limits of the binary fraction of the field O stars since only spectroscopic binaries are counted.

In the case of runaways, the binary fractions from our most realistic sequences, MS3OP_SP and MS3UQ_SP, are well consistent with the observed spectroscopic binary fraction of the runaway O stars in Gies (1987) and Mason et al. (1998, 2009), 19–29% (grey area in the lower panel of Fig. 3.11), but too small compared to the value in Chini et al. (2012),[4] 69% (grey horizontal line in the same figure). This may be due to the difference in assigning runaways between the Chini et al. (2012) work and the other studies. In Chini et al. (2012), stars are classified as runaways when they can be traced back to any cluster or associations in the study of Schilbach & Röser (2008). In other words, the runaways in their sample may be simply ejected O stars from star clusters which have masses $\lesssim 10^4$ $M_\odot$ since very massive clusters are exceedingly rare. The other studies assign stars to runaways with a large distance from the Galactic plane or with a high peculiar (radial) velocity.

In most of our cluster models (with the exception of the MS3OP_SP and MS3UQ_SP models) the binary fraction of O stars, whether they are inside a cluster or not, at 3 Myr is smaller than the observed O-star binary fraction ($\approx$70%, Chini et al. 2012; Sana et al. 2012, and references therein). This is the case because dynamical interactions between binaries and other cluster members disrupt binaries, preferentially those with a wide orbit (Kroupa 1995a; Parker et al. 2009; Marks et al. 2011) and because the Kroupa period distribution (which was constrained originally only for late-type stars) extrapolated in some of the model sequences to the O-star regime has a larger fraction of long period binaries compared to the observed distribution of O-star binaries (Fig. 3.1).

3.6 Discussion

While the mass of clusters which eject O stars most efficiently is the same for all models ($M_{\rm ecl} \approx 10^{3.5}$ $M_\odot$), it has been shown that the dynamical ejection of O stars can be highly sensitive to the initial conditions of star clusters. In this section, we further discuss the effects of our choice of initial parameters for massive stars and for the clusters, and the available observational constraints.

The ejection fraction is strongly dependent on the initial cluster size. As seen in Fig. 3.2 the shapes of the curves look similar but the values of the ejection fraction are larger for initially smaller sized

[4] We note here that the Chini et al. (2012) sample is not biased. They selected stars from the Galactic O Star Catalogue v.2.0 (Sota et al. 2008) of which 248 stars could be reached from their observatory. They additionally employed archival data from the European Southern Observatory (ESO) for those stars already contained in their survey. Thus the ESO spectra did not add any new star to their sample but increased only the number of spectra and, as a consequence, the time basis for individual stars (R. Chini, private communication).

clusters. Thus it is important to check if our models are comparable to observed young star clusters. The half-mass densities of our N-body models at 3 Myr range from 175 to $\approx 10^5\,\mathrm{M}_\odot\,\mathrm{pc}^{-3}$, from $\approx$160 to $\approx 3.4\times10^4\,\mathrm{M}_\odot\,\mathrm{pc}^{-3}$, and from $\approx$50 to $\approx$4000 $\mathrm{M}_\odot\,\mathrm{pc}^{-3}$ for $r_\mathrm{h}(0) = 0.1$, 0.3, and 0.8 pc clusters, respectively. These values are well within the densities of observed young (< 5 Myr) massive ($M_\mathrm{ecl} > 6000\,\mathrm{M}_\odot$) star clusters, classified as star burst clusters in Pfalzner (2009), which range from 1500 to $4 \times 10^5\,\mathrm{M}_\odot\,\mathrm{pc}^{-3}$ (Figer 2008). However, caution is due in directly comparing the model cluster densities to the observed values since the observed densities are closer to the central (i.e. highest) density rather than to the half-mass density. Concerning the initial sizes of the embedded clusters, these are dynamically sub-pc (Testi et al. 1999; Lada & Lada 2003; Kroupa 2005; Smith et al. 2005; Tapia et al. 2009, 2011, 2014; Marks & Kroupa 2011).

The initial binary population plays a major role in the dynamical ejections of massive stars (see the differences between the MS3OP and MS3S models). Thus it is important to adopt realistic initial binary parameters to understand massive star ejections in reality. The pairing method for massive binaries adopted in most of our models results in extreme mass ratios, e.g. most of them are larger than 0.9. This was motivated by the high fraction of twins in observed massive binaries (Pinsonneault & Stanek 2006; Kobulnicky & Fryer 2007, but see also Lucy 2006), while recent observational studies favour a rather flat mass-ratio distribution for O-type binaries (Kiminki & Kobulnicky 2012; Sana et al. 2012) still excluding random pairing from the IMF for this spectral type. Adopting a more realistic initial mass-ratio distribution for O-type binaries may reduce the efficiency of the ejection, though the shape of the $f_\mathrm{ej,O}(M_\mathrm{ecl})$ ejection fraction as a function of parent birth-cluster mass is expected to be kept (see MS3OP_SP and MS3UQ_SP sequences in Table B.1). In this contribution we include a realistic model for the observed period distribution of O-star binaries (Equation 3.3). The model with the observed period distribution, which reproduces the observed abundance of short period binaries, exhibits a substantial increase of the ejection fraction, by $\approx$30%, from massive clusters ($M_\mathrm{ecl} \geq 10^4\,\mathrm{M}_\odot$). Whether the observed distribution is a real initial distribution is still unclear as the observed distribution has been compiled from several clusters which may have already evolved dynamically despite their young ages (1–4 Myr). The authors suggested that dynamical evolution would be negligible for such massive close binaries ($\log_{10}(P/\mathrm{days}) < 3.5$). However, the population of massive binaries can evolve through the dynamical interactions with other massive stars/binaries in the clusters (Oh et al. in preparation). Moreover, short-period massive binaries are vulnerable for merging either due to stellar evolution or the perturbation-induced collision of the two binary-star companions. Thus the effect of dynamical evolution needs to be taken in to account iteratively to find the true initial period distribution of massive binaries. But this is beyond the aim of this study. For late-type binaries this has already been performed successfully by Kroupa (1995a,b, see also Marks et al. 2011; Marks & Kroupa 2012).

Unlike the other initial conditions mentioned above, initial mass segregation does not result in a difference of the O-star ejection fraction for clusters with $M_\mathrm{ecl} \geq 10^3\,\mathrm{M}_\odot$ and $r_\mathrm{h}(0) = 0.3$ pc due to efficient dynamical mass segregation. But differences do occur for lowest mass clusters: initially mass-segregated clusters more efficiently eject O stars than non-segregated clusters, as dynamical mass segregation is inefficient to gather massive stars in the core of such clusters. For clusters with larger $r_\mathrm{h}(0)$ values, as the dynamical mass segregation timescale becomes longer, the initial mass segregation can play a significant role. In observations, post gas-expulsion young massive clusters (age $\lesssim$ 5 Myr) are generally compact (effective radii $\lesssim$ a few pc, Tapia et al. 2003; Kroupa 2005; Portegies Zwart et al. 2010).

Throughout this study the $m_{\rm max}$–$M_{\rm ecl}$ relation is adopted. It follows from an intuitive theoretical concept that the mass of a star-forming molecular cloud core is finite and that star formation is a self-regulated process (Adams & Fatuzzo 1996), and it follows from the data on young stellar populations (Weidner et al. 2010, 2013a; Kirk & Myers 2011). The existence of a physical $m_{\rm max}$–$M_{\rm ecl}$ relation is thus taken to be established (Weidner et al. 2014). Although the theory has been successful in describing the stellar contents of whole galaxies (e.g. Weidner et al. 2013b), it has been debated if the relation exists (see section 2.1 in Weidner et al. 2013a, for details) or if star formation is a purely stochastic process (e.g. Krumholz 2015). This is a fundamental issue for understanding galaxy-wide IMFs and how massive stars form, and we here thus stress that the data do not support the hypothesis that star formation is stochastic (see section 7 of Kroupa 2015). For example, Hsu et al. (2012, 2013) presented that L1641, the low-density star-forming region (containing as many as ≈1600 stars) of the Orion A cloud, is deficient of massive (O and early B) stars compared to the canonical IMF with 3–4σ significance and that with a probability of only 3% the southern region of L1461 and the ONC can be drawn from the same population, supporting that the high-mass end of the IMF is dependent on environmental density. In section 4.2 of Krumholz (2015) three references (Calzetti et al. 2010; Fumagalli et al. 2011; Andrews et al. 2013) are cited as containing evidence against a physical $m_{\rm max}$–$M_{\rm ecl}$ relation. Weidner et al. (2014) critically discuss these works, showing Andrews et al. (2013) data to be entirely consistent with the physical $m_{\rm max}$–$M_{\rm ecl}$ relation. As already discussed in Section 3, whether the $m_{\rm max}$–$M_{\rm ecl}$ relation is adopted or not does not affect the results obtained here though.

We do not include a gas potential, which would subsequently be removed rapidly, in the calculation (cf., Kroupa et al. 2001; Banerjee & Kroupa 2014). The main outcomes of gas expulsion are significant stellar loss from and expansion of clusters and their possible subsequent dissolution. Therefore gas expulsion can weaken the ejection efficiency by lowering the (central) density of a cluster if that occurs at a similar time when a majority of the ejection processes take place. In the future, further studies including a gas potential are needed to understand the effect of gas expulsion on the ejection of massive stars. Inclusion of a gas potential will be possible once the statistical quantification of the gas-expulsion process is in place and computable (cf., Banerjee & Kroupa 2014). It has been argued recently that gas expulsion, if the process occurs at all, may have no effect on star cluster evolution (e.g. see Longmore et al. 2014, and references therein). It may, however, be difficult to detect the expanding signature resulting from residual gas expulsion since revirialization after gas expulsion can be rapid for massive clusters, $M_{\rm ecl} > 10^3\,{\rm M}_\odot$ (Portegies Zwart et al. 2010; Banerjee & Kroupa 2013).

To constrain which initial conditions are responsible for the observed field O-star populations, one needs the observed quantities to compare with the results from models. However, it is very difficult to find which clusters individual field O stars originate from. Some ejected O stars can travel further than a few hundred pc away from their birth cluster within a few Myr, thus, without knowledge of their full-3D kinematics and the Galactic potential, it is almost impossible to find their birth cluster. *Gaia* may help to find the birth clusters of the field O stars. However, the two-step ejection process of Pflamm-Altenburg & Kroupa (2010) complicates this. Their calculation suggests that 1–4.6% of O stars would appear to have formed in isolation because of the two-step ejection process. They used the observed values of the O-star runaway fraction (10–25%, Gies & Bolton 1986; 46%, Stone 1991), and the binary fraction among the runaways (10%, Gies & Bolton 1986). Since most, if not all, ejected O-star–O-star binaries may go through the two-step ejection process and then cannot be traced back to their birth cluster, the

fraction of O stars which appear to have formed in isolation can be higher if a binary fraction of the dynamically ejected stars is substantial. A quantitative study is required to determine the fraction of O stars experiencing the two-step ejection process.

3.7 Summary

We study how the ejection of O stars varies with cluster mass (or density as we assume a constant size for different cluster masses) under diverse initial conditions. We find that moderately massive clusters ($10^{3.5}\,M_\odot$), which have formed about 10 O-star systems, most efficiently shoot out their O stars to the field through energetic encounters between massive stars in the cluster core compared to other ones with other masses, for all model sequences, i.e. this result obtains independently of cluster size or the presence of initial mass segregation or binaries. Up to on average ≈25% of the initial O-star content is ejected from the clusters with this cluster mass in $r_{\rm h}(0) = 0.3\,{\rm pc}$ models (52% in $r_{\rm h}(0) = 0.1\,{\rm pc}$ clusters, Fig. 3.2). However, the spread is large and ejections of all O stars leading to remnant young clusters void of O stars occur in about 1% of all such clusters (Fig. 3.2). Fujii & Portegies Zwart (2011) suggested that one bully binary, dynamically formed, is mainly responsible for flinging out the stars from initially single-star clusters. Here we show that the number of ejections is significantly higher when the highly significant initial massive binary population is accounted for. The ejections, thus, occur via close encounters involving several binaries in reality since the massive stars are observed to have high multiplicity fractions in young star clusters (Chini et al. 2012; Sana et al. 2012, and references therein). Furthermore, more realistic clusters, which have O-star binaries with periods following the Sana et al. (2012) distribution (MS3OP_SP and MS3UQ_SP), lead to even larger ejection fractions, especially for massive clusters. The mass-position of the peak of $f_{\rm ej,O} = f_{\rm ej,O}(M_{\rm ecl})$, however, does not change ($M_{\rm ecl,peak} \approx 10^{3.5}\,M_\odot$).

The decrease of the O-star ejection fraction with increasing cluster mass for massive ($M_{\rm ecl} \geq 10^{3.5}\,M_\odot$) clusters can be represented by a simple power-law of cluster mass with an exponent between −0.16 and −0.43. Clusters with an initial half-mass radius $r_{\rm h}(0) = 0.3\,{\rm pc}$ and with relatively simple initial conditions (Kroupa initial period distribution for O stars or no initial binaries) have an exponent of ≈ -0.4 being in good agreement with −0.5 which is derived from the number of O stars from the IMF and the binary–single star scattering rate (Equation 3.12). Models with a high fraction of close initial binaries or smaller $r_{\rm h}(0)$ deviate from the expected theoretical value by having larger ejection fractions.

We show that not only the ejection fraction but also the properties of the ejected O-star systems depend on the initial cluster mass. The velocity distribution of the ejected O-star systems shifts to higher velocities for more massive clusters, and so does their distance distribution from the cluster. But the distribution of ejected system masses varies weakly with cluster mass. The binary fraction of the ejected systems decreases with increasing cluster mass as does the binary fraction of the systems remaining in the cluster because binary disruption via interactions with other members of the cluster is more efficient for a denser cluster, i.e. more massive cluster. The binary fraction among the ejected O-star systems is substantial, especially in the more realistic models in which the period distribution of the observed O-star binaries is implemented (MS3OP_SP and MS3UQ_SP).

Considering that the cluster mass function is approximately a power law with a near Salpeter index, the main fraction of field O stars dynamically ejected from clusters originate from low/intermediate

mass clusters ($M_{\rm ecl} \lesssim$ a few 1000 $M_\odot$, see Section 3.5). The dynamical ejection process populates ≈16% to 38% of all O stars, formed in clusters, to the field. Combining our results on the dynamical ejection fraction and the binary-supernova scenario computed by Eldridge et al. (2011) it follows that the observed fractions of the Galactic field and runaway O stars are well accounted for theoretically. It should be noted that very massive ($\gtrsim$100 $M_\odot$) runaways can only originate from massive star-burst clusters ($M_{\rm ecl} \gtrsim 10^4\,M_\odot$) because only massive clusters can harbour a sufficient number of very massive stars to eject some of them.

We thank Rolf Chini for comments on the observational data in his paper.

CHAPTER 4

Dynamical ejections of massive stars from young star clusters under diverse initial conditions

Published in Astronomy & Astrophysics
Volume 590, article id A107, pp 1–27, June 2016

S. Oh and P. Kroupa

ABSTRACT

We study the effects that initial conditions of star clusters and their massive star population have on dynamical ejections of massive stars from star clusters up to an age of 3 Myr. We use a large set of direct N-body calculations for moderately massive star clusters ($M_{\rm ecl} \approx 10^{3.5}\,{\rm M}_\odot$). We vary the initial conditions of the calculations, such as the initial half-mass radius of the clusters, initial binary populations for massive stars and initial mass segregation. We find that the initial density is the most influential parameter for the ejection fraction of the massive systems. The clusters with an initial half-mass radius $r_{\rm h}(0)$ of 0.1 (0.3) pc can eject up to 50% (30%) of their O-star systems on average, while initially larger ($r_{\rm h}(0) = 0.8$ pc) clusters, that is, lower density clusters, eject hardly any OB stars (at most ≈4.5%). When the binaries are composed of two stars of similar mass, the ejections are most effective. Most of the models show that the average ejection fraction decreases with decreasing stellar mass. For clusters that are efficient at ejecting O stars, the mass function of the ejected stars is top-heavy compared to the given initial mass function (IMF), while the mass function of stars that remain in the cluster becomes slightly steeper (top-light) than the IMF. The top-light mass functions of stars in 3 Myr old clusters in our N-body models agree well with the mean mass function of young intermediate-mass clusters in M31, as reported previously. This implies that the IMF of the observed young clusters is the canonical IMF. We show that the multiplicity fraction of the ejected massive stars can be as high as ≈60%, that massive high-order multiple systems can be dynamically ejected, and that high-order multiples become common especially in the cluster. We also discuss binary populations of the ejected massive systems. Clusters that are initially not mass-segregated

begin ejecting massive stars after a time delay that is caused by mass segregation. When a large kinematic survey of massive field stars becomes available, for instance through *Gaia*, our results may be used to constrain the birth configuration of massive stars in star clusters. The results presented here, however, already show that the birth mass-ratio distribution for O-star primaries must be near uniform for mass ratios $q \gtrsim 0.1$.

4.1 Introduction

Massive runaways (Blaauw 1961) are massive stars that move with a high peculiar velocity ($\gtrsim$30 km s^{-1}) or that are located at large distances from the Galactic plane. They have been observed in the Galaxy (Blaauw 1961; Gies & Bolton 1986; Hoogerwerf et al. 2001; Gvaramadze et al. 2012, and references therein) and nearby galaxies (Gvaramadze et al. 2012). At high redshift, massive runaways may have played an important role in reionizing the Universe (Conroy & Kratter 2012).

Blaauw (1961) proposed the binary supernova hypothesis to explain the origin of runaways, in which the initially less massive star in a binary that is composed of two massive stars obtains a high velocity when the more massive star explodes as a supernova. Poveda et al. (1967) proposed another mechanism for the origin of runaways, namely the dynamical ejection through energetic few-body interactions. When a close encounter between stars involves a binary, binding energy can be transformed into kinetic energy and a runaway can thus be produced. Leonard & Duncan (1990) showed with small-number N-body calculations that the most efficient way of producing massive runaways is a close binary–binary encounter. Dynamical ejections of massive stars have been studied numerically with three/four-body scattering experiments (e.g. Leonard 1995; Gualandris et al. 2004; Gvaramadze et al. 2009; Gvaramadze & Gualandris 2011) and with full N-body calculations of real-sized young star clusters (e.g. Fujii & Portegies Zwart 2011; Banerjee et al. 2012b; Perets & Šubr 2012; Oh et al. 2015). These two scenarios are considered as the main processes for populating massive stars outside of clusters, especially runaways, from star clusters. In reality both processes will play a role (Hoogerwerf et al. 2001; Tetzlaff et al. 2011). The combination, the two-step ejection process, is a key mechanism to provide massive field stars that cannot be traced back to their birth cluster, which leads to a misinterpretation of such stars as being formed in isolation (Pflamm-Altenburg & Kroupa 2010).

In the supernova scenario, the ejection requires a supernova explosion, implying that the ejection will occur only after a few Myr from the birth of the stars. But a dynamical ejection can occur any time in a stellar lifetime and even during the formation time, that is, at ages younger than a Myr. There are very young star clusters that are too young to have had a supernova, but which have runaway OB stars around them, for example, NGC 6611 (Gvaramadze & Bomans 2008), NGC 6357 (Gvaramadze et al. 2011), NGC 3603 (Roman-Lopes 2012, 2013; Gvaramadze et al. 2013), and Westerlund 2 (Roman-Lopes et al. 2011, cf. Hur et al. 2015). This implies that the massive stars are ejected from their natal cluster at an early age. Those field O stars that can be traced back to a star cluster or an association appear to have left their birth place at a very early age (Schilbach & Röser 2008). Very massive ($\gtrsim$100 M$_\odot$) runaways (e.g. 30 Dor 016, Evans et al. 2010) and very massive single stars and binaries in apparent isolation (e.g. VFTS 682, Bestenlehner et al. 2011; R144, Sana et al. 2013a) in the Large Magellanic Cloud are most likely the outcome of dynamical ejections (Banerjee et al. 2012b; Oh et al. 2014, Chapter 5). These observations therefore imply that the dynamical ejection process is very significant for the massive star

population within a cluster (e.g. loss of massive stars in the cluster) and outside of a cluster (e.g. origin of the field massive stars).

The dynamical ejection process is sensitive to the initial conditions of massive star populations and to the properties of their birth cluster. The runaways can therefore be used as constraints to probe the initial configuration of massive stars in star clusters, under the assumption that dynamical ejection is the dominant process in producing the massive runaways. By assuming that OB runaways are dynamically ejected from star clusters, Clarke & Pringle (1992) deduced the birth configuration of OB stars using observed properties of OB runaways, such as their proportion and the high ratio of O to B stars in the runaway population. They suggested that massive stars form in compact groups of binaries with mass ratios biased toward unity and containing a deficit of low-mass stars. This configuration would correspond to the mass-segregated core of a dense young star cluster. The authors provided analytical results and neglected the cluster potential.

If all the field O stars, not only the runaways, have formed in clusters and then populated the Galactic field dominantly by the dynamical ejection process, studying the properties of the dynamically ejected population may help to constrain the initial configuration of massive stars in their birth cluster. It is therefore our aim to study how the properties of the ejected massive stars vary with various initial conditions using direct N-body calculations that include the entire cluster.

Using the theoretical young cluster library presented in Oh & Kroupa (2012, Chapter 2) and Oh et al. (2015, Chapter 3), we here study the dynamical ejection of massive stars from young star clusters with diverse initial conditions. The chapter is structured as follows. Initial conditions of our N-body models are briefly described in Section 4.2. Section 4.3 describes the fraction of ejected OB stars in different models. Properties of ejected stars produced in the N-body models, such as the velocity distribution and mass function, are presented in Section 4.4. In Section 4.5, multiplicity fractions and binary populations of ejected massive systems are illustrated. The discussion and summary follow in Sections 4.6 and 4.7.

4.2 N-body models

We adopted N-body models of $M_{\rm ecl} = 10^{3.5}\,{\rm M}_\odot$ clusters from the theoretical young star cluster library of Oh & Kroupa (2012, Chapter 2) and its extension in Oh et al. (2015, Chapter 3). With this mass, model clusters are the most efficient at ejecting O-star systems (Oh et al. 2015, Chapter 3) and they have the largest number of ejected O-star systems per set of initial conditions because more runs (100 reailizations for each set of initial conditions) were performed than for the clusters with higher masses (e.g. 10 runs for $10^4\,{\rm M}_\odot$ models). The library contains a wide variation of the initial conditions for star clusters, such as the initial half-mass radius, initial mass segregation, binary fraction, and two pairing methods for massive binaries. Thus the cluster mass we chose here suits the aim of studying how the ejection fraction and the properties of the ejected massive stars depend on the initial conditions.

Common initial conditions for all models are briefly described as follows (see Oh & Kroupa 2012; Oh et al. 2015, Chapters 2 and 3, for more details). Stellar masses are randomly drawn from the two-part power-law canonical initial mass function (IMF),

$$\xi(m) \propto m^{-\alpha_i}, \tag{4.1}$$

with power-law indices of $\alpha_1 = 1.3$ for $0.08 \leq m/{\rm M}_\odot < 0.5$ and of $\alpha_2 = 2.3$ (the Salpeter index) for

Model	$r_{\rm h}(0)$ (pc)	IMS	$f_{\rm bin}$	IPD	Pairing method	e dist.
MS1OP	0.1	Y	1	Kroupa	OP	thermal
MS3OP_SPC	0.3	Y	1	Sana et al.	OP	$e = 0$
MS3OP_SP	0.3	Y	1	Sana et al.	OP	thermal
MS3UQ_SP	0.3	Y	1	Sana et al.	uniform q-dist.	thermal
MS3OP	0.3	Y	1	Kroupa	OP	thermal
MS3RP	0.3	Y	1	Kroupa	RP	thermal
MS3S	0.3	Y	0	-	-	-
NMS3OP	0.3	N	1	Kroupa	OP	thermal
NMS3RP	0.3	N	1	Kroupa	RP	thermal
NMS3S	0.3	N	0	-	-	-
MS8OP	0.8	Y	1	Kroupa	OP	thermal
MS8RP	0.8	Y	1	Kroupa	RP	thermal
MS8S	0.8	Y	0	-	-	-
NMS8OP	0.8	N	1	Kroupa	OP	thermal
NMS8RP	0.8	N	1	Kroupa	RP	thermal
NMS8S	0.8	N	0	-	-	-

Table 4.1. List of the N-body models and their initial conditions. Initial half-mass radius, $r_{\rm h}(0)$, is listed in column 2. Column 3 denotes initial mass segregation (IMS), N standing for the initially unsegregated cluster model and Y for the initially mass-segregated one. The initial binary fraction, $f_{\rm bin}$, is listed in column 4. Initial period distributions (IPD) applied to massive binaries are listed in column 5, where Sana et al. and Kroupa refer to the distributions introduced in Sana et al. (2012, Equation 4.3) and Kroupa (1995b, Equation 4.2). Column 6 is the pairing method for massive binaries (primary mass $m_1 \geq 5\,{\rm M}_\odot$, for details see Section 4.2). The last column gives the initial eccentricity distribution for massive binaries. In binary-rich clusters, all low-mass binaries have the period distribution of Kroupa (1995b) and a thermal eccentricity distribution, and their component masses are randomly paired for consistency with observational data (Kroupa 1995a,b; Marks & Kroupa 2011). Each model is computed $N_{\rm run} = 100$ times with different random number seeds to obtain representative statistics.

$m/{\rm M}_\odot \geq 0.5$, where m is the stellar mass (Kroupa 2001; Kroupa et al. 2013). The lower mass limit for stellar masses adopted here is $0.08\,{\rm M}_\odot$. The upper stellar mass limit of the IMF, $m_{\rm max}$, is derived from the relation between maximum stellar mass and cluster mass (Weidner & Kroupa 2006; Weidner et al. 2010, 2013a), e.g. $m_{\rm max} \approx 79.2\,{\rm M}_\odot$ for the $10^{3.5}\,{\rm M}_\odot$ cluster. Initial positions and velocities of stars (centre of mass in the case of a binary system) are generated according to the Plummer density profile with the assumption that the clusters are initially in virial equilibrium. In initially mass-segregated models (with a name starting with MS), the more massive star is more closely bound to the cluster (Baumgardt et al. 2008). Mainly two different initial half-mass radii of $r_{\rm h}(0) = 0.3$ and 0.8 pc are used, but we also include a model with $r_{\rm h}(0) = 0.1$ pc for comparison. The 0.3 pc model-sets are consistent with the radius-mass relation of very young embedded clusters (Marks & Kroupa 2012).

The typically large angular momenta of star-forming cloud cores (Goodman et al. 1993; Fig. 13 in Kroupa 1995b) imply that most, if not all, stars form in a binary multiple system (Goodwin et al. 2007; Duchêne & Kraus 2013; Reipurth et al. 2014), as shown in observations, for instance, the high binary fractions for massive stars in clusters (Sana et al. 2014; Chini et al. 2012) and for protostars (Duchêne

et al. 2007; Chen et al. 2013). We therefore include primordial binaries in most of our models for a more realistic initial set-up of the young star clusters, especially for the massive star population in them. In this study, we assume a binary fraction of 100% for the initially binary-rich models. Modelling a cluster with primordial binaries requires distributions of initial binary parameters such as eccentricity, e, period, P in days, and mass ratio, $q = m_2/m_1$ where m_1 and m_2 are the masses of the binary components and $m_1 \geq m_2$.

The models in Oh & Kroupa (2012, Chapter 2) adopted equation (8) of Kroupa (1995b),

$$f(\log_{10} P) = 2.5 \frac{\log_{10} P - 1}{45 + (\log_{10} P - 1)^2}, \tag{4.2}$$

as the initial period distribution for all binaries (Marks & Kroupa 2011; Marks et al. 2014; Leigh et al. 2015). This period distribution was deduced from studies of solar-mass binaries that have been intensively studied (Duquennoy & Mayor 1991), and is also applied to the massive binaries in the library since the period distribution of massive binaries is poorly constrained in observation and theory. However, recent observational studies show a high fraction of short-period binaries for massive (e.g. O star) binaries (Sana et al. 2012; Kobulnicky et al. 2014). Oh et al. (2015, Chapter 3) additionally performed cluster models with the Sana et al. (2012) period distribution for massive binaries with a primary mass $\geq 5\,\mathrm{M}_\odot$ (equation 3 in Oh et al. 2015, Chapter 3),

$$f(\log_{10} P) = 0.23 \times (\log_{10} P)^{-0.55}, \tag{4.3}$$

with a range $0.15 \leq \log_{10}(P/\mathrm{days}) \leq 6.7$. These models are indicated with _SP in their names, for example MS3UQ_SP, MS3OP_SP, and MS3OP_SPC.

For lower mass binaries ($m_1 < 5\,\mathrm{M}_\odot$), masses of binary components are randomly chosen from the IMF. For massive binaries ($m_1 \geq 5\,\mathrm{M}_\odot$), we use three different pairing methods. The first is random pairing (RP) as for lower mass binaries, the second is ordered pairing (OP, Oh & Kroupa 2012, Chapter 2), which produces q biased towards unity by sorting stars with decreasing mass after generating the mass-array from the IMF and then pairing them in the sorted order. The last is a uniform mass-ratio distribution (UQ, the MS3UQ_SP model) in which the companion is chosen from the stellar masses already drawn from the IMF with the closest mass ratio to a value drawn from a uniform distribution for $q \geq 0.1$. The uniform distribution is adopted to imprint the observed mass-ratio distribution of O-star binaries (Sana et al. 2012; Kobulnicky et al. 2014). The very important point we need to emphasize here is that our procedure of first drawing N stars from the IMF with a combined mass of $10^{3.5}\,\mathrm{M}_\odot$ and only then pairing stars from this array to binaries is essential so as to not change the shape of the stellar IMF.

In the model libraries, the eccentricities are generated from the thermal distribution, $f(e) = 2e$ (Kroupa 2008). While the observed eccentricity distribution of low-mass and solar-type binaries is well accounted for by the thermal distribution, that of the high-mass counterpart is not well described with a simple functional form. As a simple test, we additionally include calculations that are the same as the MS3OP_SP models, but with all massive binaries (with primary star $\geq 5\,\mathrm{M}_\odot$) being initially in a circular orbit (MS3OP_SPC).

We include single-star cluster models, that is, those with an initial binary fraction of 0, for comparison. These models are indicated in the model names with the suffix S.

Each cluster is calculated with the direct N-body code NBODY6 (Aarseth 2003) up to 5 Myr and stellar evolution is taken into account with the stellar evolution library (Hurley et al. 2000, 2002) that is implemented in the code. Throughout this chpater, however, we use the snapshots at 3 Myr because after this time, stellar evolution significantly changes the masses of the most massive stars in the clusters, and the first supernova occurs at around 4 Myr .

Table 4.1 lists the initial conditions for each of the models. The wide range of initial conditions will help us to study how properties of the ejected OB stars change with cluster initial condition and to constrain the initial configuration of massive stars in a star cluster. Sixteen models are considered in total and each model contains 100 reailizations with a different random seed number. The results are therefore either averages or the compilation of 100 runs.

4.3 Effects of the initial conditions on ejection fractions

In this section we discuss how each initial condition affects the resulting dynamical ejection fractions, especially those of massive stars. Before discussing the results, we define terms and quantities used in this chapter for clarity. We refer throughout to a star more massive than 17.5 $M_\odot$ as an O star, to one with a mass between 3 and 17.5 $M_\odot$ as a B star, and to one with a mass between 1.65 and 3 $M_\odot$ as an A star (Adelman 2004). The mass is determined from the snapshots at 3 Myr. Although we switched on stellar evolution, their masses change little from the initial values unless stars collide with other stars. We call a star massive when its mass exceeds 5 $M_\odot$ (all O and early-B stars) in this study. Throughout this chapter, we use the word system for either a single star or a multiple system (see Section 4.5.1 for the procedure for searching multiples). The spectral type of the system is defined to be that of the primary star (the most massive component) in the case of a multiple system.

From snapshots at 3 Myr, we regard a system as an escapee when it is located farther than $3 \times r_{\rm h}(3\,{\rm Myr})$ from the cluster centre and is moving faster than the escape velocity at its distance. The averaged $r_{\rm h}(3\,{\rm Myr})$ is approximately 0.5, 0.55–0.7, and 0.85–1.0 pc (depending on models) for clusters with $r_{\rm h}(0)$ = 0.1, 0.3, and 0.8 pc, respectively (Oh & Kroupa 2012; Oh et al. 2015, Chapters 2 and 3). We assume that the escapees are dynamically ejected since the dynamical ejection process is the only way to move massive stars outwards at a young age before the first supernova explosion. A cluster within an extreme environment, such as the Galactic centre, may lose its massive stars through tidal stripping by a strong tidal field if the cluster forms with a size similar to its tidal radius and without primordial mass segregation (e.g. Habibi et al. 2014, but the observation indicates that those stars are possibly ejected from young star clusters through energetic encounters with other stars, Dong et al. 2015). However, it is worth mentioning that lower mass escapees are not necessarily ejected. Slowly moving stars may be the outcome of evaporation that is driven by two-body relaxation for these escapees.

The ejection fraction of a certain spectral type (ST) star,[5] $f_{\rm ej,ST}$, is defined as

$$f_{\rm ej,ST} = \frac{N_{\rm ej,ST}}{N_{\rm sys,ST}}, \tag{4.4}$$

where $N_{\rm ej,ST}$ and $N_{\rm sys,ST}$ are the number of the ejected systems and the total number of systems for a certain stellar type in a calculation, respectively. Throughout the study, we use the average of ejection

[5] We use the term spectral type to distinguish groups with different stellar masses.

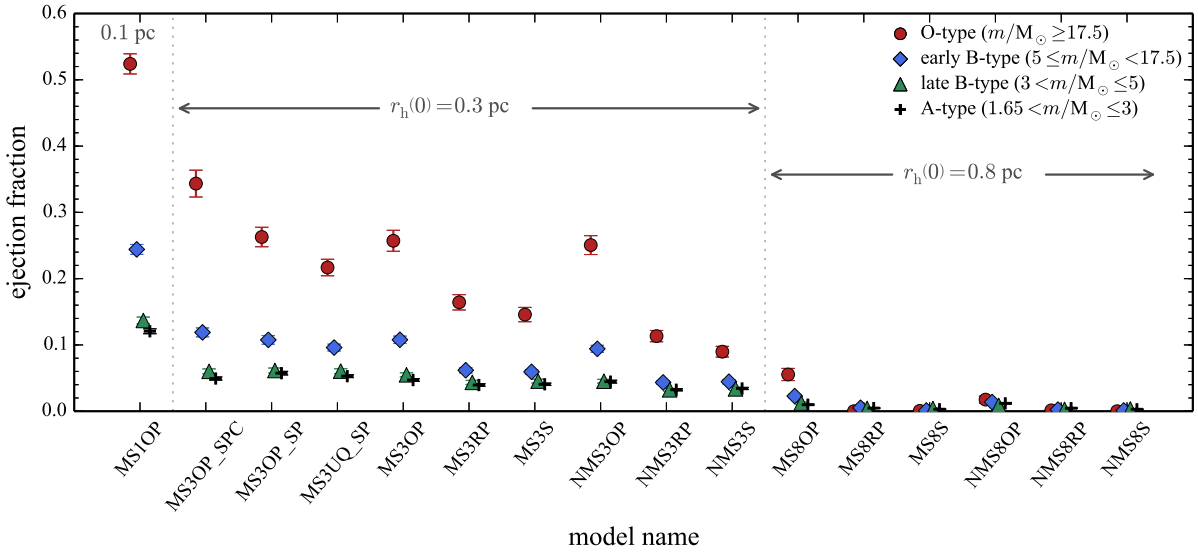

Figure 4.1. Averaged ejection fractions (Equation 4.4), $\langle f_{\mathrm{ej,ST}} \rangle$, of systems for four different primary-mass groups at 3 Myr. Model names are indicated on the x-axis (see Table 4.1). The error bars are the standard deviation of the mean.

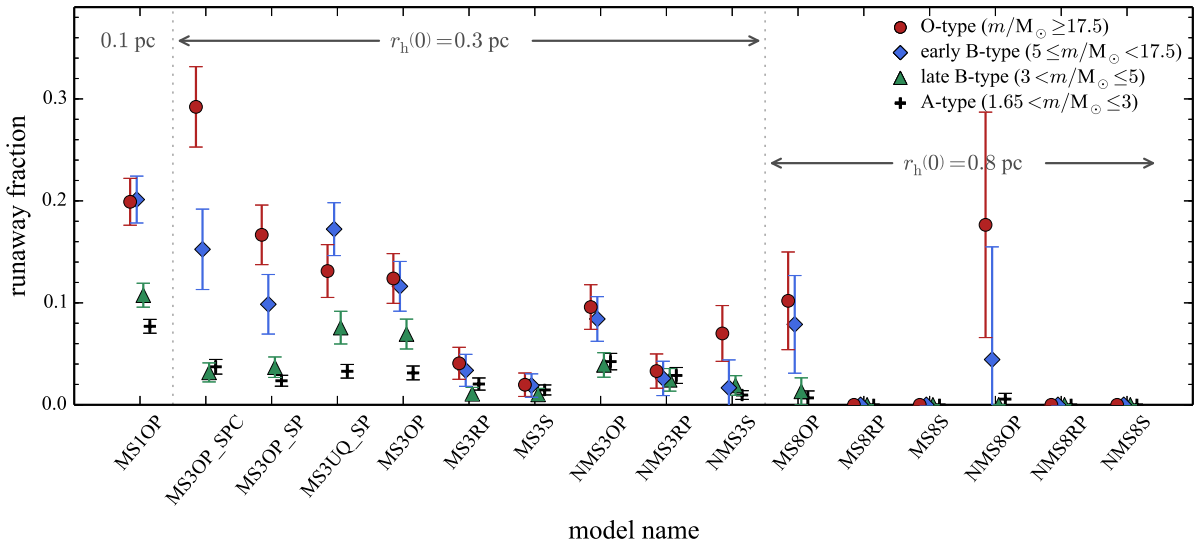

Figure 4.2. Runaway fraction among the ejected systems, the number of runaways divided by the number of ejected stars (Equation 4.5). The fraction is derived from all runs for each model. The error bars indicate Poisson uncertainties.

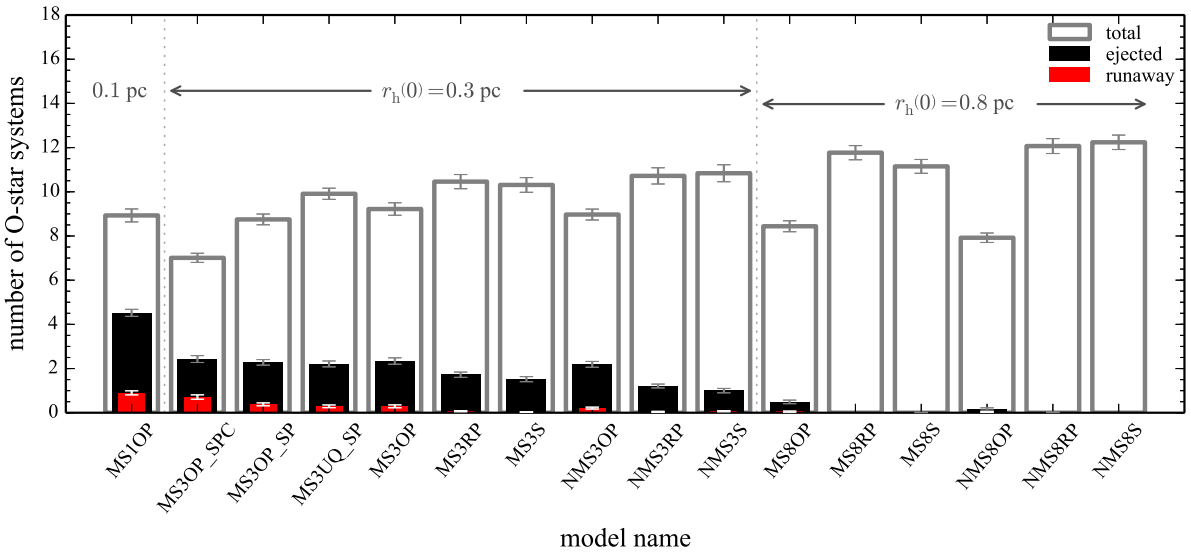

Figure 4.3. Averaged numbers, $\bar{N}$, of total (open grey), ejected (black), and runaway (red bars) O-star systems in the models at 3 Myr. The error bars are the standard deviation of the mean. The total number varies because of the different binary fraction and/or the different mass-ratio distribution at 3 Myr.

fractions from 100 reailizations of each model. An ejected system moving with a velocity greater than 30 km s^{-1} is referred to as a runaway. The runaway fraction is the ratio of the number of the runaway systems, $N_{\rm r,ST}$, to the number of ejected systems. We use the runaway fraction relative to all ejected systems of each model,

$$f_{\rm r,ST} = \frac{\sum N_{\rm r,ST}}{\sum N_{\rm ej,ST}}. \tag{4.5}$$

In the following subsections, we discuss the results depending on the initial conditions, such as initial size, mass segregation, and binary populations. Figures 4.1 and 4.2 show the averaged ejection fractions and the runaway fractions of different stellar mass groups for all models.

4.3.1 Initial size (density) of cluster

The close encounter rate is proportional to the cluster density. Since we chose the same cluster mass for all models, it is expected that the ejection is more efficient with decreasing initial size of the cluster in our models.

The highest ejection fraction appears in the most compact cluster in our model library (MS1OP) with an average O-star ejection fraction of about 52%, which is about twice higher than for the model with $r_{\rm h}(0) = 0.3$ pc (MS3OP). Clusters with $r_{\rm h}(0) = 0.3$ pc ($\rho_{\rm h} \approx 1.4 \times 10^4$ M$_\odot$ pc^{-3}) eject ≈9–34% of O-type systems depending on the initial conditions (Fig. 4.1). However, clusters with $r_{\rm h}(0) = 0.8$ pc ($\rho_{\rm h} \approx 740$ M$_\odot$ pc^{-3}) eject hardly any massive stars. Only the binary-rich clusters with OP massive binaries eject a few percent of OB stars ($\lesssim$3.5% for O-type and <1% for B-type systems). None of the single-star clusters or RP binary-rich clusters eject OB stars. It is therefore very unlikely that this or larger clusters with the mass studied here populate massive stars into the field through dynamical ejections. Most of the massive stars in the field should form in compact star clusters ($r_{\rm h}(0) \lesssim 0.5$ pc),

which eject massive stars efficiently if they have a dynamically ejected origin. But if the cluster is too compact ($r_{\rm h}(0) \lesssim 0.1$ pc), the ejection of O-star system is so efficient that it may lead to a higher fraction of O stars relative to all young stars in the field than in the cluster.

The determining factor for the number of ejected O-star systems is the initial cluster size. For the same initial half-mass radius, the averaged number of the ejected O-star systems is similar and approximately independent of the other initial conditions, although the ejection fraction varies as a result of the different number of total O-star systems, which depends on the initial binary fraction, the mass ratio of O-star binaries, and the stellar merger rate (Fig. 4.3).

Although the dependence of the O-star runaway fraction on the model properties is similar to that of the O-star ejection fraction, the runaway fraction does not seem to be strongly dependent on the initial size (i.e. density) of the cluster. The ejection velocity of a system attained after an energetic close encounter is mainly determined by configurations of the systems that are involved in the encounter. For example, for a single–binary encounter, the ejection velocity $v_{\rm ej}$ is of the order of the orbital velocity of the binary (Heggie 1980; Gies & Bolton 1986; Perets & Šubr 2012),

$$v_{\rm ej} \propto \left(\frac{m}{a}\right)^{1/2}, \tag{4.6}$$

where a and m are the semi-major axis of the binary and the typical mass of the stars engaging in the encounter, respectively. The ejection velocity is higher when a tighter binary is involved (e.g. Gvaramadze et al. 2009). It is expected that the denser cluster (i.e. the cluster with the higher velocity dispersion) is more efficient in producing runaways among ejected systems if the initial density is the only difference between clusters. The reason is that binaries with an orbital velocity similar to the velocity dispersion of the cluster are dynamically most active, and a higher velocity is required for escapees from a denser cluster because of its deeper gravitational potential (see also fig. 8 in Oh et al. 2015, Chapter 3, for the runaway fraction as a function of cluster mass for clusters with the same initial half-mass radius). Based on comparing MS1OP and MS3OP (the two models differ only in size, i.e. density) in Fig. 4.2, the initially denser cluster has a higher runaway fraction. However, clusters with a lower density (a larger size) can produce a higher fraction of runaways among ejected systems than denser (more compact) clusters if a higher fraction of energetic (e.g. close) binaries are present in the less dense clusters. For example, the model with short period (Equation 4.3) and only circular massive binaries (MS3OP_SPC) produces runaways more efficiently than the smaller cluster model that has the Kroupa period distribution (Equation 4.2) and the thermal eccentricity distribution (MS1OP). An initial binary population (especially, with which clusters maintain a high fraction of short-period binaries after an early dynamical evolution) can therefore be more important than the initial density for efficiency with which runaways are produced among ejected stars (see also Section 4.3.3). The high O-star runaway fractions in some models that have a low ejection fraction (e.g. the MS3S, MS8OP, and NMS8OP models) arise from the small number of the ejected O-star systems.

4.3.2 Initial mass-segregation

For cluster models with $r_{\rm h}(0) = 0.3$ pc, the final ejection fraction is not strongly sensitive to whether the cluster is initially mass-segregated when a massive binary is initially composed of two massive stars. The ejection fraction of OB stars for the MS3OP model, for instance, is only 1–2% higher than that of the

NMS3OP model.

However, differences are shown when the massive binaries are randomly paired or when there is no initial binary. The MS clusters eject OB stars almost twice as often as the NMS clusters. These initial conditions are unrealistic, however, because many massive stars in young star clusters are binaries and the companions are very likely massive stars.

For clusters with $r_{\rm h}(0) = 0.8$ pc, the MS8OP model is more efficient at ejecting massive stars than the NMS8OP model, even though the massive binaries are composed of two massive stars. This is due to the larger size of the clusters, which leads to a significantly longer mass-segregation timescale even if massive stars are paired with other massive stars. Such large initially not mass-segregated clusters therefore need time for the massive stars to segregate to the core. Ejections of massive stars arise from there on.

In realistic models with characteristic radii of a few tenths of a pc and a high proportion of short-period binaries with a similar spectral-type companion, it would be difficult to determine whether the cluster was initially mass-segregated by only considering the ejection fraction of massive stars because the initial mass segregation is not a strong factor for the ejection fraction at 3 Myr. But other properties, such as the time distribution when the ejections occur, may show differences between initially mass-segregated and not mass-segregated clusters. It is expected that the MS clusters would start ejecting massive stars earlier than the NMS clusters would because the dense core of massive stars already exists in the centre of the MS clusters at the beginning of the cluster evolution. This is discussed in Section 4.4.3.

4.3.3 Initial binary population

We varied four parameters for the initial binary populations of massive systems. The first was the binary fraction. The dynamical ejection process most likely involves at least one binary, regardless of whether it was primordial or dynamically formed. During the energetic close encounter between a binary and a single star or binary, the binding energy of the binary transforms into kinetic energy and a star may be ejected. Binaries have a larger cross-section, which increases the probability of energetic encounters. The dynamical formation of binaries is inefficient. Thus a high initial binary fraction enhances the interaction rate, resulting in a significantly higher ejection fraction. Including primordial binaries plays a central role in ejecting massive stars from the cluster because single-star clusters eject OB stars slightly later than binary-rich clusters. This is a result of the time that first needs to pass for binary systems to form dynamically, as is evident in the example presented here (clusters with $r_{\rm h}(0) = 0.3$ pc).

The second parameter we varied was the pairing method (i.e. mass-ratio distribution) for the massive binaries. None of the single-star clusters with $r_{\rm h}(0) = 0.8$ pc ejects OB-star systems by 3 Myr (Fig. 4.1). The situation does not change when the initial binary fraction is 100%, but the massive binaries are paired with companions randomly chosen from the whole IMF. For clusters with $r_{\rm h}(0) = 0.3$ pc, both single-star and RP binary-rich clusters eject approximately 4–6% of O-star systems and ≈1.5–2.3% of B-star systems by 3 Myr. The ejection fractions are similar for both cluster models, meaning that the difference is smaller than 1%. This is because most massive binaries paired randomly behave like single stars because their mass ratios are very low. The mass ratio of the system would be $q \approx 10^{-3}$ in the most extreme case, for instance, if the most massive star (≈80 $M_\odot$) is paired to the least massive star (≈0.08 $M_\odot$) in the cluster.

When massive binaries initially have a massive companion (OP and UQ models), however, clusters

eject massive stars more efficiently. For initially mass-segregated clusters with $r_{\rm h}(0) = 0.3$ pc, for instance, ejection fractions of massive systems for the OP cluster models are more than twice as high (differences of up to 16% for O-star systems and 6% for early-B star systems) as those of the single-star or RP clusters. Runaway fractions for the OP models are also higher than those of the single-star or RP models (Fig. 4.2). For the OP models, the massive binaries involved in the close encounters initially have a higher binding energy as a result of the higher masses of binary components, which increases the ejection velocity (Equation 4.6), compared to the massive binaries for the single-star or RP models. Not only do they show higher ejection and runaway fractions, but the ejection of massive systems from these clusters occurs when they are younger than 1 Myr (see Section 4.4.3). We also note that the OP model (MS3OP_SP) in which O-star binaries are initially paired with an O star shows higher ejection and runaway fractions of O-star systems than the UQ model (MS3UQ_SP) in which a large portion of O-star binaries initially have a B-star companion. This difference in companions of O-star binaries may result in a higher runaway fraction of B-star systems for the UQ model than for the OP model (Fig. 4.2). For the UQ model B stars can engage in close encounters with O stars more often than in the OP model. Therefore, the UQ model has a higher probability of producing B-star runaways since the least massive star among interacting stars gains the highest velocity.

The third parameter we varied was the initial period distribution function. Given two initial period distribution functions considered for the massive binaries in this study (Equations 4.2 and 4.3), the distribution is not a significant factor in determining the ejection efficiency of O-star systems. For example, the models with the two different initial period distributions (e.g. MS3OP_SP and MS3OP) show similar results for the O-star ejection fraction and the number of the ejected O-star systems (Figs. 4.1 and 4.3). However, the model with the short-period massive binaries (MS3OP_SP) produces more runaways than the model with the softer Kroupa period distribution (MS3OP) (Fig. 4.2).

The last parameter we changed was the initial eccentricity distribution function. For the initial eccentricity distribution of massive binaries, all binary-rich models but one assumed the thermal distribution, which well reproduces the observed eccentricity distribution for low-mass binaries (Kroupa 1995b). Since massive short-period binaries are mostly found in circular orbits (e.g. $e = 0$ for $P \leq 2$ days, Sana et al. 2012), we included a model (MS3OP_SPC) for which all massive binaries were in circular orbits. The two models in which only the initial eccentricity distribution differs (all systems having initial $e = 0$, MS3OP_SPC, versus the thermal distribution, MS3OP_SP) show a similar average number of the ejected O-star systems at 3 Myr (black bars in Fig. 4.3). However, the number of total O-star systems (open grey bars in Fig. 4.3) are different for the two models. For the MS3OP_SPC model, the binaries with a short period in a circular orbit hardly break up or merge at all, keeping the number close to the initial number of O-star systems, which is half of the number of individual O stars. For the MS3OP_SP model in contrast, a large portion of massive binaries, composed of similar-mass components, merge and form a single massive star as a result of their short period and high eccentricity. Thus more O stars are formed by merging of less massive stars during the evolution of the clusters. With the increase of the total number of O stars by collisions in the MS3OP_SP model and the smaller total number of O-star systems in the MS3OP_SPC model, the ejection efficiency of the latter model is higher than that of the former model, although both models result in the same average number of the ejected O-star systems. Differences also appear in the numbers of O-star runaways (Fig. 4.3) and the runaway fractions (Fig. 4.2) of the two models. With initially only circular binaries, more O-star runaways are produced than in the model

with the thermal initial eccentricity distribution. The reason may be that the eccentric orbits are mostly near their apo-centre where orbital velocities are lower and thus produce lower slingshot velocities than circular orbits with the same semi-major axis. This means that the initial eccentricity also plays a role in the ejection efficiency and in the properties of the ejected systems (Section 4.4), especially when massive binaries are initially highly biased towards short periods (e.g. an initial period distribution given by Equation 4.3).

4.4 Properties of the ejected massive systems

In this section, we consider the properties (e.g. velocities, the mass function, and multiplicities) of the ejected OB stars and study how they vary with different initial conditions. Here, we only examine the results from the clusters with $r_{\rm h}(0) = 0.3$ pc since the clusters with $r_{\rm h}(0) = 0.8$ pc eject hardly any OB stars (most models do not eject OB stars, Fig. 4.1). For the $r_{\rm h}(0) = 0.1$ pc models, the ejection fraction is high, although these clusters are too small to be realistic, and therefore only one set of models was calculated for the effect of cluster size (density) on the dynamical ejection.

4.4.1 Ratio of ejection and runaway fractions for O- to B-star systems

As already mentioned in the previous section, the ejection fraction generally increases with increasing stellar mass. For models with $r_{\rm h}(0) \leq 0.3$ pc, the ratios of the ejection fraction of the O-type to that of early-B type systems are ≈2–2.9, while the ratios of early-B to late-B type systems are <2.0. This tendency indicates that the difference of the ejection efficiency decreases with decreasing stellar mass and the difference almost disappears in the low-mass (<5 $M_\odot$) regime. The reason for this decrease of the ejection fraction with the stellar mass would be that O-star systems quickly sink into the cluster core and are ejected at the earliest time when the cluster core is in the densest phase.

In the observational studies, the fraction of runaways for the different spectral types have been presented. For example, Blaauw (1961) reported the frequency of runaways to be 21, 2.5, and 1.5% for stars with spectral types of O5–O9.5, B0–B0.5, and B1–B5, respectively. Gies & Bolton (1986) collected the runaway fractions of O- and B-type stars from several publications and listed them as 10–25% and 2%, respectively. This means that the ratio of the O- to B-star runaway fraction is between 5–10, depending on the literature. This decrease in runaway fraction with decreasing stellar mass extends to lower masses. The frequency of high-velocity A stars relative to the total number is 0.5–1.0% (Gies & Bolton 1986). Stetson (1981, 1983) found evidence for a young, high-velocity A-star population that accounts for 0.1–0.2% of the A stars in the vicinity of the Sun.

In our models, the sharp decrease of the ejection fraction with decreasing stellar mass appears as well. When only the ejected systems are considered, the runaway fractions of O-star and early-B star systems are almost the same for a few models, although the runway fractions generally decrease with decreasing stellar mass (Fig. 4.2). In the MS3UQ_SP model, which is the most realistic model in the library, the runaway fraction of the ejected systems for B-star systems is higher than that for O-star systems. If we consider entire populations of each mass group for the runaway fraction (i.e. the systems that are ejected and those that remain in clusters, for which we replace the denominator of Equation 4.5 by $\Sigma N_{\rm sys,ST}$), the sharp decrease of the runaway fraction with decreasing group mass becomes pronounced. For the MS3OP_SPC model, for example, the runaway fraction relative to the entire O-star systems is ≈10%,

while the runaway fraction of early-B type systems (primary mass $5 \leq m_1/\mathrm{M}_\odot < 17.5$) relative to the entire early-B type systems is ≈1.8%. In the MS3UQ_SP model, the fractions are 2.8% and 1.7% for O-star and early-B star systems, respectively. In all models the runaway fractions of O-star systems are higher than those of B-star systems. Although the model values are slightly lower than those of the observed ones, they agree with the observational finding that the runaway fraction increases with increasing stellar mass when the fraction of runaways of all systems, whether ejected or not, is considered. But this tendency is not a unique feature of the dynamical ejection process. It also appears in the binary supernova scenario (Eldridge et al. 2011). This means that if the observed samples are a mixture of outcomes of the two processes, the supernova scenario will enhance the tendency that appears in our models. We note that the runaway fractions reported in the literature are space frequencies or derived from given star catalogues that may include selection biases and contamination. The difference of our theoretical results compared to the observation might also be caused by the different initial configurations that the O- and B-star systems may have. In our calculations, the distribution function for periods, eccentricities, and mass ratios of initial binary population are the same for both O-star and early-B star systems, and in reality this may not be the case.

4.4.2 Velocities of the ejected massive star systems

In Fig. 4.4 we plot the system masses and velocities of all ejected systems from the MS3UQ_SP model at 3 Myr. The histograms in the upper panel of Fig. 4.4 show velocity distributions of all ejected systems with different stellar masses and the distribution of those that remain in the star cluster. Systems that remain in the cluster have a velocity lower than $10\,\mathrm{km\,s^{-1}}$, with a peak near 3–4 $\mathrm{km\,s^{-1}}$, which is the velocity dispersion of a cluster with a mass of $10^{3.5}\,\mathrm{M}_\odot$ and a size of $r_\mathrm{h} = 0.3$ pc. O-star systems ejected from the cluster show a velocity peak close to the escape velocity at the cluster centre, for example about $11\,\mathrm{km\,s^{-1}}$ for the $10^{3.5}\,\mathrm{M}_\odot$ cluster with $r_\mathrm{h}(0) = 0.3$ pc and about $19\,\mathrm{km\,s^{-1}}$ for the $10^{3.5}\,\mathrm{M}_\odot$ cluster with $r_\mathrm{h}(0) = 0.1$ pc (see the MS1OP model in Fig. C.1). Because massive stars are ejected from the cluster centre, ejected massive stars require the velocity to be higher than the central escape velocity of the cluster. This velocity peak therefore varies with the initial condition of a cluster. With the same initial half-mass radius, the peak will move to a higher velocity with increasing cluster mass.

The velocity distribution also varies with the stellar mass of the ejected systems. The top panel of Fig. 4.4 exhibits the velocity distributions of the ejected systems for different stellar masses. The more massive systems tend to have a distribution biased towards higher velocities (see also Fig. C.1 for other models), although in Fig. 4.4 the difference between the velocity distribution of ejected O-star and of ejected early-B star systems is marginal. Banerjee et al. (2012b) also showed that the average velocity of ejected stars increases with stellar mass. The lowest velocity of ejected systems slightly increases with system mass in the main panel of Fig. 4.4. This may be because fewer massive systems are ejected compared to their lower mass counterparts, but it may also caused by the effect of the stars being in the cluster. As mentioned above, massive stars are ejected from the cluster centre where the gravitational potential of the cluster is deepest, therefore a higher velocity is required to escape the cluster, while less massive stars are most likely ejected at a location farther from the cluster centre where the escape velocity is lower. Furthermore, massive systems ejected with a low velocity can fall back to the cluster, failing to escape the cluster, by dynamical mass-segregation processes if they move away from the cluster centre slowly enough to interact with low-mass stars in the outer part of the cluster.

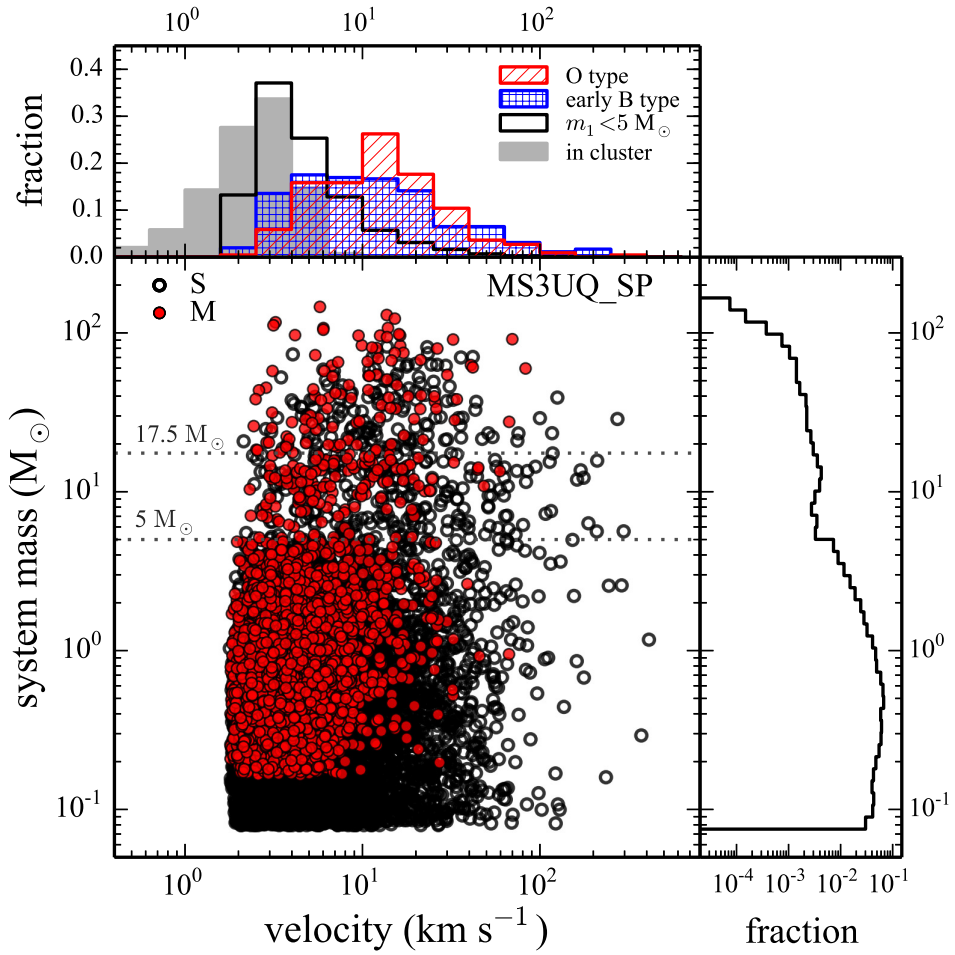

Figure 4.4. System mass versus velocity of all escapees from the most realistic model (MS3UQ_SP) of our models. Filled red and open black circles are multiple systems and single stars, respectively. The top panel presents the histograms of velocities of ejected systems for three different (primary) mass groups and all systems that remain in the clusters. The lower right panel is the histogram of the system mass for all ejected systems.

However, the relatively less massive systems have the highest velocity because the least massive of the interacting stars generally gains the highest velocity by the energy exchange. This can explain the higher runaway fraction of B-star systems compared to O-star systems for the MS3UQ_SP model in which B stars are most likely engaged because a large portion of O-star binaries initially have a B-star companion (Fig. 4.2, see also Section 4.3.3). For the same reason, the multiple systems have lower velocities than single stars (the main panel of Fig. 4.4, see also Leonard & Duncan 1990). An ejection of a binary through a single–binary or a binary–binary encounter accompanies an ejection of single star(s), and the single star very likely attains a higher velocity because its mass is lower than the mass of the ejected binary. The velocity distribution of the low-mass group ($m_1 < 5\,\mathrm{M}_\odot$) overlaps with that of stars that remain in the cluster at the peak of the distributions. The reason may be that the low-mass group includes low-mass star systems that evaporate from the cluster in addition to the ejected systems.

Figure 4.5 exhibits the velocity distribution of ejected systems for four different models that are efficient at ejecting O-star systems. In the lower panel of the figure, we show that the models with a

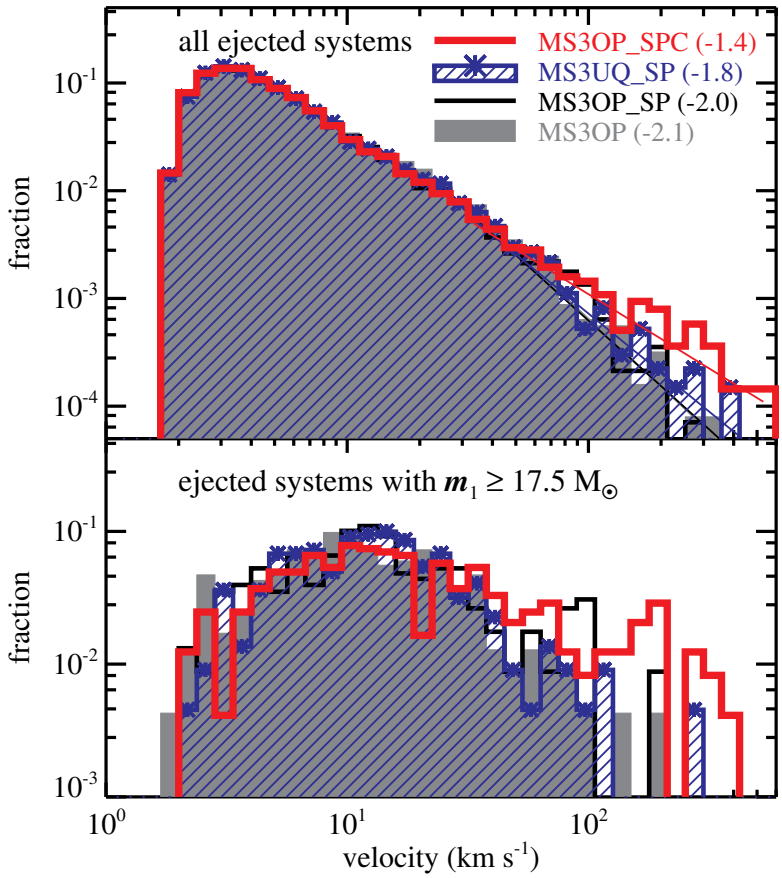

Figure 4.5. Velocity distributions of the all ejected systems (top panel) and of the ejected O-star systems (bottom panel) in four models, MS3OP_SPC, MS3UQ_SP, MS3OP_SP, and MS3OP. The solid lines in the upper panel are a linear fit for the systems with a velocity ≥30 km s^{-1}.

high proportion of short-period massive binaries produce more high-velocity stars. The model with only circular massive binaries (MS3OP_SPC) is interesting. It produces a long high-velocity tail of ejected O-star systems (Fig. C.1). Based on 100 runs of the model, seven single O stars have a velocity exceeding 200 km s^{-1}, mostly close to 300 km s^{-1}, and the fastest one has a mass of 26.6 $M_\odot$ and a velocity 381.5 km s^{-1}. Furthermore, two single massive ($m \approx 9.5$ and 12 $M_\odot$) stars in the model move faster than 400 km s^{-1} ($v \approx 462$ and 474 km s^{-1}, respectively). This indicates that with realistic massive binary populations, an energetic close encounter in a star cluster can be the origin of the high velocity of the runaway red supergiant star that has recently been discovered in M31 (J004330.06+405258.4, with an inferred initial mass of 12–15 $M_\odot$ and an estimated peculiar velocity of 400–450 km s^{-1}, Evans & Massey 2015). The production of such a high-velocity massive star in the MS3OP_SPC model is most likely due to energetic (short-period) massive binaries in the model engaging in close encounters that produce high-velocity stars, while in the MS3OP_SP and MS3UQ_SP models such systems disappear from a cluster by merging as a result of their high initial eccentricities (i.e. short peri-centre distances) at the early stage of the evolution.

The solid lines in the upper panel of Fig. 4.5 are the linear fit to all ejected systems with $v \geq 30$ km s^{-1} and their slopes are indicated next to the model names. Our results show that the velocity distribution

depends on the massive binary population, especially at high velocity ($v > 70\,\mathrm{km\,s^{-1}}$); this agrees with the results of Perets & Šubr (2012). Our study shows in particular that differences solely in the massive binary populations result in different velocity distributions of the dynamically ejected systems, even though the low-mass binaries, which constitute the majority of cluster members, are set to have identical initial binary populations for the four models shown in Fig. 4.5. Furthermore, our results suggest that the velocity distribution depends not only on the initial period (separation in Perets & Šubr 2012) distribution, but also on the initial mass ratios and eccentricities of massive binaries. Since the binary populations and cluster properties (size and mass) adopted in this study differ from those in Perets & Šubr (2012), we do not reproduce the same velocity distribution (i.e. a power-law slope) as those in their paper. The slopes we derived from our models, -1.4–-2.0, are shallower than those in the high-velocity regime in Perets & Šubr (2012), -2.5–-3.4. We were unable to separately fit the velocity distribution in the high-velocity regime ($v > 80\,\mathrm{km\,s^{-1}}$), which was done in Perets & Šubr (2012), because most of our models do not produce a sufficient number of such high-velocity stars for the analysis because our cluster mass is lower and we used fewer runs than they.

The highest velocity of the escapees from the cluster is dependent on the cluster model. None of the single-star or RP clusters ejects OB stars with velocities higher than $100\,\mathrm{km\,s^{-1}}$. In the OP models, however, some of the escapees exceed $100\,\mathrm{km\,s^{-1}}$. Especially for the MS3OP_SPC model in which massive binaries are initially on a circular orbit, several O stars have a velocity exceeding $200\,\mathrm{km\,s^{-1}}$. This clearly shows that the initial population of massive binaries is important in producing high-velocity massive stars.

4.4.3 Age of the clusters at the time of the ejections

It is not possible to determine the exact moment at which the close encounters that have resulted in ejections of the systems have occurred for individual ejected systems in our N-body models because of the complexity and the time resolution of the output. Here we calculate observationally relevant estimates for when systems are ejected from a cluster by calculating the approximate travelling time, $r_{\rm sys}/v_{\rm sys}$, where $r_{\rm sys}$ and $v_{\rm sys}$ are the present distance and velocity of the system relative to the cluster centre. From a snapshot at t (in this study $t = 3\,\mathrm{Myr}$), the cluster age when a system has been ejected, $\tau_{\rm ej}$, can be deduced from

$$\tau_{\rm ej} = t - \frac{r_{\rm sys}}{v_{\rm sys}}, \tag{4.7}$$

under the assumption that the system was ejected from the cluster centre and did not experience any further interactions with other systems after it had been ejected. This is a reasonable assumption since $r_{\rm sys} \gg r_{\rm h}(t)$ and $v_{\rm sys} \gg \sigma_{\rm cl}(t)$ the velocity dispersion in the cluster.

The distribution of $\tau_{\rm ej}$ for the ejected systems of the MS3UQ_SP model at 3 Myr is shown in Fig. 4.6. The peak of the $\tau_{\rm ej}$ distribution, at which the ejections occur most often, varies from model to model. In the most energetic case, the MS3OP model (the OP cluster with initial mass segregation), the peak appears around 0.5 Myr after the beginning of the calculations, while single-star clusters without initial mass segregation eject massive stars most efficiently after 1 Myr.

As stars move away from the cluster, the cluster potential can slow the ejected stars, especially those with low-velocities. This can result in negative values of $\tau_{\rm ej}$ for the systems that have been ejected at the very early stage of cluster evolution. The systems with negative $\tau_{\rm ej}$ indeed have a low velocity

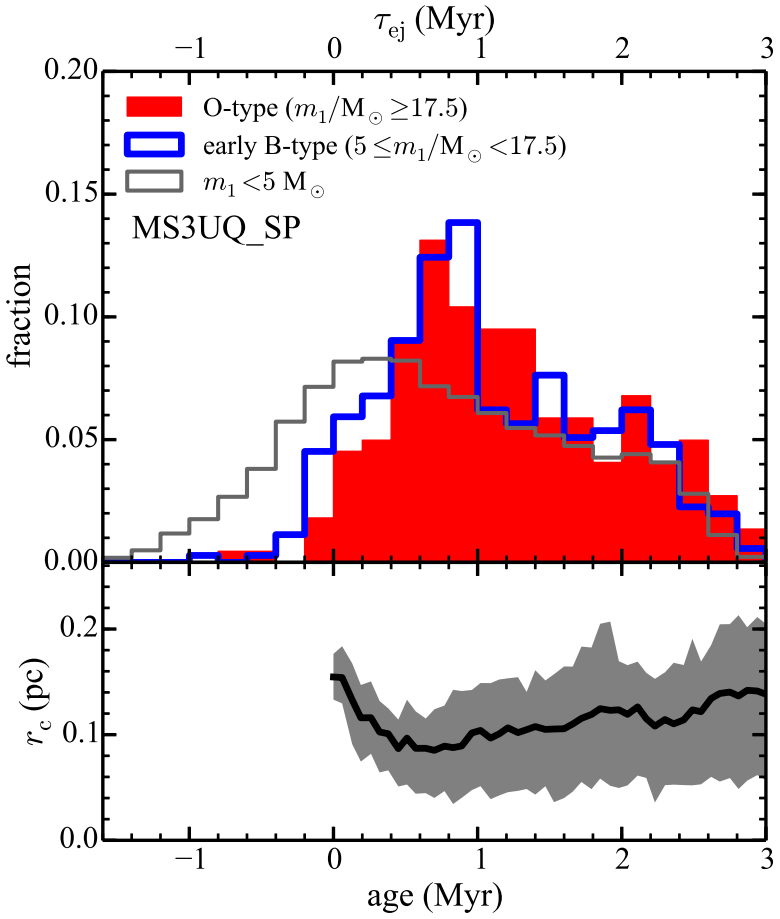

Figure 4.6. Top : distribution of estimated ages of the cluster when the massive systems are ejected from the cluster, τ_{ej}, for three different (primary star) mass groups in the MS3UQ_SP model. All ejected systems from 100 runs for each model are counted. Bottom : averaged core radius, r_c, of the same model as a function of time (black line). The lower and upper boundary of the grey shaded area are the 17th and 84th percentile, i.e. 68% of clusters have a core radius ranging within the area. The secondary maximum is shown in the top panel near 2.1 Myr when the core radius shrinks again as a result of the Spitzer instability.

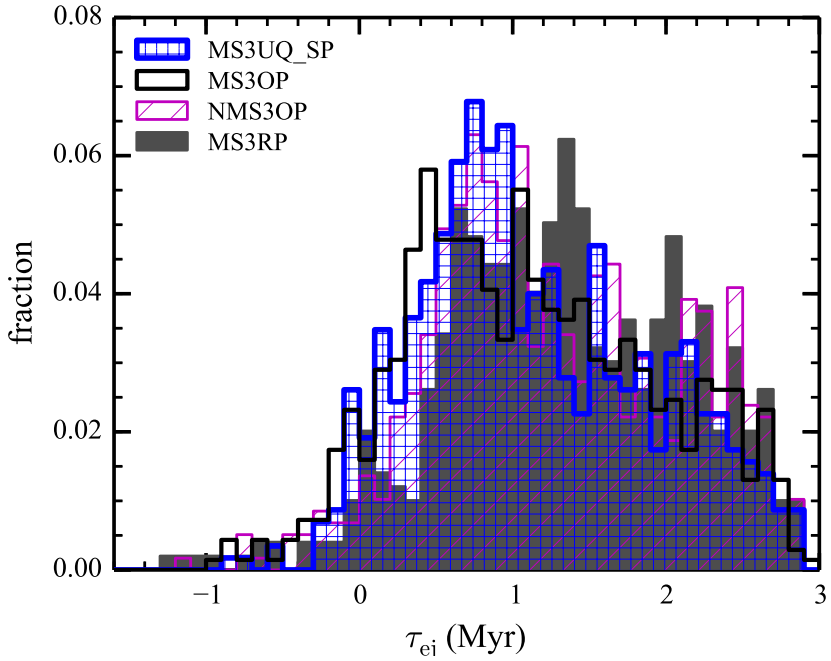

Figure 4.7. Distribution of $\tau_{\rm ej}$ of the ejected massive systems for four different models, MS3UQ_SP, MS3OP, NMS3OP, and MS3RP. All ejected massive systems from 100 runs for each model are counted.

($<10\,{\rm km\,s^{-1}}$, see Fig. C.3).

The $\tau_{\rm ej}$ distributions of the massive systems are expected to be related with the evolution of the cluster core. The core radius is as given by NBODY6 (equation 15.4 in Aarseth 2003; see also Casertano & Hut 1985). Figure 4.6 shows that the number of ejection increases as the cluster core shrinks and that the maxima of the $\tau_{\rm ej}$ distributions appear approximately when the core radius is the smallest. This shows that the number of massive systems in the core decreases and the core expands.

Figure 4.7 shows that the $\tau_{\rm ej}$ distribution is dependent on the initial configuration of the cluster. Evident dilation (the peak at later than 1 Myr) is present in the model in which massive binaries have a companion randomly chosen from the IMF (MS3RP, grey filled histogram in Fig. 4.7) compared to the models in which massive binaries preferentially have a massive companion (the other three models in the same figure). In the random-pairing models the massive primaries exchange their low-mass companions for massive companions, which causes a time delay until ejections become energetically possible. The peak of the $\tau_{\rm ej}$ distribution occurs later in the initially not mass-segregated cluster (e.g. NMS3OP, magenta hatched histogram in the figure) than in the mass-segregated one (e.g. MS3OP, black histogram in the same figure). The ejection time delay in the not mass-segregated clusters compared to the mass-segregated ones is expected to be the timescale at which dynamical mass segregation first creates a core of massive stars. The dynamical mass-segregation time, $t_{\rm ms}$, is expressed as (Spitzer 1987)

$$t_{\rm ms} = \frac{\langle m \rangle}{m_{\rm massive}} t_{\rm rh}, \tag{4.8}$$

where $\langle m \rangle \approx 0.57\,{\rm M}_\odot$, $m_{\rm massive}$, and $t_{\rm rh}$ are the average mass of the stars, the mass of the massive system, and the relaxation time at the half-mass radius, respectively. The half-mass relaxation time can be

estimated as (Binney & Tremaine 2008)

$$t_{\rm rh} = \frac{0.78\,{\rm Gyr}}{\ln(\lambda N)} \frac{1\,{\rm M}_\odot}{\langle m \rangle} \left(\frac{M_{\rm ecl}}{10^5\,{\rm M}_\odot} \right)^{1/2} \left(\frac{r_{\rm h}}{1\,{\rm pc}} \right)^{3/2}, \tag{4.9}$$

where $\lambda \approx 0.1$ (Giersz & Heggie 1994). For a $20\,{\rm M}_\odot$ star in a $10^{3.5}\,{\rm M}_\odot$ cluster with $r_{\rm h} = 0.3\,{\rm pc}$, the equation gives $t_{\rm ms}$ of about 0.18 Myr. The difference between peak locations of the MS3OP (black) and NMS3OP (magenta histogram in Fig. 4.7) models is ≈0.3 Myr. For clusters with $r_{\rm h} = 0.8\,{\rm pc}$, the $t_{\rm ms} \approx 0.78\,{\rm Myr}$ for the star with the same mass and is consistent in the difference between the peaks of the MS8OP and the NMS8OP models (≈1 Myr).

The ejections require the formation of a core of massive stars. Even though a cluster is initially mass-segregated, the cluster needs a time to build a dynamically compact core of massive stars. Both MS3OP and MS8OP models are initially mass-segregated, but thanks to its shorter mass-segregation timescale, the MS3OP model ejects massive stars more efficiently at an earlier time than the MS8OP model (see panels in Fig. C.2).

4.4.4 Present-day mass function of the ejected systems

The ejection fraction drops with decreasing stellar mass, as shown in Section 4.3 and in Banerjee et al. (2012b). It is therefore expected that the present-day mass function (MF) of the ejected stars is top-heavy compared to the IMF. In this section we investigate the slope of the present-day mass function in the high-mass regime ($m \geq 2\,{\rm M}_\odot$)[6] of the ejected stars. For comparison, the mass function of stars that remain in the cluster is also presented. We counted all individual stars with $m \geq 2{\rm M}_\odot$, that is, for a multiple system each component was counted separately, and only stars more massive than $2\,{\rm M}_\odot$ were taken into account. In reality, a fraction of the observed systems are possibly unresolved multiple systems. These systems may result in an observed MF deviating from the true stellar MF. However, Weidner et al. (2009), who studied the effect of unresolved multiple systems on the mass function of massive stars, found the difference between a slope of the observed MF and of the MF of all stars to be small, at most 0.1. The MFs of all stars can therefore be comparable with the observed MF. The slopes were obtained with the method of Maíz Apellániz & Úbeda (2005), in which bin sizes are varied for the same number of stars in each. We used ten bins for each fitting, and the number of stars in each bin was the same (5–370 stars per bin for the MFs of the ejected stars, ≈20 stars per bin for the IMF and the MFs of stars that remain in their host cluster). For the ejected stars, we used the stars from all 100 runs for each model because of their small number per cluster, especially for models that eject hardly any massive stars. We calculated the MF power-law index α and its uncertainty $\sigma(\alpha)$ with a nonlinear least-squares fit[7] (for details see Maíz Apellániz & Úbeda 2005). For the slope of stars that remain in clusters and for the initial slope, we computed the values from the individual runs and then averaged them.

In Fig. 4.8 we show the MF slopes for stars with a mass $\geq 2\,{\rm M}_\odot$ that are ejected and for those that remain in the clusters at 3 Myr. In addition, we present the fitted IMF slopes. For all models, the average values of the fitted IMF slope, $\langle \alpha_{\rm i} \rangle$, very well reproduce the adopted canonical value of the IMF,

[6] We chose the lower mass limit of $2\,{\rm M}_\odot$ for MF following Weisz et al. (2015) to compare our models to their results.

[7] We used CURVE_FIT in python (SCIPY package). Maíz Apellániz & Úbeda (2005) used CURVEFIT in the standard IDL distribution. Both CURVE_FIT and CURVEFIT are nonlinear least-squares fitting routines based on a gradient-expansion algorithm (Press et al. 1986; Bevington & Robinson 1992).

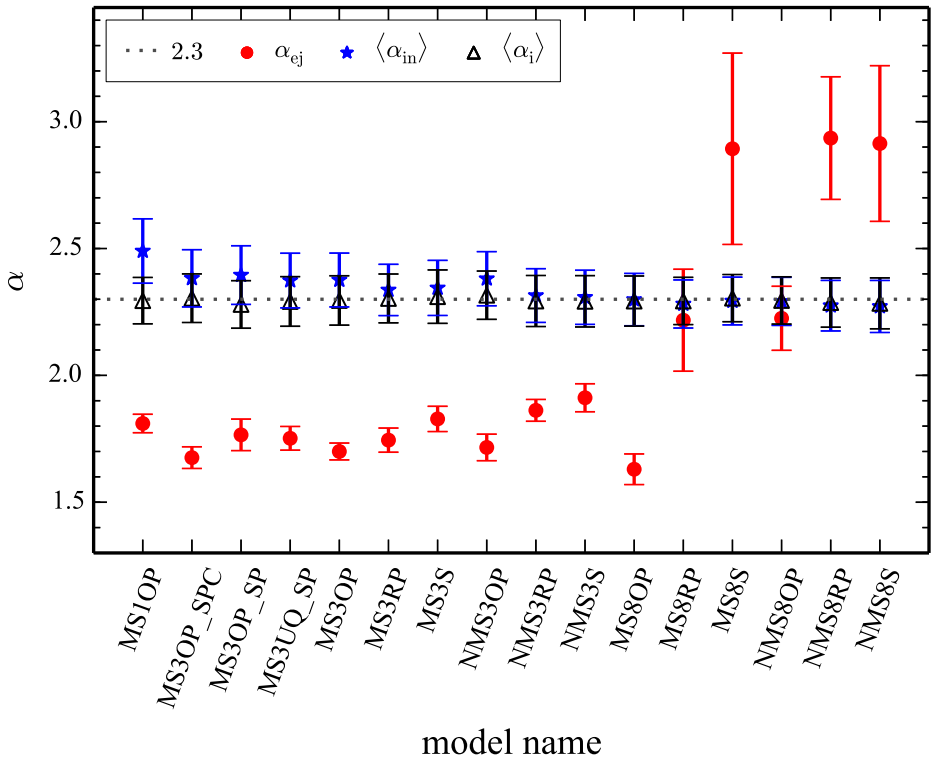

Figure 4.8. Mass function slopes for all (individual) stars with mass ≥2 $M_\odot$. Red filled circles are the present-day mass functions for the ejected stars (α_{ej}). Blue stars are the averaged present-day mass function slopes of the stars that remain in the clusters at 3 Myr ($\langle\alpha_{in}\rangle$), while black open triangles are those at 0 Myr (i.e. IMF, $\langle\alpha_{i}\rangle$). The canonical value of the upper IMF, $\alpha_2 = 2.3$ (Equation 4.1), is indicated with a dotted grey line.

$\alpha_2 = 2.3$, with uncertainties smaller than 0.1. The mass functions of the ejected stars are top-heavy with $1.7 \lesssim \alpha \lesssim 1.8$ for the clusters that actively eject massive stars ($f_{ej,O} \gtrsim 0.2$, see Fig. 4.1). As we showed in Fig. 4.1, these clusters in general eject more massive stars more efficiently. It is therefore naturally expected that the mass function of the ejected stars is top-heavy. Oh et al. (2015, Chapter 3) showed that the mass function of ejected O stars is top-heavy compared to the canonical IMF.

For the clusters with a higher ejection fraction of massive stars, a higher efficiency in ejecting more massive stars causes the mass function of stars that remain in the cluster to become steeper ($2.37 < \langle\alpha_{in}\rangle < 2.50$, Fig. 4.8), or top-light, at 3 Myr. This is similar to the mass function slope 2.45 found for stars with the same lower mass limit (2 $M_\odot$) in young (≲25 Myr) intermediate-mass (10^3–10^4 $M_\odot$) star clusters in M31 (Weisz et al. 2015). It also confirms the findings by Pflamm-Altenburg & Kroupa (2006) that the Orion nebular Cluster (ONC) is deficient in massive stars. This may imply that these star clusters have ejected massive stars and their IMFs may not be deviating from the canonical IMF. Without significant (close to none) ejection of stars, however, the average slope of the present-day mass function of stars in the cluster becomes slightly shallower than the initial values because of stellar evolution (see most of the model clusters with $r_h(0) = 0.8$ pc in Fig. 4.8).

It should be noted that this tendency can be obtained only with many clusters, not from an individual cluster. Too few stars are ejected from a single cluster to statistically derive the mass function of the ejected stars. Furthermore, it would be almost impossible to find all the stars that a cluster has ejected in

observations without the precise kinematic knowledge of all stars in the field and all nearby star clusters (cf. Pflamm-Altenburg & Kroupa 2006, on the ONC). It may therefore be difficult to determine whether the steeper mass function observed from a single cluster is due to evolutionary effects or stochastic effects in the IMF.

In addition to the MF of all stars, we derived the system MF for systems with a primary mass $\geq 2\,M_\odot$ and with a system mass $\geq 2\,M_\odot$ (Fig. 4.9) as well as the primary MF for systems with a primary mass $\geq 2\,M_\odot$ (Fig. 4.10) in the same way as described above to investigate the effect of multiplicity on these mass functions. For the ejected systems, the multiplicity does not significantly affect the system MFs and the primary MF. They are highly top-heavy for clusters that are efficient at ejecting massive systems and bottom-heavy for the clusters that eject hardly any massive stars, as shown in the individual stellar MF of the ejected stars in Fig. 4.8. This is due to their relatively low multiplicity fraction (Section 4.5). However, the system MF and the primary MF for the systems that remain in the cluster, which have a higher multiplicity fraction than the ejected systems (Fig. 4.11), are different from the MF of all stars in some models. The system MFs show that $\langle\alpha_{\rm in}\rangle$ becomes larger than the derived IMF $\langle\alpha_{\rm i}\rangle$, a similar trend as in the MF of individual stars, regardless of how we sample the systems, that is, whether we use a primary or a system mass. However, the values of the MF slopes are different when different criteria are used to sample the systems. For systems with a primary mass $\geq 2\,M_\odot$ (Fig. 4.9(a)), the slopes of the derived IMF for system masses are slightly lower than the canonical IMF value of 2.3 (especially for the RP models), but the difference is negligible, while for systems with a system mass $\geq 2\,M_\odot$ (Fig. 4.9(b)), $\langle\alpha_{\rm in}\rangle$ and $\langle\alpha_{\rm i}\rangle$ for binary-rich clusters are higher than the canonical IMF value (e.g. $2.4 \leq \langle\alpha_{\rm i}\rangle \leq 2.5$, see also Weidner et al. 2009). On the other hand, $\langle\alpha_{\rm in}\rangle$ of the primary MF becomes smaller than the derived IMF for most of the models in which massive stars are initially paired with another massive star (OP and UQ models). These models also show that the derived IMF of primary masses is very different from the canonical value (Fig. 4.10). This is mainly due to our choice for the lower limit of $2\,M_\odot$ when, in these models, two different pairing methods are used for systems with $m_1 < 5\,M_\odot$ and with $m_1 \geq 5\,M_\odot$. When $5\,M_\odot$ is chosen as the lower mass limit of the MFs, the primary MFs show indices similar to the MFs of all stars more massive than $5\,M_\odot$, while the system MFs are quite different.

This indicates that neither the primary MF nor the system MF is a good indicator for the MF of all stars because they can significantly deviate from the MF of all stars depending on the assumed parameters such as a criterion for sampling systems (see Fig. 4.9), a lower mass limit, and an initial mass-ratio distribution of binaries. Fortunately, however, our MF for all stars can be used for a comparison with the observed MF even with the high proportion of unresolved multiples since the effect of unresolved multiple systems on the observed MF is small (Weidner et al. 2009), as mentioned above. Again, the observed steeper MF for massive stars found in Weisz et al. (2015) agrees well with our MF for all stars that remain in the cluster for models that are efficient at ejecting massive stars. This suggests that the origin of these observed steeper MF slopes for massive stars in young star clusters may be the preferential loss of massive stars by dynamical ejections, even though the IMF has the canonical slope (in agreement with the conclusion drawn by Pflamm-Altenburg & Kroupa 2006 on the IMF in the ONC).

(a) system MF for systems with a *primary mass* ≥2 $M_\odot$

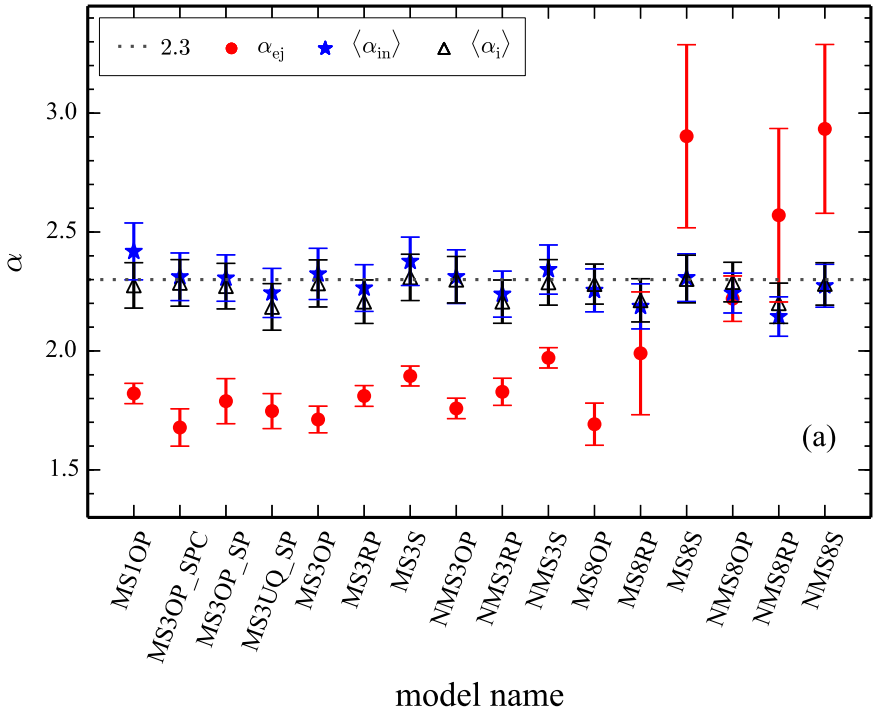

(b) system MF for systems with a *system mass* ≥2 $M_\odot$

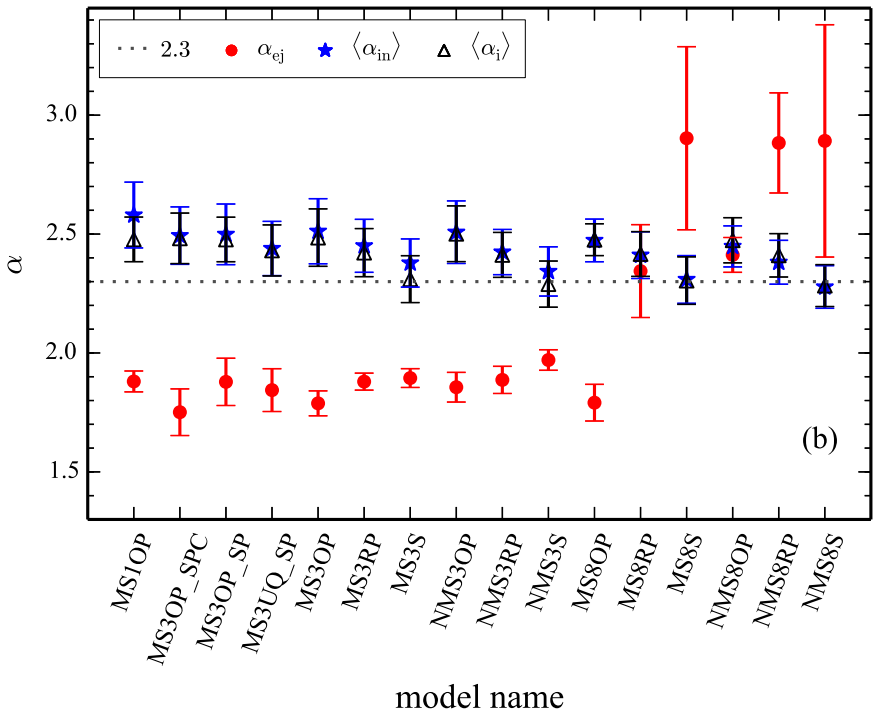

Figure 4.9. System mass function slopes for systems (a) with a primary mass ≥2 $M_\odot$ and (b) with a system mass ≥2 $M_\odot$. Symbols are the same as in Fig. 4.8.

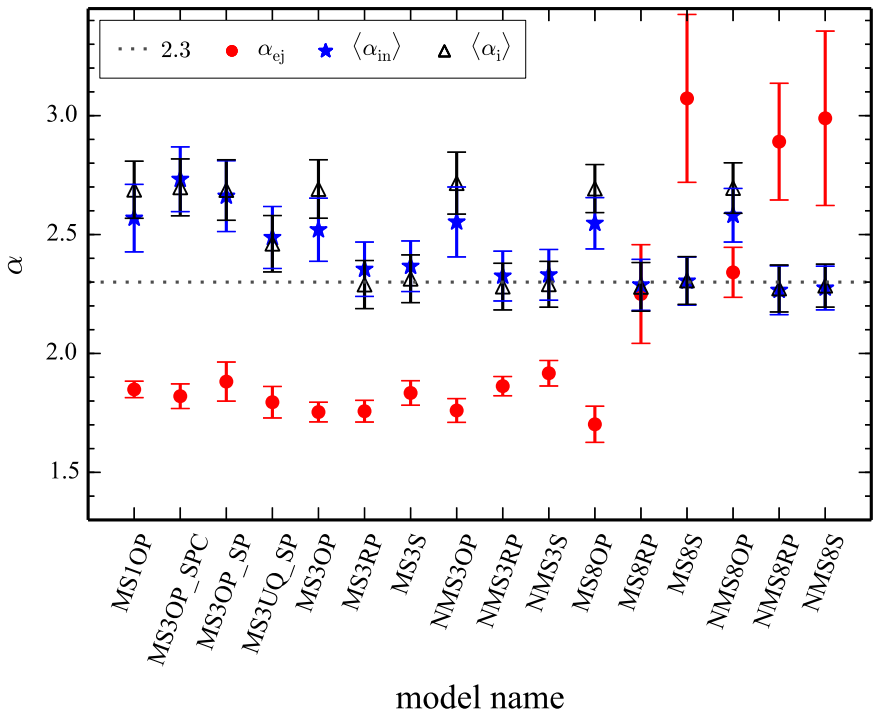

Figure 4.10. Primary mass function slopes for systems with a primary mass ≥2 $M_\odot$. Symbols are the same as in Fig. 4.8.

4.5 Dynamically ejected massive multiple systems

It has been shown that binary systems involving massive stars, even very massive ones (≳100 $M_\odot$, Oh et al. 2014, Chapter 5), can be ejected from a star cluster in theory (e.g. Fujii & Portegies Zwart 2011; Banerjee et al. 2012b; Oh et al. 2015) and in observations (e.g. Gies & Bolton 1986; Sana et al. 2013a), and that some are even runaways. Here we show that higher order multiple systems (e.g. a system with $N \geq 3$ components) can be dynamically ejected as well. We present multiplicity fractions among the ejected massive systems in the following subsections. We only discuss the initially mass-segregated cluster models with $r_{\rm h}(0) = 0.3$ pc in this section. Unsegregated cluster models would show only little different values compared to those of the segregated models, and their trend of the binary fraction related with the other initial conditions is similar as for the mass-segregated models. The larger sized models eject only a few systems and are therefore inappropriate to study the multiplicity fraction of the ejected systems.

4.5.1 Finding all multiple systems

Binary systems are found in a snapshot by searching a closest companion for each star and calculating whether the binding energy is negative. After this, the identified binaries are replaced by their centre-of-mass system and the search is repeated to find triple and quadruple systems. See also Kroupa (1995a) for further details.

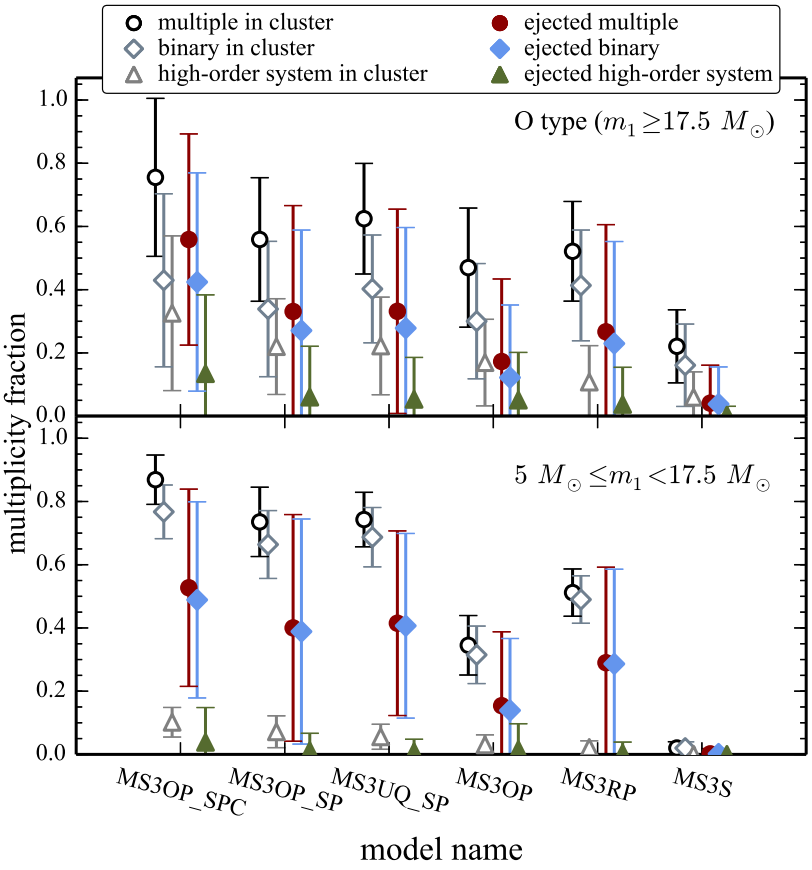

Figure 4.11. Averaged multiplicity fractions of O-star systems (top) and less massive systems (bottom) at 3 Myr. Open and filled symbols are the values of the systems that remain in their host cluster and those of the ejected systems, respectively. The error bars are standard deviations of the values from the individual clusters.

4.5.2 Multiplicity fraction

Considering that higher order multiple systems form during few-body interactions, it is not surprising that some of them are ejected, although the incidence is very rare. The multiplicity fraction is defined as

$$f_{\rm multi} = \frac{N_{\rm multi}}{N_{\rm sys}}, \tag{4.10}$$

where $N_{\rm multi}$ and $N_{\rm sys}$ are the number of multiple (binary, triple, quadruple, etc.) systems and all systems, respectively. The binary fraction ($f_{\rm bin}$) can be described as $f_{\rm multi}$ by using the number of binary systems ($N_{\rm bin}$) in place of $N_{\rm multi}$ (similarly for $f_{\rm trip}$, $f_{\rm quad}$, etc.).

In Fig. 4.11 we show the multiplicity, binary, and higher order multiple fractions of massive systems for systems that remain in their host cluster and for dynamically ejected systems. The multiplicity fractions vary with the initial conditions. However, all the models in the figure show that the multiplicity fractions of ejected massive systems are generally lower than those of systems that remain in a cluster. This is because the ejection efficiency is lower for binaries because on average they have higher system masses than single stars. Binary or multiple systems are also usually decomposed during the ejecting encounter.

For the ejected systems, the O-star systems have a higher high-order multiple fraction than less massive systems. This is because the O-star systems undergo significant dynamical processing, including captures into binaries, in the cluster centre, and because they have a high binding mass.

For O-star systems that remain in their host cluster, high-order multiple fractions are significantly high, even comparable to the binary fraction, while most multiple systems of the ejected systems are binaries. The fraction of the ejected high-order multiple O-star systems is small, but their occurrence implies that the energetic interactions that eject O-star systems can be more complicated than just binary-binary scattering. We note that the companions of many high-order massive multiple systems are generally low-mass stars. Even though most of the massive star systems are centrally concentrated, many low-mass stars are also present in the central part of the cluster, which means that the probability of a massive system to capture a low-mass system is higher than to capture another massive system. This is also favourable energetically because capturing a low-mass star requires a smaller amount of energy that has to be absorbed.

For less massive multiple systems, binary systems dominate mostly (the lower panel of Fig. 4.11) compared to O-star systems. The high-order multiple fraction is significantly lower than the binary fraction because of the rare occurrences of their formation by dynamical interactions in the majority of clusters. Especially for the ejected systems, the multiplicity fraction is almost equal to their binary fraction for all models shown in Fig. 4.11.

The ejected less massive systems generally show a slightly higher multiplicity fraction than O-star systems. In Fig. 4.12 the multiplicity fraction of the ejected systems decreases with increasing primary mass in all three models, although the trend varies with the model for the systems that remain in the cluster. We note that the multiplicity fractions of systems at the high-mass end (grey shaded area in Fig. 4.12) are high, particularly for the systems that remain in their host cluster. These systems contain primaries that are merger products and do not follow the general trends shown in lower mass counterparts. Because they are the most massive systems in the clusters, the systems are generally situated close to the centre of their cluster, where the probability of capturing other cluster members is high. An observer would see these stars as blue stragglers (because of their merger nature), but above the main sequence because of their multiplicity nature (cf. Dalessandro et al. 2013).

The differences in the multiplicity fractions for massive systems that remain in their host cluster indicate that the main mechanism for the removal of natal massive binary systems depends on the initial binary population. For the SP models, the multiplicity fraction is higher for less massive ($5 \leq m_1/\mathrm{M}_\odot < 17.5$) systems than for O-star systems. The reason is that in these models the main mechanism for reducing the binary fraction is merging of the two stars in the system, which has a higher probability to occur in a binary system with more massive (i.e. larger) components. This is more clearly shown in the left panel (MS3OP_SP) of Fig. 4.12, where the multiplicity fraction decreases with increasing primary mass, especially for systems that remain in their host cluster. Furthermore, the merger products naturally have a higher mass than the primary mass of the progenitor system, which leads to an increase of the number of single stars in the high-mass regime. Moreover, the significantly lower value of the multiplicity fraction in the MS3OP_SP model compared to the MS3OP_SPC model means that it is more likely for the short-period binaries with eccentric orbits to merge than it is for those with circular orbits. Likewise, the slightly smaller multiplicity fraction of O-star systems in the MS3OP_SP models than in the MS3UQ_SP models is probably due to the larger components of the initial binary systems, which more frequently

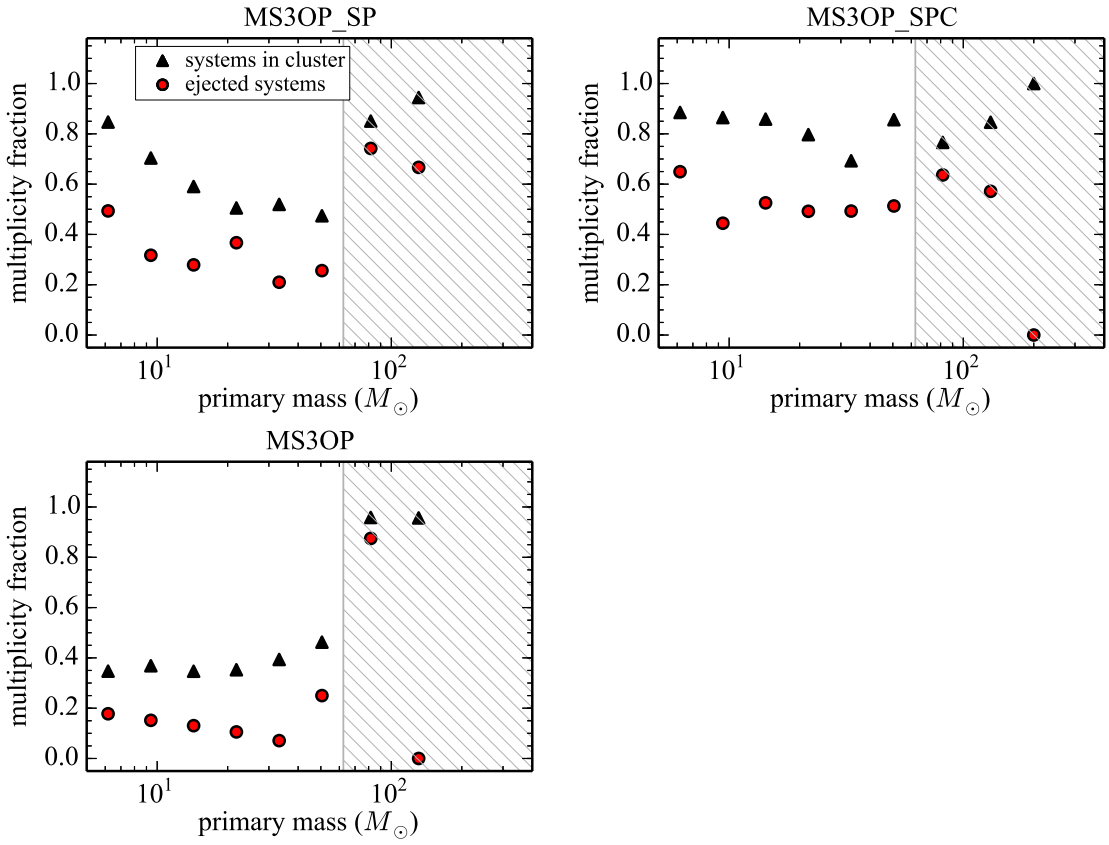

Figure 4.12. Averaged multiplicity fraction as a function of primary mass of systems for primary mass ≥5 $M_\odot$ from three models (MS3OP_SP, MS3OP_SPC, and MS3OP). Black triangles and red circles are the multiplicity fractions of systems that remain in the cluster and of the dynamically ejected systems, respectively. Model names are indicated at the top of subfigures. Grey hatched area indicates where a primary mass is higher than 62.4 $M_\odot$, that is, the evolved mass of a $m_{\rm max}$ star (79.2 $M_\odot$ at t = 0 Myr) at 3 Myr, evolved by single stellar evolution. Primary stars of all systems inside the area are therefore stellar mergers. Technically, these stars are blue stragglers that lie above the main sequence (cf. Dalessandro et al. 2013).

lead to mergers. The MS3OP_SPC model in Fig. 4.12 shows generally higher multiplicity fractions than the other models and little dependency of the multiplicity fraction on primary mass. The effect of pairing more massive companions in the MS3OP_SP model is less prominent among less massive ($5 \leq m_1/M_\odot < 17.5$) systems. The multiplicity fractions of the MS3OP_SP and MS3UQ_SP models are almost the same in the lower panel of Fig. 4.11. This again confirms that the merging of binaries is the main mechanism that removes initial binary systems for the models with the Sana et al. (2012) period distribution.

However, for the models with the Kroupa period distribution (Equation 4.2), the main mechanism of binary removal is the disruption of binary systems through dynamical interactions with other cluster member systems. The less massive systems are more vulnerable to a binary disruption because their absolute binding energy is lower than that of the more massive systems. For these models, the multiplicity fraction of less massive systems is therefore lower than those of O-star systems. In the right panel (MS3OP) of Fig. 4.12 we show that the multiplicity fraction of systems that remain in their birth cluster

(weakly) increases with increasing primary mass. The following mechanism naturally explains why the multiplicity fraction in the MS3OP model is lower than that in the MS3RP model (Fig. 4.11). While in the former model two single massive stars generally emerge when a massive binary system is ionized, only one single massive star appears in the latter. The difference between the two models increases for less massive systems because they are more prone to be ionized by the dynamical interactions than O-star systems, which is a result of their lower binding energy.

4.5.3 Binary populations

A majority of the ejected massive (O-star) binaries (or of the inner binary systems in the case of high-order multiple systems) from the initially binary-rich models have a period shorter than 10^5 (10^4) days, except in the MS3S models, in which all stars are initially single (Fig. 4.13). Compared to the period distribution of massive binaries that remain in a cluster (blue lines in the figures), the period distribution of the ejected binaries is more biased towards shorter periods.

With the thermal distribution for the initial eccentricity distribution, the fraction of very short-period binaries (P/days < 1) is lower among ejected binaries than in the initial distribution in the models with the Sana et al. (2012) period distribution (MS3OP_SP and MS3UQ_SP). This is due to stellar collisions. This naturally explains that the reduction in the number of very short-period massive binaries is not seen for the model with only circular binaries (MS3OP_SPC).

For the models with the Kroupa period distribution (Equation 4.2, the right-column panels in Fig. 4.13), the skewness to shorter periods for the period distribution of the ejected binaries is more prominent. The peak of the distribution, for example, appears at a shorter period than that of the systems in the clusters.

The evolution of the period distribution of massive systems, particularly of those that remain in their host cluster, depends on the initial period distribution, which determines the dominant binary-removal mechanism as discussed in Section 4.5.2. For the SP models, a fraction of short-period binaries is significantly smaller at 3 Myr than the initial distribution, which is a result of the merging of close binaries in a highly eccentric orbit. For the models with the Kroupa period distribution, in contrast, the binary fraction decreases for long periods, as a result of the binary disruption.

The mass-ratio distributions of the ejected systems are similar to those of the systems that remain in the clusters. But binaries with the lowest mass ratio ($q < 0.1$) are slightly more deficient among the ejected binaries than in those that remain in clusters. Unlike the other two orbital parameters discussed above, the mass-ratio distributions of massive binaries are not significantly altered from the initial distributions (Fig. 4.14), as is also the case for the lower mass counterparts (Marks et al. 2011).

A fraction of binaries exchanged their partner, which led to a small change in the mass-ratio distribution. However, neither models with random pairing nor those with ordered pairing reproduce the observed mass-ratio distribution of massive binaries, which is an almost uniform distribution, as a result of the dynamical evolution. The uniform mass-ratio distribution, taking all primaries together, is thus the initial distribution for massive binaries ($m_1 \geq 5\,\mathrm{M}_\odot$)

All binary-rich models but one (MS3OP_SPC) adopt the thermal distribution for the initial eccentricity distribution. The models that are initially biased towards short periods present a significant decrease of high-eccentricity ($e \geq 0.9$) orbits in populations within clusters as well as in ejected populations. This is because stellar mergers result from close binaries with high eccentricity (i.e. the peri-centre distance is very small). There is no significant difference between the eccentricity distribution of the ejected systems

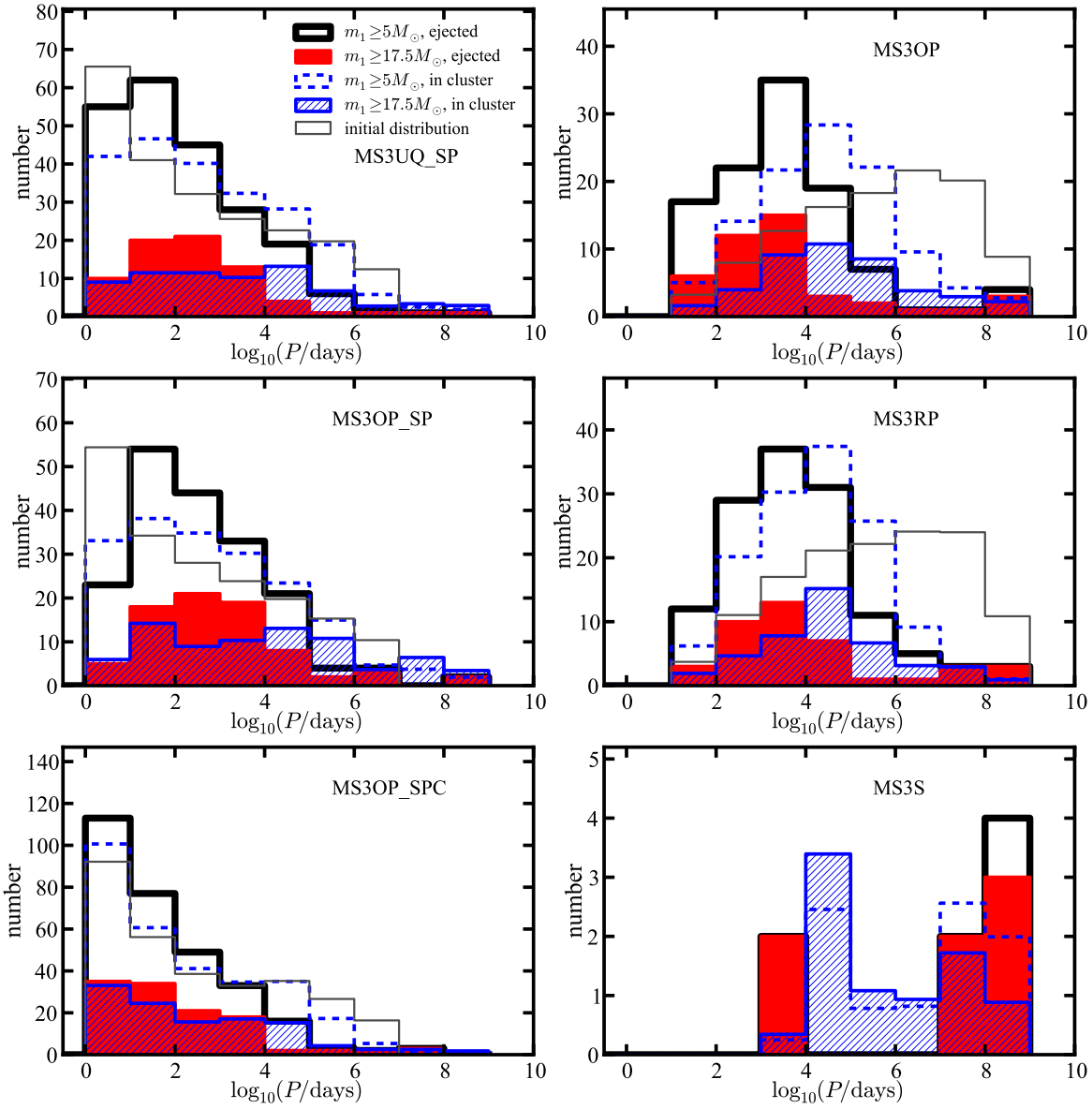

Figure 4.13. Period distribution (number of binaries in a period bin) of the ejected massive binary systems for initially mass-segregated clusters with $r_{\rm h}(0) = 0.3$ pc. Figures in the left column are the clusters with an initial period distribution according to Sana et al. (2012) for massive binaries (Equation 4.3), while those in the right column are the clusters with the Kroupa (1995b) period distribution (Equation 4.2). The grey solid line indicates the initial distribution. Initial distribution and the distributions of systems that remain in their birth cluster are scaled to the total number of the ejected binary systems.

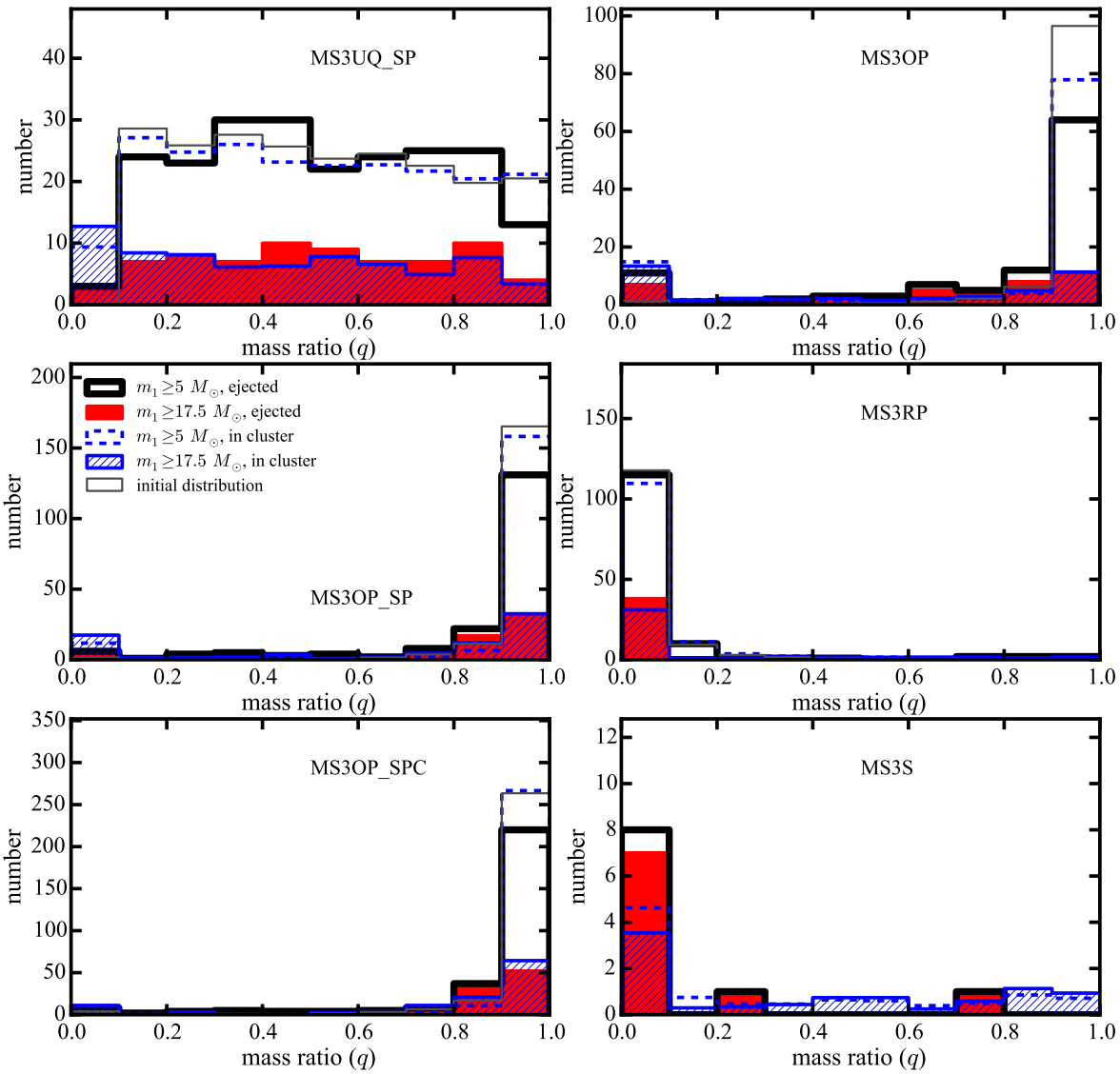

Figure 4.14. Same as Fig. 4.13, but for the mass-ratio distributions.

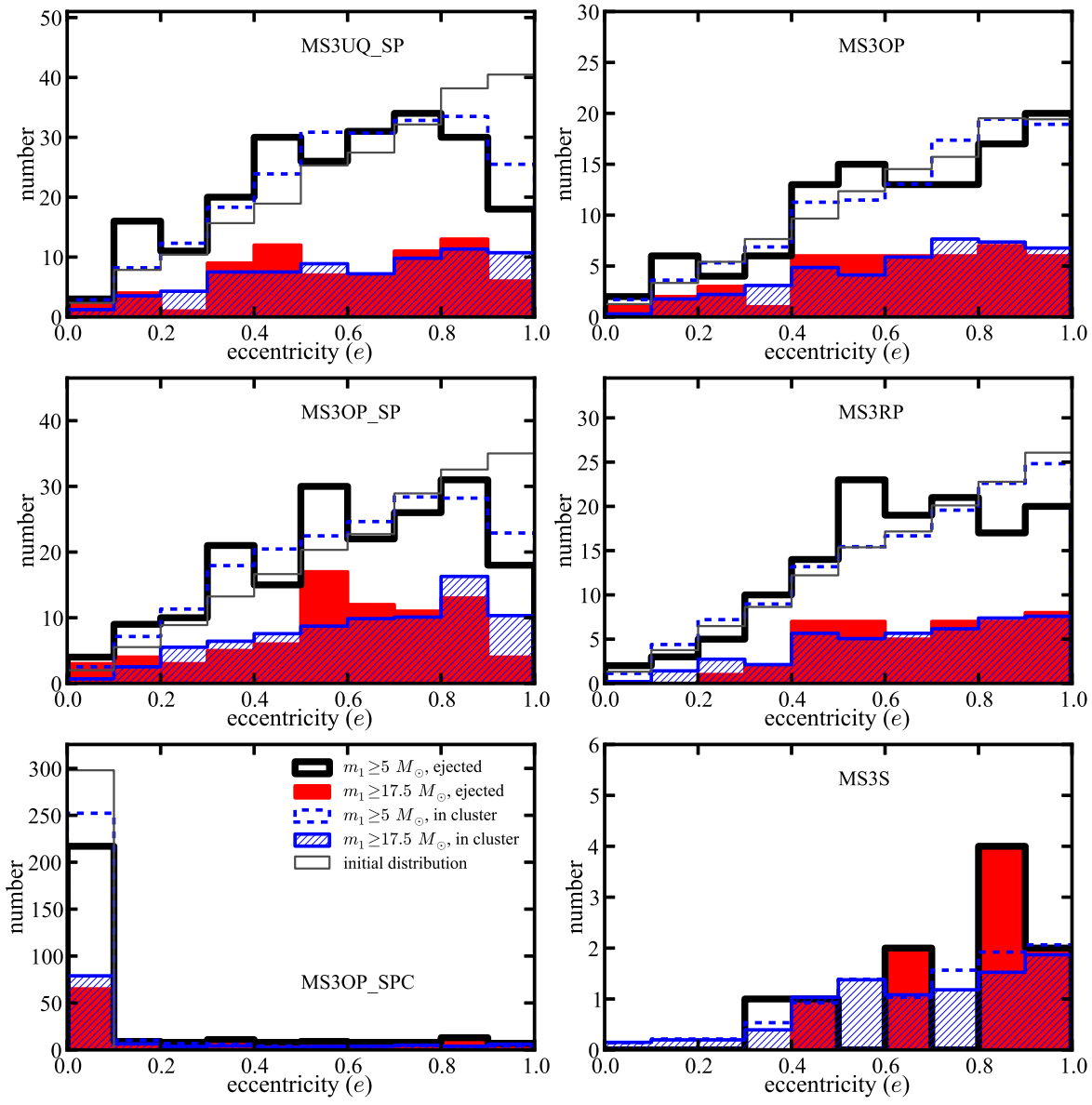

Figure 4.15. Same as Figs. 4.13 and 4.14, but for the eccentricity distributions.

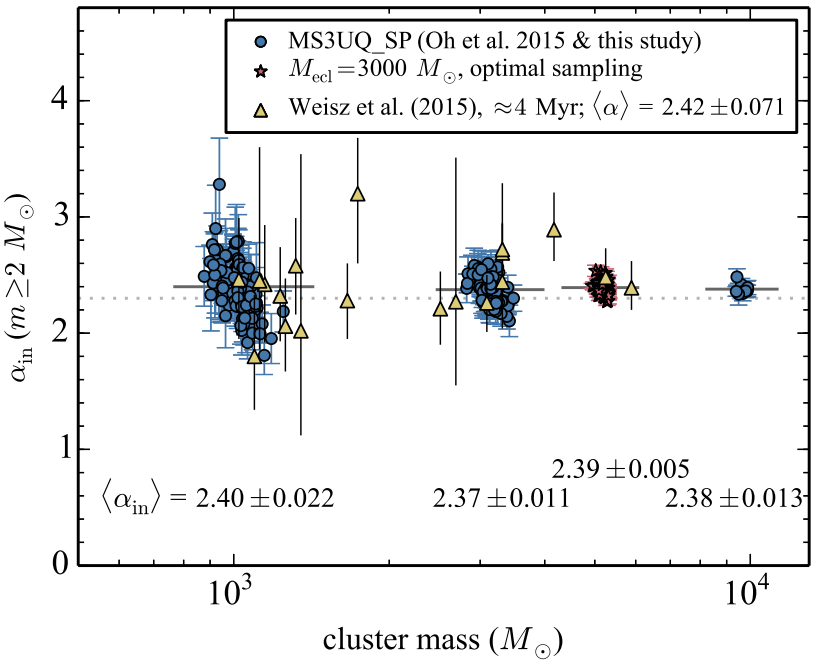

Figure 4.16. Present-day MFs of all stars ≥2 $M_\odot$ for clusters with $M_{\rm ecl}$ = 10^3, $10^{3.5}$, and 10^4 $M_\odot$ at 3 Myr. Grey horizontal bars and numbers below the points are the average values for each *N*-body model with different cluster mass. The uncertainties on the average $\langle\alpha_{\rm in}\rangle$ values are standard deviations of the mean. The red star is the model with $M_{\rm ecl}$ = 3000 $M_\odot$ and with initial conditions similar to the MS3UQ_SP model, but stellar masses derived by optimal sampling (see text). For this model, cluster masses are shifted to higher masses by 0.25 on the logarithmic scale to separate the model from the MS3UQ_SP model. The triangles are clusters with an age of ≈4 Myr in M31 from Weisz et al. (2015).

and the systems that remain in the cluster (Fig. 4.15).

Above we briefly mentioned the dynamical evolution of massive binary populations. Although it is important to study how the dynamical evolution affects the binary populations to understand the true initial binary population of massive systems formed in a cluster, given the observed (i.e. dynamically already evolved) distribution function, this is beyond the scope of this study. A more detailed discussion on the dynamical evolution of the massive binary populations in clusters will appear in a future study (Oh et al. in preparation), where the true physical initial or birth distribution functions of massive binaries will be constrained similarly to the procedure applied in Kroupa (1995a,b) for late-type stars.

4.6 Discussion

In Section 4.4.4 we showed that the average values of the present-day MF slopes for all stars ≥2 $M_\odot$ that remain in the clusters that are efficient in ejecting massive stars ($2.37 < \langle\alpha_{\rm in}\rangle < 2.5$) are similar to the mean MF slope of young star clusters in M31 derived by Weisz et al. (2015), α = 2.45. The cluster masses in Weisz et al. span 10^3–10^4 $M_\odot$, while in this study we only considered one cluster mass, $M_{\rm ecl}$ = $10^{3.5}$ $M_\odot$, which is the middle value of their cluster mass range on the logarithmic scale. It is therefore necessary to check whether the agreement between our present-day MF and that of Weisz et al. only appears for the specific cluster mass we used in this study, or whether it is also there for

different cluster masses that are similar to the cluster mass range of Weisz et al.. Here, we derive $\langle\alpha_{\rm in}\rangle$ for two additional cluster masses, $M_{\rm ecl} = 10^3$ and $10^4\,{\rm M}_\odot$, for the most realistic model in our library, MS3UQ_SP. We adopted the MS3UQ_SP models with these two cluster masses from Oh et al. (2015, Chapter 3) and derived the present-day MF slope of all stars with a mass $\geq$2 $\rm M_\odot$ that remain in the cluster, $\alpha_{\rm in}$, for each cluster with the same procedure as described in Section 4.4.4. Additionally, we included one model similar to MS3UQ_SP, but in which stellar masses are obtained using the optimal sampling procedure in which the IMF has no Poissonian sampling scatter (Kroupa et al. 2013).

The MF slopes are plotted as a function of cluster mass in Fig. 4.16. We note that in Fig. 4.16 the data points of the optimal sampling model are shifted to a higher cluster mass (by adding 0.25 on the logarithmic scale to the cluster masses) to separate them from the MS3UQ_SP models. The mean MF slopes of youngest clusters (only ages of $\approx$4 Myr) in Weisz et al. is 2.42, slightly smaller than that of their whole sample clusters, 2.45. For all three cluster masses of the MS3UQ_SP model, the averaged present-day MFs at 3 Myr are $\langle\alpha_{\rm in}\rangle \approx 2.4$, regardless of cluster mass, and this agrees very well with the mean MF of the Weisz et al. sample for $\approx$4 Myr old clusters (see also the numbers in Fig. 4.16). The averaged MF slope for the model with optimal sampling is 2.39, very similar to the values of the other models. Our analysis implies that the canonical IMF evolves to a steeper present-day MF even in the first few Myr because of dynamical and stellar evolution, at least within the cluster mass range shown here, and that the IMF of young clusters in M31 should be the canonical IMF. The steeper averaged MF in the observations would have resulted from the (dynamical and stellar) evolution of the clusters. However, we note that some additional degree of IMF steepening above a few solar masses could be present in the clusters in M31 because of a possible metallicity dependence of the IMF (cf. Marks et al. 2012).

The scatter of MFs of individual clusters is larger for clusters with lower mass (i.e. smaller N) as a result of the stochastic behaviour of random sampling. For the model with optimal sampling, the scatter of the MF slopes is smaller than that for the MS3UQ_SP model with a similar cluster mass, and so are their uncertainties. This is because there is no stochasticity in optimal sampling for the IMF since the optimal sampling produces only one set of stellar masses for a cluster mass. The spread of the present-day MFs then appears as a result of the slightly different evolution of the individual clusters. It should also be noted that the canonical IMF, 2.3, the input IMF for our N-body models, is reproduced for the averaged IMFs from these three additional models deduced with the procedure described in Section 4.4.4, as is shown in all models with $M_{\rm ecl} = 10^{3.5}\,{\rm M}_\odot$. The similar steepening of the MFs at 3 Myr for all cluster masses is not caused by any initial systematic biases that are due to different cluster mass.

In the previous sections, we described that the dynamical ejections of massive stars vary with the initial conditions of their birth cluster and its massive star population. To constrain the initial configurations of massive stars in a star cluster, our results need to be compared with observations and should be able to rule out sets of initial conditions in the models that result in outcomes that are inconsistent with observations.

Since individual $10^{3.5}\,{\rm M}_\odot$ clusters eject only a small number of O-star systems, the number of ejected O-star systems can vary strongly from cluster to cluster. Some clusters, for instance, eject no O-star systems, while others loose 3–4 O-star systems. A cautionary remark is due when comparing our averaged results to an individual cluster. For the comparison, a large sample of clusters and of O stars in the field are needed. From the N-body calculations we can find all stars ejected from a star cluster. In reality, a fraction of the ejected massive systems may not be traced back to their birth cluster and may not

be recognised as ejected systems if they have travelled too far from their birth place or have experienced the two-step ejection process (Pflamm-Altenburg & Kroupa 2010), which makes it almost impossible to trace the stars to their origin. Furthermore, O stars form in a wide range of cluster masses in a galaxy. The ejection fractions and their properties also depend on the cluster mass (Oh et al. 2015, Chapter 3). Thus this study cannot represent the true observed field population or be compared to the general properties of the field O stars since here we only studied a single cluster mass and snapshots at 3 Myr to make the analysis manageable and to pave the way towards even more comprehensive work. Ultimately, such work should include the cluster mass function in terms of a full-scale dynamical population synthesis approach (see Marks & Kroupa 2011 for more details and also Oh et al. 2015, Chapter 3).

It is expected that *Gaia* will deliver vast data on the kinematics of stars in the Galaxy, including the O-star population. Comprehensive *N*-body studies on the evolution of young star clusters formed in the Milky-Way-like galaxy incorporating the cluster mass function are thus required to interpret the data thoroughly.

4.7 Summary

We investigated the effects of initial conditions of star clusters on the dynamical ejections of massive stars from moderately massive ($M_{\rm ecl} = 10^{3.5}\,{\rm M}_\odot$) young star clusters by means of direct *N*-body calculations with diverse initial conditions. The ejection fraction of massive systems is most sensitive to the initial density of the cluster (i.e. the initial size in this study because we used the same mass for all clusters) compared to other properties. But the binary population is also an important factor for the ejection efficiency. The ejection fraction is higher, for example, when massive binaries are composed of massive components, and the properties of the ejected systems, such as their velocities and multiplicity, strongly depend on the properties of the initial binary population.

The mass function of ejected stars is highly top-heavy because ejections with increasing stellar mass becomes more efficient. This tendency with stellar mass also alters the mass function of stars in a cluster so that it becomes steeper (top-light) than the IMF. The observed stellar mass functions in young (but more than a few Myr old) clusters may therefore deviate from their IMF (Pflamm-Altenburg & Kroupa 2006; Banerjee & Kroupa 2012). This may be evident in the MF slopes of young star clusters in M31 for which the MFs are homogeneously derived with high-resolution observations by Weisz et al. (2015). The mean MF for the clusters is steeper than the canonical IMF, but is in excellent agreement with the average present-day (at 3 Myr) MFs for our *N*-body models with the most realistic initial conditions and with different cluster masses (Sections 4.4.4 and 4.6). We stress that the IMFs of young clusters in M31 in Weisz et al. (2015) therefore do appear to be indistinguishable from the canonical IMF and that the stellar MF of clusters can be altered even within the first few Myr of cluster evolution through dynamical ejections and collisions of massive stars, and through stellar evolution.

We showed that high-order multiple systems containing O stars can also be ejected readily. The ejected systems have a lower multiplicity fraction, especially high-order multiplicity, than those that remain in the cluster. The period distributions of the ejected binary systems are biased to shorter periods than those for systems that remain in the cluster. The mass ratio and eccentricity distributions of the ejected systems are similar to those of the systems that remain in the cluster. The evolved mass-ratio distribution of massive stars almost preserves the shape of the initial distribution. We thus emphasize that the birth

mass-ratio distribution of massive (particularly O star) binaries must be close to a uniform distribution as in observations of O-star binaries (Sana et al. 2012; Kobulnicky et al. 2014; cf. B-star binaries, Shatsky & Tokovinin 2002).

The ejection fraction and the properties of ejected systems depend on the initial conditions of the clusters and their massive population. Applying our results to a large survey of the kinematics of massive stars in the Galactic field, as will be possible with *Gaia*, for instance, will help to constrain the birth configuration of massive stars and of the star clusters in which they form. Further research using N-body models is required to achieve a full-scale dynamical population synthesis to be applied to the *Gaia* data.

We thank Sverre Aarseth for his comments and Dan Weisz for kindly providing the data on MF slopes of young star clusters in M31 from Weisz et al. (2015).

CHAPTER 5

R144 : a very massive binary likely ejected from R136 through a binary–binary encounter

Published in Monthly Notices of the Royal Astronomical Society
Volume 437, pp 4000–4005, February 2014
S. Oh, P. Kroupa, and S. Banerjee

ABSTRACT

R144 is a recently confirmed very massive, spectroscopic binary which appears isolated from the core of the massive young star cluster R136. The dynamical ejection hypothesis as an origin for its location is claimed improbable by Sana et al. due to its binary nature and high mass. We demonstrate here by means of direct N-body calculations that a very massive binary system can be readily dynamically ejected from an R136-like cluster, through a close encounter with a very massive system. One out of four N-body cluster models produces a dynamically ejected very massive binary system with a mass comparable to R144. The system has a system mass of $\approx$355 $M_\odot$ and is located at 36.8 pc from the centre of its parent cluster, moving away from the cluster with a velocity of 57 km s^{-1} at 2 Myr as a result of a binary–binary interaction. This implies that R144 could have been ejected from R136 through a strong encounter with another massive binary or single star. In addition, we discuss all massive binaries and single stars which are ejected dynamically from their parent cluster in the N-body models.

5.1 Introduction

The formation process of massive stars is still poorly understood. Among many issues, whether massive stars form only in clusters or whether they can form in isolation has been a major debate to this day. de Wit et al. (2005) suggested that about 4% of the Galactic field O stars are formed in isolation. Later, every one of these candidates for isolated massive star formation were found to be runaways (Gvaramadze et al.

2012, and references therein) or to be consistent with having been generated via the two-step ejection process described by Pflamm-Altenburg & Kroupa (2010). This indicates that probably all O stars in the Galactic field likely originate from star clusters (Gvaramadze et al. 2012).

Isolated massive stars have been found not only in the Galaxy but also in our nearest-neighbour galaxies, the Magellanic Clouds (Bressert et al. 2012; Gvaramadze et al. 2012; Oey et al. 2013, and references therein). Even stars more massive than $100\,M_{\odot}$ are found in apparent isolation in the 30 Dor region in the Large Magellanic Cloud (LMC), among them VFTS 682 (Bestenlehner et al. 2011) and R144 (Sana et al. 2013a). The presence of these massive stars in isolation has been interpreted by the respective authors to mean that very massive stars can form in isolation. Although dynamical ejection as the origin of VFTS 682 was claimed challenging due to its high mass ($\approx 150\,M_{\odot}$, Bestenlehner et al. 2011), with the direct N-body calculations of R136-like clusters Banerjee, Kroupa & Oh (2012b) showed that the star would have been dynamically ejected from R136. The dynamical ejection process can thus explain these observed very massive isolated stars, suggesting there is no need to postulate isolated massive star formation. In this study, our main interest is R144, a recently confirmed very massive spectroscopic binary which is located at a projected distance of 59 pc from R136 (Sana et al. 2013a). Sana et al. (2013a) argued that the ejection from R136 via a dynamical interaction is improbable. It is thus important to investigate whether a very massive binary, such as R144, can be dynamically ejected from a cluster like R136, in order to prove that the system can originate only from in situ formation.

Using three-body scattering experiments, Gvaramadze & Gualandris (2011) showed that a very massive star can attain a high velocity through a close encounter with a very massive binary such as WR20a and NGC3603-A1. They also suggested that the ejection of a very massive star can accompany a recoiled very massive binary. However, so far there has been no study to find a very massive binary ejected dynamically from its parent cluster with full N-body calculations for a realistic cluster model comparable to R136. It is only recently that massive young star cluster models comparable to R136 have been computed with the direct N-body method (Fujii & Portegies Zwart 2011; Banerjee et al. 2012b; Fujii, Saitoh & Portegies Zwart 2012). Among them, Banerjee et al. (2012b) constitute the only theoretical data set which initially applied a realistic high fraction of massive close binaries, including ones with primary masses larger than $100\,M_{\odot}$. Observed O-star binaries in the Tarantula Nebula, in which R136 is at the centre, are found to favour short binary orbital periods (Sana et al. 2013b). Banerjee et al. (2012b) performed direct N-body calculations for R136-like cluster models with primordial massive binaries but mainly focused on ejected massive single stars which have similar properties as VFTS 682. Here, we revisit the N-body data to study if a very massive binary such as R144 in the LMC could be ejected from its birth cluster via a close encounter with other cluster members. We would like to stress that the models used here are the exact same ones as used in Banerjee et al. (2012b) and that they were not generated with the specific purpose of addressing the problem at hand (can R144-type objects be ejected?).

We briefly describe the N-body models of Banerjee et al. (2012b) in Section 5.2. A dynamically ejected very massive binary found in the N-body calculations is described and compared to R144 in Section 5.3. Section 5.4 presents dynamically ejected massive binaries and single stars from the N-body calculations. The conclusion is presented in Section 5.5.

5.2 *N*-body Models

We revisit the direct *N*-body calculations for an R136-like cluster performed by Banerjee et al. (2012b) to study if a very massive binary, as massive as R144, can be dynamically ejected. The models used here are thus not specially made to study the ejection of binaries. The models were integrated with the Aarseth NBODY6 code (Aarseth 1999, 2003).

The initial cluster mass is set as $10^5\,M_\odot$ with 170 667 stars. The model clusters have initial half-mass radii, $r_h(0)$, of 0.8 pc. The initial positions and velocities of stellar systems, single stars or centre-of-mass of binary systems, are generated following the Plummer density profile and assuming the cluster to be in virial equilibrium. Individual stellar masses are randomly derived from the two-part power-law canonical initial mass function (IMF) with power indices of $\alpha_1 = 1.3$ for $0.08\,M_\odot \leq m < 0.5\,M_\odot$ and of $\alpha_2 = 2.3$ for $m \geq 0.5\,M_\odot$ (Kroupa et al. 2013) in a stellar mass range $0.08\,M_\odot \leq m \leq 150\,M_\odot$. The model clusters are initially fully mass-segregated by assigning more massive stars to be more bound to the cluster (Baumgardt, De Marchi & Kroupa 2008). Due to the high computational cost, only stars more massive than $5\,M_\odot$, i.e. ≈2000 stars, are initially in a binary system (≈1000 binary systems). The exact number of binaries slightly differs from model to model as it is determined by the number of stars more massive than $5\,M_\odot$ which fluctuates among the models. For a realistic initial setup of massive binaries, for them to be consistent with their observed orbital parameters (Sana et al. 2012, 2013b), a star is paired with the next less massive star and periods are generated using a uniform distribution over a period range between 10 and 10^4 days for binaries with a primary more massive than $20\,M_\odot$, and using the Kroupa (1995b) distribution for lower mass binaries. The thermal distribution was used for the initial eccentricity distribution of binary orbits. Stellar evolution was included and stellar collisions were allowed. Four calculations with initial configurations generated by different random seed numbers were carried out. More details can be found in Banerjee et al. (2012b).

In the following sections we discuss results from the snapshots of the *N*-body integrations at 2 Myr. It is worthy to mention that by 2 Myr the total number of stars is reduced by 30–35 due to stellar collisions and that most of the collisions took place at the very beginning of the calculations due to initially short periods and high eccentricities of massive binaries (Banerjee, Kroupa & Oh 2012a).

5.3 A very massive binary dynamically ejected via a binary–binary interaction

Our motivation for this study is the recently confirmed massive binary star R144 which is found about 60 pc away from R136 in projection and has an estimated mass of 200–300 $M_\odot$ (Sana et al. 2013a). Apparently not being inside of any star cluster and its high mass are interpreted such that the system is very unlikely to have been ejected via a close encounter and thus that it is a good candidate of isolated massive star formation (Sana et al. 2013a). To check this argument, we study if such a system can appear in the direct *N*-body calculations of realistic R136-like cluster models.

We find that one very massive binary system with a system mass, $m_{sys} = 355.9\,M_\odot$, has been dynamically ejected and is located 36.8 pc away from the centre of its birth cluster moving with a velocity of $57\,km\,s^{-1}$ at 2 Myr (system ID 4-5 in Table 5.1).[8]

[8] Note that the binary system was misclassified as two single stars in Banerjee et al. (2012b).

ID	$m_{\rm sys}$ ($M_\odot$)	r (pc)	v (km s^{-1})	m_1 ($M_\odot$)	m_2 ($M_\odot$)	P (d)	a (au)	e	$v_{\rm orb}$ (km s^{-1})	$E_{\rm b}/E_{\rm tot,ecl}$
1-59[a]	110.8	29.1	43.8	55.5	55.3	19.4	0.68	0.44	381.0	0.19
3-301	40.6	20.9	11.1	20.3	20.3	7.7	0.26	0.57	371.0	0.07
4-5	355.9	36.8	57.0	244.0	111.9	1 955.7	21.69	0.78	120.8	0.05
4-47	108.9	29.1	27.5	60.2	48.6	35.1	1.00	0.86	310.9	0.13

Table 5.1. List of massive binaries ejected from all four model-cluster integrations by 2 Myr. ID in column 1 indicates identification of run and the system. System mass, $m_{\rm sys}$, distance from the cluster centre, r, and 3D velocity, v, of the systems are listed in columns 2–4. Furthermore, columns 5–10 list parameters of binaries such as primary and secondary mass (m_1 and m_2, respectively), orbital period (P), semi-major axis (a), eccentricity (e) and orbital velocity ($v_{\rm orb}$) when a circular orbit is assumed. Ratio of binding energy of the binaries (Equation 5.2) to the initial total energy of the cluster (Equation 5.3) is listed in column 11. All values are from snapshots at 2 Myr.
[a]The initial orbital parameters of the system are $P = 30.7$ days, $a = 0.93$ au, and $e = 0.53$.

Theoretically, after an energetic encounter between a binary and a single star, the recoil of the very massive binary can be accompanied by an ejection of a very massive star because of momentum conservation (Gvaramadze & Gualandris 2011). However, it was not certain whether such an event can occur in a cluster. Here, we show that a binary system even more massive than R144 can be ejected via a few-body close encounter in an R136-type cluster.

The above binary is composed of two stars with present masses of 244.0 $M_\odot$ and 111.9 $M_\odot$. The primary of the binary with a present mass of 244.0 $M_\odot$ is, in fact, a merger product which was initially a binary with initial component masses of 134.9 and 129.2 $M_\odot$. The secondary star was initially in a binary with an ejected single star 4-10 in Table 5.2 which is found on the opposite side of the cluster with respect to the binary system.

The orbital period of the binary found in the N-body model is 1955.7 days with a highly eccentric orbit (eccentricity, $e = 0.78$). The period estimates of R144 from observations are between two and six months or can be up to one year if the orbit is highly eccentric (Sana et al. 2013a). Even though the very massive, ejected binary found in the N-body model has a relatively long period, a massive binary with a period as short as 7.7 days can also readily be dynamically ejected (Section 5.4 and Table 5.1).

Gvaramadze & Gualandris (2011) suggested that R145, another very massive binary ($m_{\rm sys} \approx 240\,M_\odot$, Chené et al. 2011; period ≈159 days, Schnurr et al. 2009) located outside of the R136 core (at a projected distance ≈19 pc), could be such a recoiled very massive binary having been involved in an energetic encounter which would have ejected the runaway B2 star Sk–69◦206. In the case of the N-body models here, there is a single massive star ejected in the opposite direction of the ejected binary (star 4-10 in Table 5.2 and see the panel RUN4 in Fig. 5.1). If R144 is such a case as well, then one may find an ejected massive star on the opposite side of its birth cluster.

5.4 Dynamically ejected massive systems

In this study, we define an ejected massive system as a system whose current (primary, in case of a binary) mass is larger than 20 $M_\odot$ and whose distance from the parent cluster density centre is greater than 10 pc at 2 Myr. A ‘system’ refers to either a single star or a binary. We find 26 ejected massive

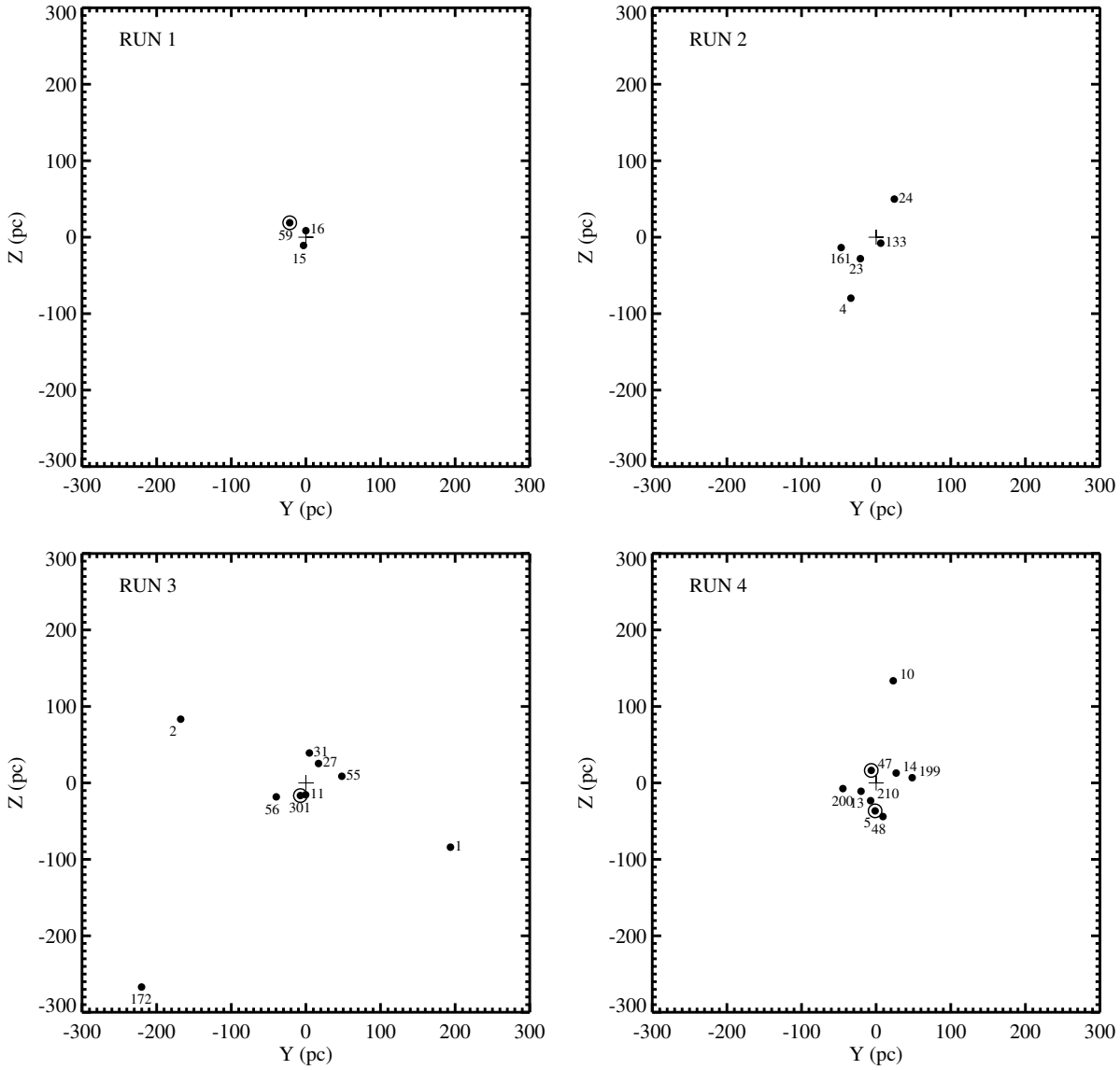

Figure 5.1. Snapshots of the ejected massive stars for each run projected on the *YZ* plane at 2 Myr. Dots are single stars and dots with an outer circle are binary systems. Cluster centre is indicated with a cross in each panel. System identification numbers are noted.

ID	$m_{\rm sys}$ ($M_\odot$)	r (pc)	v (km s^{-1})
1-15	90.9	12.6	73.3
1-16	90.6	10.7	59.9
2-4	129.9	87.9	69.7
2-23	69.3	35.8	38.8
2-24	67.9	62.0	69.0
2-133	33.6	10.4	9.3
2-161	49.0	53.6	72.8
3-1	132.4	211.4	131.8
3-2	129.0	187.4	117.0
3-11	116.9	36.9	32.8
3-27	169.1	30.8	28.9
3-31	74.3	40.4	75.0
3-55	61.3	49.5	39.9
3-56	61.2	44.1	35.0
3-172	29.2	348.3	343.0
4-10	111.2	137.3	215.8
4-13	106.5	32.1	50.5
4-14	105.9	30.8	48.1
4-48	59.1	57.1	55.6
4-199	26.1	48.9	55.2
4-200	26.1	46.8	53.2
4-210	25.3	24.5	93.9

Table 5.2. List of the ejected massive single stars by 2 Myr. Same as columns 1–4 in Table 5.1.

systems from all four calculations. Four systems are binaries (Table 5.1) and the other 22 systems are single stars (Table 5.2).

Among all four dynamically ejected binary systems, three have system masses larger than 100 $M_\odot$ including the one discussed in the previous section. Furthermore, about half (10) of the single stars are more massive than 90 $M_\odot$. This indicates that very massive stars can be efficiently ejected from a massive young star cluster within the first few Myr of cluster evolution (see fig. 4 in Banerjee et al. 2012b) since those very massive stars are formed in or migrate into (Bonnell, Vine & Bate 2004) the cluster core dynamically at a very early age of the cluster, given the high densities of star-burst clusters such as R136.

In the models studied here, the binaries are ejected with relatively lower velocities and are found relatively close ($r < 38$ pc) to the clusters compared to the ejected single stars which are found up to about 350 pc away from their birth clusters at 2 Myr (Figs 5.2 and 5.3). A few single stars more massive than 100 $M_\odot$ are ejected with a velocity greater than 100 km s^{-1} up to $\approx$200 km s^{-1}. Especially, one star with a mass of 111.2 $M_\odot$ moves away from its parent cluster with a velocity of 215.8 km s^{-1}. This was probably ejected by the same binary–binary interaction which has ejected the very massive binary described in Section 5.3; it is located on the opposite side of the cluster.

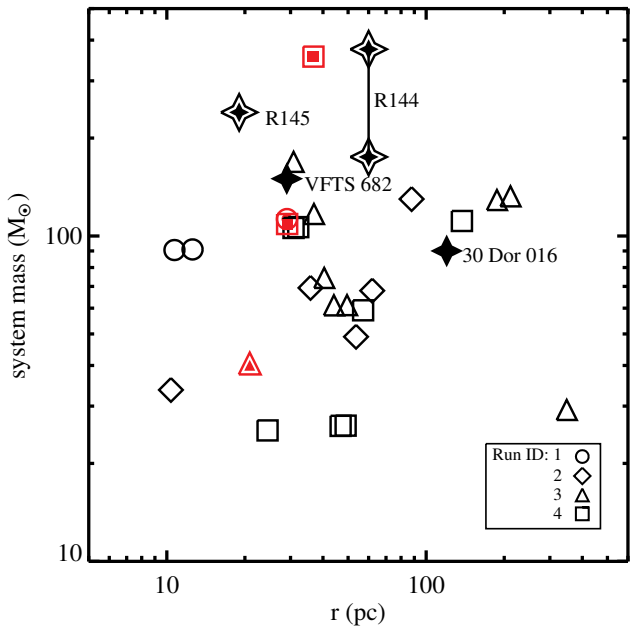

Figure 5.2. Distance from the cluster centre versus system mass of the ejected massive systems. Single stars are black open symbols. Red symbols with small filled symbols inside are binary systems. Star symbols are the *observed* massive systems located outside of the R136 core, e.g. R144 (Sana et al. 2013a), R145 (Schnurr et al. 2009; Chené et al. 2011), 30 Dor 016 (Evans et al. 2010), and VFTS 682 (Bestenlehner et al. 2011). The filled stars are single stars while open stars with small filled symbols confirmed binary systems. The two mass estimates of R144 are connected with a solid line. As is evident, the theoretical systems cover the range of observed cases.

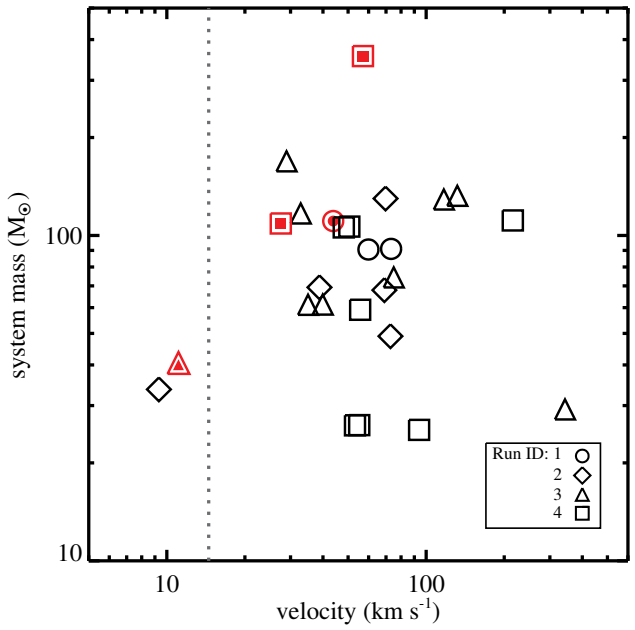

Figure 5.3. Velocity of the ejected massive system with respect to the cluster centre versus system mass of the ejected massive systems. Symbols are the same as in Fig. 5.2. The dotted line represents the initial rms velocity dispersion of the model clusters, $\approx$14.5 km s^{-1}.

As shown in Fig. 5.2, the ejected massive systems in the models cover the range of observed very massive systems outside of the R136 core in the system mass – distance from the cluster centre space. The Jacobi radius of the cluster with a mass of $10^5\,M_\odot$ at the location of R136 in the LMC, ≈1 kpc in projection relative to the H I rotation centre of the LMC (Mackey & Gilmore 2003), would be ≈43 pc (Baumgardt et al. 2013),[9] so some of the ejected massive systems are still located inside the Jacobi radius and may be under the influence of the cluster potential. However, all ejected massive systems are unbound to the cluster, i.e. their velocities exceed the escape velocity at their location (e.g. initial escape velocity at 10 pc of the model clusters ≈9.5 km s^{-1}). Therefore most of those still remaining inside the Jacobi radius at 2 Myr will move outside the Jacobi radius within less than 0.5 Myr considering their high velocity.

Like the distances from the cluster centre, the velocities of the ejected massive systems are also spread over a large range, from 9 to 350 km s^{-1}. There seems no evident correlation between the system mass and the velocity of ejected massive systems (Fig. 5.3) though there is a little tendency that more massive systems have on average higher velocities (Banerjee et al. 2012b). The initial rms velocity dispersion of the model clusters, ≈14.5 km s^{-1} (equation 8.69 in Kroupa 2008), is indicated in Fig. 5.3. Most of the ejected systems have attained velocities significantly larger than the rms velocity dispersion.

One of the interesting findings here is that all ejected binaries but one have a short period ($P \lesssim 35$ days, Fig. 5.4). This may mainly result from the initial period distribution which the N-body models adopted. Indeed the two shortest period binaries are natal pairs (1-59 and 3-301 in Table 5.1). However, even a binary which has dynamically formed probably after a binary–binary interaction (4-47[10] in Table 5.1) also has a short period, $P = 35.1$ days. We expect that ejected massive binaries from R136 would preferentially have short periods like the result presented here, because the observed period distribution of O-type star binaries in the Tarantula Nebula, which hosts the cluster R136 at its centre, favours short periods (Sana et al. 2013b), in fact even shorter ones than used in the N-body models here. Furthermore, an energetic encounter between a binary and another system can result in the shrinkage of the binary's orbit. Indeed, the orbit of one ejected binary, 1-59, has shrunk compared to its initial one: the period has changed from 30.7 to 19.4 days, the semi-major axis from 0.93 to 0.68 au, and the eccentricity from 0.51 to 0.44. Note that the other natal binary, 3-301, keeps its initial binary orbital parameters implying that the binary was treated as a single star in the interaction which has caused its ejection.

By fixing the binding energy, E_b, and mass ratio of a binary, $q = m_2/m_1$, where m_1 and m_2 are masses of the binary components in $M_\odot$ and $m_1 \geq m_2$, the binary period can be expressed as a function of system masses,

$$P_\mathrm{yr} = \left[-\frac{206264.8\,Gq}{2(1+q)^2 E_\mathrm{b}}\right]^{3/2} m_\mathrm{sys}^{5/2}, \tag{5.1}$$

where P_yr is the period in years, G is the gravitational constant ($G = 0.0045\,\mathrm{pc^3\,M_\odot^{-1}\,Myr^{-2}}$) and the binding energy of the binary in units of $\mathrm{M_\odot\,pc^2\,Myr^{-2}}$ is

$$E_\mathrm{b} = -\frac{Gm_1m_2}{2a_\mathrm{pc}} = -\frac{Gq}{2(1+q)^2}\frac{m_\mathrm{sys}^2}{a_\mathrm{pc}}, \tag{5.2}$$

[9] Tidal field is not included in the N-body calculations.

[10] This binary system is also not found in a list of ejected stars in Banerjee et al. (2012b) because the system merges before 3 Myr due to its highly eccentric orbit.

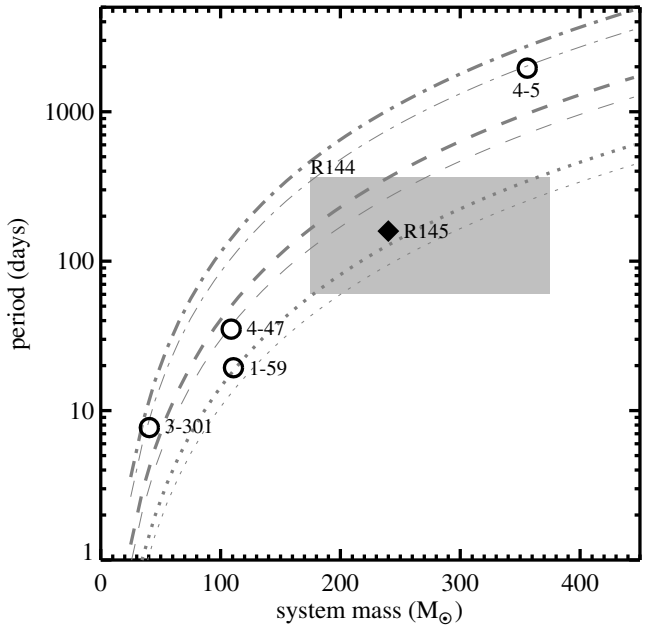

Figure 5.4. System mass versus period of the ejected binary systems. Open circles are the binaries from the *N*-body models while the filled diamond is R145 (Schnurr et al. 2009; Chené et al. 2011). A large grey box indicates the range of the values of R144 in Sana et al. (2013a). Curves present equal binding energies, i.e. 5% (dot-dashed), 10% (dashed), 20% (dotted) of the total energy of the cluster (Equation 5.3) assuming a certain mass ratio (thick lines, $q = 1$; thin lines, $q = 0.4$).

where $a_{\rm pc} = a_{\rm au}/206264.8\,{\rm pc}$ and $a_{\rm au}$ is the semi-major axis in au. Curves in Fig. 5.4 indicate 5, 10 and 20% of initial total binding energy of the cluster (Heggie & Hut 2003),

$$E_{\rm tot,ecl} = -\frac{3\pi}{32}\frac{GM_{\rm ecl}^2}{r_{\rm Pl}}, \tag{5.3}$$

in units of $M_\odot\,{\rm pc}^2\,{\rm Myr}^{-2}$ where $r_{\rm Pl}$ is the Plummer radius $\approx 0.766 r_{\rm h}$ in units of pc. The figure indicates a possible correlation between system mass and a period of the ejected massive binaries, but the number of cases is too small to be conclusive. The ejected binaries have binding energies between 5 and 20% of the initial total energy of the cluster. They thus contain a significant amount of energy.

As stellar identification numbers in the NBODY6 code are consecutive for initial binary components, we can identify if the ejected stars have been initially paired with other ejected stars. Among the ejected single stars, six natal pairs (i.e. 12 stars) can be deduced. Furthermore, two of the ejected single stars, 4-10 and 4-48, were a companion of the two ejected binaries, 4-5 and 4-47, respectively, which have exchanged their companions. Both components of one binary are shot out into opposite directions (Fig. 5.1) almost conserving momentum. However, there should be a third body, likely another binary system, to operate the ejection process; thus the momentum of one ejected star is not exactly identical to the other's. In addition, dynamically ejected systems are still under the influence of the gravitational potential of the cluster right after ejection while they move away from the cluster. This can reduce the velocity of the systems, especially of massive ones with a low velocity. Associating isolated massive

stars with particular ejection events is thus not straightforward.

5.5 Conclusion

We find a very massive binary ($m_{\rm sys} \approx 355.9\,{\rm M}_\odot$) with a period $P \approx 2000$ days, which is dynamically ejected via a binary–binary interaction in previously published direct N-body models of an R136-like cluster. This suggests that a very massive binary system such as R144 can be dynamically ejected via a close encounter with another very massive binary or single star and that they then appear in isolation. Three other massive binaries are found being ejected in the four R136-model clusters studied here. Among them two have a system mass larger than $100\,{\rm M}_\odot$. Three out of four binaries have a period shorter than ≈35 days. From this result and the observed period distribution of O-type star binaries in the Tarantula Nebula (Sana et al. 2013b), we expect that ejected massive binaries from R136 would preferentially have short periods contrary to the discussion in Sana et al. (2013a).

We show that very massive stars can be ejected with a high velocity via a three- or four-body interaction in a realistic full-cluster size N-body calculation, even a star more massive than $100\,{\rm M}_\odot$ can obtain a velocity of more than $200\,{\rm km\,s^{-1}}$. The ejected massive stars travel up to 350 pc away from their birth clusters within the first 2 Myr of their cluster evolution.

Among the 26 dynamically ejected massive systems, 15 systems (≈58%) are more massive than $90\,{\rm M}_\odot$. Thus, in the first few Myr of evolution of a massive cluster like R136, mostly very massive stars are dynamically ejected since they are the ones located at the very centre of the cluster where the probability for close encounters is the highest. Massive young star clusters such as R136 would mainly contribute very massive stars into the field during the first few Myr of their evolution. Correcting the measured stellar mass function within R136 for the likely massive stars lost from the cluster through ejections reveals a flattening of the IMF at high stellar masses (Banerjee & Kroupa 2012).

Thus, more than one very massive binary can be ejected from a massive young star cluster by dynamical interactions. One out of four runs produced two very massive binaries ejected dynamically by 2 Myr. Thus, the cluster R136 probably produced both R144 and R145 through close encounters with other very massive systems. In particular, the isolated formation scenario of R144 is unnecessary.

CHAPTER 6

Summary and Outlook

We established a theoretical young star cluster library by performing a large set of the direct N-body calculations. The library, which is the largest and most comprehensive to have been computed, includes a large range of initial conditions, varying initial cluster mass, cluster size, binary populations of massive stars. By using the direct N-body code NBODY6, we performed in total about 8300 realizations for this thesis which used a CPU time of more than 30 000 hours. We have studied several aspects of the dynamical ejections of massive stars from young star clusters using different subsets of our library (but overlapping in large parts) in Chapters 2–4 and using the very-large-N N-body calculations for a R136-like cluster by Banerjee et al. (2012b) in Chapter 5.

In Chapter 2, we studied the effect of dynamical processes, such as dynamical ejections and stellar collisions, on the relation between the maximum stellar mass and cluster mass. We used twelve sets of the direct N-body calculations with various initial conditions, that are composed of 7210 realizations in total. For each set the cluster mass spans from 10 to $10^{3.5}\,\mathrm{M}_\odot$ ($10^4\,\mathrm{M}_\odot$ for one set). We analysed the snapshots at 3 Myr of the calculations. For lower mass clusters, their most massive stars are rarely ejected for all sets. For higher mass clusters, the initially most massive star in a cluster can be dynamically ejected, particularly when massive binaries initially consist of two similar mass components and are initially concentrated in the cluster centre. The ejection frequency of the most massive star for these clusters can be as high as 20% but the clusters likely host a few stars that are nearly as massive as the initially most massive star. This means that the dynamical ejection rarely changes the mass of the most massive star in the cluster. For dense and massive clusters, stellar collisions can be more significant in changing the maximum stellar mass in a cluster. Overall, (dynamical) evolutionary effects hardly produce a spread of m_{max} in the relation for low-mass ($M_{\mathrm{ecl}} \lesssim 10^{2.5}\,\mathrm{M}_\odot$) or less dense ($r_{\mathrm{h}}(0) = 0.8\,\mathrm{pc}$) clusters. Massive ($M_{\mathrm{ecl}} \gtrsim 10^{2.5}\,\mathrm{M}_\odot$), binary-rich clusters with $r_{\mathrm{h}}(0) = 0.3\,\mathrm{pc}$ do lead to a significant spread of m_{max} values, mostly produced by stellar collisions, becoming comparable to the observed spread. We stress here that star clusters can dynamically eject their initially most massive member via an energetic close encounter.

In Chapter 3, we studied how the ejection fraction of O-star systems varies with cluster mass. Seven sequences in the library were considered. We used cluster models that have O stars initially ($M_{\mathrm{ecl}} = 10^{2.5}$–$10^{4.5}\,\mathrm{M}_\odot$. For each sequence a single cluster size is assigned, thus the cluster mass increases so does the cluster density. The number of ejected O-star systems increases with increasing cluster mass since the close encounter rate is expected to be proportional to the cluster density. For massive star clusters $M_{\mathrm{ecl}} \geq 10^{3.5}\,\mathrm{M}_\odot$, however, the ejection efficiency of O-star systems decreases with increasing cluster

mass because the number of O-star systems increases more steeply with increasing cluster mass than the number of ejected O-star systems does. For lower mass clusters $M_{\rm ecl} \leq 10^3\,{\rm M}_\odot$, the efficiency increases with increasing cluster mass because of too low number of massive stars in the lowest mass cluster. The number of ejected O-star systems increases more slowly than the total number of O-star systems with increasing cluster mass because the O-star-core becomes an increasingly smoother potential. All seven sequences studied here show the trend that the ejection fraction of O-star systems peaks at a cluster mass of $10^{3.5}\,{\rm M}_\odot$ although the amplitude of the efficiency depends on models. This implies that, regardless of initial conditions (at least those considered in this thesis), moderately massive star clusters $M_{\rm ecl} \approx 10^{3.5}\,{\rm M}_\odot$ are most efficient in ejecting O-star systems. The properties of ejected O-star systems depend on the cluster mass. For example, the velocities of ejected stars become more biased to higher velocities and binary fraction of the ejected systems decreases as the cluster mass increases.

By synthesizing a young star cluster mass function that follows a power law with the index -2, we estimated that about 15% of O-star systems in our most realistic model are dynamically ejected from their birth cluster to the field in a Milky-Way-type galaxy within a star-formation epoch of 10 Myr. We found that the most prominent contributors to the population of ejected O stars are $\approx$400 $\,{\rm M}_\odot$ clusters and that a high proportion of field O stars that are dynamically ejected from clusters originate from low/intermediate mass clusters ($M_{\rm ecl} \lesssim$ few1000 $\,{\rm M}_\odot$). Given the result presented in this chapter, the observed fractions of field and runaway O stars, and the binary fractions among them can be well understood theoretically if all O stars form in embedded clusters.

In Chapter 4, we investigated how the initial conditions of massive stars and of their birth star clusters affect the dynamical ejections of massive stars. We used sixteen $10^{3.5}\,{\rm M}_\odot$ cluster models with different initial conditions, such as initial cluster size, initial binary populations (particularly massive binaries), and initial mass-segregation. Each model was computed 100 times with different random seed numbers, and thus 1600 realizations were considered in this chapter. We found that the density is the most influential factor for the ejection fraction of massive systems. The clusters with a smaller size (i.e. higher density) eject the massive stars more efficiently. The ejection efficiency increases with increasing stellar mass, particularly for models that are efficient in ejecting massive stars. This results in the mass functions to be top-heavy ($1.7 < \alpha < 1.8$) for ejected stars and bottom-heavy ($2.37 < \alpha < 2.5$) for stars that remain in the cluster for these models. The mass functions of stars that remain in the cluster for our realistic N-body models are in good agreement with the observed stellar mass function of young intermediate-mass clusters in M31 (Weisz et al. 2015). This implies that the initial mass function of those clusters in M31 would be canonical and that their bottom-heavy present-day mass function can be the outcome of cluster evolution. This suggests that the present-day mass function can be different from the initial mass function even within the first few Myr as a result of evolutionary stellar-dynamical processes.

We showed that the multiplicity is lower for the ejected systems than for the systems that remain in the cluster and that not only binaries but also high-order (e.g. triple and quadruple) multiple massive systems can be dynamically ejected. The period distribution of the ejected massive binaries is more biased to shorter periods than that of the binaries that remain in the cluster. However, the eccentricity and mass-ratio distributions are similar for the two populations.

In this chapter, we presented that the properties of the ejected systems, such as velocity distribution, the time of ejection, and multiplicity fraction, vary with the initial conditions. This suggests that studying massive stars outside of star clusters can constrain the initial dynamical configuration of massive stars, by

assuming that they all form in star clusters.

In Chapter 5, we investigated the origin of the very massive binary R144 (estimated system mass of 200–300 $M_\odot$, Sana et al. 2013a) that is apparently in isolation near the young massive star cluster R136 in the Large Magellanic Cloud. We revisited the direct N-body calculations for the R136-like cluster (mass 10^5 $M_\odot$) by Banerjee et al. (2012b) and, then, showed that a very massive binary (system mass >300 $M_\odot$) can be dynamically ejected from a young massive star cluster through a binary–binary encounter. This implies that the very massive binary R144 could have been dynamically ejected from the young massive star cluster R136 and that the isolated formation scenario of R144 is unnecessary. In addition, we presented that a massive cluster such as R136 can populate several very massive stars ($\gtrsim$100 $M_\odot$) outside of the cluster through dynamical ejections.

Throughout the thesis, we have shown that the massive stars can be efficiently ejected from their birth cluster through energetic close encounters. Even the initially most massive stars in the cluster or (binary) stars more massive than 100 $M_\odot$ can be expelled. The ejection efficiency is the highest when star clusters form with a smaller size (e.g. half-mass radius $\lesssim$0.3 pc) and with a high portion of short-period massive binaries that have a massive companion. Such configurations seem to be common in reality (e.g. Testi et al. 1999; Tapia et al. 2009; Sana et al. 2012; Kobulnicky et al. 2014). This implies that a large fraction of massive stars in the field have been likely ejected from star clusters through close encounters. Considering also the other mechanisms that make unable to trace back stars to their birth cluster, such as dissolution of a star cluster and two-step ejection (Chapter 3), all the field massive stars have formed in star clusters and isolated massive star formation would be unnecessary to explain their origin.

As mentioned above, the efficiency of dynamical ejection and the properties of ejected massive systems depend on the initial conditions of star clusters and their massive star population. This suggests that studying massive stars outside of star clusters can constrain the initial configuration of massive stars, by assuming that they all form in star clusters. When a large kinematic survey of O stars in the Galaxy becomes available, for example through the *Gaia* mission, our models can be used to constrain the initial configurations of massive stars and their birth cluster, which are end-products of the star formation, leading towards a better understanding of massive star formation.

Ongoing and future studies

Initial massive-binary populations

The multiple stellar system is a dominant mode of star formation (Duchêne & Kraus 2013; Sana et al. 2014). Thus binaries are one of the key elements to understand star formation. In fact, since $N > 3$ multiple systems decay on a crossing time ($\approx 10^4$–10^5 yr) while the observed binary fraction is very high in $\approx 10^6$ yr old populations, star formation must predominantly yield binary systems (Goodwin & Kroupa 2005). The initial distribution functions of the binary population can be used to constrain the theory of star formation (Kroupa & Petr-Gotzens 2011; Duchêne & Kraus 2013). The discrepancies in binary fractions and period distributions between field late-type stars and low-mass stars in star-forming regions are often misunderstood as they form in different ways. However, binary populations in clusters do evolve because of interactions between systems. For solar- and late-type binaries, Kroupa (1995a) and Marks & Kroupa (2011) showed that initial binary populations similar to those in star-forming regions with a binary fraction of 100% can dynamically evolve into the field late-type binary populations that

have a binary fraction of ≈50% (Duquennoy & Mayor 1991; Raghavan et al. 2010).

The observed orbital-parameter distributions of massive binaries are significantly different from those of late-type binaries. For example, a high proportion of O-star binaries are short-period spectroscopic binaries (Kiminki & Kobulnicky 2012; Sana et al. 2012; Kobulnicky et al. 2014), while the majority of low-mass binaries in star-forming regions have a long period (Kroupa & Petr-Gotzens 2011, and references therein). Based on our calculations, we found that dynamical evolution alone cannot reproduce the observed massive binary populations if the same initial distributions as those of low-mass binaries are adopted. This means that different initial populations from those of the low-mass binaries are needed for massive binaries. The observational studies on the massive binary populations have assumed that the observed distributions from a few ($\lesssim$3) Myr old clusters are the initial distribution, arguing that the dynamical evolution is insignificant for the binary populations. But this assumption has not been tested with N-body models and thus needs to be investigated. Furthermore, in the case that the dynamical evolution alters the binary populations, we aim to find the true initial binary populations of massive binaries that can be consistent with observed binary populations in young star clusters after a few dynamical times. This can be done by performing N-body calculations iteratively with varying initial orbital parameter distributions of massive binaries, a similar procedure invented by Kroupa (1995a).

Modelling the young massive star cluster NGC 6611

Even though we have studied a large parameter space for the initial conditions of star clusters and their massive star populations, our N-body models have not been directly compared with observed quantities because the observational kinematical data of young massive stars are incomplete. However, it is possible to compare between N-body models and the observational data for a star cluster that has been well studied by observations. Such a case study can constrain the initial conditions of the cluster and further provide a better understanding on the formation of similar star clusters.

NGC 6611 is a young (2–3 Myr) massive ($\lesssim 2 \times 10^4$ $M_\odot$) star cluster in the Eagle nebula at a distance of ≈2 kpc from the Sun (Dufton et al. 2006; Wolff et al. 2007). It has been well studied observationally on the issue of possibly ejected O stars (e.g. bow-shock-producing OB stars in the vicinity of the cluster, Gvaramadze & Bomans 2008) and on binary populations of O stars in the cluster (Sana et al. 2009). Therefore, the cluster is a good target for the case study on constraining initial conditions by studying the dynamical ejections of massive stars and dynamical evolution of massive binary populations. N-body modelling of NGC 6611 can readily be applied to examine the results of our ongoing study to constrain initial binary populations of massive binaries.

Reproducing massive-star populations in the Galaxy with N-body calculations

In reality, young star clusters in the Galaxy have broad ranges of mass and age. For our theoretical star-cluster library, however, only a few cluster masses are selected to be calculated because we studied a large parameter space and some calculations are computationally expensive. Furthermore, we mainly use a single snapshot of 3 Myr for the analysis.

In Chapter 3, we utilised the cluster mass function to our result using the fitting functions for N-body models and obtained only rough estimates for the proportion of O-star systems that can be dynamically ejected to the field. For a better understanding of the Galactic O-star populations originated from star clusters, it is required to incorporate the cluster mass function and the age-distributed cluster population. About 12 000 clusters would form with a mass $\gtrsim$240 $M_\odot$ within a cluster-population formation timescale

of 10 Myr under the same assumptions for the star formation rate in the galaxy ($3\,M_\odot\,yr^{-1}$) and for the cluster mass function ($\beta = 2$) as in Chapter 3. Though the number of clusters that need to be calculated is very high, the calculations can be feasible because most of the clusters have a low mass (i.e. computationally inexpensive). Furthermore, we need to evolve them only about 10 Myr which is the lifetime of O stars. With these calculations, one can quantify what fraction of O stars would be dynamically populated to the field from the clusters and thus provide an answer for the long-debating question whether stars form only in star clusters. In addition, such calculations can be used to study several subjects relevant to the young star (cluster) population in the Galaxy; for example, the evolution of the cluster mass function and of the stellar mass function and the dissolution rate of young star clusters by dynamical processes. Also, this set of calculations can provide a better theoretical model to compare to the observational data for studying the dynamical evolutionary effects on the relation between the maximum stellar mass and cluster mass (cf. Chapter 2).

Bibliography

Aarseth S. J., 1999, PASP, 111, 1333

Aarseth S. J., 2003, Gravitational N-Body Simulations. Cambridge Univ. Press, Cambridge

Aarseth S. J., Henon M., Wielen R., 1974, A&A, 37, 183

Adams F. C., 2010, ARA&A, 48, 47

Adams F. C., Fatuzzo M., 1996, ApJ, 464, 256

Adelman S. J., 2004, in Zverko J., Ziznovsky J., Adelman S. J., Weiss W. W., eds, IAU Symposium Vol. 224, The A-Star Puzzle. pp 1–11

Ahmad A., Cohen L., 1973, Journal of Computational Physics, 12, 389

Aldoretta E. J., et al., 2015, AJ, 149, 26

Andrews J. E., et al., 2013, ApJ, 767, 51

Banerjee S., Kroupa P., 2012, A&A, 547, A23

Banerjee S., Kroupa P., 2013, ApJ, 764, 29

Banerjee S., Kroupa P., 2014, ApJ, 787, 158

Banerjee S., Kroupa P., Oh S., 2012a, MNRAS, 426, 1416

Banerjee S., Kroupa P., Oh S., 2012b, ApJ, 746, 15

Bastian N., Gieles M., Lamers H. J. G. L. M., Scheepmaker R. A., de Grijs R., 2005, A&A, 431, 905

Bate M. R., 2009, MNRAS, 392, 590

Bate M. R., 2012, MNRAS, 419, 3115

Baumgardt H., Klessen R. S., 2011, MNRAS, 413, 1810

Baumgardt H., De Marchi G., Kroupa P., 2008, ApJ, 685, 247

Baumgardt H., Parmentier G., Anders P., Grebel E. K., 2013, MNRAS, 430, 676

Bestenlehner J. M., et al., 2011, A&A, 530, L14

Bestenlehner J. M., et al., 2014, A&A, 570, A38

Bevington P. R., Robinson D. K., 1992, Data reduction and error analysis for the physical sciences. New York: McGraw-Hill

Binney J., Tremaine S., 1987, Galactic dynamics. Princeton Univ. Press, Princeton, NJ

Binney J., Tremaine S., 2008, Galactic Dynamics: Second Edition. Princeton: Princeton Univ. Press

Blaauw A., 1961, Bull. Astron. Inst. Netherlands, 15, 265

Bonnell I. A., Bate M. R., Clarke C. J., Pringle J. E., 1997, MNRAS, 285, 201

Bonnell I. A., Vine S. G., Bate M. R., 2004, MNRAS, 349, 735

Bressert E., et al., 2012, A&A, 542, A49

Calzetti D., Chandar R., Lee J. C., Elmegreen B. G., Kennicutt R. C., Whitmore B., 2010, ApJ, 719, L158

Casertano S., Hut P., 1985, ApJ, 298, 80

Chen L., de Grijs R., Zhao J. L., 2007, AJ, 134, 1368

Chen X., et al., 2013, ApJ, 768, 110

Chené A.-N., Schnurr O., Crowther P. A., Fernández-Lajús E., Moffat A. F. J., 2011, in Neiner C., Wade G., Meynet G., Peters G., eds, Proc. IAU Symp. 272, Active OB stars: Structure, Evolution, Mass Loss, and Critical Limits. Cambridge Univ. Press, Cambridge, p. 497

Chernoff D. F., Shapiro S. L., 1987, ApJ, 322, 113

Chini R., Hoffmeister V. H., Nasseri A., Stahl O., Zinnecker H., 2012, MNRAS, 424, 1925

Clarke C. J., Pringle J. E., 1992, MNRAS, 255, 423

Cohn H., 1979, ApJ, 234, 1036

Conroy C., Kratter K. M., 2012, ApJ, 755, 123

Crowther P. A., Schnurr O., Hirschi R., Yusof N., Parker R. J., Goodwin S. P., Kassim H. A., 2010, MNRAS, 408, 731

Da Rio N., Gouliermis D. A., Rochau B., Pasquali A., Setiawan J., De Marchi G., 2012, MNRAS, 422, 3356

Dalessandro E., et al., 2013, ApJ, 778, 135

Dong H., Mauerhan J., Morris M. R., Wang Q. D., Cotera A., 2015, MNRAS, 446, 842

Duchêne G., Kraus A., 2013, ARA&A, 51, 269

Duchêne G., Bontemps S., Bouvier J., André P., Djupvik A. A., Ghez A. M., 2007, A&A, 476, 229

Dufton P. L., et al., 2006, A&A, 457, 265

Duquennoy A., Mayor M., 1991, A&A, 248, 485

Einsel C., Spurzem R., 1999, MNRAS, 302, 81

Eldridge J. J., Langer N., Tout C. A., 2011, MNRAS, 414, 3501

Evans K. A., Massey P., 2015, AJ, 150, 149

Evans C. J., et al., 2010, ApJ, 715, L74

Figer D. F., 2005, Nature, 434, 192

Figer D. F., 2008, in Bresolin F., Crowther P. A., Puls J., eds, IAU Symp. Vol. 250, Massive Stars as Cosmic Engines. Cambridge: Cambridge Univ. Press, p. 247

Forbes D. A., Kroupa P., 2011, Publ. Astron. Soc. Australia, 28, 77

Fujii M. S., Portegies Zwart S., 2011, Science, 334, 1380

Fujii M. S., Saitoh T. R., Portegies Zwart S. F., 2012, ApJ, 753, 85

Fumagalli M., da Silva R. L., Krumholz M. R., 2011, ApJ, 741, L26

Gaburov E., Gualandris A., Portegies Zwart S., 2008, MNRAS, 384, 376

García B., Mermilliod J. C., 2001, A&A, 368, 122

Giersz M., 1998, MNRAS, 298, 1239

Giersz M., Heggie D. C., 1994, MNRAS, 268, 257

Gies D. R., 1987, ApJS, 64, 545

Gies D. R., Bolton C. T., 1986, ApJS, 61, 419

Goodman A. A., Benson P. J., Fuller G. A., Myers P. C., 1993, ApJ, 406, 528

Goodwin S. P., Kroupa P., 2005, A&A, 439, 565

Goodwin S. P., Kroupa P., Goodman A., Burkert A., 2007, in Reipurth B., Jewitt D., Keil K., eds, Protostars and Planets V. Tucson, AZ: Univ. Arizona Press, p. 133

Gouliermis D., Keller S. C., Kontizas M., Kontizas E., Bellas-Velidis I., 2004, A&A, 416, 137

Gualandris A., Portegies Zwart S., Eggleton P. P., 2004, MNRAS, 350, 615

Gvaramadze V. V., Bomans D. J., 2008, A&A, 490, 1071

Gvaramadze V. V., Gualandris A., 2011, MNRAS, 410, 304

Gvaramadze V. V., Gualandris A., Portegies Zwart S., 2009, MNRAS, 396, 570

Gvaramadze V. V., Kniazev A. Y., Kroupa P., Oh S., 2011, A&A, 535, A29

Gvaramadze V. V., Weidner C., Kroupa P., Pflamm-Altenburg J., 2012, MNRAS, 424, 3037

Gvaramadze V. V., Kniazev A. Y., Chené A.-N., Schnurr O., 2013, MNRAS, 430, L20

Habibi M., Stolte A., Harfst S., 2014, A&A, 566, A6

Heggie D. C., 1975, MNRAS, 173, 729

Heggie D. C., 1980, in Hanes D., Madore B., eds, Globular Clusters. p. 281

Heggie D., Hut P., 2003, The Gravitational Million-Body Problem: A Multidisciplinary Approach to Star Cluster Dynamics. Cambridge Univ. Press, Cambridge

Hillenbrand L. A., 1997, AJ, 113, 1733

Hillenbrand L. A., Hartmann L. W., 1998, ApJ, 492, 540

Hills J. G., 1975, AJ, 80, 809

Hills J. G., Fullerton L. W., 1980, AJ, 85, 1281

Hoogerwerf R., de Bruijne J. H. J., de Zeeuw P. T., 2001, A&A, 365, 49

Hsu W.-H., Hartmann L., Allen L., Hernández J., Megeath S. T., Mosby G., Tobin J. J., Espaillat C., 2012, ApJ, 752, 59

Hsu W.-H., Hartmann L., Allen L., Hernández J., Megeath S. T., Tobin J. J., Ingleby L., 2013, ApJ, 764, 114

Hur H., Park B.-G., Sung H., Bessell M. S., Lim B., Chun M.-Y., Sohn S. T., 2015, MNRAS, 446, 3797

Hurley J. R., 2008, in Aarseth S. J., Tout C. A., Mardling R. A., eds, Lecture Notes in Physics Vol. 760, The Cambridge N-Body Lectures. Springer-Verlag, Berlin, p. 283

Hurley J. R., Pols O. R., Tout C. A., 2000, MNRAS, 315, 543

Hurley J. R., Tout C. A., Pols O. R., 2002, MNRAS, 329, 897

Hut P., Bahcall J. N., 1983, ApJ, 268, 319

Huthoff F., Kaper L., 2002, A&A, 383, 999

Joshi K. J., Rasio F. A., Portegies Zwart S., 2000, ApJ, 540, 969

Kiminki D. C., Kobulnicky H. A., 2012, ApJ, 751, 4

King I. R., 1966, AJ, 71, 64

Kirk H., Myers P. C., 2011, ApJ, 727, 64

Kirsten F., Vlemmings W., Campbell R. M., Kramer M., Chatterjee S., 2015, A&A, 577, A111

Kobulnicky H. A., Fryer C. L., 2007, ApJ, 670, 747

Kobulnicky H. A., et al., 2014, ApJS, 213, 34

Kouwenhoven M. B. N., Brown A. G. A., Goodwin S. P., Portegies Zwart S. F., Kaper L., 2009, A&A, 493, 979

Kroupa P., 1995a, MNRAS, 277, 1491

Kroupa P., 1995b, MNRAS, 277, 1507

Kroupa P., 2000, New Astron., 4, 615

Kroupa P., 2001, MNRAS, 322, 231

Kroupa P., 2002, Science, 295, 82

Kroupa P., 2005, in Turon C., O'Flaherty K. S., Perryman M. A. C., eds, ESA Special Publication Vol. 576, The Three-Dimensional Universe with Gaia. Noordwijk: ESA, p. 629

Kroupa P., 2008, in Aarseth S. J., Tout C. A., Mardling R. A., eds, Lecture Notes in Physics Vol. 760, The Cambridge N-Body Lectures. Springer-Verlag, Berlin, p. 181

Kroupa P., 2015, CaJPh, 93, 169

Kroupa P., Boily C. M., 2002, MNRAS, 336, 1188

Kroupa P., Petr-Gotzens M. G., 2011, A&A, 529, A92

Kroupa P., Aarseth S., Hurley J., 2001, MNRAS, 321, 699

Kroupa P., Weidner C., Pflamm-Altenburg J., Thies I., Dabringhausen J., Marks M., Maschberger T., 2013, in Oswalt T. D., Gilmore G., eds, Planets, Stars and Stellar Systems. Vol. 5: Galactic Structure and Stellar Populations. Springer, Dordrecht, p. 115

Krumholz M. R., 2015, in Vink J. S., ed., Astrophysics and Space Science Library Vol. 412, Very Massive Stars in the Local Universe. Springer International Publishing Switzerland, p. 43

Kuiper R., Klahr H., Beuther H., Henning T., 2010, ApJ, 722, 1556

Kuiper R., Klahr H., Beuther H., Henning T., 2011, ApJ, 732, 20

Kustaanheimo P., Stiefel E., 1965, J. Reine Angew. Math., 218, 204

Lada C. J., Lada E. A., 2003, ARA&A, 41, 57

Larsen S. S., 2002, AJ, 124, 1393

Larsen S. S., 2004, A&A, 416, 537

Larson R. B., 1970, MNRAS, 147, 323

Leigh N. W. C., Giersz M., Marks M., Webb J. J., Hypki A., Heinke C. O., Kroupa P., Sills A., 2015, MNRAS, 446, 226

Leonard P. J. T., 1995, MNRAS, 277, 1080

Leonard P. J. T., Duncan M. J., 1988, AJ, 96, 222

Leonard P. J. T., Duncan M. J., 1990, AJ, 99, 608

Longmore S. N., et al., 2014, in Beuther H., Klessen R. S., Dullemond C. P., Henning T., eds, Protostars and Planets VI. Tuscon, AZ: Univ. Arizona Press, pp 291–314

Louis P. D., Spurzem R., 1991, MNRAS, 251, 408

Lucy L. B., 2006, A&A, 457, 629

Lynden-Bell D., Eggleton P. P., 1980, MNRAS, 191, 483

Mackey A. D., Gilmore G. F., 2003, MNRAS, 338, 85

Mackey J., Langer N., Gvaramadze V. V., 2013, MNRAS, 436, 859

Maíz Apellániz J., Úbeda L., 2005, ApJ, 629, 873

Makino J., 1991, ApJ, 369, 200

Makino J., Aarseth S. J., 1992, PASJ, 44, 141

Makino J., Taiji M., 1998, Scientific Simulations with Special-Purpose Computers–the GRAPE Systems

Makino J., Taiji M., Ebisuzaki T., Sugimoto D., 1997, ApJ, 480, 432

Marks M., Kroupa P., 2011, MNRAS, 417, 1702

Marks M., Kroupa P., 2012, A&A, 543, A8

Marks M., Kroupa P., Oh S., 2011, MNRAS, 417, 1684

Marks M., Kroupa P., Dabringhausen J., Pawlowski M. S., 2012, MNRAS, 422, 2246

Marks M., Leigh N., Giersz M., Pfalzner S., Pflamm-Altenburg J., Oh S., 2014, MNRAS, 441, 3503

Maschberger T., Clarke C. J., 2008, MNRAS, 391, 711

Mason B. D., Gies D. R., Hartkopf W. I., Bagnuolo Jr. W. G., ten Brummelaar T., McAlister H. A., 1998, AJ, 115, 821

Mason B. D., Hartkopf W. I., Gies D. R., Henry T. J., Helsel J. W., 2009, AJ, 137, 3358

Massey P., Hunter D. A., 1998, ApJ, 493, 180

McMillan S. L. W., Aarseth S. J., 1993, ApJ, 414, 200

Megeath S. T., et al., 2016, AJ, 151, 5

Mikkola S., Aarseth S. J., 1990, Celestial Mechanics and Dynamical Astronomy, 47, 375

Mikkola S., Aarseth S. J., 1993, Celestial Mechanics and Dynamical Astronomy, 57, 439

Moeckel N., Clarke C. J., 2011, MNRAS, 410, 2799

Moeckel N., Holland C., Clarke C. J., Bonnell I. A., 2012, MNRAS, 425, 450

Nitadori K., Aarseth S. J., 2012, MNRAS, 424, 545

Oey M. S., Clarke C. J., 2005, ApJ, 620, L43

Oey M. S., Lamb J. B., 2012, in Drissen L., Rubert C., St-Louis N., Moffat A. F. J., eds, ASP Conf. Ser. Vol. 465, Four Decades of Research on Massive Stars. San Francisco, CA: ASP, p. 431

Oey M. S., Lamb J. B., Kushner C. T., Pellegrini E. W., Graus A. S., 2013, ApJ, 768, 66

Oh S., Kroupa P., 2012, MNRAS, 424, 65

Oh S., Kroupa P., 2016, A&A, 590, A107

Oh S., Kroupa P., Banerjee S., 2014, MNRAS, 437, 4000

Oh S., Kroupa P., Pflamm-Altenburg J., 2015, ApJ, 805, 92

Parker R. J., Goodwin S. P., 2007, MNRAS, 380, 1271

Parker R. J., Goodwin S. P., Kroupa P., Kouwenhoven M. B. N., 2009, MNRAS, 397, 1577

Perets H. B., Šubr L., 2012, ApJ, 751, 133

Peters T., Klessen R. S., Mac Low M.-M., Banerjee R., 2010, ApJ, 725, 134

Pfalzner S., 2009, A&A, 498, L37

Pfalzner S., 2013, A&A, 549, A82

Pflamm-Altenburg J., Kroupa P., 2006, MNRAS, 373, 295

Pflamm-Altenburg J., Kroupa P., 2010, MNRAS, 404, 1564

Pflamm-Altenburg J., Weidner C., Kroupa P., 2007, ApJ, 671, 1550

Pflamm-Altenburg J., González-Lópezlira R. A., Kroupa P., 2013, MNRAS, 435, 2604

Pinsonneault M. H., Stanek K. Z., 2006, ApJ, 639, L67

Plummer H. C., 1911, MNRAS, 71, 460

Portegies Zwart S. F., 2000, ApJ, 544, 437

Portegies Zwart S. F., McMillan S. L. W., Gieles M., 2010, ARA&A, 48, 431

Poveda A., Ruiz J., Allen C., 1967, BOTT, 4, 86

Press W. H., Flannery B. P., Teukolsky S. A., 1986, Numerical recipes. The art of scientific computing. Cambridge: Cambridge Univ. Press

Raghavan D., et al., 2010, ApJS, 190, 1

Ramírez Alegría S., et al., 2016, A&A, 588, A40

Randriamanakoto Z., Escala A., Väisänen P., Kankare E., Kotilainen J., Mattila S., Ryder S., 2013, ApJ, 775, L38

Reipurth B., Clarke C. J., Boss A. P., Goodwin S. P., Rodríguez L. F., Stassun K. G., Tokovinin A., Zinnecker H., 2014, Protostars and Planets VI, pp 267–290

Roman-Lopes A., 2012, MNRAS, 427, L65

Roman-Lopes A., 2013, MNRAS, 435, L73

Roman-Lopes A., Barba R. H., Morrell N. I., 2011, MNRAS, 416, 501

Röser S., Schilbach E., Piskunov A. E., Kharchenko N. V., Scholz R.-D., 2011, A&A, 531, A92

Salpeter E. E., 1955, ApJ, 121, 161

Sana H., Evans C. J., 2011, in Neiner C., Wade G., Meynet G., Peters G., eds, Proc. IAU Symp. 272, Active OB Stars: Structure, Evolution, Mass Loss, and Critical Limits. Cambridge Univ. Press, Cambridge, p. 474

Sana H., Gosset E., Nazé Y., Rauw G., Linder N., 2008, MNRAS, 386, 447

Sana H., Gosset E., Evans C. J., 2009, MNRAS, 400, 1479

Sana H., et al., 2012, Science, 337, 444

Sana H., et al., 2013a, MNRAS, 432, L26

Sana H., et al., 2013b, A&A, 550, A107

Sana H., et al., 2014, ApJS, 215, 15

Scheepmaker R. A., Haas M. R., Gieles M., Bastian N., Larsen S. S., Lamers H. J. G. L. M., 2007, A&A, 469, 925

Schilbach E., Röser S., 2008, A&A, 489, 105

Schnurr O., Casoli J., Chené A.-N., Moffat A. F. J., St-Louis N., 2008, MNRAS, 389, L38

Schnurr O., Moffat A. F. J., Villar-Sbaffi A., St-Louis N., Morrell N. I., 2009, MNRAS, 395, 823

Shatsky N., Tokovinin A., 2002, A&A, 382, 92

Shu F. H., Adams F. C., Lizano S., 1987, ARA&A, 25, 23

Smith N., Stassun K. G., Bally J., 2005, AJ, 129, 888

Smith R. J., Longmore S., Bonnell I., 2009, MNRAS, 400, 1775

Sota A., Maíz Apellániz J., Walborn N. R., Shida R. Y., 2008, RMxAC, 33, 56

Spitzer Jr. L., 1969, ApJ, 158, L139

Spitzer L., 1987, Dynamical evolution of globular clusters. Princeton: Princeton Univ. Press

Spurzem R., 1999, Journal of Computational and Applied Mathematics, 109, 407

Stetson P. B., 1981, AJ, 86, 1882

Stetson P. B., 1983, AJ, 88, 1349

Stone R. C., 1979, ApJ, 232, 520

Stone R. C., 1991, AJ, 102, 333

Takahashi K., 1995, PASJ, 47, 561

Tapia M., Roth M., Vázquez R. A., Feinstein A., 2003, MNRAS, 339, 44

Tapia M., Rodríguez L. F., Persi P., Roth M., Gómez M., 2009, AJ, 137, 4127

Tapia M., Roth M., Bohigas J., Persi P., 2011, MNRAS, 416, 2163

Tapia M., Persi P., Roth M., Elia D., Molinari S., Saldaño H. P., Gómez M., 2014, MNRAS, 437, 606

Testi L., Palla F., Natta A., 1999, A&A, 342, 515

Tetzlaff N., Neuhäuser R., Hohle M. M., 2011, MNRAS, 410, 190

Thies I., Kroupa P., 2007, ApJ, 671, 767

Verbunt F., 2003, in Piotto G., Meylan G., Djorgovski S. G., Riello M., eds, ASP Conf. Ser. Vol. 296, New Horizons in Globular Cluster Astronomy. San Francisco, CA: ASP, p. 245

Wang L., Spurzem R., Aarseth S., Nitadori K., Berczik P., Kouwenhoven M. B. N., Naab T., 2015, MNRAS, 450, 4070

Wang L., et al., 2016, MNRAS, 458, 1450

Weidner C., Kroupa P., 2004, MNRAS, 348, 187

Weidner C., Kroupa P., 2006, MNRAS, 365, 1333

Weidner C., Kroupa P., Larsen S. S., 2004, MNRAS, 350, 1503

Weidner C., Kroupa P., Nürnberger D. E. A., Sterzik M. F., 2007, MNRAS, 376, 1879

Weidner C., Kroupa P., Maschberger T., 2009, MNRAS, 393, 663

Weidner C., Kroupa P., Bonnell I. A. D., 2010, MNRAS, 401, 275

Weidner C., Kroupa P., Pflamm-Altenburg J., 2013a, MNRAS, 434, 84

Weidner C., Kroupa P., Pflamm-Altenburg J., Vazdekis A., 2013b, MNRAS, 436, 3309

Weidner C., Kroupa P., Pflamm-Altenburg J., 2014, MNRAS, 441, 3348

Weisz D. R., et al., 2015, ApJ, 806, 198

Whitmore B. C., 2003, in Livio M., Noll K., Stiavelli M., eds, A Decade of Hubble Space Telescope Science. Cambridge: Cambridge Univ. Press, p. 153

Wolff S. C., Strom S. E., Dror D., Venn K., 2007, AJ, 133, 1092

Wu S.-W., Bik A., Bestenlehner J. M., Henning T., Pasquali A., Brandner W., Stolte A., 2016, A&A, 589, A16

Yorke H. W., Sonnhalter C., 2002, ApJ, 569, 846

Zinnecker H., Yorke H. W., 2007, ARA&A, 45, 481

de Wit W. J., Testi L., Palla F., Vanzi L., Zinnecker H., 2004, A&A, 425, 937

de Wit W. J., Testi L., Palla F., Zinnecker H., 2005, A&A, 437, 247

Šubr L., Kroupa P., Baumgardt H., 2008, MNRAS, 385, 1673

van Buren D., McCray R., 1988, ApJ, 329, L93

van Buren D., Noriega-Crespo A., Dgani R., 1995, AJ, 110, 2914

APPENDIX A

Ejection estimates of S_{MAXI} using the half-mass radius

The tidal radius is used in Chapter 2 to determine if a star belongs to the cluster. In some cases, even though S_{MAXI} is dynamically ejected through a strong close encounter the star may have not left the cluster yet at a given time, especially if it has obtained a relatively low velocity from the encounter. Thus, the real probability for ejection of S_{MAXI} may be higher than that presented in this study. Considering that the massive stars are generally seated in the central part of the cluster due to dynamical interactions, relatively small distance such as the half-mass radius can be used as the ejection criterion for S_{MAXI}. However, it should be noted that S_{MAXI} being found outside of the half-mass radius does not necessarily mean that is ejected, especially when the cluster is initially unsegregated and dynamically unevolved. Here, therefore, we provide tables (Table A.1 and A.2) which contain the mean half-mass radius and the numbers of clusters whose S_{MAXI} is found outside of r_h, $2r_h$ and $4r_h$ and additionally has a velocity greater than the escape velocity at the given time. For most of the cluster models the mean half-mass radii do not change much within 3 Myr due to the clusters' dynamical evolution. Note that the initial crossing time of the clusters with $M_{ecl} \leq 100\,M_\odot$ and $r_h(0) = 0.8$ pc is longer than 3 Myr (Table 2.2). The most expanded half-mass radius is ≈ 1 pc at 3 Myr, although a few massive cluster models have expanded up to twice their initial half-mass radius.

The initial positions of S_{MAXI} distinctly show whether the models are generated with initial mass segregation. For the initially unsegregated clusters (Table A.1), more than half of the realizations for each models show that the S_{MAXI} is initially located outside of the half-mass radius. Even in up to 23 (8) per cent of the clusters the star is located further out than $2r_h$ ($4r_h$) at 0 Myr. For the initially mass-segregated clusters, only in few low-mass clusters (less than 5% at most) is S_{MAXI} located outside of r_h at 0 Myr (Table A.2). It may be strange for the mass-segregated cluster to show its most massive star having an initial position beyond the half-mass radius at all. But for the initially mass-segregated clusters with low masses ($M_{ecl} < 100\,M_\odot$) the initial position of S_{MAXI} can, sometimes, be generated slightly beyond the half-mass radius due to the shallow gravitational potential, the low number statistics and the algorithm generating the initially mass-segregated cluster (the heaviest star being the *most bound* to the cluster, but not requiring it to be at the most central position). None of the initially mass-segregated clusters have S_{MAXI} located initially further out than $2r_h$.

For the initially not mass-segregated clusters with relatively high masses ($\geq 100\,M_\odot$) and/or $r_h(0) = 0.3$ pc, $N(r_{S_{MAXI}} > r_h)$ in Table A.1 significantly decreases at 3 Myr as a result of dynamical evolution, i.e.

dynamical mass segregation. But there are still a large number of the unsegregated clusters, particularly the low-density ones, which have S_{MAXI} beyond the half-mass radius. In many cases the star has a velocity lower than the escape velocity. As those clusters are dynamically young and the velocity of the star is too small to escape from its cluster, it is unlikely that these stars are dynamically ejected. Either the star was initially located beyond the half-mass radius and has not fallen into the cluster centre yet. Or, if S_{MAXI} of the low-density clusters has an initial orbit as large as the half-mass radius (note that the half-mass radius is less than a parsec), it could be temporarily found beyond the half-mass radius since the dynamical interactions which lead to the massive star being confined to the central part of the cluster are insufficient by 3 Myr for these low-density clusters. This can also explain that for the mass-segregated clusters with low masses, especially with $10\,M_\odot$, $N(r_{S_{MAXI}} > r_h)$ increases at 3 Myr and most of these clusters have S_{MAXI} moving slower than the escape velocity. There are only two initially mass-segregated clusters with $10\,M_\odot$ whose S_{MAXI} is found beyond twice the half-mass radius at 3 Myr. These are due to low-energy encounters expelling the stars from the core without ejecting them from the cluster. However, in the NMS3OP and MS3OP models, and in massive ($\geq 10^3\,M_\odot$) clusters from the other models, a number of clusters have S_{MAXI} being beyond the half-mass radius with a velocity larger than the escape velocity, which implies that the S_{MAXI} stars are dynamically ejected. The probability of S_{MAXI} ejection increases with cluster mass. For the MS3OP model, 40% of the $10^4\,M_\odot$ clusters have probably ejected their S_{MAXI}.

$M_{\rm ecl}$ ($M_\odot$)	$\langle r_{\rm h}\rangle$ (pc)		$N(r_{\rm S_{MAXI}} > r_{\rm h})$			$N(r_{\rm S_{MAXI}} > 2r_{\rm h})$			$N(r_{\rm S_{MAXI}} > 4r_{\rm h})$		
	0 Myr	3 Myr	0 Myr	3 Myr	3 Myr†	0 Myr	3 Myr	3 Myr†	0 Myr	3 Myr	3 Myr†
NMS3S											
10	0.27	0.27	49	31	0	14	6	0	2	1	0
$10^{1.5}$	0.29	0.30	47	6	0	9	3	0	2	0	0
10^{2}	0.30	0.36	52	11	0	21	8	0	3	4	0
$10^{2.5}$	0.30	0.41	54	6	0	16	3	0	3	0	0
10^{3}	0.30	0.50	45	2	0	15	2	0	7	1	0
$10^{3.5}$	0.30	0.55	48	10	6	18	8	6	3	5	4
NMS3RP											
10	0.25	0.31	53	23	1	6	0	0	0	0	0
$10^{1.5}$	0.28	0.31	46	12	0	9	3	0	1	1	0
10^{2}	0.29	0.37	53	17	0	21	10	0	4	3	0
$10^{2.5}$	0.30	0.47	54	12	0	19	1	0	3	0	0
10^{3}	0.30	0.54	47	6	2	17	3	1	7	1	0
$10^{3.5}$	0.30	0.55	50	13	6	18	9	6	3	7	6
NMS3OP											
10	0.26	0.30	46	23	0	12	6	0	1	1	0
$10^{1.5}$	0.28	0.31	44	18	0	12	4	0	0	1	0
10^{2}	0.29	0.38	47	9	2	18	4	1	1	0	0
$10^{2.5}$	0.30	0.56	44	14	7	19	8	3	5	3	2
10^{3}	0.30	0.68	44	15	11	16	9	9	6	7	7
$10^{3.5}$	0.30	0.65	48	17	15	15	16	15	3	14	14

Continued on next page

M_{ecl} ($M_\odot$)	$\langle r_h \rangle$ (pc)		$N(r_{S_{MAXI}} > r_h)$			$N(r_{S_{MAXI}} > 2r_h)$			$N(r_{S_{MAXI}} > 4r_h)$		
	0 Myr	3 Myr	0 Myr	3 Myr	3 Myr†	0 Myr	3 Myr	3 Myr†	0 Myr	3 Myr	3 Myr†
NMS8S											
10	0.70	0.67	45	39	0	11	10	0	4	4	0
$10^{1.5}$	0.79	0.77	58	50	0	17	19	0	3	3	0
10^2	0.79	0.81	49	35	0	10	9	0	1	1	0
$10^{2.5}$	0.80	0.82	49	25	0	22	16	0	8	8	0
10^3	0.80	0.84	43	18	0	16	5	0	4	3	0
$10^{3.5}$	0.81	0.86	38	10	0	16	3	0	3	1	0
NMS8RP											
10	0.68	0.67	51	46	0	12	12	0	0	1	0
$10^{1.5}$	0.74	0.75	46	46	0	18	16	0	3	3	0
10^2	0.79	0.82	43	34	0	15	13	0	1	1	0
$10^{2.5}$	0.80	0.82	51	20	0	16	13	0	2	1	0
10^3	0.80	0.84	41	13	0	14	9	0	4	4	0
$10^{3.5}$	0.80	0.85	52	18	0	15	7	0	5	2	0
NMS8OP											
10	0.69	0.68	39	42	0	8	11	0	0	0	0
$10^{1.5}$	0.76	0.76	48	34	0	10	10	0	1	2	0
10^2	0.77	0.81	45	20	0	10	7	0	2	2	0
$10^{2.5}$	0.79	0.85	63	32	0	23	13	0	6	6	0
10^3	0.81	0.88	53	18	2	18	8	2	2	4	1
$10^{3.5}$	0.80	0.93	44	12	1	17	3	0	0	2	0

Table A.1. The averaged half-mass radius, $\langle r_h \rangle$, and the number of clusters whose S_{MAXI} is found beyond the half-mass radius, $N(r_{S_{MAXI}} > r_h)$, beyond $2r_h$, $N(r_{S_{MAXI}} > 2r_h)$, and beyond $4r_h$, $N(r_{S_{MAXI}} > 4r_h)$ at 0 and 3 Myr from the initially unsegregated clusters. The latter numbers at 3 Myr marked with †, are the number of clusters whose S_{MAXI} fulfils the distance criteria and moves faster than the escape velocity ($v_{S_{MAXI}} > v_{esc}$).

$M_{\rm ecl}$ ($M_\odot$)	$\langle r_{\rm h}\rangle$ (pc)		$N(r_{\rm S_{MAXI}} > r_{\rm h})$			$N(r_{\rm S_{MAXI}} > 2r_{\rm h})$			$N(r_{\rm S_{MAXI}} > 4r_{\rm h})$		
	0 Myr	3 Myr	0 Myr	3 Myr	3 Myr†	0 Myr	3 Myr	3 Myr†	0 Myr	3 Myr	3 Myr†
MS3S											
10	0.24	0.25	0	10	0	0	0	0	0	0	0
$10^{1.5}$	0.28	0.31	0	0	0	0	0	0	0	0	0
10^{2}	0.32	0.35	0	0	0	0	0	0	0	0	0
$10^{2.5}$	0.31	0.44	0	2	1	0	0	0	0	0	0
10^{3}	0.31	0.55	0	2	1	0	2	1	0	1	1
$10^{3.5}$	0.31	0.59	0	7	5	0	5	4	0	4	4
MS3RP											
10	0.23	0.29	4	25	1	0	2	0	0	0	0
$10^{1.5}$	0.29	0.30	3	2	0	0	0	0	0	0	0
10^{2}	0.30	0.39	0	3	0	0	0	0	0	0	0
$10^{2.5}$	0.31	0.47	0	3	3	0	1	1	0	1	1
10^{3}	0.31	0.57	0	3	3	0	3	3	0	2	2
$10^{3.5}$	0.31	0.59	0	11	6	0	9	6	0	8	6
MS3OP											
10	0.23	0.26	2	11	0	0	0	0	0	0	0
$10^{1.5}$	0.28	0.33	0	3	1	0	1	1	0	0	0
10^{2}	0.29	0.42	0	4	4	0	4	4	0	2	2
$10^{2.5}$	0.30	0.60	0	19	16	0	12	12	0	3	3
10^{3}	0.31	0.72	0	20	13	0	15	11	0	11	8
$10^{3.5}$	0.31	0.70	0	26	22	0	24	22	0	19	19
10^{4}	0.31	0.50	0	4	4	0	4	4	0	4	4

Continued on next page

M_{ecl} ($M_\odot$)	$\langle r_h \rangle$ (pc)		$N(r_{S_{MAXI}} > r_h)$			$N(r_{S_{MAXI}} > 2r_h)$			$N(r_{S_{MAXI}} > 4r_h)$		
	0 Myr	3 Myr	0 Myr	3 Myr	3 Myr†	0 Myr	3 Myr	3 Myr†	0 Myr	3 Myr	3 Myr†
MS8S											
10	0.63	0.59	0	6	0	0	0	0	0	0	0
$10^{1.5}$	0.77	0.74	1	5	0	0	0	0	0	0	0
10^2	0.87	0.82	0	1	0	0	0	0	0	0	0
$10^{2.5}$	0.81	0.86	0	0	0	0	0	0	0	0	0
10^3	0.82	0.90	0	0	0	0	0	0	0	0	0
$10^{3.5}$	0.83	0.93	0	0	0	0	0	0	0	0	0
MS8RP											
10	0.60	0.57	3	3	0	0	0	0	0	0	0
$10^{1.5}$	0.74	0.70	0	8	0	0	0	0	0	0	0
10^2	0.81	0.82	0	3	0	0	0	0	0	0	0
$10^{2.5}$	0.82	0.85	0	2	0	0	0	0	0	0	0
10^3	0.83	0.90	0	0	0	0	0	0	0	0	0
$10^{3.5}$	0.83	0.95	0	0	0	0	0	0	0	0	0
MS8OP											
10	0.61	0.55	0	3	0	0	0	0	0	0	0
$10^{1.5}$	0.75	0.67	0	4	0	0	0	0	0	0	0
10^2	0.78	0.80	0	2	0	0	0	0	0	0	0
$10^{2.5}$	0.80	0.93	0	3	2	0	0	0	0	0	0
10^3	0.83	1.02	0	7	4	0	2	2	0	0	0
$10^{3.5}$	0.83	1.05	0	5	3	0	3	2	0	2	2

Table A.2. Same as Table A.1 but for the initially mass-segregated cluster models. Note that only 10 realizations are performed for 10^4 $M_\odot$ clusters due to the expensive computing cost.

APPENDIX B

Results of individual models in Chapter 3

Here we append the table containing the results and properties of each model cluster in Chapter 3 (Table B.1).

$M_{\rm ecl}$ ($M_\odot$)	$m_{\rm max}$ ($M_\odot$)	$\langle r_{\rm h}\rangle$ (pc)	$\langle {}^{\rm com}N_{\rm O}\rangle$	$\langle {}^{\rm com}N_{\rm ej,O}\rangle$	$\langle {}^{\rm com}f_{\rm ej,O}\rangle$	$\langle f_{\rm b,O}\rangle$	$\langle f_{\rm b,ej,O}\rangle$	$N_{\rm run}$
MS3OP								
$10^{2.5}$	21.2	0.60	1.11	0.09	0.080	0.84	0.78	100
10^{3}	43.9	0.72	2.96	0.61	0.172	0.66	0.33	100
$10^{3.5}$	79.2	0.70	9.57	2.38	0.252	0.45	0.17	100
10^{4}	114.7	0.50	30.10	4.40	0.149	0.23	0.13	10
$10^{4.5}$	136.2	0.50	105.00	11.25	0.105	0.15	0.05	4
NMS3OP								
$10^{2.5}$	21.2	0.56	1.14	0.03	0.020	0.87	0.50	100
10^{3}	43.9	0.68	3.11	0.54	0.166	0.70	0.25	100
$10^{3.5}$	79.2	0.65	9.26	2.21	0.244	0.51	0.15	100
10^{4}	114.7	0.57	30.00	5.30	0.177	0.32	0.17	10
$10^{4.5}$	136.2	0.50	98.25	9.25	0.092	0.27	0.12	4
MS3OP_SP								
$10^{2.5}$	21.2	0.62	1.23	0.09	0.090	0.79	0.67	100
10^{3}	43.9	0.74	2.92	0.71	0.228	0.65	0.43	100
$10^{3.5}$	79.2	0.72	9.11	2.32	0.257	0.51	0.32	100
10^{4}	114.7	0.66	26.40	5.70	0.218	0.40	0.27	10
$10^{4.5}$	136.2	0.55	96.50	14.00	0.145	0.27	0.21	4
MS3UQ_SP								
$10^{2.5}$	21.2	0.58	1.34	0.12	0.097	0.86	0.67	100
10^{3}	43.9	0.73	3.32	0.62	0.177	0.66	0.56	100
$10^{3.5}$	79.2	0.69	10.28	2.23	0.209	0.59	0.32	100
10^{4}	114.7	0.63	33.60	6.30	0.188	0.45	0.29	10
$10^{4.5}$	136.2	0.54	103.00	10.50	0.104	0.36	0.26	4

Continued on next page

$M_{\rm ecl}$ ($M_\odot$)	$m_{\rm max}$ ($M_\odot$)	$\langle r_{\rm h}\rangle$ (pc)	$\langle {}^{\rm com}N_{\rm O}\rangle$	$\langle {}^{\rm com}N_{\rm ej,O}\rangle$	$\langle {}^{\rm com}f_{\rm ej,O}\rangle$	$\langle f_{\rm b,O}\rangle$	$\langle f_{\rm b,ej,O}\rangle$	$N_{\rm run}$
MS3S								
$10^{2.5}$	21.2	0.44	1.17	0.00	0.000	0.84	0.00	100
10^{3}	43.9	0.55	2.88	0.17	0.043	0.56	0.13	100
$10^{3.5}$	79.2	0.59	10.40	1.52	0.145	0.22	0.04	100
10^{4}	114.7	0.52	34.30	3.30	0.096	0.06	0.00	10
$10^{4.5}$	136.2	0.48	114.50	6.25	0.054	0.02	0.04	4
MS8OP								
$10^{2.5}$	21.2	0.93	1.10	0.00	0.000	0.97	0.00	100
10^{3}	43.9	1.02	2.45	0.12	0.036	0.92	0.26	100
$10^{3.5}$	79.2	1.05	8.81	0.49	0.053	0.54	0.20	100
10^{4}	114.7	1.02	27.90	1.10	0.038	0.39	0.00	10
$10^{4.5}$	136.2	1.00	86.50	2.25	0.026	0.35	0.00	4
10^{5}[a]	145.3	0.90	207.25	17.50	0.084	0.62	0.05	4
MS1OP								
$10^{2.5}$	21.2	0.60	1.16	0.28	0.248	0.91	0.64	100
10^{3}	43.9	0.63	3.09	1.48	0.415	0.72	0.35	100
$10^{3.5}$	79.2	0.49	9.10	4.55	0.516	0.47	0.15	100
10^{4}	114.7	0.40	30.90	14.30	0.468	0.22	0.05	10
$10^{4.5}$	136.2	0.33	106.00	33.75	0.320	0.12	0.04	4

Table B.1. Results of all models at 3 Myr. Columns 1 and 2 show the initial stellar mass of the model clusters and the initial maximum stellar mass, respectively. Columns 3 and 4 present the averaged half-mass radius,$\langle r_{\rm h}\rangle$, and the average number of O-star systems present in the calculations, $\langle {}^{\rm com}N_{\rm O}\rangle$, at 3 Myr, respectively. Columns 5 and 6 are the average number of ejected O-star systems, $\langle {}^{\rm com}N_{\rm ej,O}\rangle$, and the average O-star system ejection fraction, $\langle {}^{\rm com}f_{\rm ej,O}\rangle$. The average binary fraction of O-star systems remaining in the cluster, $\langle f_{\rm b,O}\rangle$, and the average binary fraction of ejected O-star systems, $\langle f_{\rm b,ej,O}\rangle$, at 3 Myr are listed in columns 7 and 8, respectively. Note that the fraction of binaries among all O-star systems is smaller than the initial value of $f_{\rm b,O} = 1$ because systems are disrupted in these models. The number of realizations, $N_{\rm run}$, for each cluster mass is listed in the last column. Only clusters with $M_{\rm ecl} \geq 10^{2.5}\,M_\odot$ are listed as less massive clusters do not have O stars in our models.

[a]The $10^5\,M_\odot$ cluster model is adopted from Banerjee et al. (2012b). The initial conditions of the model from Banerjee et al. (2012b) are slightly different from ours. Their O-star binaries are mostly close binaries (see Figure 3.1) and this results in higher ejection fractions and less dynamical disruptions of O-star binaries (higher binary fraction of O-star systems at 3 Myr) compared to our models.

APPENDIX C

Additional figures for Chapter 4

C.1 System mass versus velocity of the ejected systems for all models with $r_h(0) \leq 0.3$ pc in Chapter 4.

The velocity and system mass of ejected systems, same as Fig. 4.4, are plotted in Fig. C.1 for all models with $r_h(0) \leq 0.3$ pc in Chapter 4.

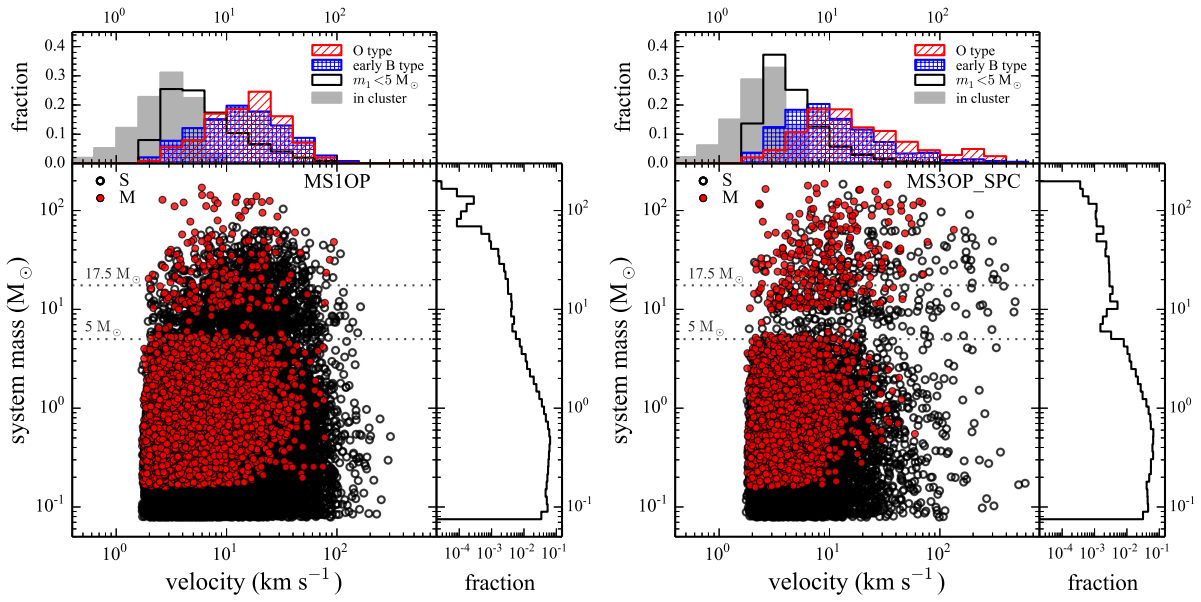

Figure C.1. Same as Fig. 4.4 but for all models with $r_h(0) \leq 0.3$ pc in Chapter 4.

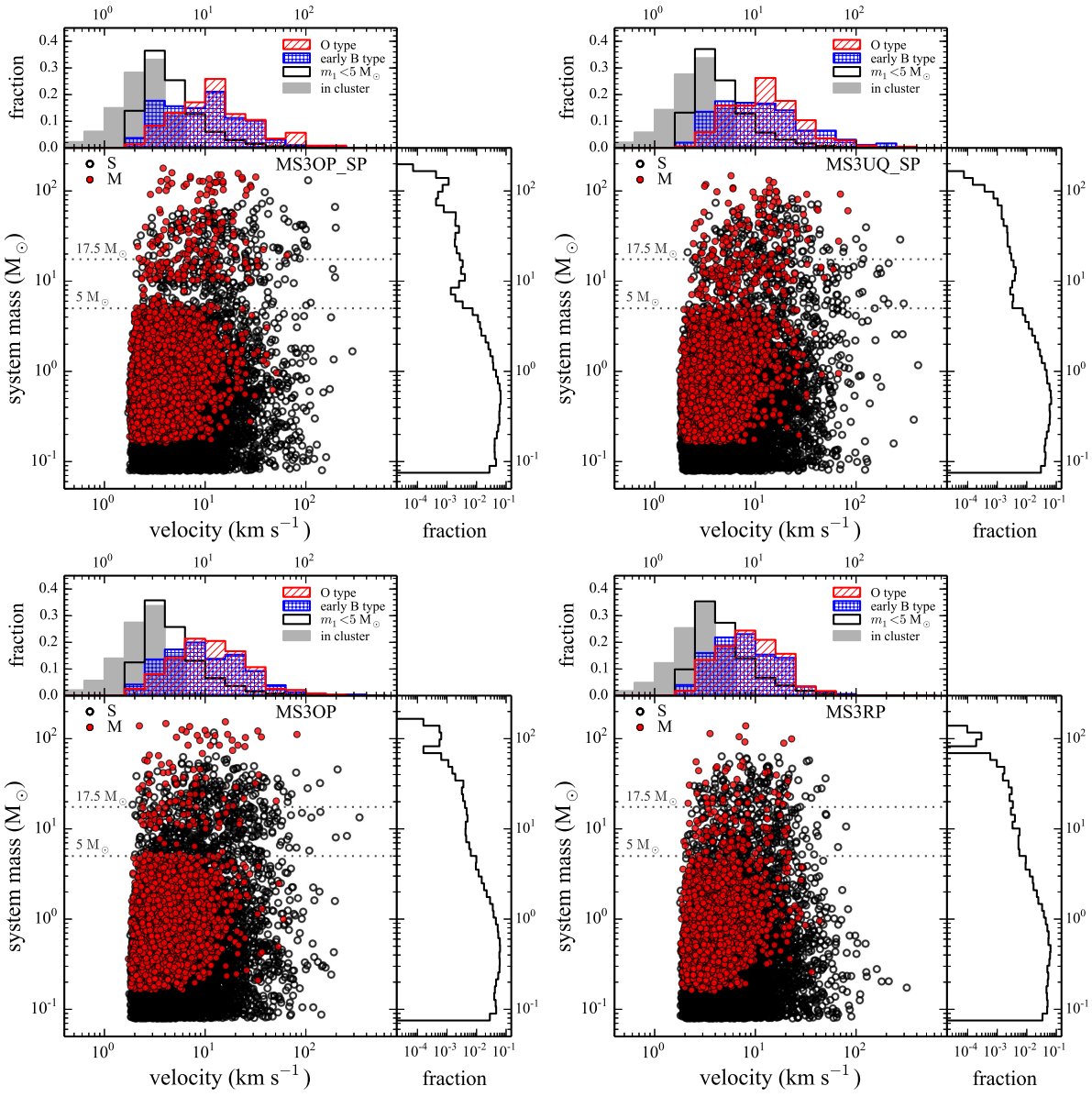

Figure C.1. (Continued.)

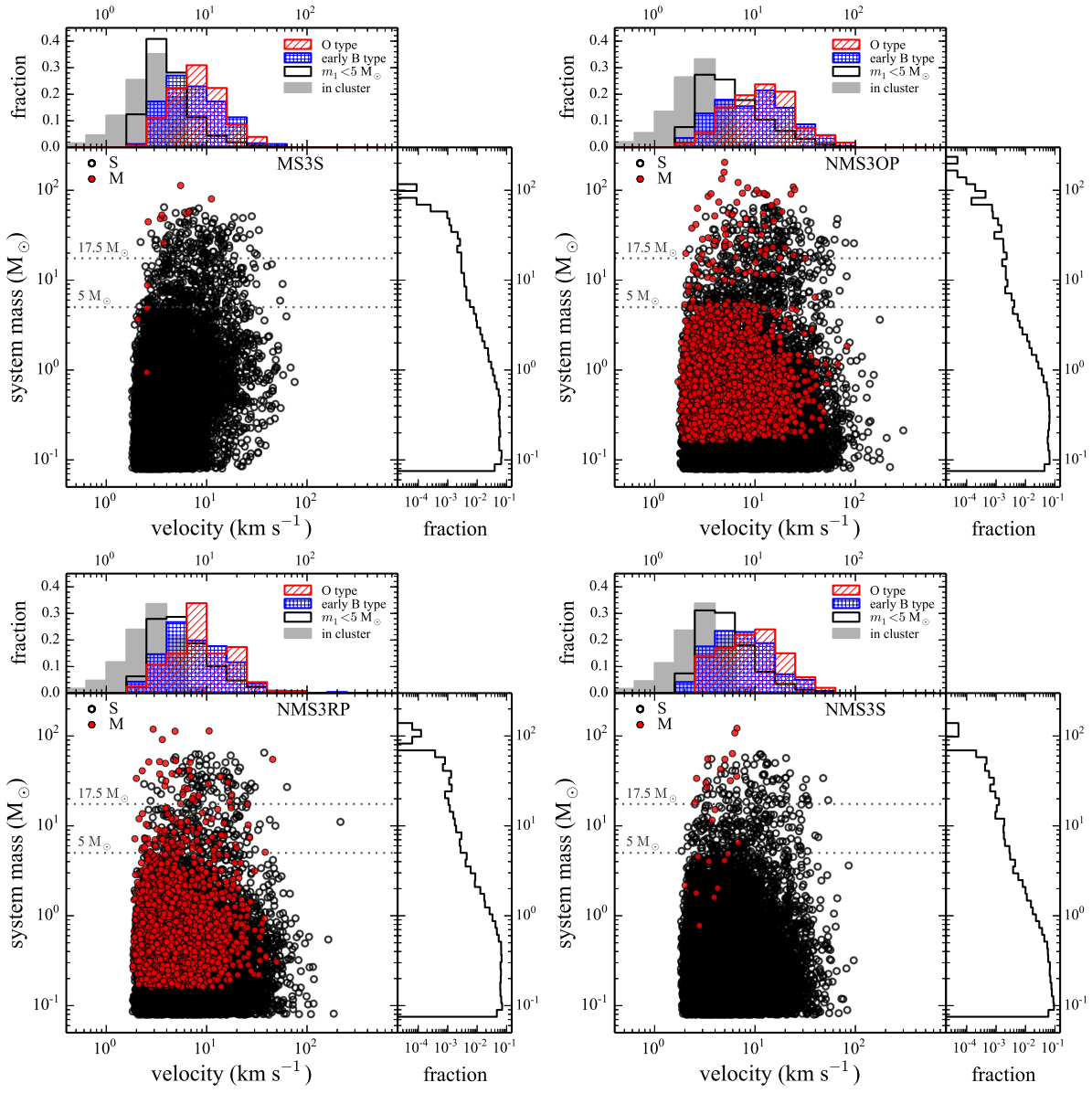

Figure C.1. (Continued.)

C.2 τ_{ej} and the core radius

The distributions of τ_{ej} and core radius as a function of time, same as Fig. 4.6, are plotted in Fig. C.2 for all models with $r_h(0) \leq 0.3$ pc in Chapter 4.

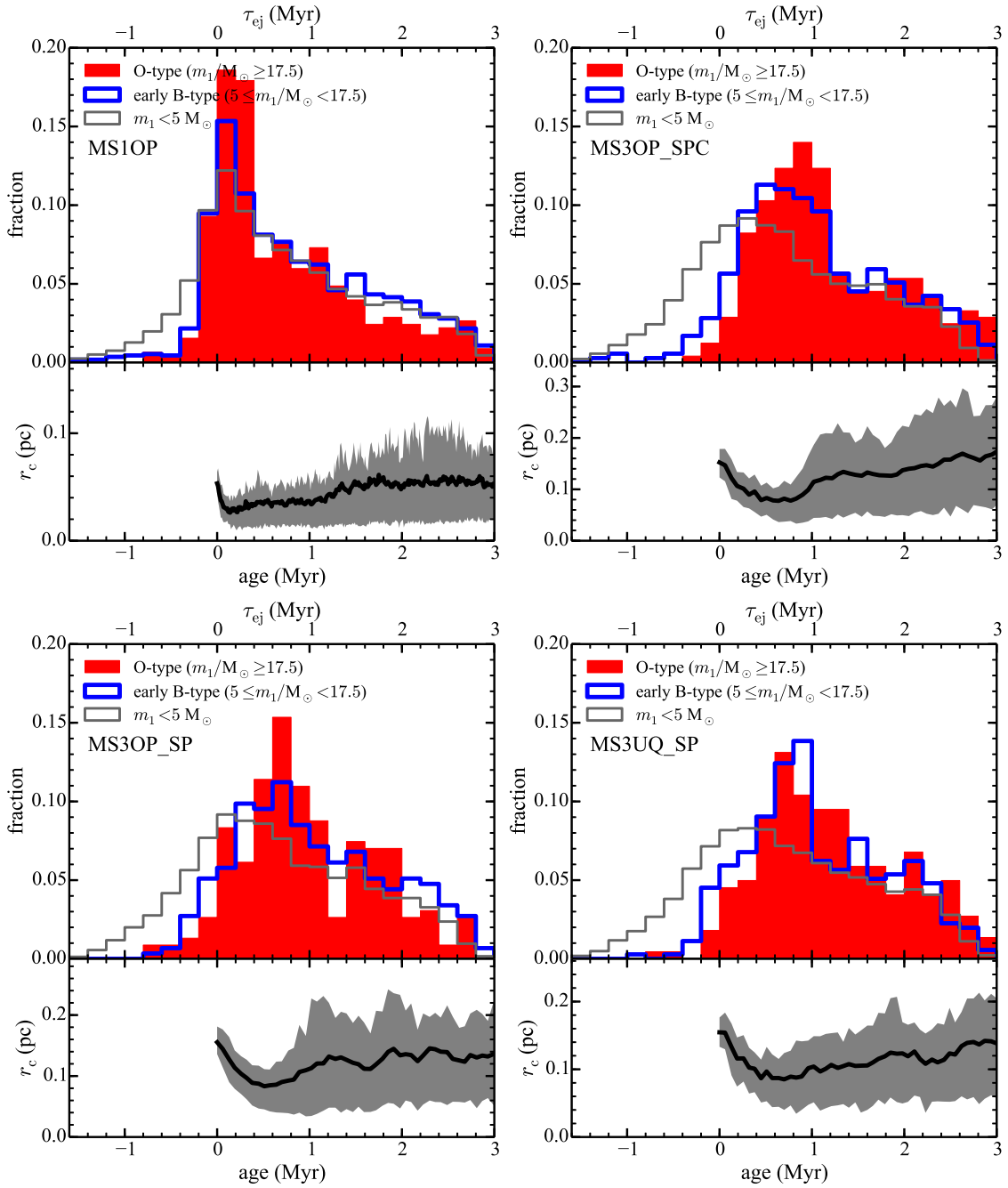

Figure C.2. Same as Fig. 4.6 but for all models with $r_h(0) \leq 0.3$ pc in Chapter 4.

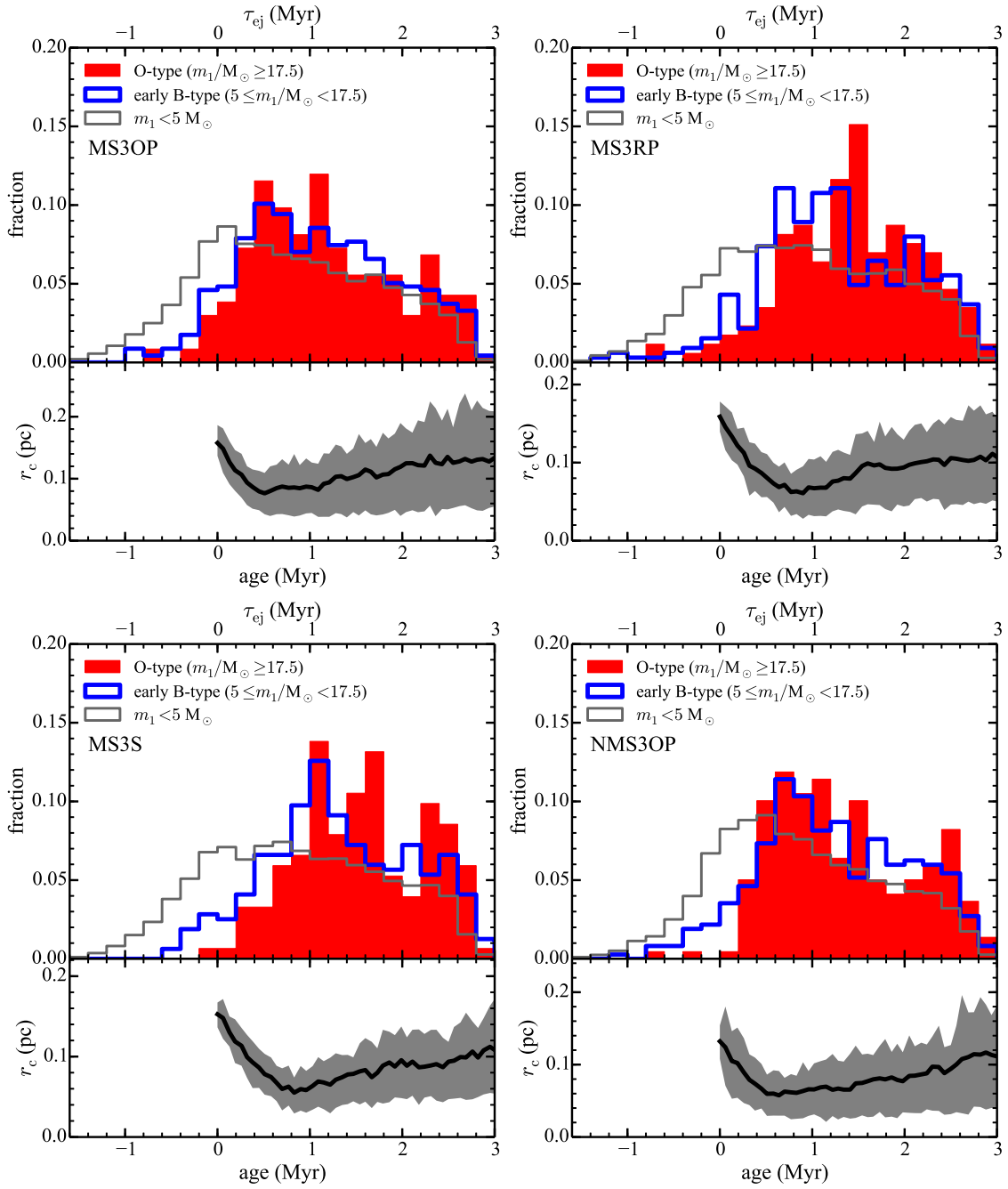

Figure C.2. (Continued.)

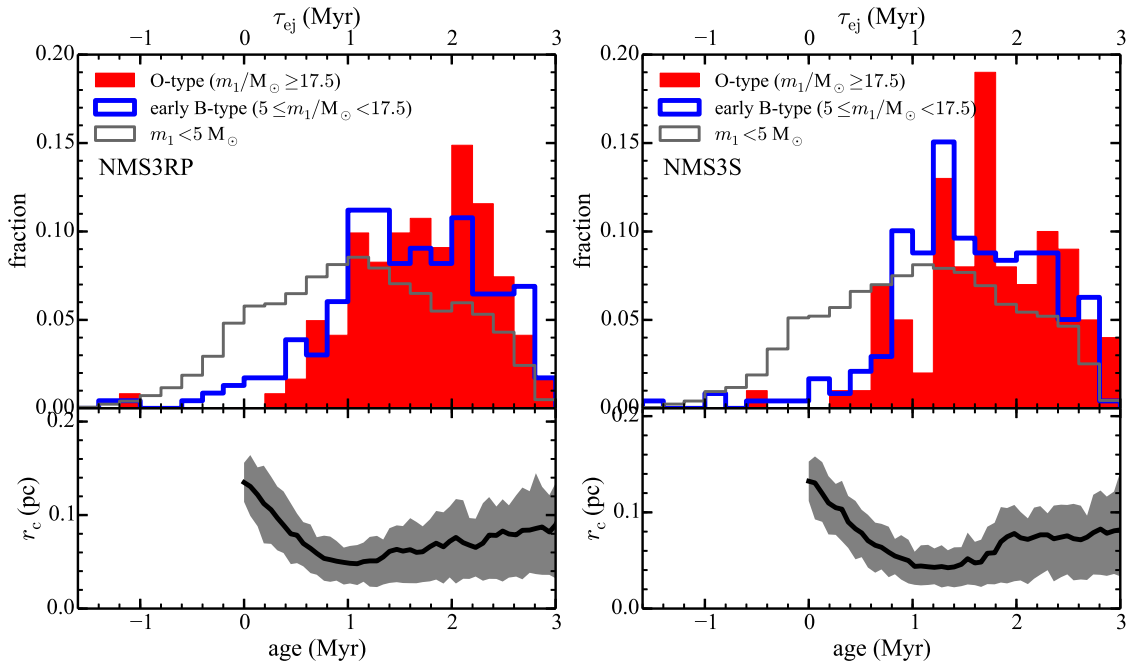

Figure C.2. (Continued.)

C.3 τ_{ej} versus velocity

Heat maps of τ_{ej} versus velocity are plotted in Fig. C.2 for all models with $r_h(0) \leq 0.3$ pc in Chapter 4. The systems with a negative τ_{ej} mostly have a low velocity, implying deceleration by the potential of their birth cluster.

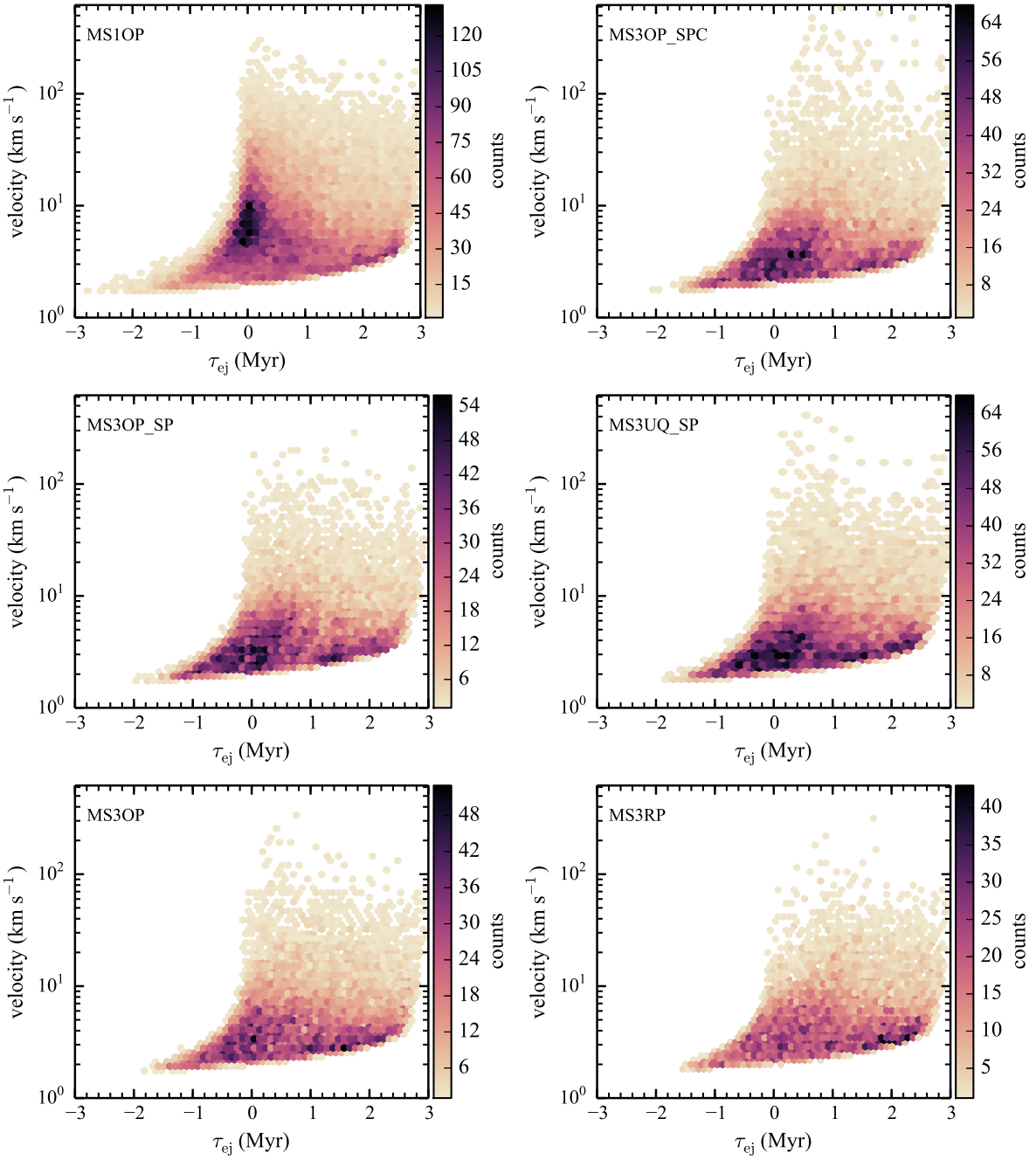

Figure C.3. Heatmaps of τ_{ej} versus velocity for all models with $r_h(0) \leq 0.3$ pc in Chapter 4.

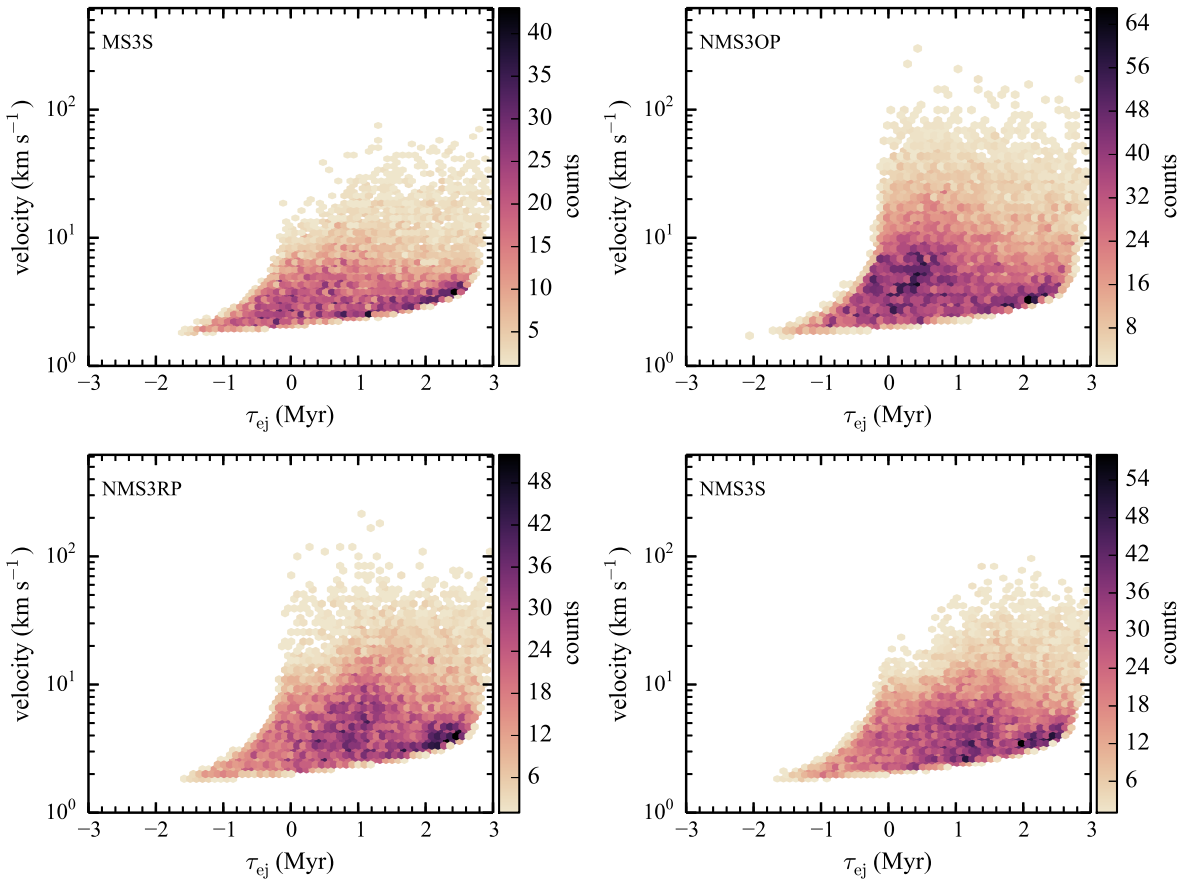

Figure C.3. (Continued.)

List of Figures

List of Tables

Acknowledgements

Firstly, I deeply thank my advisor Pavel Kroupa for his continuous support of my PhD studies and for his motivation and immense knowledge. His guidance has taught me how to be a good researcher and has helped me develop my own thoughts and ideas.

I would like to express my sincere gratitude to Sverre Aarseth. My research has been only possible with his great work and long-time devotion to the development of N-body codes. He has been a great inspiration to me in many ways, not only with his passion for astronomy but also with his love for wildlife.

I appreciate the Max Planck Society (International Max Planck Research School for Astronomy and Astrophysics) for the financial support in my first three years of PhD study and wish to thank Gabi Breuer for helping me to settle in Bonn when many things were new to me as I came to Germany for the first time in my life. I thank Prof. Karl Menten for his support from the beginning of my PhD studies and for kindly being a member of my thesis examination board. I also thank my other examination board members, Prof. Carsten Urbach and Prof. Hubert Schorle.

Many thanks to people with whom I have crossed paths in Bonn for the funs or the fruitful discussions I had with them; my late lunch buddies Yujin and Miju, my old office mate Iskren, Rob who introduced various whiskies and wines, old party friends Rosie and Nanase, Andrea Stolte who always encouraged me, my colleagues in SPODYR group, Marcel, Michael, Andreas, Andrea Dieball, Ingo, Sambaran, and Jan, and special thanks to Ahmed for kindly answering my questions on the thesis submission and to Ole Marggraf for his technical support related to computers. I also thank all the people whom I cannot recall to list here right now, but who have been a help of my PhD study.

I am thankful to Laura, Ilka, Mayumi, Hui, Xufen for their friendship. They are now far away but I hope to see them soon again. My life in bonn cannot be described without Yoon Kyung who did so many activities together with me. She has always given me positive energy and warm wishes. I feel so lucky to know her and to share many years in Bonn with her and her lovely family.

I thank my friends in Korea for their warm friendship; Jieun, Eunjung, Soyoung, and Jiwon. I would like to give my special thanks to Namhee who had kept me from feeling lonely, listened my boring whines and always checked if I am doing well.

My big thanks go to Joachim who has kept me happy for the last couple of years and will keep doing the job well, hopefully!

Last but not least, I am wholeheartedly grateful to my family, my parents, my two brothers and sister, for their endless love, support, and patience.